Characterisation and prediction of membrane separation performance: An industrial assessment.

Oatley, Darren Lee

Department of Chemical and Biological Process Engineering

University of Wales Swansea

CHARACTERISATION AND PREDICTION OF MEMBRANE SEPARATION PERFORMANCE – AN INDUSTRIAL ASSESSMENT

by

Darren Lee Oatley

M. Eng. (Wales)

A Thesis Submitted in Fulfilment of the Requirement

for the Degree

DOCTOR OF PHILOSOPHY

Philosophiae Doctor (Ph.D.)

June 2004

ProQuest LLC.
789 East Eisenhower Parkway
P.O. Box 1346
Ann Arbor, MI 48106 – 1346

Summary

The main objective of this work was to develop the existing predictive models for membrane nanofiltration, previously verified at the laboratory scale, and apply these theoretical descriptions to separations of real industrial importance.

A detailed comparison was made between the updated Donnan steric partitioning model (UDSPM) model and the simplified linear UDSPM model and the extent of deviation over a wide range of possible nanofiltration conditions was small. This result justified the use of the simplified model for predicting multi-component separations reducing computational time and complexity.

A theoretical and experimental comparison was made between two existing continuum descriptions of dielectric exclusion phenomenon. The two models were found to calculate the total contribution of dielectric exclusion effects to the same order of magnitude. The Born model was suggested as the most practical description at present because of the model's inherent simplicity.

The UDSPM and linear UDSPM were then employed as a predictive tool in the isolation of *N*-acetyl-D-neuraminic acid, an important precursor in the production of the influenza antiviral Relenza™. The Nanomax™-50 commercially available NF membrane was characterised and a membrane charge isotherm was developed from a study of the diafiltration components. Excellent agreement between the experimental findings and the model predictions was observed when the membrane charge was varied with pyruvate ion concentration. The linear UDSPM model was then used to assess the performance of a possible full scale industrial process for the recovery of sodium cefuroxime from a process effluent. The model results indicate that inclusion of nanofiltration technology will indeed facilitate the recovery of the high value antibiotic and produce an effluent of significantly improved quality.

Overall, as a result of the rational approach taken in this study, the application of existing predictive nanofiltration models for the design, optimisation and scale-up of more complex industrially relevant separations has been established. This will further promote the use of membrane technology in the process industries, such as pharmaceutical and fine chemical manufacture, by significantly reducing development risk and time.

Each time new experiments are observed to agree with predictions our confidence in the model is increased. However, if a new observation is found to disagree, we have to abandon or modify the theory...

At least that is what is supposed to happen, but we can always question the competence of the observer.

-Stephen Hawking

Declaration

This work has not previously been accepted in substance for any degree and is not being concurrently submitted in candidature for any degree.

Signed: ..... (*Candidate*: Darren Lee Oatley)
Date: 6-Sep-04

STATEMENT 1

This thesis is the result of my own investigation, except where otherwise stated. Other sources are acknowledged by footnotes giving explicit references. A bibliography is appended.

Signed: ..... (*Candidate*: Darren Lee Oatley)
Date: 6-Sep-04

STATEMENT 2

I hereby give consent for my thesis, if accepted, to be available for photocopying and inter-library loan, and for the title and summary to be made available to outside organisations.

Signed: ..... (*Candidate*: Darren Lee Oatley)
Date: 6-Sep-04

Acknowledgements

To fully acknowledge the part that some people have played in my time at Swansea is simply impossible. However, I offer my deepest gratitude to the following:

Professor W. Richard Bowen, my supervisor, for his insight, encouragement and unfailing guidance throughout the course of the present work and especially during difficult times.

Professor Steve Wilks, for all his help during the final stages of the project.

Professor Paul Preece, a man who has opened my eyes to possibilities and cultures I most likely would have never experienced…bon chance sur votre retrait.

GlaxoSmithKline Research and Development Ltd. Stevenage and **GlaxoSmithKline Global Manufacturing and Supply** Ulverston, for support of this work via a fully funded PhD studentship. I would especially like to thank **Eur. Ing. Peter Jones** and **Dr. Barrie Cassey**, industrial supervisors, for their continued support and assistance throughout this project.

The lecturing and technical staff at Swansea, particularly Dr. Tony Knights, Dr. Bob Lovitt, Dr. Meirion Jones, Glyn, Phil, Adrian and Gary, for their help and support in my work.

My friends within the department for providing a stimulating alternative when necessary, especially Paulo, Brownie, Karlos, Shaner, Sej, Filthy, Richie, Cordy and Wrighty.

Finally, and most importantly, **Theresa** and **Anthony**, my parents, whose love, support, understanding and encouragement has guided me through life thus far. I love you both more than I could ever tell you.

Table of Contents

1 Introduction

This chapter introduces the reader to a general overview of membrane processes and then focuses on nanofiltration (NF) in particular. A brief discussion of microfiltration (MF), ultrafiltration (UF) and hyperfiltration commonly referred to as reverse osmosis (RO) will be given. A detailed discussion of NF membranes related to types of membrane, separation mechanisms and industrial applications will also be given. Finally, the last section will discuss the overall objectives of the present work and how they contribute to the development of NF technology.

1.1 Overview of membrane processes

Although chemists, physicists and biologists were performing research into the barrier properties of membranes at the start of the twentieth century, the first artificial laboratory membranes were not manufactured for some twenty years [Mulder (1996)]. The most significant breakthrough in the industrial application of membrane technology was the development of the first asymmetric membrane in the late 1950s [Loeb and Sourirajan (1960)]. Since then, membrane processes have carved a niche in various industries as an alternative to traditional separation processes such as distillation, adsorption, extraction and chromatography.

Membrane processes offer many distinct advantages over traditional separation processes such as highly selective separation, relatively low capital investment and operating costs, low energy consumption, constant temperature operation with no phase change, continuous and automatic operation and simple modular construction. These advantages are beneficial to wide range of applications and are especially important for certain types of materials that have been inherently difficult and expensive to separate [Bowen (1994)]:

- Finely dispersed solids, especially those which are compressible, have a density close to that of the liquid phase, have high viscosity or are gelatinous.
- Low molecular weight, non-volatile organics or pharmaceuticals and dissolved salts.

- Biological materials which are very sensitive to their physical and chemical environment.

A membrane is defined, according to the International Union of Pure and Applied Chemistry [IUPAC (1996)], as a "structure having lateral dimensions much greater than thickness, through which mass transfer may occur under a variety of driving forces". Membranes are able to separate components due to differences in physical and chemical properties between the membrane and the solutes. Transport of both solvent and solute across a membrane is caused by the action of a driving force or driving potential on the feed solution. The possibility exists to classify membrane processes based upon the nature of the driving force or driving potential (gradients in concentration, electrical potential, temperature or pressure) and the physical state of the phase on either side of the membrane. A classification on this basis of membrane processes is presented in Table 1.1.

Table 1.1: A classification of membrane processes [Mulder (1996)].

Membrane Process	Feed Phase	Permeate Phase	Driving Force
Microfiltration	Liquid	Liquid	ΔP
Ultrafiltration	Liquid	Liquid	ΔP
Nanofiltration	Liquid	Liquid	ΔP
Reverse Osmosis	Liquid	Liquid	ΔP
Piezodialysis	Liquid	Liquid	ΔP
Gas Separation	Gas	Gas	Δp
Vapour Permeation	Gas	Gas	Δp
Pervaporation	Liquid	Gas	Δp
Electrodialysis	Liquid	Liquid	ΔE
Membrane Electrodialysis	Liquid	Liquid	ΔE
Dialysis	Liquid	Liquid	Δc
Diffusion Dialysis	Liquid	Liquid	Δc
Membrane Contactors	Liquid	Liquid	Δc
	Gas	Liquid	Δc / Δp
	Liquid	Gas	Δc / Δp
Thermo-osmosis	Liquid	Liquid	ΔT / Δp
Membrane Distillation	Liquid	Liquid	ΔT / Δp

The liquid-liquid pressure driven processes of MF, UF, NF and RO will now be considered in further detail. MF membranes are normally used to separate suspended particles in the range of approximately 0.05 – 10 μm such as aggregates, bacteria and yeast at low operating pressures ($\Delta P < 0.2$ MPa). The separation mechanism of MF

membranes is primarily due to steric rejection (sieving). UF membranes have pore dimensions ranging from 5 – 100 nm and are suitable for the separation of macromolecules (molecular weight ~ 10^4 – 10^6 Da) and colloids such as proteins and enzymes. Initially it was thought that the separation mechanisms involved in UF were predominantly steric but increasingly attention was given to charge effects, which are now considered to play a significant role. The separating layer of UF membranes is denser than that in MF membranes and leads to a larger hydraulic resistance. As a direct result, the operating pressures are greater in UF membranes than MF membranes ($0.1 < \Delta P < 0.5$ MPa). RO membranes ideally only allow the solvent (in most cases water) to permeate the membrane. These membranes are denser still and so the operating pressure must be large ($1 < \Delta P < 10$ MPa) to overcome both the hydraulic resistance and the large osmotic pressure gradient (typically the osmotic pressure of sea water is 2.5 MPa). NF membranes, that will be described in further detail, have properties that lie between those of UF and RO membranes. Figure 1.1 illustrates the main separation features of the four processes considered.

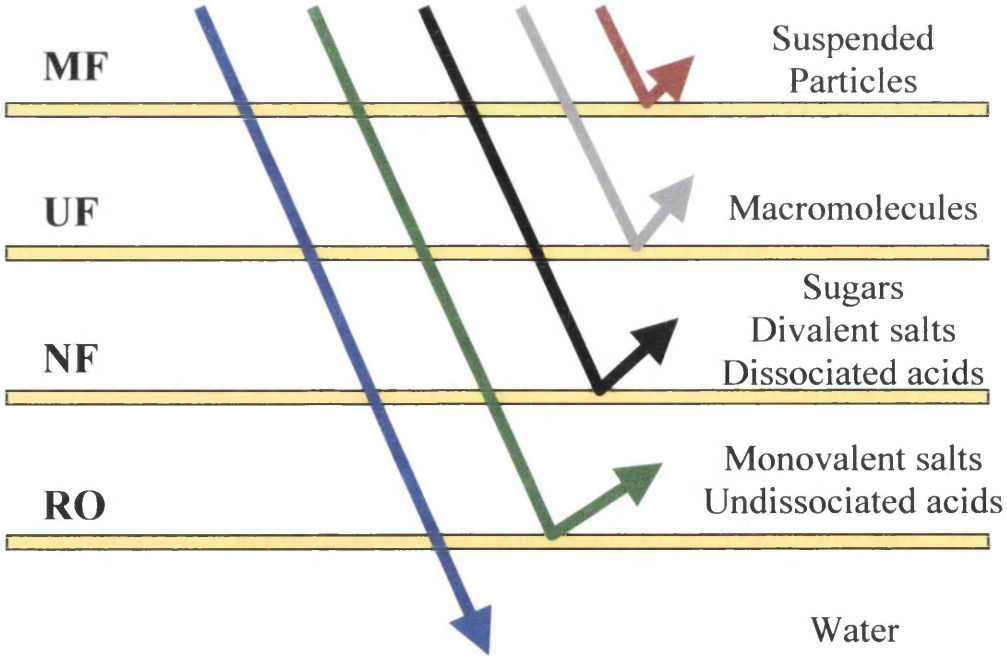

Figure 1.1: The separation features of different liquid-liquid pressure driven membrane processes [Raman *et al.* (1994)].

The membranes used in all four of the processes considered are commonly made from polymeric materials. In the early years of membrane development, cellulose acetate was widely used throughout industry, however, this polymer has been replaced by polyamide, polysulphone, polyethersulphone, polycarbonate and a number of more advanced polymers and blends. These synthetic polymers offer improved chemical and mechanical stability and higher resistance to microbial degradation than the original cellulose acetate membranes and are very suitable for use in a wide range of applications.

As a result of the ever increasing industrial demand for use of membranes in elevated temperatures, pressures and corrosive environments, a number of workers are now developing inorganic membranes fabricated from ceramics and metals. Weber *et al.* (2003) developed a ceramic membrane with properties in the NF range. This membrane had superior permeation rates to polymeric NF membranes and was successfully applied to the filtration of textile wastewaters, alkaline wash solutions and pickling bath solutions. Tsuru *et al.* (2003) used the Sol-Gel method to develop an NF membrane from a 9:1 silica:zirconia blend and showed that the membrane had an average pore size in the range 1-3 nm. The transport mechanism for the membrane did not obey the viscous-flow mechanism as the pure solvent permeation rate multiplied by the solvent viscosity ($L_p\mu$) was not constant for a range of different solvents. However, modification of the membrane with trimethylchlorosilane produced a membrane which did obey the viscous-flow mechanism and had a pore size of 1 nm, with a molecular weight cut-off (MWCO) equal to 200 Da.

Most MF membranes have a symmetrical porous structure with porosities as high as 80 % and thickness in the range of 50 – 100 μm. UF membranes are also porous although their pore structure is asymmetric with a 1 – 2 μm thick top layer of very fine pore dimensions supported by an openly porous bottom layer of approximately thickness 100 μm. Both layers may be fabricated from the same material. The thin film composite (TFC) membrane is another type of UF membrane. This type of membrane consists of an extremely thin layer, typically 1 μm thickness, of the finest pore structure deposited on a more openly porous matrix. The two materials for the active layer and support matrix are not the same for TFC membranes. RO membranes

are generally considered to have no porous structure but consist of a very dense polymer network, within which transfer takes place by the solution diffusion method.

1.2 Nanofiltration membranes and modules

NF membranes have been on the market for the last fifteen years but have gained in popularity during the last eight years. They have been referred to in the past as 'loose', 'leaky' or low pressure RO membranes [Tsuru *et al.* (1991b)]. Eriksson (1998) and Cadotte *et al.* (1988) were among the first workers to use the term 'nanofiltration' to describe a membrane to signify the fact that the MWCO corresponded to a hypothetical pore of approximate diameter 1 nm.

The properties of NF membranes lie between those of porous UF membranes and homogeneous non-porous RO membranes. The flux characteristics through the membrane are as important as selectivity and so most NF membranes are either thin film or composite membranes to minimise hydraulic resistance. The operating pressures used in NF ($1 < \Delta P < 3$ MPa) are lower than in RO because of the more open pore structure which allows some permeation of solutes, reducing the osmotic potential gradient. UF membranes are often used as the porous support layer with the dense separating or 'active' layer (thickness approximately 1 – 2 nm), which is assumed to control all separation characteristics, normally being deposited on the support using either dip coating or interfacial polymerisation. Merry (2001) stated that polyamide is commonly used as the thin film layer in NF and RO membranes while Petersen (1993) stated that other polyelectrolytes such as sulphonated polyethersulphone are also used in the fabrication of NF membranes. The presence of ionisable groups in the active layer provides the membrane with an ionic charge. These charges can either be positive (formed from cationic groups such as NH_4^+) or negative (formed from anionic groups such as COOH, SO_3H and H_2PO_4), however, most NF membranes tend to be negatively charged.

Industrial NF modules can be configured in tubular, hollow-fibre or spiral-wound geometries. The latter of these configurations is often used because the high packing density (300 – 1000 $m^2\ m^{-3}$) allows greater filtration areas than tubular membranes

and higher fluxes than hollow-fibre membranes. The spiral-wound membrane configuration is prone to fouling and requires careful pre-treatment for feed streams that contain potential fouling materials. Flat sheet membranes are arranged around a central permeation collection tube in a Swiss roll arrangement (see Figure 1.2) with the membranes being separated by spacers and turbulence promoters.

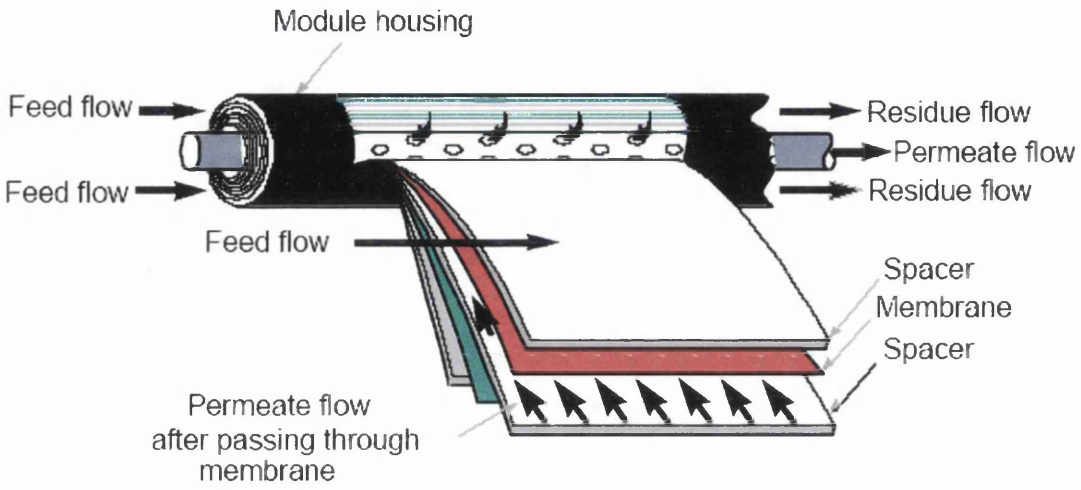

Figure 1.2: A spiral wound membrane module.

1.3 Separation mechanisms of NF membranes

Understanding the factors that affect the separation properties of NF membranes is very important for engineering applications. The development of good predictive models must take into account all of the following factors:

- The NF membrane itself – structural parameters such as pore radius and membrane thickness, electrical parameters such as charge density and other factors such as degree of fouling and polymer swelling.
- The feed solution – characteristics of ions or solutes, concentration, pH and fouling potential.
- The operating unit – capacity, dimensions, flow rate, mass and heat transfer parameters.
- The process environment – temperature and pressure.

The last two factors involve fundamental principles of chemical engineering and are elaborated in great detail in various chemical engineering text books [Coulson and Richardson (1996), Bird *et al.* (1960)]. The first two factors, which are specific to the NF membrane system, are interrelated and are very important in understanding the separation behaviour in NF systems.

The development of NF membranes was driven by the requirement to process the range of materials that pass freely through UF membranes while being fully retained by RO membranes. Conventional RO membranes reject almost all solutes while UF membranes are used for the concentration and separation of colloids, proteins and other relatively large macromolecules. As a result, the pore sizes in NF membranes were designed to make them very effective in the separation of uncharged and polar organic solutes with molecular weights in the range 100 – 1000 Da. The rejection of uncharged solutes is assumed to be through a purely steric mechanism and, as such, dependent only on the relative sizes of the solute and pore.

Unlike other pressure-driven liquid phase membrane processes (where either complete rejection or transmission is desired), NF offers the added ability of fractionation of molecules of similar size. The combination of small pore size and fixed surface charges make NF membranes especially suitable for the fractionation of small organic molecules and low molecular weight ions of different valences [Tsuru *et al.* (1991b), Rautenbach and Gröschl (1990) and Cadotte *et al.* (1988)]. Practically, rejection at NF membranes is low for salts with monovalent ions and uncharged solutes with molecular weights < 150 Da, while high for salts with divalent and multivalent ions and organics with molecular weights > 200 Da.

The assumption has been widely made that ions undergo equilibrium partitioning at the entrance and exit of NF pores. Initial descriptions were based solely on the Donnan exclusion principle [Donnan (1911)] where the efficiency of ion exclusion decreases as the valence of the counter-ion increases or increases as the valence of the co-ion increases. As an example, for a negatively charged membrane, rejection of salts with divalent anions such as Na_2SO_4 is always high compared to monovalent salt such as NaCl.

In addition to the charge effect, Tsuru *et al.* (1994) discussed the potential importance of the steric mechanism in the partitioning of ions. Bowen and Mukhtar (1996) included steric effects (important because of the fact that hydrated ions can have similar size to that of an NF pore) in their analysis of salt rejection. Bowen *et al.* (1997) and Bowen and Mohammad (1998) further investigated the relative importance of the size effect by studying the order of rejection for LiCl, NaCl and KCl form the CA30 NF membrane. The order of rejection was found to be LiCl > NaCl > KCl indicating that rejection was indeed a function of size (as well as charge density) in the narrow pores of NF membranes.

Yaroshchuk (1998) further discussed the rejection mechanisms of NF membranes and proposed two other non-steric mechanisms that could be of importance, namely dielectric exclusion and the hydration mechanism. The basis of the discussion was the extensive experimental studies of salt rejection at NF membranes [Peeters *et al.* (1998)] which identified three types of salt rejection characteristics:

a) membranes where $R(Na_2SO_4) > R(NaCl) > R(CaCl_2)$,
b) membranes where $R(CaCl_2) > R(NaCl) > R(Na_2SO_4)$, and
c) membranes where $R(Na_2SO_4) > R(CaCl_2) > R(NaCl)$.

where R signifies rejection. If Donnan mechanisms are dominant, rejection has to increase with increasing co-ion valence and decrease with increasing counter-ion valence. Therefore, membranes that exhibit separation behaviour of a) and b) represent negatively and positively charged membranes respectively.

Yaroshchuk (1998) suggested that the dielectric exclusion occurred due to interactions of ions with polarisation charges that are induced at the solvent-membrane surface. This effect was dependent on the square of the ion charge and so the rejection of divalent ions was greater than monovalent ions, irrespective of the sign of the charge. This effect would explain both the behaviour of the membranes in c) above (and the rejection of the magnesium salts in Table 1.2). However, the statement was made that the presence of fixed charges on the membrane surface would diminish the importance of this method of dielectric exclusion due to screening of the interactions

by the counter-ions that compensate for the fixed membrane charge (indicating an extremely important coupling of Donnan and dielectric mechanisms).

Bowen and Welfoot (2002) proposed that dielectric exclusion could be attributed to the solvation energy barrier formed when an ion passes from a solvent of one dielectric constant to a solvent of different dielectric constant. The argument was made that the unique confinement of an NF pore causes a spacial reorientation of the solvent molecules from that of the bulk solution. This realignment of the solvent into discreet yet diffuse layers causes a shift in the physical and electrical properties of the solvent and, as a consequence, the dielectric constant of the solvent changes. This behaviour was described through a Born model [Born (1920)] and again was dependent on the square of the ion valence.

The hydration mechanism was suggested to be caused by a loss in the dissolving ability of the solvent (which is related to the solvent dielectric properties) within the NF pore. Multivalent ions are again more highly rejected than monovalent ions and so this mechanism is also capable of describing the behaviour of the membranes in c).

Therefore, at present, the separation characteristics of ions at charged membranes are thought to be caused by the following three mechanisms:

- Steric effects – related to the relative size of the solute and pore.
- Electrostatic (Donnan) effects – can be either attractive or repulsive depending on the valence of the ion and the sign and magnitude of the fixed membrane charge.
- Dielectric interactions – where multivalent ions are rejected to a higher degree than monovalent ions due to interactions between the ions, membrane and solvent at the surface and inside the NF pores.

Recently, Schaep *et al.* (2001) reported experimental evidence to support the suggested three separation mechanisms. Four NF membranes were studied using a range of salts. The results are summarised in Table 1.2.

Table 1.2: Rejection characteristics of four NF membranes [Schaep *et al.* (2001)].

Salt	CA30	NTR7450	NF40	UTC20
	R	*R*	*R*	*R*
NaCl	0.08	0.41	0.41	0.47
$MgCl_2$	0.20	0.15	0.97	0.94
Na_2SO_4	0.29	0.88	0.98	0.98
$MgSO_4$	0.56	0.53	1.00	0.97

Clearly, the NTR7450 membrane exhibits classical Donnan exclusion behaviour for a negatively charged membrane. The CA30 membrane indicates dielectric exclusion characteristics as $MgSO_4$ is significantly more highly rejected than either Na_2SO_4 or $MgCl_2$. However, the other two membranes appear to show characteristics related to a combination of all three mechanisms.

Many studies of salt rejection at NF membranes have stated the strong influence of feed salt concentration (not a characteristic of RO membranes). Li *et al.* (2003), Garba *et al.* (2003) and Mohammad and Takriff (2003) have been among the latest to report the observation that rejection decreases as the concentration in the feed solution increases. As concentrations increase, the membrane fixed charge becomes increasingly neutralised (shielded) by the counter-ions in solution, resulting in lower rejection. Thus, the importance of the Donnan mechanism becomes progressively diminished with increasing feed concentration. However, some workers [Bowen and Welfoot (2002), Vezzani and Bandini (2003)] have reported rejection actually increasing with an increase in feed concentration for solutions of $MgCl_2$ and $CaCl_2$. This is in contrast to expectation and neither authors have explained their findings.

Recent studies have attempted to quantify the variation of salt rejection with pH through analysis of the variation of membrane charge caused by the dissociation of ionisable surface groups [Hall *et al.* (1997), Hagmeyer and Gimbel (1998), Ernst *et al.* (2000)]. Also, there are a number of small molecules (molecular weight < 500 Da) such as amino acids, humic acids, lactic acid and other simple organics that can be charged to different extents, or neutral, depending on the pH of the solution. In addition, specific ion-membrane interactions could cause a change in membrane electrical characteristics which would affect the rejection behaviour [Childress and Elimelech (1996), Aitkuliev *et al.* (1984)] and the fouling characteristics [Nystrom *et*

al. (1995, 1996)]. Thus the feed conditions can be modified to tailor the charge properties of the membrane and the molecules for a particular separation.

Bhattacharya *et al.* (1989) studied the rejection of phenol using the negatively charged NF40 membrane. Phenol has a $pK_a = 9.9$, which means that at pH 9.9 50 % of the phenol molecules will be in the phenolate anion form. At pH values < 8, phenol rejections were < 5 % but increased significantly to 50 % at pH 10. At pH 8, phenol was almost entirely neutral and easily passed through the membrane due to the molecules small size. Phenolate anion formation increases at higher pH values and rejection increases due to the Donnan effect. Similar observations have been obtained for propionic acid and lactic acid. More recently, Tsuru *et al.* (1994) and Garem *et al.* (1997) discussed the dependence of the rejection behaviour of amino acids at NF membranes on pH through the isoelectric point of the amino acid.

The rejection of mixtures of ions displays similar behaviour to single electrolytes. Studies with negatively charged membranes have indicated that the presence of multivalent electrolytes such as SO_4^{2-} [Hagmeyer and Gimbel (1998)] or a negatively charged polyelectrolyte [Gilron *et al.* (2001)] causes the rejection of NaCl to significantly decrease and, under some conditions, become negative. Negative rejection signifies that the concentration of solute is higher in the permeate than in the feed solution. This phenomenon results directly from the requirement of electroneutrality in the permeate solution. The Donnan effect predicts that multivalent co-ions will be strongly rejected from the membrane while counter-ions are preferentially transmitted through the membrane. For single salts, both co-ion and counter-ion must transmit together to maintain electroneutrality and, as a direct result, the rejection is controlled by the co-ion exclusion. For mixtures, monovalent co-ions are more readily transported with the counter-ion than multivalent co-ions and so the rejection of the monovalent ions (NaCl) is controlled by the preferential transport of the counter-ion and negative rejection is possible. The magnitude of the negative rejection is reduced significantly (and in many cases completely) as pressure increases because of the effect of convective transport. This observation has important implications for the operation of desalting applications such as dye-salt diafiltration because a more efficient separation will be obtained at pressure only slightly higher than the osmotic pressure difference and not the normal pressures used in NF.

Experimental evaluation and theoretical prediction of negative salt rejection remains an area of active interest for this reason [Rios *et al.* (1996), Hagmeyer and Gimbel (1999), Dey *et al.* (2000), Gilron *et al.* (2001)].

1.4 Industrial applications of nanofiltration

NF membranes have found applications in a wide range of industries over the past fifteen years. Currently 65 % of the NF market accounts for water treatment, 25 % for the food and dairy industry and less than 10 % for the chemical industry [Bessarabov and Twardowski (2002)]. Table 1.3 lists some of the most recently reported applications of NF membranes [Mukhtar (1995) and Mohammad (1998) have reviewed some of the more established applications].

Table 1.3: Recently reported applications of nanofiltration.

Application	Reference
Water Treatment	
Beverage industry effluent	Chmiel *et al.* (2002)
Fruit juice industry effluent	Noronha *et al.* (2002)
Colour removal from effluent	Frank *et al.* (2002)
Evolution in seawater desalination	Bruggen and Vandecasteele (2002)
Tanning industry effluent	Shaalan *et al.* (2001)
Desalination of process cooling water	Radier *et al.* (2001)
Removal of pesticides	Boussahel *et al.* (2000)
Arsenic removal	Vrijenhoek and Waypa (2000)
Treatment of deep well water	Pervov *et al.* (2000)
Removal of hexavalent chromium	Hafiane *et al.* (2000)
Electroplating effluent	Ahn *et al.* (1999)
Dissolved uranium removal	Raff and Wilken (1999)
Food and Biotechnology	
Dairy by-product recovery	Nguyen *et al.* (2003)
Pharmaceutical recovery	Zhu *et al.* (2003)
Marine flavours from cooking water	Vandanjon et al. (2002)

Purification of oligosaccharides	Goulas *et al.* (2002)
Biopharmaceutical production	Christy and Vermant (2002)
Dairy cleaning-in-place	Dresch *et al.* (2001)
Separation of amino acids	Grib *et al.* (2000)
Fractionation of whey proteins	Pouliot *et al.* (1999)
Bean curd wastewater	Chai *et al.* (1999)
Edible oil processing	Ebert and Cuperus (1999)
Chemical Industry	
Separation of organometallic catalysts	Scarpello *et al.* (2002)
Benzene/cyclohexane separation	Villaluenga and Mohammadi (2000)

1.5 Objectives of the present work

For traditional separation processes, such as distillation, there are reliable process design methodologies for scale up and optimisation. These methods allow the prediction of performance and operation of a distillation column from a detailed knowledge of the physiochemical properties of the components to be separated. Similarly, the design and operation of membrane separation processes in industry also requires quantitative methods for the prediction of separation performance, especially filtration rates and rejection. Predictive models reduce development risk and time, thus promoting the use of membrane technology in process industries such as pharmaceutical manufacturing processes.

Methods now exist for prediction in the case of simple aqueous systems such as small molecule separations and simple salt separations at the laboratory scale. At full industrial scale, model calculations are already valuable in predicting the separation performance of uncharged solutes [Bowen and Welfoot (2002b)]. However, there is currently insufficient knowledge of NF separations of concentrated aqueous electrolytes and/or organic solvents [Bessarabov and Twardowski (2002)].

A collaborative research project funded by GlaxoSmithKline (GSK) Research and Development Ltd. (Stevenage, Herts., U.K.) and supported by GSK Global Manufacturing and Supply (Ulverston, Cumbria, U.K.) has provided an opportunity to

evaluate the scientific and engineering challenges of NF separations and to provide a basis for the selection of scale-up methods.

The present work is intended to significantly contribute to the understanding of NF membranes and processes through application of existing NF theory to real industrial separations. Such a development should encompass a study of existing NF theory, a practical evaluation of the mechanisms for dielectric exclusion, and finally, applying the existing theory to relevant industrial separation processes. These overall objectives will be achieved specifically by:

a) A detailed description of the existing NF theory for neutral and charged solutes derived as the original Donnan Steric Partitioning Model (DSPM) [Bowen *et al.* (1997)] which predicts solute rejection as a function of volumetric flux. A description and explanation of how Bowen and Welfoot (2002) updated the original theory to produce a more rigorous model based on rejection in terms of effective pressure and included dielectric effects, and finally, how simplification of the model is possible to produce a linear model for solute transport.
b) A theoretical comparison will be made over a range of NF conditions between the updated DSPM model (UDSPM) and the linearised UDSPM model to evaluate model deviations as a result of the simplifying assumptions.
c) A theoretical and experimental comparison between the different mechanisms of dielectric exclusion will evaluate which mechanism, if any, is predominant and should be included in the model descriptions.
d) Both the full UDSPM and linearised UDSPM models will then be used to characterise a separation of real industrial importance. This will allow us to evaluate if the current NF theoretical models are indeed capable of fully describing real processes as opposed to simple laboratory experiments with ideal solutions.
e) Finally, the models will be used to demonstrate the rationale for modelling the performance of NF separations as a tool in the design, optimisation and scale-up of a real industrial process. Outlining the relevant process options, operating regions, design considerations and improvements possible by incorporation of NF technology.

2 Materials, Methods and Supporting Experiments

This chapter details the materials and methods used in the experimental work. Firstly, the laboratory scale dead-end filtration cell employed in all filtration experiments will be described in detail. Then the materials used for experimental work and sample analysis will be provided along with the sample analysis methods. Finally, supporting experiments will be presented to investigate the mass transfer characteristics of the dead-end filtration cell and the experimentation required to determine the diffusion coefficients of some of the molecules used in this study.

2.1 Laboratory scale rig

A stirred Amicon™ UF cell model 8400 supplied by Millipore (U.K.) Ltd. (Watford, Herts., U.K.) was used for the experimentation in this study and is illustrated in Figure 2.1. The cell has a capacity of 4 $x10^{-4}$ m^3 and supports a membrane disc of 7.8 $x10^{-2}$ m diameter. The effective area of the of the membrane is 41.8 $x10^{-4}$ m^2 and the maximum operating pressure of the cell is 517 kPa (~ 5 bar). The cell consists of a cylindrical body, a membrane support, small channels to allow permeate to flow out, a quick fit base (which holds the membrane support and body), a magnetic stirrer assembly which is mounted inside the body, a top cap containing a pressure relief valve and an inlet to the body and a retaining stand which supports the entire cell when under pressure. The magnetic stirrer has a diameter of 0.031 m. The design of the body allows the positioning of the stirrer as close to the membrane surface as possible. The cap and membrane support were sealed using an O-ring gasket fabricated from silicone rubber.

Two modifications were made to the cell. Firstly, an external water jacket was fitted around the body of the cell to enable isothermal operation during experiments. Secondly, a 0.5 μm grade porous steel plate supplied by Mott Corp. (Farmington, CT, U.S.A) was placed between the membrane and the support plate to avoid any compaction of the membrane on the top of the support plate channels by the exertion of pressure.

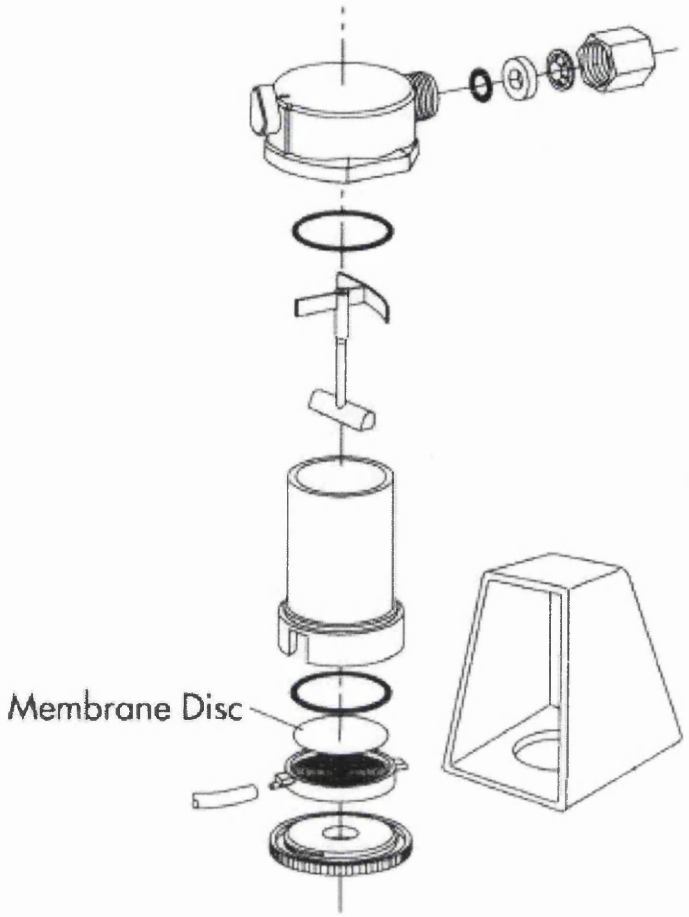

Figure 2.1: A schematic diagram of the Amicon™ 8400 stirred ultrafiltration cell.

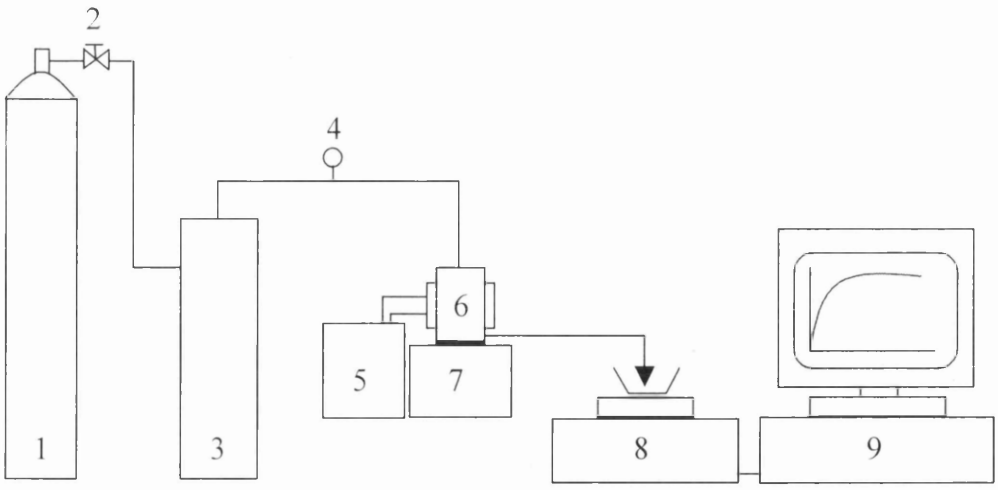

Figure 2.2: A schematic diagram of the dead-end filtration equipment. (1) nitrogen cylinder, (2) valve, (3) 1.5 L reservoir, (4) pressure sensor, (5) water bath, (6) Amicon cell, (7) magnetic stirrer, (8) electronic balance, (9) PC.

When operating the cell, the membrane was placed on the porous steel plate and then slotted into the cell support plate. The O-ring gasket was carefully placed on the membrane peripheral surface and the cell support plate was inserted into the body of the cell and the quick fit base screwed on tight, completing the base assembly of the cell. The magnetic stirrer was then placed inside the body of the cell and the experimental solution poured in. Next, the top cap was secured to the body and the cell was placed inside the retaining stand and set onto a magnetic stirring table. The stirring speed was set at 300 rev min^{-1} for all experiments unless otherwise stated. The pressure relief valve was then set to the vertical closed position and the cell was pressurised using compressed nitrogen gas from a free standing cylinder. The applied pressure to the cell was measured using a digital pressure meter supplied by PSI-Tronix (Tulare, CF, U.S.A.). Permeate flux was measured by collection of the permeate over time and was recorded by mass via an electronic balance connected to a personal computer. The cell was maintained at 25 ± 0.5 °C by connection of the water jacket to an external water bath. On completion of the experiment, the nitrogen gas supply was cut and the pressure released from the system by opening the pressure relief valve. The top cap was then removed and the contents of the cell emptied. At this point, either fresh solution was poured into the cell and a new experiment started or the cell was dismantled and cleaned. The experimental set-up of the dead end filtration is illustrated in Figure 2.2.

In order to use the experimental rig for diafiltration experiments, the above procedure was again employed with pure water added to the 1.5 L reservoir. The application of pressure from the nitrogen gas cylinder would then supply pressure to the water reservoir and force pressurised water to the top of the Amicon cell. As the system is closed, pressurised water can only enter the cell at the same rate as membrane flux, providing the constant volume required.

Prior to experimental runs, the cell was purged at 0.5 MPa for 1 hour with ultra pure water obtained from a RiOs™ water purification system supplied by Millipore (U.K.) Ltd. (Watford, Herts., U.K.). This was carried out in order to avoid any compression effects of the membranes and ensure that operation was always under constant

conditions. The cell was also purged with pure water at the end of experimental runs to clean the membrane.

The dead-volume beneath the membrane support plate and in the collection tube were calculated to be approximately 6 mL. Thus, the membrane was purged for 10 mL before any samples were taken to be sure of clearing the dead-volume and obtaining a representative sample.

2.2 Materials

All reagents used in this study were analytical grade. Glucose and sodium chloride were obtained in high purity form from Fisher Scientific U.K. Ltd. (Loughborough, Liecs., U.K.). The reagents used in the HPLC assays were supplied by Sigma-Aldrich Ltd. (Poole, Dorset, U.K.). Polyethylene glycol (PEG) in all forms were also obtained from Sigma-Aldrich Ltd. (Poole, Dorset, U.K.). GSK Global Manufacturing and Supply (Ulverston, Cumbria, U.K.) kindly supplied *N*-acetyl-D-mannosamine (ManNAc), *N*-acetyl-D-neuraminic acid (Neu5Ac), sodium cefuroxime and sodium pyruvate in crystal form of purity greater than 95 % and also supplied sodium lactate in liquid form of 60 wt % solution (equivalent to 7000 mol m^{-3}). No further purification was carried out in order to simulate real process streams.

Three commercially available NF membranes were used in this study, all in flat sheet format. Nanomax™-50, a thin film polyamide membrane, was obtained from Millipore (U.K.) Ltd. (Watford, Herts., U.K.). SelRO® MPF-44, a hydrophilic solvent stable membrane, was obtained from Koch Membrane Systems Inc. (Stafford, U.K.). Desal-5-DK, a thin film polyamide membrane, was kindly supplied by Osmonics (France).

2.3 Sample analysis

Sample analysis involved several different techniques. Glucose concentrations were analysed by either the GOD-Perid assay kit supplied by Roche Diagnostics GmbH (Mannheim, Germany) or the GAGO-20 assay kit supplied by Sigma-Aldrich Ltd.

(Poole, Dorset, U.K.) and a spectrophotometer [Philips Scientific (Cambridge, U.K.) model No. PU 8625 UV/Vis]. Single salt concentrations of sodium chloride, sodium pyruvate, sodium lactate, Neu5Ac were calculated from conductivity measurements at 25 °C, using a conductivity meter supplied by Thermo Russell (Auchtermuchty, Fife, U.K.) model No. RL105 and probe. Lactate ion concentrations were analysed using the lactate reagent 735-10 assay kit supplied by Trinity Biotech U.K. Sales Ltd. (Abingdon, Oxford, U.K.). Particle size analysis was measured using the High Performance Particle Sizer (HPPS) with NIBS™ technology from Malvern Instruments (Malvern, Worces., U.K.). HPLC analysis was carried out using a Waters™ HPLC system consisting of the following components: Waters 600E system controller, Waters temperature controller module, Waters 600 multi-solvent delivery system, Waters 990 photodiode array detector and software, Waters 5200 printer plotter.

HPLC Assay 1: Sodium cefuroxime was determined using high performance liquid chromatography. 1 μL sample of the reaction mixture was analysed through a Spherisorb® hexyl, 5 μm, column (150 x 4.6 mm, Alltech Associates Applied Science Ltd., Carnforth, Lancs., U.K.): assay conditions 30 °C, mobile phase, sodium acetate 0.37 g, glacial acetic acid 5.16 g, water 901 g and acetonitrile 78 g; flow rate 2.0 mL min^{-1}; UV detection at 273 nm.

HPLC Assay 2: ManNAc, pyruvate and Neu5Ac concentrations were determined using ion-moderated partition chromatography [Kragl *et al.* (1991)]. 1 μL sample of the reaction mixture was analysed through a Spherisorb® NH_2, 5 μm, column (150 x 4.6 mm, Alltech Associates Applied Science Ltd., Carnforth, Lancs., U.K.): assay conditions 35°C, mobile phase, isocratic 0.01M ammonium dihydrogen orthophosphate: acetonitrile 20:80 by volume, adjusted to pH 3.0 with phosphoric acid; flow rate 1.5 mL min^{-1}; UV detection at 210 nm.

Details of the individual analysis procedures are found in Appendix A3.

2.4 Determination of the diffusion coefficients and hydrodynamic radii

In order to use the theoretical descriptions of NF, some fundamental physical properties or characteristics of the solutes in question must be known or evaluated. Namely, the diffusion coefficient at infinite dilution and the hydrodynamic Stokes radius. For many simple solutes and ions this information is readily available in the literature. However, for the more complex organic ions used in this study, this information is not freely available and these properties must be obtained by either experimental procedures or empirical relationships.

2.4.1 Theory for conductivity of strong electrolytes

Conductivity measurement can provide an accurate determination of the diffusion coefficient for a given ionic species in aqueous solution [Cussler (1995)]. This section briefly describes the theory and results of the measurements of conductivity to determine the diffusion coefficient values for the lactate ion, pyruvate ion and cefuroxime ion.

For strong electrolytes, the electrical conductivity which is the reciprocal of the electrical resistance is measured easily using a conductivity meter. The resistance is inversely proportional to the current flowing between the electrodes, which is a measure of the ionic mobility.

$$(R)^{-1} = K_{cell} i = K_{cell}(z_1 j_1 + z_2 j_2) \qquad (2.1)$$

The proportionality constant K_{cell} in Eq. 2.1 is a function of the electrode area, the electrode separation and the cell shape. The ion flux is proportional to the ion concentration

$$j_i = c_i v_i \qquad (2.2)$$

The ion velocity is proportional to the electrical force acting on the ion

$$v_i = -u_i z_i F \Delta\psi \tag{2.3}$$

Therefore, the resistance can be expressed in terms of the ion mobilities

$$(R)^{-1} = K_{cell}\left(z_1^2 c_1 u_1 + z_2^2 c_2 u_2\right) F \Delta\psi \tag{2.4}$$

The individual ion concentrations in the solution are related to the total ion concentration, c_T, for a binary salt as

$$c_T = \frac{c_1}{|z_1|} = \frac{c_2}{|z_2|} \tag{2.5}$$

The above equations can be combined to define the equivalent conductance, Λ, which is the most convenient measure of conductivity

$$\Lambda = \left(z_1 u_1 + z_2 u_2\right) F = \{(R)[K_{cell}\Delta\psi] \mid z_1 z_2 \mid c_T\}^{-1} \tag{2.6}$$

Where u is the ionic mobility of the ion in question and is related to the diffusion coefficient through the Einstein relationship

$$D_i = \frac{u_i RT}{z_i F} \tag{2.7}$$

Substitution of the Einstein relationship into the equivalent conductance for a binary salt gives

$$D_1 = \frac{1}{z_1^2}\left(\frac{\Lambda RT}{F^2} - z_2^2 D_2\right) \tag{2.8}$$

If we now consider the limiting conductance, i.e. the conductance at infinite dilution, then we can obtain the diffusion coefficient at infinite dilution

$$D_{1,\infty} = \frac{1}{z_1^2}\left(\frac{\Lambda_o RT}{F^2} - z_2^2 D_{2,\infty}\right) \qquad (2.9)$$

The equivalent conductance is known to vary with concentration and is expressed with equations of the form of that of Crow [Crow (1994)].

$$\Lambda = \Lambda_o - (B_1\Lambda_o + B_2)\sqrt{c_T} + B_3 c_T(1 - B_1\sqrt{c_T}) \qquad (2.10)$$

Where all the B_i's are constants.

The limiting conductance, Λ_o, is a property of the ions and is not well understood theoretically. This limiting value can be used to determine the infinite dilution diffusion coefficient of the ions. The constant of the second term in Eq. (2.10) is a function only of the charges on the ions and is thus characteristic of the electrostatic interactions between the ions. The constants in subsequent terms include other interactions such as ion-solute interactions and the ion associations more commonly encountered with weak electrolytes.

In this study, the conductance of the sodium lactate, sodium pyruvate and sodium cefuroxime solutions was measured at different concentrations and the data fitted using Eq. (2.10). As the infinite dilution diffusion coefficient of Na^+ is known, the diffusion coefficient of the other species is easily calculated using Eq. (2.9). The hydrodynamic radius (effective spherical radius) of the ionic species was then calculated using the Stokes-Einstein relation

$$a_i = \frac{k_B T}{6\pi\mu D_{i,\infty}} \qquad (2.11)$$

2.4.2 Experimental method and results

Different samples of the three solutions were prepared to give concentrations ranging from 1.5 to 250 mol m^{-3}. Each sample was then put into a water bath at 25 °C and allowed to equilibrate and then the conductivity measured. The conductivity meter

and probe have been described previously in section 2.3. The results of the experiments are illustrated in Figure 2.3 in the form of equivalent conductance versus square root of the molar concentrations as required for the Crow equation.

The experimental findings were fitted using Eq. (2.10) and good agreement was observed. The limiting equivalent conductance was found to be 89.8, 89.5 and 70.3 $x10^{-4}$ m^2 S mol^{-1} for sodium lactate, sodium pyruvate and sodium cefuroxime respectively. Based on the literature value for $D_{Na+,\infty}$, the diffusion coefficient for the three ionic species was evaluated as 1.06, 1.05 and 0.54 $x10^{-9}$ m^2 s^{-1} respectively. This gives corresponding hydrodynamic radii of 0.231, 0.233 and 0.453 nm. The hydrodynamic radius for cefuroxime was confirmed by particle size analysis using the Malvern HPPS and was found to be 0.44 ± 0.01 nm, agreeable with the value obtained from conductivity measurements. Unfortunately the lactate and pyruvate ions are below the detectable size range for this device so no meaningful value could be obtained for these species.

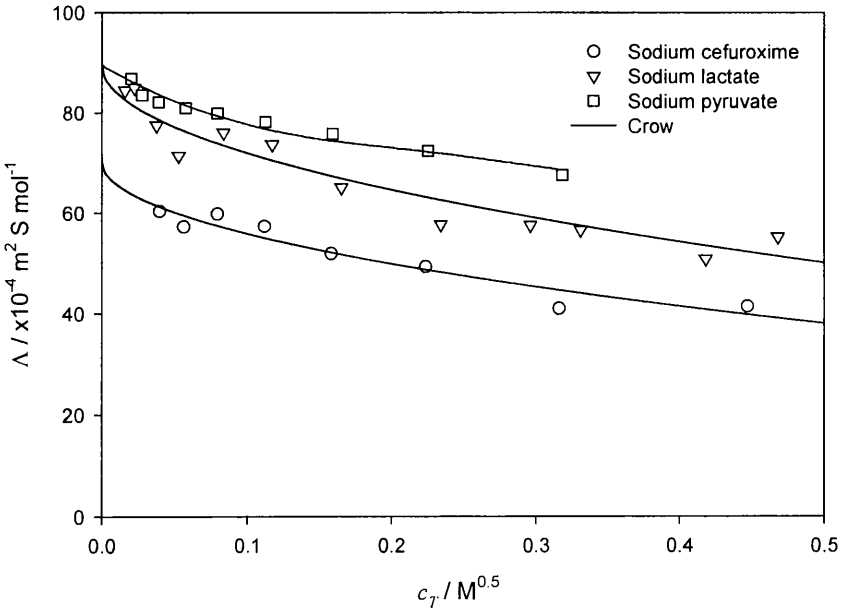

Figure 2.3: Equivalent conductances of sodium lactate, sodium pyruvate and sodium cefuroxime solutions as a function of concentration.

2.4.3 Determination of diffusion coefficients via correlations

Unfortunately the conductivity method of evaluating the diffusion coefficient is not valid for neutral solutes and difficult to determine for weak electrolytes due to the sharp rise in ionic conductance at low concentration (for weak electrolytes only). For this reason, an alternative method is required for the evaluation of the diffusion coefficients of ManNAc and Neu5Ac.

Wilke and Chang (1955) proposed an equation to calculate the diffusivity of a molecular species in dilute solution. The method relies on a general correlation derived from the Stokes-Einstein equation for spherical particles and is represented as

$$D = 7.4\times10^{-8}\frac{(xM)^{0.5}T}{\mu\overline{V}^{0.6}} \qquad (2.12)$$

where D is diffusivity ($cm^2\ s^{-1}$), x is an association parameter, M is molecular weight, T is absolute temperature (K), μ is viscosity (cP) and $\overline{V}$ is molar volume. The association parameter x is of great importance. The method itself was developed for unassociated solvents, but the x term allows the inclusion of polar solvents. Association values are provided for water, methyl alcohol, ethyl alcohol, benzene, ether and heptane. Contained within the method is the partial molar volume ($\overline{V}$). Molar volumes are values at the normal boiling point estimated for complex molecules by the atomic contributions of Lebas [Lebas (1915)]. The method claims sufficient precision for most engineering purposes, i.e. 10 % average error. However, the correlation relies upon only a few data points taken from the International Critical Tables (1926). Hayduk and Laudie (1974) tested the available correlations for diffusion coefficients in order to determine the extent to which the correlations were still applicable, only data reported from 1950 onwards was used. The new equation derived for aqueous systems was

$$D_{12} = \frac{13.26\times10^{-5}}{\mu_2^{1.4}\overline{V}_1^{0.589}} \qquad (2.13)$$

The conclusion was made that true molar volumes should be used where available. However, the Lebas molar volumes yield only slightly less accurate results with the absolute error being similar for both cases.

The diffusion coefficients calculated for ManNAc and Neu5Ac were 6.41 and 5.06 $x10^{-10}$ m^2 s^{-1} respectively. The diffusion coefficient calculated for glucose was 7.74 $x10^{-6}$ m^2 s^{-1}. This value is an over estimation by 8 % from the literature diffusion coefficient for glucose. For this reason, the values obtained for ManNAc and Neu5Ac were scaled by the ratio of the calculated to literature value for the diffusion coefficient of glucose. The new values obtained were 6.05 and 4.99 $x10^{-10}$ m^2 s^{-1} respectively. This gives corresponding hydrodynamic radii of 0.404 and 0.490 nm. Table 2.1 below gives the physical properties of all solutes used in this study.

Table 2.1: Physical properties of solutes used in this study.

Species	Valence	MW Da	$D_{eff,\infty}$ $x10^9$ m^2 s^{-1}	a_i nm	Source
Glucose	0	180	0.690	0.365	Welfoot (2001)
ManNAc	0	209	0.605	0.404	Prediction
Neu5Ac	0	309	0.499	0.490	Prediction
Cefuroxime	-1	408	0.540	0.453	Experiment
Cl	-1	35.5	2.030	0.121	Cussler (1995)
H	+1	1	9.311	0.026	Cussler (1995)
Lactate	-1	89	1.060	0.231	Experiment
Mg	+2	24.3	0.720	0.350	Cussler (1995)
Na	+1	23	1.333	0.184	Cussler (1995)
Neu5Ac	-1	308	0.499	0.490	Prediction
Pyruvate	-1	88	1.050	0.233	Experiment
SO_4	-2	96	1.060	0.230	Cussler (1995)

2.5 Description of mass transfer

An inherent feature of membrane operation is concentration polarisation at the membrane surface due to local increases in the concentration of rejected solutes. The induced diffusive flow back into the feed solution will eventually attain a steady state. If flow conditions are such that a boundary layer will be established at the membrane surface, the concentration gradient will be retained within this layer [Mulder (1996)]. The extent of concentration polarisation depends on several factors [Dresner and Johnson (1980)]:

- Competition between solute convection towards the membrane and diffusion away from the membrane,
- Fraction of solute rejected by the membrane,
- Flow regime at the membrane surface (whether laminar or turbulent),
- Stirrer geometry.

The rejection characteristics of a membrane are typically defined by observed rejection:

$$R_{obs} = 1 - \frac{C_p}{C_f} \qquad (2.14)$$

The quantity represents an experimental measurement of the degree of rejection of a solute by a membrane. However, in the presence of concentration polarisation, this definition of rejection is not accurate because the solute concentration at the membrane surface C_w is higher than the feed concentration, C_f. The real rejection of the solute, R, which is always higher than observed rejection, is defined as follows:

$$R = 1 - \frac{C_p}{C_w} \qquad (2.15)$$

Figure 2.4 shows a schematic diagram of the interface between the bulk feed solution and the membrane surface for a single electrolyte.

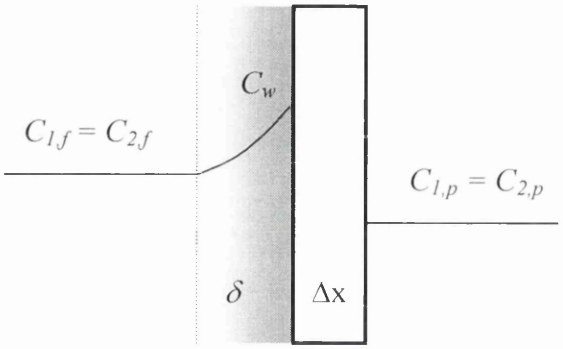

Figure 2.4: Concentration profiles within the polarised boundary layer.

However, the value of C_w is not directly measurable and so must be calculated indirectly with a suitable model for concentration polarisation. Concentration polarisation will be assumed to occur within a boundary film layer of thickness, δ. For a single salt such as NaCl, the cation and anion move together due to the requirement of electroneutrality and so there is no electromigrative transport of ions. Transport within the film layer is, in this case, due to convection and diffusion only and so a mass balance yields

$$j_+ = j_- = -D_{eff,\infty} \frac{dC_\pm}{dx} + C_\pm J_v \qquad (2.16)$$

Where J_v is volumetric flux though the membrane and $D_{eff,\infty}$ is the effective diffusivity of the salt [Krishna and Wesselingh (1997)], defined as

$$D_{eff,\infty} = \frac{D_+ D_- (z_+ - z_-)}{z_+ D_+ - z_- D_-} \qquad (2.17)$$

Eq. (2.16) is solved using the relationship $j_+ = C_p J_v$ and the boundary conditions: $C_\pm(0) = C_w$ and $C_\pm(-\delta) = C_f$ to allow C_w to be correlated to measurable parameters

$$\frac{J_v}{k} = \ln\left(\frac{C_w - C_p}{C_f - C_p}\right) \qquad (2.18)$$

Where k is the mass transfer coefficient in the polarised boundary layer, defined as:

$$k = \frac{D_{eff,\infty}}{\delta} \tag{2.19}$$

This result is equally applicable to a system of uncharged solutes but the correction for a multicomponent electrolyte system requires the solution of the extended Nernst-Planck equation [Bowen and Mohammad (1998)]. Many mass transfer correlations have been derived to predict k for simple membrane modules such as tubular and hollow-fibre membranes [Levesque (1928), Rautenbach and Albrecht (1994)] and dead-end stirred cells [Opong and Zydney (1991)]. These correlations relate dimensionless Sherwood number (Sh) to Reynolds number (Re) and Schmidt number (Sc)

$$N_{Sh} = \frac{kr}{D_{eff,\infty}} = \varphi(N_{\mathrm{Re}})^n (N_{Sc})^{0.33} \tag{2.20}$$

where

$$N_{\mathrm{Re}} = \frac{\omega r^2}{\upsilon}, \quad N_{Sc} = \frac{u}{D_{eff,\infty}} \tag{2.21}$$

The most suitable value for the empirical constant n was found to be 0.567 [Smith *et al.* (1968), Malone and Anderson (1977)]. The value for φ will be taken as 0.23 as suggested by Opong and Zydney (1991).

Bowen *et al.* (1997) used the infinite rejection method proposed by Nakao and Kimura (1981) to evaluate the mass transfer coefficient within the Amicon cell as

$$k = 0.23\left(\frac{r^2}{\upsilon}\right)^{0.567}\left(\frac{\upsilon}{D_{eff,\infty}}\right)^{0.33}\frac{D_{eff,\infty}}{r}\omega^{0.567} \tag{2.22}$$

An experimental method for the evaluation of k is also available. Linearisation of Eq. (2.18) gives

$$\ln\left(\frac{1-R_{obs}}{R_{obs}}\right) = \ln\left(\frac{1-R}{R}\right) + \frac{J_v}{k} \qquad (2.23)$$

From Eq. (2.22), the mass transfer coefficient can be expressed as

$$k = k'\omega^{0.567} \qquad (2.24)$$

Hence, the real rejection of a membrane is determined from the experimentally observed rejection by extrapolation to infinite ω on plotting $\ln[(1 - R_{obs})/R_{obs}]$ against $J_v/\omega^{0.567}$. The slope of the best fit line will be equal to $1/k'$.

2.5.1 Experimental method and results

Concentration polarisation effects within the Amicon™ 8400 stirred cell were studied using 1.67 mol m^{-3} glucose solution and the Nanomax™-50 membrane. Figure 2.5 represents the experimental findings. The value calculated for k' from the plot and using Eq. (2.24) was 1.17 x10^{-5} m $s^{-0.433}$. This value is significantly higher than that obtained from Eq. (2.22) of 2.85 x10^{-6} m $s^{-0.433}$. This indicates that the mass transfer within the Amicon™ 8400 stirred cell is much better than the theory would predict and concentration polarisation is low.

The maximum practical stirrer speed for the Amicon cell was 300 rev min^{-1}, above this speed the stirrer begins to rotate in a non-uniform manner and the motion is no longer smooth. The observed rejection at this stirrer speed was 0.543. The value obtained for infinite stirrer speed using Eq. (2.23) was 0.564. This value is only 3.7 % different from that at 300 rev min^{-1}, also indicating that concentration polarisation effects are small. For this reason, the effects of concentration polarisation using the Amicon™ 8400 stirred cell and the Nanomax™-50 membrane were deemed small and neglected from further calculations. The small effect of concentration polarisation was attributed to the low flux of the membrane, 4.6 m^3 m^{-2} s^{-1} for pure water at 0.5 MPa applied pressure, and the high mass transfer coefficient in the Amicon 8400 stirred cell. This result is equally applicable to both the SelRO® MPF-44 and the

Desal-5-DK membrane as the flux of these membranes is also very low and, as a result, no significant mass transfer will occur.

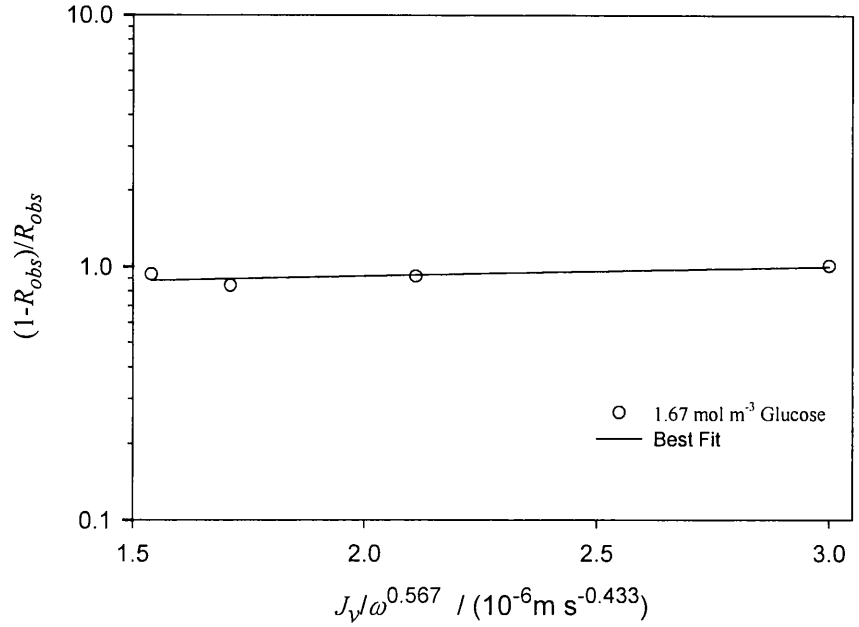

Figure 2.5: Determination of concentration polarisation effects in the Amicon™ 8400 stirred cell.

2.6 Conclusions

In this chapter, the materials and equipment used in this study were described in detail. In addition, experimental results and analysis for the characterisation of the solutes used was explained and the effects of concentration polarisation determined.

Solute diffusivity was determined from the electrical conductance in solution for strong electrolytes and from empirical relationships for the other species. The values obtained were then used to evaluate the solute hydrodynamic radius using the Stokes-Einstein equation. The calculated radii were consistent with that expected for materials in the molecular weight range studied and the hydrodynamic radius of sodium cefuroxime was confirmed by high performance particle sizing using the Malvern HPPS system.

The study of mass transfer characteristics within the Amicon™ 8400 stirred cell has demonstrated that the effects of concentration polarisation for NF membranes studied are small and the observed rejection will be very close to the real rejection for a stirring speed of 300 rev min^{-1}. The small effect of concentration polarisation was attributed to the low flux of NF membranes and to the high mass transfer coefficient (determined experimentally) within the cell.

3 Review of Nanofiltration Theory

The prediction of NF performance has been an active area of research over the last decade. During that time, the emphasis has shifted from empirical black box models based on irreversible thermodynamics to models based on the extended Nernst-Planck equation due to the ability of the latter to provide information related to actual membrane properties. The present chapter will first describe recent developments in physical measurement of NF membrane properties including an assessment of their limitations. Models for uncharged solute and electrolyte rejection based on the extended Nernst-Planck equation will be provided and the merits of each will be discussed in turn. The purpose of these models is to describe real physical membrane properties in order to better match measurable quantities to adjustable model parameters.

3.1 Measurement of membrane properties

The major limitation of NF modelling is the requirement for characteristic model parameters, such as pore radius and membrane charge, that are not readily measured at the near atomic NF length scale. Similarly, the development of rigorous physical descriptions (such as Molecular Dynamics simulations) has been limited by the lack of a detailed knowledge of the physical structure and electrical properties of real NF membranes. As a result, developments in modelling have moved in parallel with improvements in the measurement techniques employed in the characterisation of NF membranes, since only then will it be possible to check the appropriateness of model parameters. Therefore, the current trend in NF modelling is to predict NF separations using experimentally measured values of model parameters.

Until recently, one of the fundamental unanswered questions in the study of NF membranes has been whether or not real NF membranes have distinct pores. The lack of reliable measurement techniques for the investigation of pores around 1 nm in size has undoubtedly hindered the early development of NF models because the assumption of either a porous or homogeneous membrane structure could not easily

be validated [Bowen and Mukhtar (1996)]. A significant development in this respect has been the use of atomic force microscopy (AFM).

Since invention [Binnig *et al.* (1986)], AFM has been increasingly used to provide ultra-high resolution images of industrial membranes. Bowen *et al.* (1997) reported the use of AFM to image the PES5 NF membrane where the existence of distinct pores was apparent. However, no confirmation with another method was made to check the reliability of the determined pore size and so it was quite possible, since the AFM tip had a diameter of around 10 nm, that the image obtained using AFM underestimated the actual pore size due to convolution between the tip and the pore. These measurements enabled Bowen to propose a predictive NF model based on a porous structure. Subsequently, direct measurement of pore size distributions in NF membranes by Combe *et al.* (1997), using a nitrogen adsorption-desorption technique, and Bowen and Doneva (2000), using AFM, have provided further physical evidence for this porous structure assumption. Recently, Bowen and Doneva (2000b) compared the mean pore radii obtained from AFM measurements of NF membranes to those estimated from molecular weight cut-off and found reasonable agreement for pores of approximately 1 nm in diameter.

The electrical properties of NF membranes also play an important role in electrolyte rejection. Two main mechanisms for charge development on NF membranes are usually assumed. The variation of membrane charge with pH is due to dissociation of ionisable groups at the membrane surface as follows [Hall *et al.* (1997)]:

$$RH \Leftrightarrow R^- + H^+ \qquad RH + H^+ \Leftrightarrow RH_2^+$$

These reactions indicate that membrane charge can be either positive or negative depending on the operating pH. However, the increase in membrane charge with increasing electrolyte concentration is attributed to the specific adsorption of ions [Xu *et al.* (1997)], which in the limiting case may be the sole charging mechanism [Bowen *et al.* (1997)].

In recent years, many workers have attempted to investigate the development of membrane charge due to both of these mechanisms. The direct measurement of the volumetric membrane charge density used in existing NF models is not feasible and so this property has been derived from other electrical properties of the membrane.

Combe *et al.* (1997) measured the variation of surface charge density (expressed as charge per unit area) with pH of a ceramic NF membrane by acid-base titration. Xu *et al.* (1997) and Hall *et al.* (1997b) used the membrane potential (the sum of Donnan and diffusional potentials) to study the charge properties of an NF and RO membrane respectively. The electrokinetic measurement of membrane zeta-potential is well established in membrane technology and has become a popular measurement technique for NF membranes. Several authors [Hagmeyer and Gimbel (1998, 1999), Peeters *et al.* (1999), Ernst *et al.* (2000), Afonso *et al.* (2001)] have all studied the variation of membrane zeta-potential with either pH or concentration for polymeric NF membranes from streaming potential measurements in various electrolyte solutions. However, streaming potentials are measured across the outer surface of the membrane and not through the pores and so it is necessary to assume that the membrane charge is distributed uniformly throughout the membrane.

A dependence of membrane charge on electrolyte concentration suggests that the membrane charge within pores (where co-ion concentrations are much smaller than feed concentrations) should differ from the outer surface [Xu *et al.* (1997), Ernst *et al.* (2000)]. Bearing in mind this fundamental discrepancy, the above mentioned authors have all attempted (with various degrees of success) to predict both single and multicomponent electrolyte separations. In many of these studies, the zeta-potential was converted into the effective charge density used in the transport models. In addition, researchers have attempted to compare the values of membrane charge density obtained from the analysis of electrolyte rejection data to the adsorption isotherms proposed from these experimental measurements.

3.2 Assessment of NF models

The nano-scale phenomena involved in uncharged solute and salt separations by NF are extremely complex and, as such, likely to be a rigorous test of any macroscopic description of ion transport and partitioning. The transport of uncharged solutes is reasonably well established through numerous studies of UF membranes. There have been many works over the past thirty years on modelling the transport of charged solutes across a charged membrane. A large number of predictive NF models have been based on either the charged capillary model [Jacazio *et al.* (1972)], models based on the extended Nernst-Planck equation [Tsuru *et al.* (1991)] or the irreversible thermodynamic model [Levenstein *et al.* (1996)]. In this study, the model used is based upon an updated version of the Donnan Steric Partitioning Model (DSPM) which is derived from the extended Nernst-Plank equation.

Tsuru and co-workers [Tsuru *et al.* (1991, 1991b)] were among the first to develop a substantive model of electrolyte transport in charged porous UF and RO membranes based on the extended Nernst-Planck equations. They realised the possible importance of volume flux in ion transport and modified the fixed-charge Teorell-Meyer-Sievers (TMS) model [Teorell, (1951), Meyer and Sievers (1936)] used in equilibrium studies of ion-exchange membranes. Equilibrium partitioning at the pore inlet and outlet was included through a Donnan expression and the model was successful in describing the rejection characteristics of binary and ternary electrolyte mixtures. Their model contained two adjustable parameters, the effective membrane charge density, X_d, and membrane thickness, Δx. The governing equation for the flux of ions was given as

$$j_i = -D_{i,p}\frac{dc_i}{dx} - \frac{z_i c_i D_{i,p}}{RT} F \frac{d\psi}{dx} + c_i V \qquad (3.1)$$

Bowen and Mukhtar (1996) later used a similar model but incorporated hindrance factors to account for the hindered nature of the movement of ions inside the membrane. The model was solved as if the membrane were homogenous (non-porous) but hindrance factors for diffusion and convection were included to allow for the transport of ions in the membrane taking place within a confined space. They

found that the inclusion of the hindrance factors improved the accuracy of the model when fitted to experimental data while also allowing the determination of the effective pore radius of the membrane (in addition to the effective charge density and effective membrane thickness).

The space charge model (SCM) originally proposed by Gross and Osterle (1968) is a more rigorous (and complex) model that takes into account a radial distribution of both concentration and electric potential. Ion transport within the pores is described by the extended Nernst-Planck equation and pore volume flow by the Navier-Stokes equations. Ions are treated as point charges (i.e. no steric effects due to the ion sizes) and total electric potential, $\overline{\Psi}$, is subdivided into two parts as follows

$$\overline{\Psi} = \Psi(x,r) + \psi(x) \tag{3.2}$$

Ψ originates from the surface charge of the capillaries and ψ is due to the streaming potential in the x direction. For a small axial variation in potential [Wang *et al.* (1995)], the radial distribution of concentration, $c_i(x,r)$, can be calculated from the Poisson-Boltzmann equation using the electric potential, $\Psi(x,r)$, and a reference concentration, $c_i(x)$:

$$c_i(x,r) = c_i(x)\exp\left(-\frac{z_i F}{RT}\Psi(x,r)\right) \tag{3.3}$$

The extended Nernst-Planck equation, Eq. (3.1), then becomes

$$j_i = \exp\left(-\frac{z_i F}{RT}\Psi\right)\left[Vc_i - D_i\left(\frac{dc_i}{dx} + \frac{z_i c_i F}{RT}\frac{d\psi}{dx}\right)\right] \tag{3.4}$$

The solution of this system of equations to obtain ion fluxes requires the use of complex numerical techniques and model parameters that are not measurable although the solution can be simplified by the assumption of a Hagen-Poiseuille velocity distribution inside the pore [Jacazio *et al.* (1972)]. Recent workers have attempted to develop this space-charge approach. Hall *et al.* (1997) formulated a rigorous model of

multicomponent ion transport in RO membranes where specific ion interactions were included in partitioning and H^+ and OH^- transport was included in a chemical model for membrane charge formation. Basu and Sharma (1997) included ion hydration and dielectric saturation effects where the change in pore dielectric constant induced by the radial electric field was defined by the Booth (1951) equation.

Wang *et al.* (1995) compared the TMS model to the SCM and found the results to be in good agreement provided the pore radius was significantly smaller than the Debye length. In such a case, the electrical double layers formed within the pore overlap and the radial variation in concentration and potential is small. Bowen *et al.* (1997) showed this assumption of radial homogeneity to be satisfied by a wide range of NF conditions since surface charge density is reasonably small and pores are narrow. Therefore, at present, the most widely adopted models of NF are based on this approximation and so are effectively developments of the original model of Tsuru *et al.* (1991). Many similar versions of this model have been proposed although it is perhaps the work of Rios *et al.* (1996), Wang *et al.* (1997), Combe *et al.* (1997) and Bowen *et al.* (1997) that have made the greatest contributions in this field.

3.2.1 The Donnan Steric Partitioning Model (DSPM)

The original DSPM model forms the basis of the models used in this study and will therefore be described in detail.

3.2.1.1 Transport equations

The application of the extended Nernst-Planck equations was originally proposed by Schlogl (1966) for the description of transport of electrolytes in RO through ion-exchange membranes. The equation is particularly useful for NF as consideration is given to the mechanisms of transport, namely diffusion, electrical potential and convection. The following assumptions are made when using the extended Nernst-Planck equation:

- The activity coefficients are assumed as unity.
- The effective membrane charge density is constant throughout the membrane.
- All ions inside the membrane are transportable.
- Donnan equilibrium is assumed at the interface between the membrane pore and bulk solution.

In terms of the diffusivity of ions, the extended Nernst-Planck equation is

$$j_i = -\frac{c_i K_{i,d} D_{i,\infty}}{RT}\frac{d\mu}{dx} + K_{i,c} c_i V \qquad (3.5)$$

Where j_i is the ionic flux, c is the concentration, V is the solvent velocity and $K_{i,c}$ and $K_{i,d}$ are hindrance factors to account for the convection and diffusion in the confined NF pore. Mukhtar (1995) showed that for NF membranes the correction factor could be important, even for small electrolytes. Note should be taken of the fact that this is a porous model and the convective term uses the symbol V not J_v as would have been used previously in non-porous models and were defined on a membrane area basis [Mukhtar (1995)].

The hindrance factors are defined as

$$K_{i,d} = \frac{D_{i,p}}{D_{i,\infty}} \qquad K_{i,c} = \frac{u_s}{u_x} \qquad (3.6)$$

Where $D_{i,p}$ is the hindered diffusivity inside the NF pore, u_s is the solute velocity and u_x is the maximum solvent velocity. Both hindrance factors are related to the ratio of solute to pore radius, λ, and will be discussed in detail later. Therefore, Eq. (3.5) becomes

$$j_i = -\frac{c_i D_{i,p}}{RT}\frac{d\mu}{dx} + K_{i,c} c_i V \qquad (3.7)$$

The electrochemical potential is written as

$$\mu_i = RT \ln a_i + V_{si} P + z_i F \psi + \text{constant} \qquad (3.8)$$

Where R is the universal gas constant, T is the absolute temperature, V_{si} is the specific volume of the ion, P is the operating pressure, z is the ion valence, F is the Faraday constant and ψ is the electrical potential inside the membrane.

If we differentiate Eq. (3.8) we obtain

$$\frac{d\mu}{dx} = RT \frac{d}{dx}[\ln a_i] + V_{si} \frac{dP}{dx} + z_i F \frac{d\psi}{dx} \qquad (3.9)$$

Using the mathematical relationship $\frac{d}{dx}[\ln a] \approx \frac{1}{a}\frac{da}{dx}$ and $a_i = c_i \gamma_i$ we obtain

$$\frac{d\mu}{dx} = \frac{RT}{c_i}\frac{dc_i}{dx} + \frac{RT}{\gamma_i}\frac{d\gamma_i}{dx} + V_{si}\frac{dP}{dx} + z_i F \frac{d\psi}{dx} \qquad (3.10)$$

Substitution of Eq. (3.10) into Eq. (3.7) yields the result

$$j_i = -D_{i,p}\frac{dc_i}{dx} - \frac{c_i D_{i,p}}{\gamma_i}\frac{d\gamma_i}{dx} - \frac{c_i D_{i,p}}{RT} V_{si}\frac{dP}{dx} - \frac{c_i D_{i,p}}{RT} z_i F \frac{d\psi}{dx} + K_{i,c} c_i V \qquad (3.11)$$

Eq. (3.11) represents the full extended Nernst-Planck equation and must be simplified for solution. Schlogl (1966) proposed that the contribution to ion transport of the activity coefficient, γ, is negligible. Also, Dickson (1988) and Burghoff *et al.* (1980) demonstrated that the effects of pressure on the chemical potential were small at low pressure ($\Delta P < 0.5$ MPa). Therefore, Eq. (3.11) is simplified to

$$j_i = -D_{i,p}\frac{dc_i}{dx} - \frac{c_i D_{i,p}}{RT} z_i F \frac{d\psi}{dx} + K_{i,c} c_i V \qquad (3.12)$$

From the definition of solute flux through the membrane we obtain

$$j_i = VC_{i,p} \tag{3.13}$$

Substitution of Eq. (3.13) into Eq. (3.12) yields the result

$$\frac{dc_i}{dx} = \frac{V}{D_{i,p}}\left[K_{i,c}c_i - C_{i,p}\right] - \frac{z_i c_i}{RT}F\frac{d\psi}{dx} \tag{3.14}$$

This expression describes the concentration gradient of ion i across the membrane. The condition of electroneutrality in the bulk solution is expressed as

$$\sum_{i=1}^{n} z_i C_i = 0 \tag{3.15}$$

Where C_i is the bulk concentration. Electroneutrality inside the membrane pore is expressed as

$$\sum_{i=1}^{n} z_i c_i = -X_d \tag{3.16}$$

Where c is the concentration inside the membrane pore and X_d is the effective membrane charge density. If we differentiate Eq. (3.16) and substitute the result into Eq. (3.14) we obtain an expression for the electrochemical potential

$$\frac{d\psi}{dx} = \frac{\sum_{i=1}^{n}\frac{z_i V}{D_{i,p}}\left[K_{i,c}c_i - C_{i,p}\right]}{\frac{F}{RT}\sum_{i=1}^{n} z_i^2 c_i} \tag{3.17}$$

Substitution of Eq. (3.17) into Eq. (3.14) yields the result

$$\frac{dc_i}{dx} = \frac{V}{D_{i,p}}\left[K_{i,c}c_i - C_{i,p}\right] - z_i c_i\left[\frac{\sum_{i=1}^{n}\frac{z_i V}{D_{i,p}}\left[K_{i,c}c_i - C_{i,p}\right]}{\sum_{i=1}^{n} z_i^2 c_i}\right] \tag{3.18}$$

Eq. (3.18) forms the basis for the transport of ions through the NF pore in terms of solvent flux for the DSPM model.

3.2.1.2 Equilibrium partitioning

In order to solve the transport equations, the solute concentrations at the feed side and permeate side, $c_i(0)$ and $c_i(\Delta x)$, of the membrane must be known. These values are obtained from equilibrium partitioning, which relates the concentration in the bulk solution to that within the membrane pore. This relationship is expressed as

$$\frac{\gamma_i c_i}{\gamma_i^o C_i} = \Phi_i \exp\left(-\frac{z_i F}{RT}\Delta\psi_D\right) \tag{3.19}$$

The terms on the right hand side of Eq. (3.19) are the classic expressions for both steric and Donnan effects respectively [Deen *et al.* (1980), Giddings *et al.* (1968), Donnan (1911)]. Where

$$\Phi_i = (1-\lambda)^2 \tag{3.20}$$

$$\lambda = \frac{a_i}{r_p} \tag{3.21}$$

The steric partitioning coefficient, Φ_i, approaches unity when the ratio of solute to pore radius tends to 0 and becomes 0 when $\lambda \rightarrow 1$.

3.2.1.3 Solution of the DSPM model for uncharged solutes

For the case of uncharged solutes, the transport of solutes through the membrane is only affected by diffusion and convection and Eq. (3.18) simplifies to

$$\frac{dc_i}{dx} = \frac{V}{D_{i,p}}\left[K_{i,c}c_i - C_{i,p}\right] \tag{3.22}$$

In order to obtain an expression for rejection of the solute we must integrate Eq. (3.22) across the membrane with the solute concentrations on the feed side and permeate side given from equilibrium partitioning. Again, neglecting electrical and activity terms, Eq. (3.19) simplifies to

$$\frac{c_i}{C_i} = \Phi_i \tag{3.23}$$

If we now consider the boundary conditions across the membrane, then from Eq. (3.23) we obtain

$$c_i(0) = \Phi_i C_{i,w} \text{ and } c_i(\Delta x) = \Phi_i C_{i,p} \tag{3.24}$$

Separating the variables in Eq. (3.22) gives

$$\int_{\Phi_i C_{i,w}}^{\Phi_i C_{i,p}} \left(\frac{C_{i,p}}{K_{i,c}} - c_i \right) dc_i = -\frac{VK_{i,c}}{D_{i,p}} \int_0^{\Delta x} dx \tag{3.25}$$

$$\int_{\Phi_i C_{i,w}}^{\Phi_i C_{i,p}} \left(\frac{C_{i,p}}{K_{i,c}} - c_i \right) dc_i = -\frac{VK_{i,c}}{D_{i,p}} \Delta x \tag{3.26}$$

The quantity $\frac{VK_{i,c}}{D_{i,p}}\Delta x$ is commonly known as the Peclet number, *Pe*, and is the ratio of convective transport to diffusive transport inside the membrane pore.

$$Pe = \frac{K_{i,c}}{K_{i,d}} \frac{V\Delta x}{D_{i,\infty}} \tag{3.27}$$

Substitution of Eq. (3.27) into Eq. (3.26) and integration gives

$$\frac{C_{i,p}}{C_{i,w}} = \frac{\Phi_i K_{i,c}}{1 - \left[1 - \Phi_i K_{i,c}\right] \exp(-Pe)} \tag{3.28}$$

Eq. (3.28) represents the ratio of the bulk concentrations across the membrane and from the definition of rejection we obtain the result

$$R = 1 - \frac{C_{i,p}}{C_{i,w}} = 1 - \frac{\Phi_i K_{i,c}}{1 - \left[1 - \Phi_i K_{i,c}\right] \exp\left(-Pe\right)} \tag{3.29}$$

Thus, the rejection of uncharged solutes is defined by a simple algebraic expression in terms of pore radius and pore length. In the limiting case of $Pe \rightarrow \infty$, the asymptotic rejection value provides a method for comparing the limiting rejections of solutes of various size and is represented by

$$R_{Lim} = 1 - \Phi_i K_{i,c} \tag{3.30}$$

The effects of pore length (Δx) on rejection are not available, however, the ratio of pore length to membrane porosity ($\Delta x/A_k$) is available and, as A_k is constant for a given membrane, is considered to exhibit the pore length [Nakao and Kimura (1981)]. The Hagen-Poiseuille equation describes the relationship between the pure water flux of a membrane and the applied pressure across the membrane [Nakao and Kimura (1981)] and is expressed as

$$J_w = \frac{r_p^2 \Delta P}{8\eta\left(\Delta x / A_k\right)} \tag{3.31}$$

Therefore, an experimental investigation of the pure water flux versus applied pressure will provide the ratio $\frac{r_p^2}{\Delta x / A_k}$. Then, from the rejection data of an uncharged solute of known size versus membrane flux one can perform a fitting operation using Eq. (3.29) and evaluate the membrane pore radius, r_p. Once the value of r_p and $\Delta x/A_k$ are known, Eq. (3.29) can be used to predict the rejection versus membrane flux for any given uncharged solute.

3.2.1.4 Solution of the DSPM model for charged solutes

For the case of charged solutes, there is no analytical expression available as in the case of uncharged solutes and, as a result, the transport equations must be solved using and iterative numerical integration method. This will be demonstrated using the simple case of a binary electrolyte system (examples NaCl, $MgCl_2$ and $MgSO_4$). Firstly, we must consider the transport equations. From Eq. (3.18) and the conditions of electroneutrality we obtain

$$\frac{dc_i}{dx} = \frac{V}{D_{i,p}}\left[K_{i,c}c_i - C_{i,p}\right] - z_i c_i \left[\frac{z_1 V\left(\frac{K_{1,c}}{D_{1,p}} - \frac{K_{2,c}}{D_{2,p}}\right)c_1 + z_1 V\left(\frac{1}{D_{2,p}} - \frac{1}{D_{1,p}}\right)C_{1,p} - V\frac{K_{2,c}}{D_{2,p}}X_d}{\left(z_1^2 - z_1 z_2\right)c_1 - z_2 X_d}\right] \tag{3.32}$$

Eq. (3.32) is valid for ion 1 and ion 2 in solution, however, we only need to solve for ion 1 as the concentration for ion 2 is then evaluated from electroneutrality. Note that Eq. (3.32) also contains the permeate concentration $C_{1,p}$, thus, in order to solve the equation the answer must be known. Therefore, solution of the transport equations requires an iterative procedure.

If we now consider equilibrium partitioning and focus attention on the feed side of the membrane. From Eq. (3.19) we obtain

$$\Delta\psi_D = -\frac{RT}{z_i F}\ln\left(\frac{c_i}{\Phi_i C_{i,w}}\right) \tag{3.33}$$

The Donnan potential term $\Delta\psi_D$ will have the same magnitude for each ion. Therefore, for ion 2 we obtain

$$c_2(0) = C_{2,w}\Phi_2\left(\frac{c_1(0)}{\Phi_1 C_{1,w}}\right)^{\frac{z_2}{z_1}} \tag{3.34}$$

If we now substitute Eq. (3.34) into the electroneutrality equation, Eq. (3.16), we obtain

$$z_1 c_1(0) + z_2 C_{2,w} \Phi_2 \left(\frac{c_1(0)}{\Phi_1 C_{1,w}} \right)^{\frac{z_2}{z_1}} = -X_d \qquad (3.35)$$

Eq. (3.35) is a simple equation with all values for a given feed stream known, therefore, the concentration $c_1(0)$ is easily calculated. As a result, the feed side concentrations required for the solution of the transport model are available from Eqs. (3.35) and (3.16). If we now consider the permeate side of the membrane, then a similar expression to Eq. (3.35) exists

$$z_1 c_1(\Delta x) + z_2 C_{2,p} \Phi_2 \left(\frac{c_1(\Delta x)}{\Phi_1 C_{1,p}} \right)^{\frac{z_2}{z_1}} = -X_d \qquad (3.36)$$

Eq. (3.36) is completely analogous to equation Eq. (3.35) from which the permeate concentrations can be calculated for given membrane-permeate interface concentrations, i.e. $c_1(\Delta x)$ and $c_2(\Delta x)$. Thus, the iteration procedure is established.

- First, from the feed conditions calculate the feed-membrane interface concentrations $c_1(0)$ and $c_2(0)$ using Eqs. (3.35) and (3.16).

- Second, guesstimate the permeate concentrations $C_{1,p}$ and $C_{2,p}$ and solve the transport equations to obtain the membrane-permeate interface concentrations $c_1(\Delta x)$ and $c_2(\Delta x)$.

- Third, using the values obtained for $c_1(\Delta x)$ and $c_2(\Delta x)$, calculate the permeate concentrations from Eqs. (3.36) and (3.15). If the calculated values for permeate concentration match the initial guesstimate values then the answer is correct. Otherwise, refine the guesstimates and iterate for permeate concentration.

Thus, the solution to the problem is the minimisation of the error function

$$Error = f_i = C_{i,p(transport)} - C_{i,p(partitioning)} \quad (3.37)$$

In the case of several electrolytes in solution, the numerical solution becomes a combined error minimisation where the overall error function becomes

$$f_{Overall} = f_1^2 + f_2^2 + \ldots + f_{n-1}^2 \quad (3.38)$$

In order to use the DSPM model for the prediction of electrolyte concentration three parameters must be known, namely r_p, $\Delta x/A_k$ and X_d. Both r_p and $\Delta x/A_k$ can be calculated for a given membrane from the procedure outlined in Section (3.2.1.3). The effective membrane charge density, X_d, is also obtainable from a similar fitting procedure. As detailed in Chapter 1, the membrane charge density is known to vary with feed concentration and pH. Many characterisation studies of NF membranes have attempted to describe the variation in X_d in terms of an adsorption isotherm. A widely adopted isotherm is the Freundlich isotherm [Bowen and Mukhtar (1996), Afonso and de Pinho (2000)] where X_d is related to concentration as

$$|X_d| = aC_w^b \quad (3.39)$$

Thus, a study of different salt rejections at different concentrations and at given pH is used to formulate an experimental best fit isotherm, which can then be used in the model simulations. However, care should be taken as membrane charge is inherently difficult to predict accurately and is known to vary (often significantly) from one salt to another and for different mixtures of salts (as will be demonstrated in later chapters).

3.2.2 The Updated Donnan Steric Partitioning model (UDSPM)

The DSPM as a predictive model of NF processes has proved to be very successful in describing relatively simple systems such as organic molecules and univalent electrolytes. However, the quality of agreement with experimental data is less good in studies of multivalent cations such as Mg^{2+} and SO_4^{2-} [Schaep *et al.* (1999, 2001)] and

mixtures of electrolytes. A physical assessment of the separation phenomena involved in these complex systems indicates that many factors are being taken into account implicitly in the DSPM. In general, one can conclude that the success of the DSPM model has largely been due to the fact that the characterisation parameters (r_p, $\Delta x/A_k$ and X_d) are in many ways fitting parameters that have only limited correspondence to the structural and electrical properties of the membrane. Such a model can only be described as semi-empirical.

For this reason, Bowen and Welfoot (2002) updated the original DSPM model to include more of the complex phenomena that govern the separation characteristics of NF processes in order to improve the physical relevance of the NF model. This new UDSPM model was developed to include the dependence of chemical potential on pressure in solute transport, an increased solvent viscosity within the NF pore and the contributions of dielectric exclusion on ion partitioning at the feed-membrane interface. These effects have been included into the model in such a fashion as not to increase either the complexity of calculation or the number of undefined parameters and so does not reduce the practical applications of the model as a predictive tool.

A discussion of the UDSPM now follows.

3.2.2.1 Transport equations

If we now consider the full version of the extended Nernst-Planck equation derived previously as Eq. (3.11)

$$j_i = -D_{i,p}\frac{dc_i}{dx} - \frac{c_i D_{i,p}}{\gamma_i}\frac{d\gamma_i}{dx} - \frac{c_i D_{i,p}}{RT}V_{si}\frac{dP}{dx} - \frac{c_i D_{i,p}}{RT}z_i F\frac{d\psi}{dx} + K_{i,c}c_i V \qquad (3.40)$$

Again, eliminating the negligible effects (in this case we do not eliminate the pressure term as was the case with the DSPM model) we obtain

$$j_i = -D_{i,p}\frac{dc_i}{dx} - \frac{c_i D_{i,p}}{RT}V_{si}\frac{dP}{dx} - \frac{c_i D_{i,p}}{RT}z_i F\frac{d\psi}{dx} + K_{i,c}c_i V \qquad (3.41)$$

The assumption of lamina flow through the membrane pore enables the pressure gradient to be defined from a Hagen-Poiseuille type relationship, where the pressure gradient is constant along the pore [Welfoot (2001)] and is expressed as

$$\frac{dP}{dx} = \frac{\Delta P_e}{\Delta x} = \frac{8\eta V}{r_p^2} \tag{3.42}$$

Where $\Delta P_e = \Delta P - \Delta\pi$. The introduction of an osmotic pressure difference across a pore, $\Delta\pi$, is important for systems such as multivalent electrolytes at higher concentrations as the effective pressure driving force, ΔP_e, will differ significantly from the applied pressure, ΔP. Care should be taken when using Eq. (3.42) as the viscosity term, η, is not that of the bulk viscosity (this will be discussed later).

Following the same treatment as in Section (3.2.1.1) the result obtained is

$$\frac{dc_i}{dx} = \frac{V}{D_{i,p}}\left[\{K_{i,c} - Y\}c_i - C_{i,p}\right] - z_i c_i \left[\frac{\sum_{i=1}^{n} \frac{z_i V}{D_{i,p}}\left[\{K_{i,c} - Y\}c_i - C_{i,p}\right]}{\sum_{i=1}^{n} z_i^2 c_i}\right] \tag{3.43}$$

The extra term, Y, in Eq. (3.43) when compared to Eq. (3.18) is a dimensionless parameter and arises as a direct result of the inclusion of pressure effects on the chemical potential. The term is expressed as

$$Y = \frac{D_{i,p}}{RT} V_{si} \frac{8\eta}{r_p^2} \tag{3.44}$$

3.2.2.2 Equilibrium partitioning

As with the DSPM model, the solute concentrations at the feed side and permeate side of the membrane must be known in order to solve the transport equations. Again, these values are obtained from equilibrium partitioning, however the description of

the partitioning expression is significantly different in the UDSPM model to account for dielectric contributions. This relationship is expressed as

$$\frac{\gamma_i c_i}{\gamma_i^o C_i} = \Phi_i \exp\left(-\frac{z_i F}{RT}\Delta\psi_D\right)\exp\left(-\frac{\Delta W_i}{k_B T}\right) \tag{3.45}$$

Where ΔW_i is the ion solvation energy barrier and k_B is the Boltzmann constant. Ion solvation forces are one proposed mechanism [Bowen and Welfoot (2002)] by which the contributions of dielectric exclusion of ions from NF membranes is possible. A detailed description of dielectric exclusion will be presented in Chapter 5. The solvation energy barrier is described using a Born (1920) expression

$$\Delta W_i = \frac{z_i^2 e^2}{8\pi\varepsilon_o a_i}\left(\frac{1}{\varepsilon_p} - \frac{1}{\varepsilon_b}\right) \tag{3.46}$$

Where e is elemental electron charge, ε_o is the permitivity of free space, ε_p is the pore dielectric constant and ε_b is the bulk dielectric constant. The Born model requires a knowledge of the pore dielectric constant. Bowen and Welfoot (2002) proposed that the solvent structure within the pores will consist of one layer of oriented water molecules at the pore wall and an inner annulus (central part) having bulk dielectric properties. The variation of average pore dielectric constant can then be calculated on a geometric basis (assuming $\varepsilon_b = 80$)

$$\varepsilon_p = 80 - 2(80-\varepsilon^*)\left(\frac{d}{r_p}\right) + (80-\varepsilon^*)\left(\frac{d}{r_p}\right)^2 \tag{3.47}$$

Where d is the diameter of a water molecule and ε^* is the dielectric constant of the single layer of water molecules.

3.2.2.3 Solution of the UDSPM for uncharged solutes

The solution of the UDSPM model for neutral solutes is completely analogous in approach to that of the DSPM model. However, in this case the resulting equation derived from Eq. (3.43) is

$$R = 1 - \frac{C_{i,p}}{C_{i,w}} = 1 - \frac{\{K_{i,c} - Y\}\Phi_i}{1 - [1 - \{K_{i,c} - Y\}\Phi_i]\exp(-Pe')} \tag{3.48}$$

Where the modified Peclet number (Pe') is

$$Pe' = \frac{\{K_{i,c} - Y\}}{K_{i,d}} \frac{V\Delta x}{D_{i,\infty}} = \frac{\{K_{i,c} - Y\}}{K_{i,d}} \frac{r_p^2}{8\eta D_{i,\infty}} \Delta P_e \tag{3.49}$$

This result is extremely important as redefining the NF driving force in terms of the effective pressure, ΔP_e, (as opposed to the volumetric membrane flux, J_v) has removed the membrane thickness from the rejection equation and, as a direct result, the rejection equation is now dependent only on the pore radius, r_p. In addition, the integration of the concentration gradient over the distance $\Delta x/A_k$ with the inherent assumption that $A_k = 1$ (as was the case with the DSPM model) is inconsistent with the assumption of a porous model.

Therefore, fitting the experimental rejection versus effective pressure for a solute of known size will give a direct characterisation of the membrane pore radius. Once the pore radius is obtained, the rejection of any neutral solute may be estimated for a given effective pressure using Eq. (3.48)

3.2.2.4 Solution of the UDSPM for charged solutes

The rejection of charged solutes is more complicated than that for neutral solutes as no analytical solution to the extended Nernst-Planck equation is possible, as detailed in Section (3.2.1.4.). The solution of the UDSPM model is identical to that of the DSPM with only subtle differences.

The transport equations will be described using Eq. (3.43), analogous to that used in Section (3.2.1.4.) apart from the inclusion of the parameter Y. The equilibrium partitioning equations include the extra dielectric partitioning terms, however, these are easily made analogous to those used in the DSPM by considering the expression

$$\frac{c_i}{C_i} = \Phi_i' \exp\left(-\frac{z_i F}{RT}\Delta\psi_D\right) \tag{3.50}$$

Where

$$\Phi_i' = \Phi_i \exp\left(-\frac{\Delta W_i}{kT}\right) \tag{3.51}$$

All parameters in the UDSPM model are now available except the dielectric constant of the orientated water molecules at the pore wall, ε^*. This parameter is obtained using a fitting procedure of salt rejection at the membrane isoelectric point or at high salt concentrations ($C_{i,w}$ > 100 mol m^{-3}) [Welfoot (2001)]. A detailed description of this procedure will be provided in Chapter 6. Thus, the iteration procedure is established and for a binary salt will be:

- First, evaluate the parameter Φ_i' using the experimentally determined value for ε^* and the Born model, Eqs. (3.46), (3.47) and Eq. (3.51).
- Second, from the feed conditions calculate the feed-membrane interface concentrations $c_1(0)$ and $c_2(0)$ using Eq. (3.50) and the method described in Section (3.2.1.4)
- Third, make initial guesstimates of the permeate concentrations $C_{1,p}$ and $C_{2,p}$ and solve the transport equation, Eq. (3.43), to obtain the membrane-permeate interface concentrations $c_1(\Delta x)$ and $c_2(\Delta x)$.
- Fourth, using the values obtained for $c_1(\Delta x)$ and $c_2(\Delta x)$, calculate the permeate concentrations from Eq. (3.50). If the calculated values for permeate concentration match the initial guesstimate values then the answer is correct. Otherwise, refine the guesstimate values and iterate for permeate concentration.

Again, the solution to the problem is the minimisation of the error function

$$Error = f_i = C_{i,p(transport)} - C_{i,p(partitioning)} \quad (3.52)$$

In the case of several electrolytes in solution, the numerical solution becomes a combined error minimisation where the overall error function becomes

$$f_{Overall} = f_1^2 + f_2^2 + \ldots + f_{n-1}^2 \quad (3.53)$$

Therefore, in order to use the UDSPM model for the prediction of electrolyte concentration three parameters must be known, namely r_p, ε^* and X_d. The parameter r_p is calculated for a given membrane from the procedure outlined in Section (3.2.2.1), the parameter ε^* is obtained from the fitting procedure outlined in Section (3.2.2.2.) and the effective membrane charge density, X_d, is also obtainable from the fitting procedure outlined for the DSPM model in Section (3.2.1.4).

3.2.2.5 Variation in pore viscosity

As stated earlier, the assumption of bulk solvent properties may not be valid within narrow NF pores. The use of the bulk water viscosity is likely to overestimate the water permeability since the actual viscosity may be increased due to greater solvent structure caused by orientation of the water molecules at the pore wall. Whilst some work has been performed on the effects of confinement on water structure, there remain severe limitations on the level of knowledge available. Welfoot (2001) reviewed the available literature and concluded that overall there is sufficient evidence for an increase in viscosity with decreasing pore radius. However, the conclusion was made that the increase in viscosity is extremely difficult to quantify because of the lack of relevant data for pores in the NF size range.

Experimental evidence suggests the presence of a single layer of adsorbed water molecules at the pore wall, which will remain intact when subjected to shear. Belfort *et al.* (1974) performed NMR studies of the relaxation of water adsorbed on glass surfaces and found that only one layer of water molecules was adsorbed to the

glass surfaces, the viscosity of which was estimated to be 10 times greater than that of bulk water. The cylindrical NF pores are thus to be approximated in the present work as having an annulus with the thickness of one water molecule (d = 0.28 nm) having an increased viscosity ($\eta_{layer} = 10\eta_o$). The central part of the pore is then assumed to have the viscosity of bulk water. The assumed pore solvent structure is shown in Figure 3.1 below.

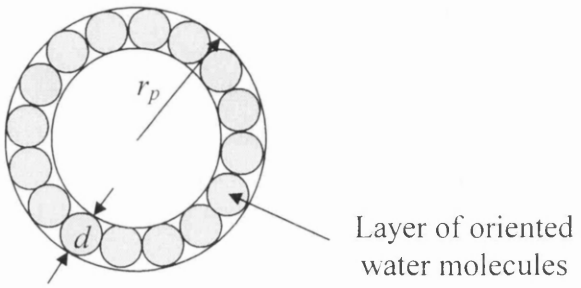

Figure 3.1: Diagram of assumed pore solvent structure.

This approach is physically consistent with the description of the solvent structuring used to evaluate the NF pore dielectric properties in Section (3.2.2.2.).

If viscosity is averaged in terms of area, substitution for η_{layer} and rearrangement yields the following expression:

$$\frac{\eta}{\eta_o} = 1 + 18\left(\frac{d}{r_p}\right) - 9\left(\frac{d}{r_p}\right)^2 \qquad (3.54)$$

Where η is the pore viscosity and η_o is the bulk solvent viscosity. The diffusivity of the solutes inside the NF pore will also be affected by the change in viscosity. Pore diffusivity, $D_{i,p}$, in the expressions for the UDSPM model should be corrected as follows:

$$D_p^* = D_p \frac{\eta_o}{\eta} = K_d D_\infty \frac{\eta_o}{\eta} \qquad (3.55)$$

The modified Peclet number defined by Eq. (3.32) is now rewritten to give

$$Pe' = \frac{\{K_{i,c} - Y\}}{K_{i,d}} \frac{r_p^2}{8\eta_o D_{i,\infty}} \Delta P_e = \frac{\{K_c - Y\} r_p^2}{8\eta D_p^*} \Delta P_e \qquad (3.56)$$

Examination of Eq. (3.56) shows that the definition of modified Peclet number is identical to that where bulk solvent viscosity is assumed, showing that uncharged solute rejection is independent of changes in pore solvent viscosity. The convective and diffusive transport terms are both scaled linearly by the factor η/η_o and so their effects cancel. Eman and Churaev (1990) have also reported this independence of Peclet number on pore viscosity. However, the increase in pore viscosity is extremely important if membrane pore-size distributions are considered (not included in this study) as the overall solute rejection (obtained by integration over the pore-size distribution) is controlled by the proportion of the total flux flowing through each pore-size range. This will be governed by the water permeability of the membrane, which will be significantly affected by the solvent viscosity.

3.2.3 The linearised UDSPM model

The lack of application of NF modelling to real industrial applications, in terms of design, optimisation and scale-up, has highlighted the limitations of the existing theoretical descriptions for NF technology. Current trends in modelling are to incorporate as much physical realism into the derived models as possible, with the aim of improving the agreement of the model parameters with measured physical properties. This incorporation of realism can lead to models of extreme complexity that are almost impossible to apply in practice. An example of this is the overall solution to the UDSPM (and equally the DSPM) requiring non-linear numerical integration of the transport equations using a Runga-Kutta integration technique. This process, especially for multi-ion systems, is time consuming and computationally demanding and has no doubt hindered the use of NF modelling by non-specialist engineers. For this reason, Bowen and Welfoot (2002c) proposed to simplify the UDSPM model through linearisation of the transport equations by considering an average solute concentration within the NF pore. This simplification greatly diminishes the complexity in solving the UDSPM model by negating the use of numerical integration and reduces the problem to a set of linear algebraic equations

that can be solved on any spreadsheet application. The incorporation of a linear concentration gradient into the UDSPM model will now be described.

Consider the UDSPM transport equation

$$\frac{dc_i}{dx} = \frac{V}{D_{i,p}}\left[\{K_{i,c} - Y\}c_i - C_{i,p}\right] - \frac{z_i c_i}{RT} F \frac{d\psi}{dx} \tag{3.57}$$

If this expression is now linearised by considering an average pore concentration, c_{av}, then Eq. (3.57) becomes

$$\frac{\Delta c_i}{\Delta x} = \frac{V}{D_{i,p}}\left[\{K_{i,c} - Y\}c_{i,av} - C_{i,p}\right] - \frac{z_i c_{i,av}}{RT} F \frac{d\psi}{dx} \tag{3.58}$$

The electrical potential across the membrane is then expressed as

$$\frac{d\psi}{dx} = \frac{\sum_{i=1}^{n} \frac{z_i V}{D_{i,p}}\left[\{K_{i,c} - Y\}c_{i,av} - C_{i,p}\right]}{\frac{F}{RT}\sum_{i=1}^{n} z_i^2 c_{i,av}} \tag{3.59}$$

Where the average solute concentration and the linearised solute concentration gradient are defined as

$$\frac{dc_i}{dx} \approx \frac{\Delta c_i}{\Delta x} = \frac{c_i(\Delta x) - c_i(0)}{\Delta x} \tag{3.60}$$

$$c_{i,av} = \frac{c_i(0) + c_i(\Delta x)}{2} \tag{3.61}$$

Solution of the linearised UDSPM model for a binary system is then

- Calculate the feed-membrane interface concentrations, $c_1(0)$ and $c_2(0)$, using the feed conditions and Eqs. (3.50) and (3.16).

- Make initial guesstimate values for the permeate concentrations, $C_{1,p}$ and $C_{2,p}$, and calculate the concentrations at the membrane-permeate interface, $c_1(\Delta x)$ and $c_2(\Delta x)$, using Eqs. (3.50) and (3.16).
- Calculate the average membrane concentrations, $c_{1,av}$ and $c_{2,av}$, using Eq. (3.61).
- Calculate the value of the linearised concentration gradient, $\Delta c_i/\Delta x$, using Eqs. (3.58) and (3.59).
- Calculate the concentrations at the membrane-permeate interface, $c_1(\Delta x)$ and $c_2(\Delta x)$, using Eq. (3.60) and then calculate the permeate concentrations, $C_{1,p}$ and $C_{2,p}$, from Eqs. (3.50) and (3.16).

Again, the solution to the problem is the minimisation of the error function

$$Error = f_i = C_{i,p(transport)} - C_{i,p(partitioning)} \tag{3.62}$$

In the case of several electrolytes in solution, the numerical solution becomes a combined error minimisation where the overall error function becomes

$$f_{Overall} = f_1^2 + f_2^2 + \ldots + f_{n-1}^2 \tag{3.63}$$

Therefore, in order to use the linearised UDSPM model for the prediction of electrolyte concentration the same three parameters must be known, namely r_p, ε^* and X_d. These parameters are obtained using exactly the same methods as described in Section (3.2.2.4) only using the linearised versions of the UDSPM model. Aspects of the linear UDSPM model related to validity under real NF conditions and practical application are described in Chapter 4.

3.3 Hindrance factors

The hindrance factors $K_{i,c}$ and $K_{i,d}$ have been used throughout the derivation of both the DSPM and UDSPM models in Section (3.2) and will be described in detail here.

Hindrance factors are introduced into the NF models to account for the hindered passage of solutes through the confined polymer structure of the NF membrane. The hindrance factors for movement inside an interconnecting network of polymers are difficult to derive and have not been reported so far. Therefore, all of the work in this area to date has assumed a solute of rigid spherical shape moving through a perfectly cylindrical pore of infinite length. For such a case, expressions for the hindrance factors can be derived theoretically from a fundamental knowledge of the system hydrodynamics [Deen (1987)]. A detailed derivation for the hindrance factors was presented by Mohammad (1998) and will be described briefly here, this will allow the reader to gain at least an understanding of the origins of hindered flow. Figure 3.2 illustrates the spherical particle inside the membrane pore.

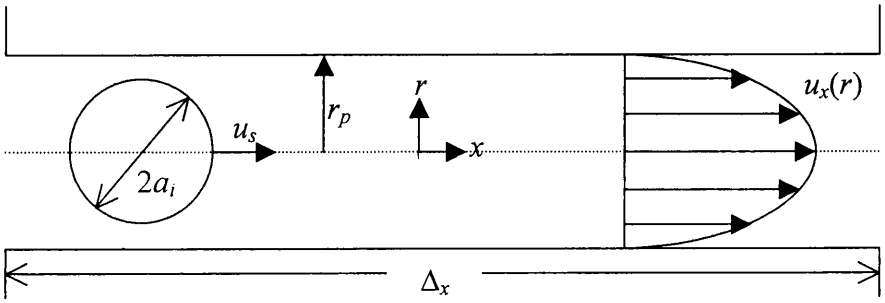

Figure 3.2: Schematic diagram of the movement of a spherical solute inside a pore.

If we consider that the radial position inside the pore is described as

$$\beta = \frac{r}{r_p} \tag{3.64}$$

Then, the hindrance factors $K_{i,c}$ and $K_{i,d}$ are expressed as

$$K_{i,c} = \frac{2\int_0^{1-\lambda} G\left(1-\beta^2\right)\exp\left(-E/RT\right)\beta d\beta}{\int_0^{1-\lambda} \exp\left(-E/RT\right)\beta d\beta} \tag{3.65}$$

$$K_{i,d} = \frac{\int_0^{1-\lambda} K^{-1} \exp(-E/RT)\beta d\beta}{\int_0^{1-\lambda} \exp(-E/RT)\beta d\beta} \tag{3.66}$$

Where E is the electrostatic potential between the solute and the pore wall, G is the lag coefficient and K^{-1} is the enhanced drag. If we limit ourselves to purely steric interactions, then Eqs. (3.65) and (3.66) simplify to give

$$K_{i,c} = (2 - \Phi_i) G(\lambda,0) \tag{3.67}$$

$$K_{i,d} = K^{-1}(\lambda,0) \tag{3.68}$$

3.3.1 Evaluation of the hindrance factors

The hydrodynamic coefficients, $K^{-1}(\lambda,0)$ and $G(\lambda,0)$, have been approximated in terms of the centreline values, where the spherical particle travels axially along the central radial axis. Such an approximation is necessary due to the shear lack of hydrodynamic information for calculating the functions radially, i.e. $K^{-1}(\lambda,\beta)$ and $G(\lambda,\beta)$. Most calculations have been reported over a wide range of λ values only for the centreline case [Hyberman and Sayre (1958), Anderson and Quinn (1974), Bungay and Brenner (1973)].

More recently, Bowen and Sharif (1994) have calculated the enhanced drag coefficients in a cylindrical pore by solving the governing equations using the finite element technique. Assuming a centreline approach, they investigated three different cases:

- A single moving spherical particle in a stationary liquid,
- a moving liquid in a stationary particle, and
- a moving particle in a moving liquid.

This approach led to point value solutions for both $K^{-1}(\lambda,0)$ and $G(\lambda,0)$ for given values of λ, which are illustrated in Figure 3.3. Regression of the numerical calculations presented in Figure 3.3 were represented by the third order polynomial expressions over the range $0 < \lambda < 0.95$ [Mohammad (1998)].

$$K^{-1}(\lambda,0) = 1.0 - 2.401\lambda + 1.530\lambda^2 - 0.118\lambda^3 \tag{3.69}$$

$$G(\lambda,0) = 1.0 + 0.042\lambda - 0.941\lambda^2 + 0.399\lambda^3 \tag{3.70}$$

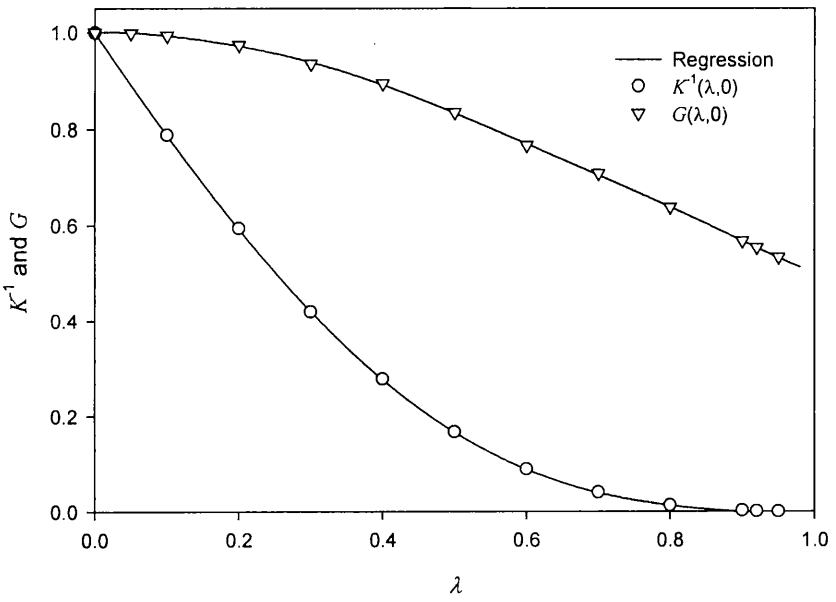

Figure 3.3: The enhanced drag, K^{-1}, and the lag coefficient, G, as a function of the ratio of solute to pore radius. The symbols are the results of the finite element calculations [Bowen and Sharif (1994)].

Welfoot (2001) performed the regression of the original data from Bowen and Sharif (1994) in terms of a seventh-order polynomial expression. The representation of both $K^{-1}(\lambda,0)$ and $G(\lambda,0)$ was significantly improved in the region of $\lambda > 0.8$, necessary when pore size distributions of membranes are included in the NF models. The expressions developed by Welfoot are valid in the range $0 < \lambda < 0.98$ and are defined as

$$K^{-1}(\lambda,0) = 1 - 2.20\lambda + 0.75\lambda^2 + 0.0006\lambda^3 + 2.07\lambda^4 - 1.02\lambda^5 - 1.82\lambda^6 + 1.22\lambda^7 \quad (3.71)$$

$$G(\lambda,0) = 1 - 0.007\lambda - 0.64\lambda^2 + 0.00005\lambda^3 - 0.46\lambda^4 + 0.87\lambda^5 + 0.24\lambda^6 - 0.51\lambda^7 \quad (3.72)$$

However, closer inspection of the expression developed by Welfoot for the enhanced drag in the range $\lambda > 0.9$ shows that the values calculated using Eq. (3.71) are negative. This result, by definition, is clearly invalid and is caused by truncation errors in the number of significant places presented for each order of λ in the expression. The negative values calculated using Eq. (3.71) are best illustrated by re-plotting Figure 3.3 using a log scale, the negative values will be indicated by a disappearance of the regression line as negative logarithms are invalid, the re-plot of Figure 3.3 with log scale values is provided as Figure 3.4.

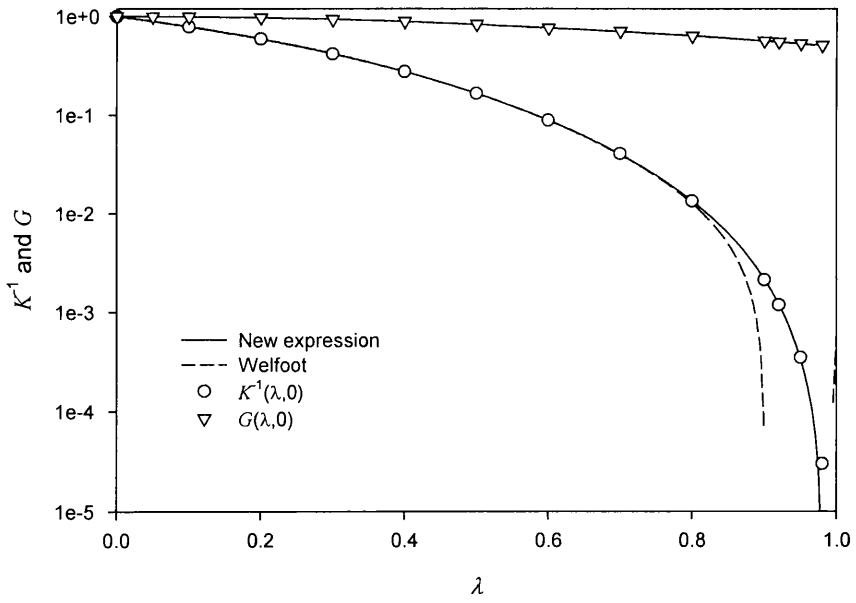

Figure 3.4: A re-plot of Figure 3.3 with a logarithmic y-axis.

For this reason, statistical regression of the original hydrodynamic data [Bowen and Sharif (1994)] was repeated (see Appendix A5) and new expressions proposed which avoid the calculation error for the enhanced drag. The new expressions for the

enhanced drag and the lag coefficient are also plotted in Figure 3.4 and are represented by

$$K^{-1}(\lambda,0) = 1.0000 - 2.1812\lambda + 0.7328\lambda^2 - 0.9065\lambda^3 + 6.7272\lambda^4 \quad (3.73)$$
$$-10.2324\lambda^5 + 6.3293\lambda^6 - 1.4692\lambda^7$$

$$G(\lambda,0) = 1.0000 + 0.0650\lambda - 1.9370\lambda^2 + 8.5211\lambda^3 - 27.3398\lambda^4 \quad (3.74)$$
$$+44.4150\lambda^5 - 34.5582\lambda^6 + 10.3358\lambda^7$$

The variation of the hindrance factors with λ are shown in Figure 3.5 where the correction factor for hindered diffusion is substantially greater than the correction for hindered convection.

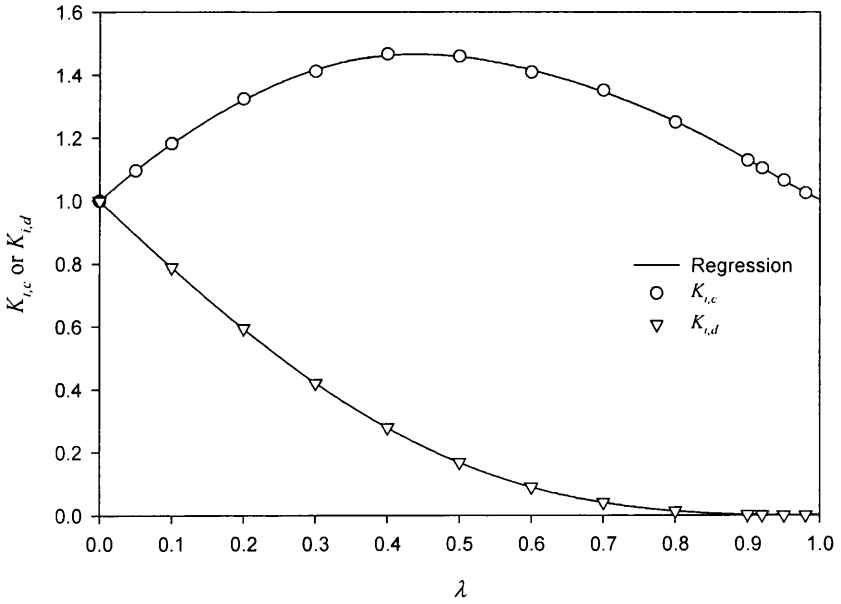

Figure 3.5: Hindrance factors for convection and diffusion.

3.4 Description of diafiltration and concentration

Consider a diafiltration vessel of volume V, membrane area A and volumetric flux J_v, with an initial feed concentration of $C_{i,f}$ and a permeate concentration of $C_{i,p}$. A mass balance over the diafiltration vessel yields

$$\frac{d}{dt}\left(VC_{i,f}\right) = -J_v A C_{i,p} \tag{3.74}$$

Expanding the derivative for constant volume and substituting for $C_{i,p}$ gives

$$\frac{dC_{i,f}}{dt} = -\frac{J_v A}{V}\left(1 - R_i\right)C_{i,f} \tag{3.75}$$

For the case of uncharged solutes, R_i is constant, and Eq. 3.75 can be solved algebraically. However, for the case of charged solutes, Eq. 3.75 must be integrated numerically. The numerical integration method used in this study was the classic fourth order Runga-Kutta method defined by Chapra and Canale (1989).

The concentration phase will take place in the same vessel as diafiltration, thus from Eq. 3.74 a mass balance yields

$$\frac{d}{dt}\left(VC_{i,f}\right) = -J_v A C_{i,p} \tag{3.76}$$

Expanding the derivative using the product rule gives

$$V\frac{dC_{i,f}}{dt} + C_{i,f}\frac{dV}{dt} = -J_v A C_{i,p} \tag{3.77}$$

In the concentration phase the volume will change with time, thus the simple expression obtained for diafiltration is no longer valid. Consider the case for two components in solution, one permeating the membrane and the other fully retained. Then, for the component fully retained

$$V = \frac{M}{C_{i,f}} \tag{3.78}$$

Where M is the mass of the component and will not change with time. Also, the description of membrane flux gives

$$\frac{dV}{dt} = -J_v A \tag{3.79}$$

By substituting Eqs. 3.78 and 3.79 into Eq. 3.77 yields (for the fully retained component)

$$\frac{dC_{i,f}}{dt} = \frac{J_v AR}{M} C_{i,f}^2 \tag{3.80}$$

Note that strictly $R = 1$ in Eq. 3.80, however, the symbol has not been omitted to simplify later explanations. Similarly, for the permeating component the following expression is obtained

$$\frac{dC_{i,f}}{dt} = \frac{J_v AR}{\dot{M}} \dot{C}_{i,f} C_{i,f} \tag{3.81}$$

Where $\dot{M}$ and $\dot{C}_{i,f}$ refer to the material fully retained. Thus, Eqs. 3.80 and 3.81 represent a series of differential equations that can be solved simultaneously using the same fourth order Runga-Kutta method [Chapra and Canale (1989)].

4 Numerical Investigation of the UDSPM Model

In order to successfully implement the models derived in Chapter 3 for characterisation and prediction of NF membrane processes mathematical techniques for solving the transport models must be developed. Solution of the UDSPM model is a simple mater for uncharged solutes as there is a direct analytical result. However, for the case of charged solutes (and more importantly multi-ion systems) the techniques required are extremely complex, labour intensive, time consuming and require the solution of a series of non-linear differential equations. This chapter will discuss the merits and issues involved in developing such mathematical techniques and solution using the computer language Fortran™ in order to control calculation error, optimise calculation efficiency and, most importantly, focus on producing mathematical techniques that are reliable.

The linearised version of the UDSPM model offers many advantages over the full UDSPM model including a significant reduction in complexity (as no numerical integration is required), reduced calculation time and easy of use. Therefore, a comprehensive comparison between the UDSPM model and the linearised UDSPM model will be made over a range of defined NF conditions and for a number of NF solutes; namely uncharged solutes, binary systems, ternary systems and quaternary systems. This will provide a thorough investigation into the assumption of a linear concentration gradient through the NF membrane pore and allow the user to have confidence that there will be no significant deviation between both model results.

4.1 Solution of the UDSPM model

There are three main areas that require attention when solving the UDSPM model; Namely, the effect of step-size in the numerical integration, the initial seed guess for the iteration procedure and the required accuracy of the result.

4.1.1 Effects of step-size on numerical integration

The numerical integration method used in this study was the classic fourth-order Runge-Kutta method defined by Chapra and Canale (1989). This method is an initial condition solution for differential equations. As with any numerical solution of this type, the method is derived from truncation of the Taylor series function and in order to reduce the global error in the solution, an appropriate step-size must be selected. If the step size is too large, the speed of the calculation will be high but the solution accuracy will be poor. If the step-size is too small, the truncation error will be low and the solution accuracy improved but the calculation will take more time. Therefore, an optimisation is required to determine an appropriate step-size. Figure 4.1 illustrates the effect of step-size on the integration of the transport function [Eq. (3.43)] to calculate rejection from a hypothetical membrane for NaCl.

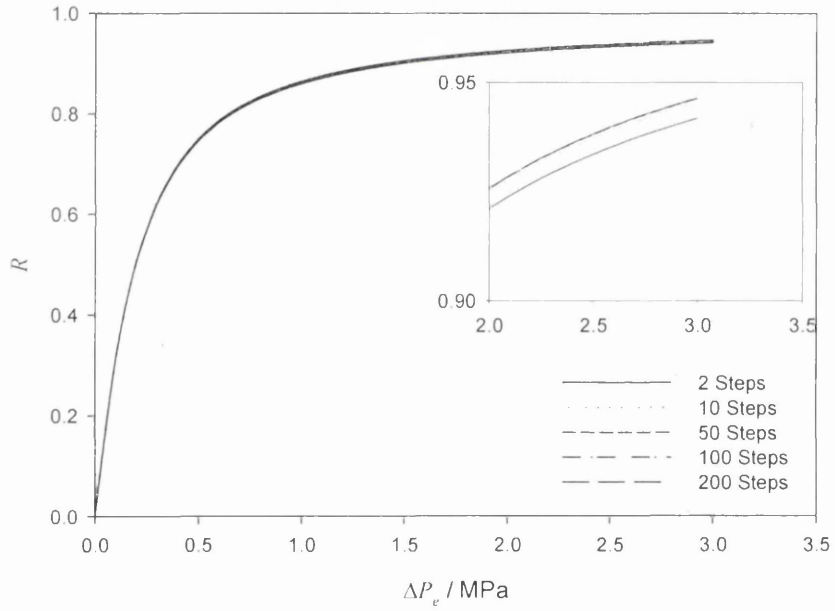

Figure 4.1: Variation in NaCl rejection from a hypothetical membrane with decreasing step-size (r_p = 0.5 nm, ε^* = 35, ξ = -1).

The rejection calculation exhibits little dependence on the number of steps used in the integration of the transport equation for NaCl, with only a 0.5 % difference in the result at 3 MPa between that calculated using 2 steps and 200 steps. However, solutions of NaCl are generally considered as one of the simplest cases to solve (i.e. mono-valent binary system) and therefore 50 steps are recommended as a minimum

level to obtain reliable solutions (200 steps were used in all subsequent calculations). The calculation to predict concentration over time during diafiltration also involves numerical integration [Eq. (3.75)]. The effects of step-size on this equation is illustrated in Figure 4.2 for an NaCl:Na_2SO_4 mixture (molar ratio 1:1).

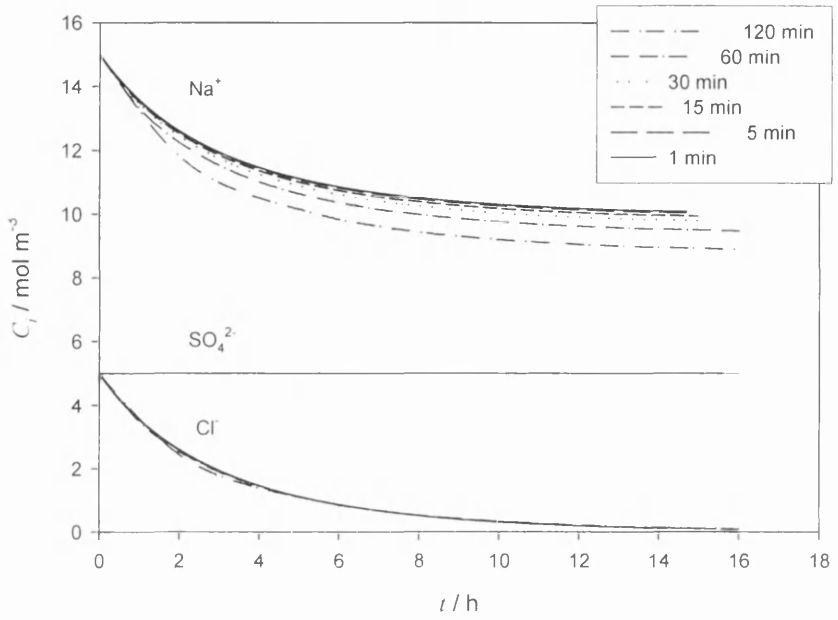

Figure 4.2: Variation in diafiltration vessel concentration over time for an NaCl:Na_2SO_4 mixture versus integral step-size (r_p = 0.5 nm, ε^* = 35, ξ = -0.2, V = 1 m^3, A = 100 m^2, ΔP_e = 1.5 MPa).

The dependence of calculated concentration on integral step-size is significant in this case and greater than that observed in Figure 4.1. The calculated concentration of Na^+ ions in solution after 10 hours operation is 10.7 % higher for a step-size of 1 minute than for a step-size of 120 minutes. Therefore a small step-size is required for increased accuracy and a step-size of less than 5 minutes is recommended.

4.1.2 Initial seed guess

Solution of the UDSPM model is obtained by an iterative procedure minimising the error function [Eq. (3.53)]. For a binary system a simple method such as the bisection method is sufficient to obtain convergence. However, for more complicated ternary

and quaternary systems a curve crawling method described by Acton (1970) was used. The nature of the error function is always positive and is illustrated for a ternary system of NaCl:$MgCl_2$ in Figure 4.3. The plateau in Figure 4.3 represents the invalid concentration range, i.e. where electroneutrality no longer exists. If the initial guesstimate for permeate concentration were to be placed on this plateau no meaningful solution would be found. Therefore, the user must take care to select an initial start position that is on the slope region of the error function, this will allow the curve crawling technique to find a minima.

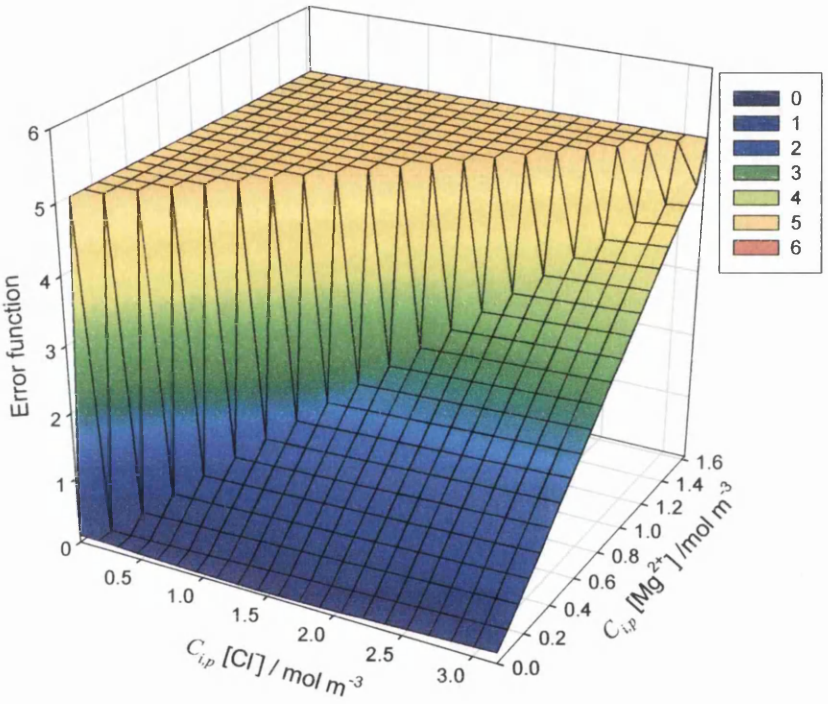

Figure 4.3: The error function for an NaCl:MgCl2 solution.

4.1.3 Required accuracy

The tolerance employed when obtaining convergence of the error function is an important consideration when obtaining a result in the rejection calculation. As the tolerance is reduced, i.e. $f_T \rightarrow 0$, the accuracy of the iteration solution is increased, however, this yields an increase in the computational time. Therefore, as with the desired step-size for integration, an optimisation is required between the desired level

of accuracy and the computational time. Figure 4.4 illustrates the error function tolerance for the NaCl:$MgCl_2$ mixture used in Figure 4.3. If the tolerance of $1x10^{-3}$ is selected, then the percentage error in concentration is 1.3, 2.3 and 2.4 % for Mg^{2+}, Cl^- and Na^+ respectively. If the tolerance is reduced by an order of magnitude to $1x10^{-4}$, then the percentage error in concentration reduces to 0.7, 0.6 and 0.6 % respectively.

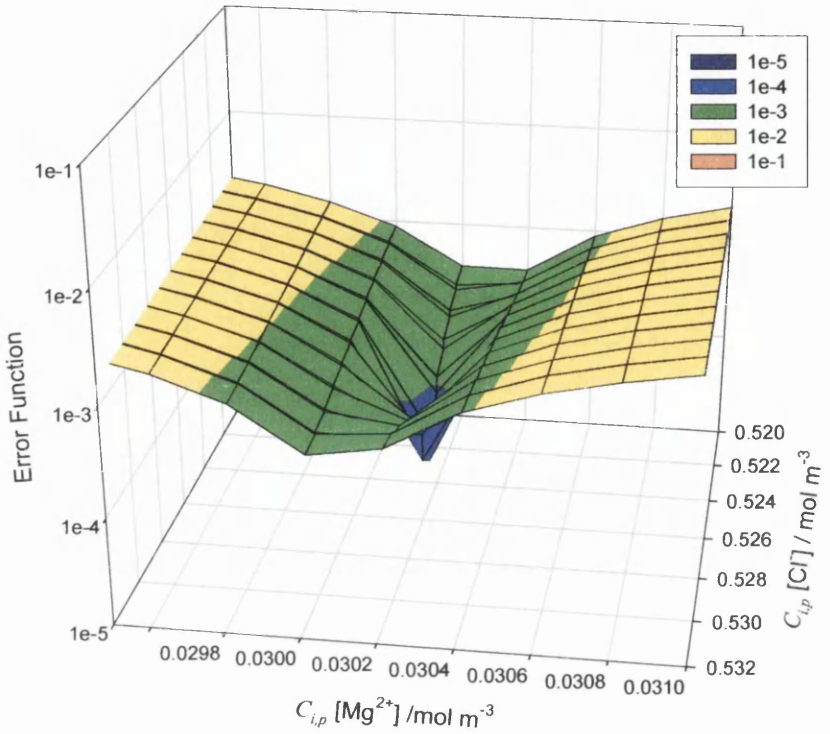

Figure 4.4: Effect of tolerance on the desired accuracy when solving the UDSPM model by iteration.

The improvement in accuracy as the tolerance is decreased is a direct result of the sharp "spike-like" nature of the error function and below a tolerance of $1x10^{-5}$ the bore of the spike is extremely narrow. A tolerance of $1x10^{-12}$ was used in all calculations.

4.2 Comparison of the UDSPM and linearised UDSPM models

The assumption of a linear concentration gradient through the NF pore greatly reduces the computational demands required when solving the UDSPM model, which has obvious benefits when applying the model to real multi-component separations.

However, the characteristics of NF membranes and NF processes vary considerably and so the validity of this assumption must be tested over a wide range of possible NF conditions. Welfoot (2001) tested the validity of the linearisation procedure and concluded that the linearisation of concentration gradients in the transport equations was reasonably valid over the range of NF pore sizes. However, this validation of the linearisation procedure was only made for uncharged solutes and single mono-valent salt systems. In order to apply the linear UDSPM model to real systems there is a need to validate the assumption of linear concentration gradients over a wider range of solutes and solutions to include multi-valent ions and multi-ion systems.

Firstly, a consideration of the reasons why linearisation of the concentration gradients should cause any significant deviation in the model results is required. The linearised transport equation (derived in Chapter 3) gives

$$\frac{\Delta c_i}{\Delta x} = \frac{V}{D_{i,p}}\left[\{K_{i,c} - Y\}c_{i,av} - C_{i,p}\right] - \frac{z_i c_{i,av}}{RT} F \frac{\sum_{i=1}^{n} \frac{z_i V}{D_{i,p}}\left[\{K_{i,c} - Y\}c_{i,av} - C_{i,p}\right]}{\frac{F}{RT}\sum_{i=1}^{n} z_i^2 c_{i,av}} \qquad (4.1)$$

Welfoot (2001) concluded that any deviation of the linearised UDSPM model from the UDSPM model would be directly dependent on the ion-specific group $K_c V/D_p$. All three variables exhibit significant dependence on r_p. However, the effects of the hindrance factors will be greater in small pores and the effect of solvent velocity will be greater in larger pores, so there will be some cancellation in the overall combined effect. As solvent velocity is also dependent on ΔP_e, any significant deviation in the linearised model would be expected at higher values of ΔP_e where the magnitude of $K_c V/D_p$ will be greater. This is in agreement with the calculations presented by Welfoot (2001). In addition to the dependence of linear concentration gradients on r_p the concentration gradients are also dependent on X_d. Therefore, the effects of both r_p and X_d will be considered in this analysis.

4.2.1 Deviation of the Linearised UDSPM model

Deviation between the UDSPM and the linearised UDSPM model must be established as reality and not a simple artefact developed from the numerical techniques employed. The apparent deviation is easily established quantitatively for uncharged solutes as there is a direct analytical result. Consider Eq. (4.1) above and remove the electrical terms to obtain

$$\frac{\Delta c_i}{\Delta x} = \frac{V}{D_{i,p}}\left[\left\{K_{i,c} - Y\right\}c_{i,av} - C_{i,p}\right] \tag{4.2}$$

Re-arrangement of Eq. (4.2) and substitution for the definition of rejection yields (see Appendix A1 for full derivation)

$$R = \frac{1 - \Phi_i\left\{K_{i,c} - Y\right\}}{1 - \frac{1}{2}\Phi_i\left\{K_{i,c} - Y\right\} + \frac{\Phi_i\left\{K_{i,c} - Y\right\}}{Pe}} \tag{4.3}$$

Comparison of this result with that obtained for the UDSPM model [Eq. (3.48)], shows that there is an additional term in the denominator such that as $Pe \rightarrow \infty$, the limiting rejection becomes

$$R_{Lim} = \frac{1 - \Phi_i\left\{K_{i,c} - Y\right\}}{1 - \frac{1}{2}\Phi_i\left\{K_{i,c} - Y\right\}} \tag{4.4}$$

This result differs from the UDSPM model, where $R_{Lim} = 1 - \Phi_i\left\{K_{i,c} - Y\right\}$, and the fact that the linearised UDSPM result differs from the UDSPM is an important result for two reasons. Firstly, this result is mathematically different to that obtained for the UDSPM model, which proves that the results obtained from both models should indeed deviate. Secondly, as the product of the term $0.5\Phi_i K_{i,c}$ is less than unity, the denominator of Eq. (4.4) will always be less than unity. This indicates that the limiting rejection calculated using the linearised UDSPM will always be higher than that obtained for the UDSPM over the range $0 < \lambda < 1$.

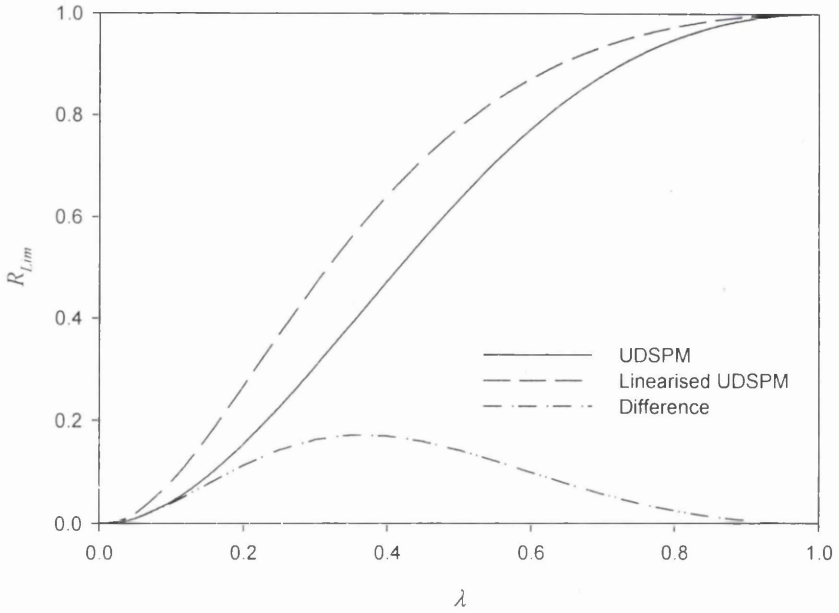

Figure 4.5: Deviation of the linearised UDSPM model for uncharged solutes.

This result is illustrated in Figure 4.5. Interesting to note from Figure 4.5 is that the deviation is not consistent over the range of λ and is largest in the range $0.2 < \lambda < 0.6$ with a maximum deviation of 0.17. This has a significant effect when considering the characterisation of NF membranes as discrepancies between the calculated pore radii obtained from the analysis of uncharged solute rejection with both the UDSPM and linearised UDSPM will be highest for the case of limiting rejection.

A mathematical comparison between the UDSPM and linearised UDSPM is not possible for charged solutes as the transport equations do not reduce to form simple algebraic solutions. However, a qualitative assessment is possible between the results obtained for the minimisation of the error function used for convergence in the iteration procedure. Figure 4.6 illustrates the error function for both the UDSPM and linearised UDSPM for a solution of $MgCl_2$. From Figure 4.6 one can clearly observe that there is indeed a significant deviation between the minimum in the error function calculated for the two models. This result confirms that the two models should also deviate for charged solutes as well as for uncharged solutes. In addition, the permeate concentrations required to calculate the minimum in the error function are less for the linearised UDSPM model than for the full UDSPM. This suggests that the calculated rejection should be higher for the linearised UDSPM model than the UDSPM, similarly to that observed previously for uncharged solutes.

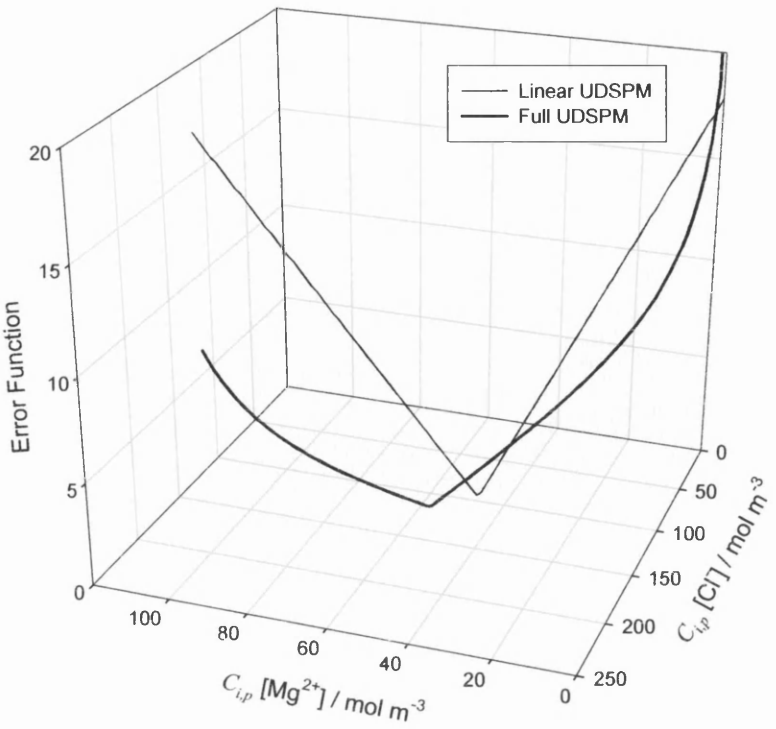

Figure 4.6: The error function for a 100 mol m^{-3} $MgCl_2$ solution from a hypothetical NF membrane (r_p = 1.0 nm, X_d = -1 mol m^{-3}, ε^* = 35, ΔP_e = 0.7 MPa).

4.2.2 Binary salt solutions

Figure 4.7 illustrates the predicted rejection from a hypothetical membrane for an NaCl solution (example of a 1:1 electrolyte). There are no apparent deviations in the predicted rejection values for NaCl with a small pore radius, even when the membrane is highly charged. The agreement between the two models is also good for a large pore radius and a highly charged membrane, although there is a small deviation at ΔP_e > 1.5 MPa. This deviation is approximately 6 % for the uncharged membrane and 10 % for the charged membrane at ΔP_e = 3.0 MPa, the linearised model predicting the higher values in both cases.

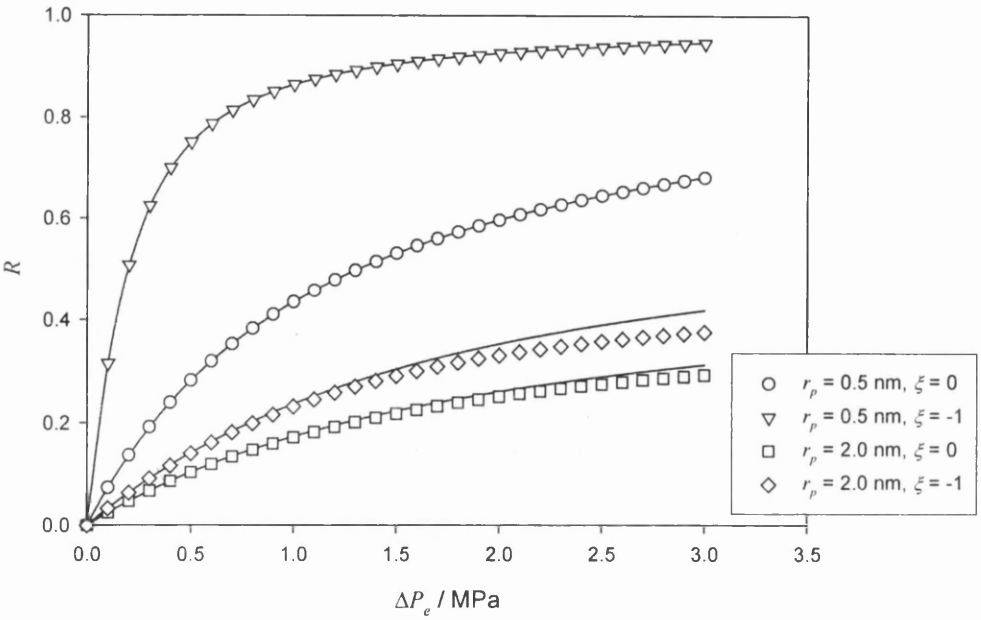

Figure 4.7: Predicted rejection for NaCl with the full UDSPM and linearised UDSPM models. Symbols represent full model, lines are linear model ($\varepsilon^* = 35$).

For purely steric interactions at limiting rejection the deviation from the UDSPM model for Cl^- ($\lambda = 0.06$) is 1.5 %. Therefore, the additional discrepancy must be attributed to charge interactions and the fact that electrolyte rejection is more complex than simple uncharged solute rejection.

Figure 4.8 represents the dimensionless Na^+ ion concentration, normalised using the initial membrane concentration $c_{Na^+}(0)$, through the hypothetical membrane for the calculations presented in Figure 4.7. The corresponding Cl^- ion concentration profiles are not included here because electroneutrality within the pore forces the concentration profiles to be parallel. Figure 4.8 shows excellent linearity at the smaller pore radius and for the highly charged membrane. This linearity justifies the assumption of a linear concentration gradient and explains the excellent agreement between the UDSPM and linearised UDSPM in this region. For the larger pore radius, there is excellent linearity at low values of pressure ($\Delta P_e < 1.0$ MPa), however, slight curvature is apparent at higher pressures and increased curvature is noted for the highly charged membrane. The curvature is only really significant at the highest

pressure and explains the slight deviation between the UDSPM and linearised UDSPM models in this region.

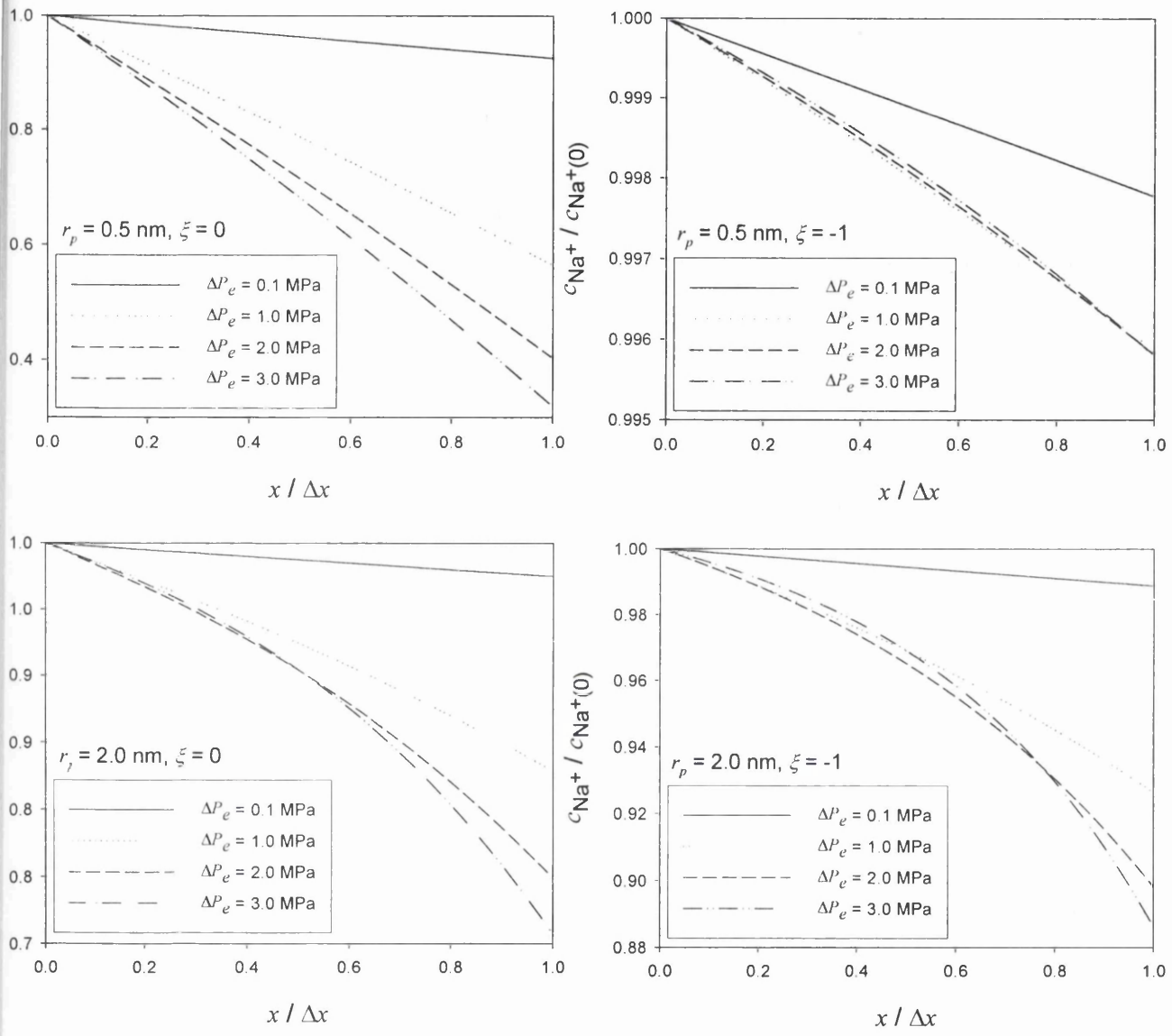

Figure 4.8: The concentration profile of Na^+ ions through the hypothetical membrane for the calculations presented in Figure 4.7.

Figure 4.9 illustrates the predicted rejection from a hypothetical membrane for an Na_2SO_4 solution (example of a 1:2 electrolyte). The rejection profiles at the smaller pore radius calculated from both the UDSPM and linearised UDSPM show excellent agreement. For the larger pore radius, as the pressure is increased (ΔP_e > 1 MPa),

slight deviation between the models is apparent for the uncharged membrane and increased deviation is notable for the highly charged membrane. This deviation is approximately 8 % for the uncharged membrane and 12 % for the charged membrane at ΔP_e = 3.0 MPa, the linearised model predicting the higher values in both cases.

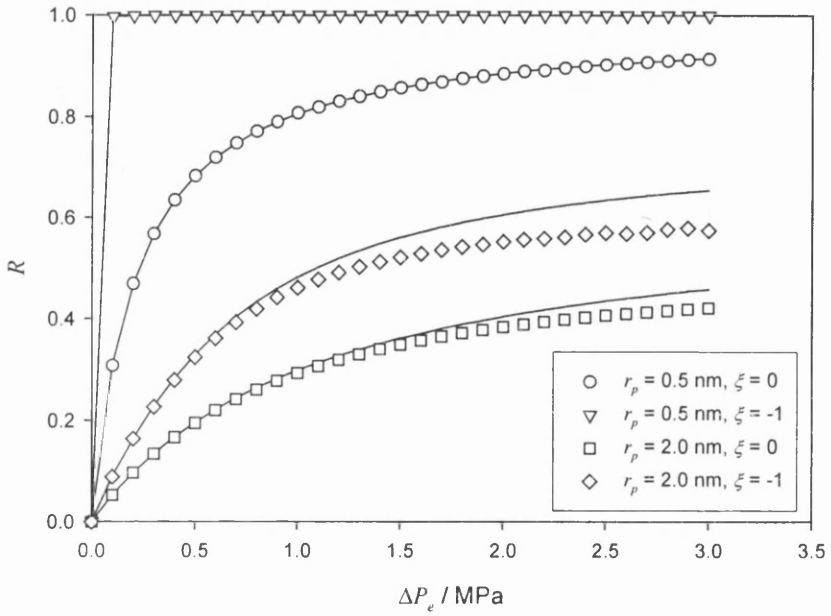

Figure 4.9: Predicted rejection for Na_2SO_4 with the full UDSPM and linearised UDSPM models. Symbols represent full model, lines are linear model (ε^* = 35).

Figure 4.10 illustrates the dimensionless concentration of Na^+ ions through the theoretical membrane corresponding to the calculations presented in Figure 4.9. Figure 4.10 shows excellent linearity at the smaller pore radius for the uncharged membrane. For the highly charged membrane the calculated rejection was close to 1 at all times and, as a direct result, the normalised concentration profile remained close to 1. For the larger pore radius, there is excellent linearity at low values of pressure (ΔP_e < 1.0 MPa), however, slight curvature is apparent at higher pressures and increased curvature is noted for the highly charged membrane. This curvature is only observed at the highest pressures and is significantly increased for the highly charged membrane.

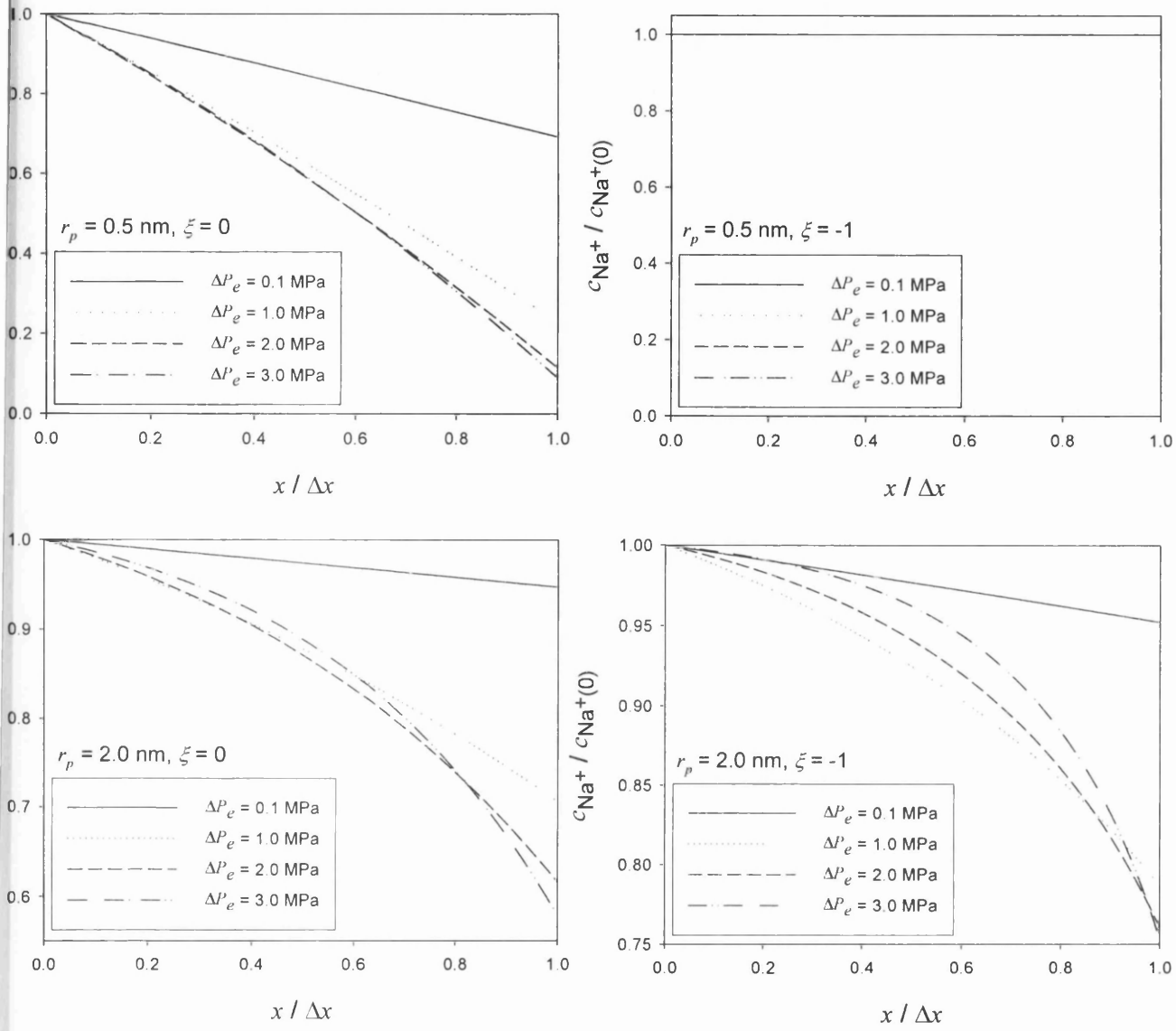

Figure 4.10: The concentration profile of Na^+ ions through the hypothetical membrane for the calculations presented in Figure 4.9.

Figure 4.11 illustrates the predicted rejection from a hypothetical membrane for an $MgCl_2$ solution (example of a 2:1 electrolyte). The rejection profiles at the smaller pore radius calculated from both the UDSPM and linearised UDSPM show excellent agreement. For the larger pore radius, as the pressure is increased (ΔP_e > 1 MPa), slight deviation between the models is apparent for the uncharged membrane, although the deviation is less notable for the highly charged membrane. The deviation is approximately 7 % for the uncharged membrane and 2 % for the charged membrane at ΔP_e = 3.0 MPa, the linearised model predicting a higher value in the

uncharged case and a lower value in the charged case. Interestingly, for both models and charged membranes, the calculated rejection value decreases slightly as the pressure is increased.

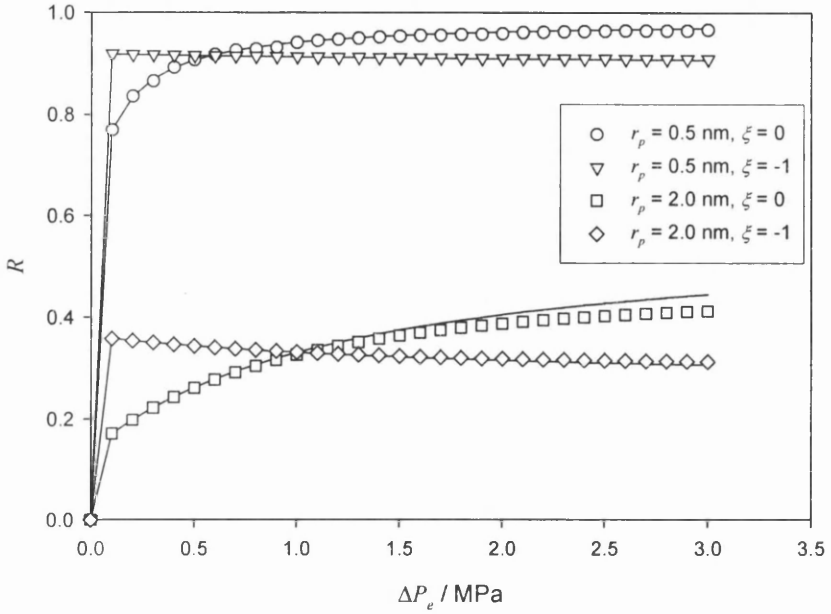

Figure 4.11: Predicted rejection for $MgCl_2$ with the full UDSPM and linearised UDSPM models. Symbols represent full model, lines are linear model ($\varepsilon^* = 35$).

Figure 4.12 illustrates the predicted rejection from a hypothetical membrane for an $MgCl_2$ solution. Figure 4.12 shows linearity at low pressure and slight curvature at higher pressures for the smaller pore radius and the uncharged membrane. For both highly charged membranes the calculated rejection was close to 1 at all times and, as a direct result, the normalised concentration profile remained close to 1. For the larger pore radius, again there is linearity at low pressure and slight curvature is apparent at higher pressures

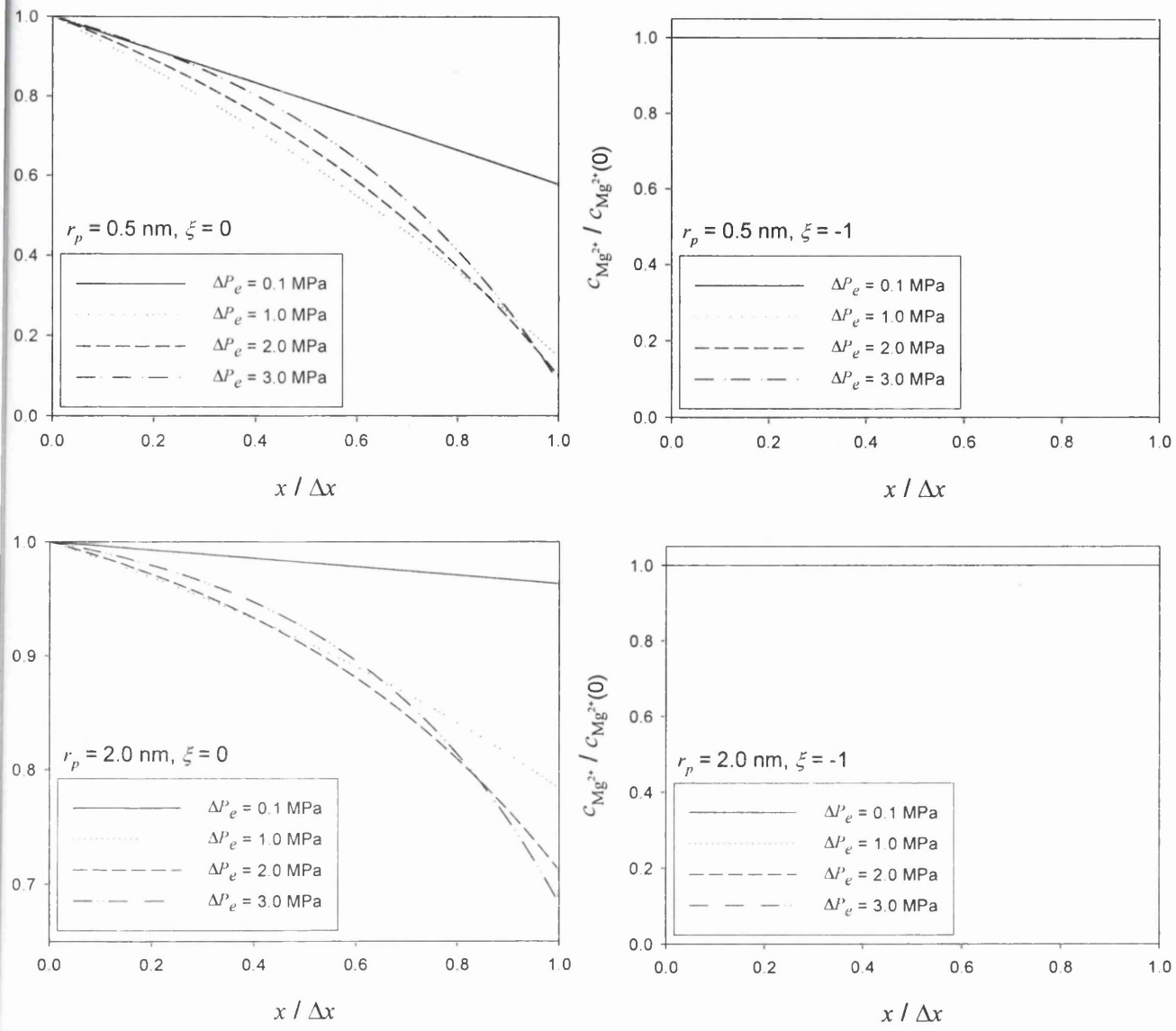

Figure 4.12: The dimensionless Mg^{2+} ion concentration through the hypothetical membrane for the calculations presented in Figure 4.11.

Figure 4.13 illustrates the predicted rejection from a hypothetical membrane for an $MgSO_4$ solution (example of a 2:2 electrolyte). The rejection profiles at the smaller pore radius calculated from both the UDSPM and linearised UDSPM show excellent agreement and both predict rejection values close to 1. For the larger pore radius, as the pressure is increased (ΔP_e > 0.75 MPa), a deviation between both models is apparent. The deviation is approximately 10 % for the uncharged membrane and 12 % for the charged membrane at ΔP_e = 3.0 MPa, the linearised model predicting a higher value in both cases.

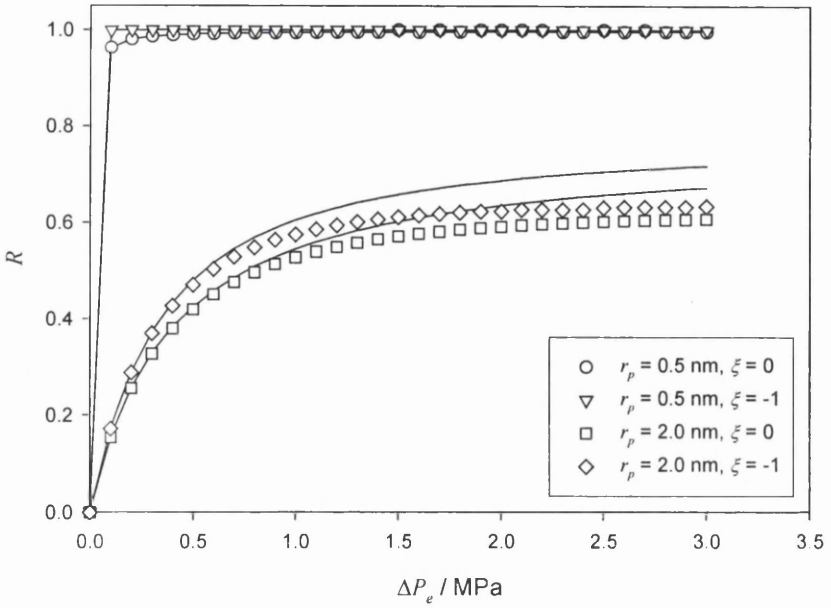

Figure 4.13: Predicted rejection for $MgSO_4$ with the full UDSPM and linearised UDSPM models. Symbols represent full model, lines are linear model ($\varepsilon^* = 35$).

Figure 4.13 illustrates the predicted rejection from a hypothetical membrane for an $MgSO_4$ solution. Figure 4.14 shows linearity at low pressure and slight curvature at higher pressures for the smaller pore radius and the uncharged membrane. For the highly charged membrane, the calculated rejection was close to 1 at all times and, as a direct result, the normalised concentration profile remained close to 1. For the larger pore radius, again there is linearity at low pressure and slight curvature at higher pressures, with the curvature being more apparent for the highly charged membrane.

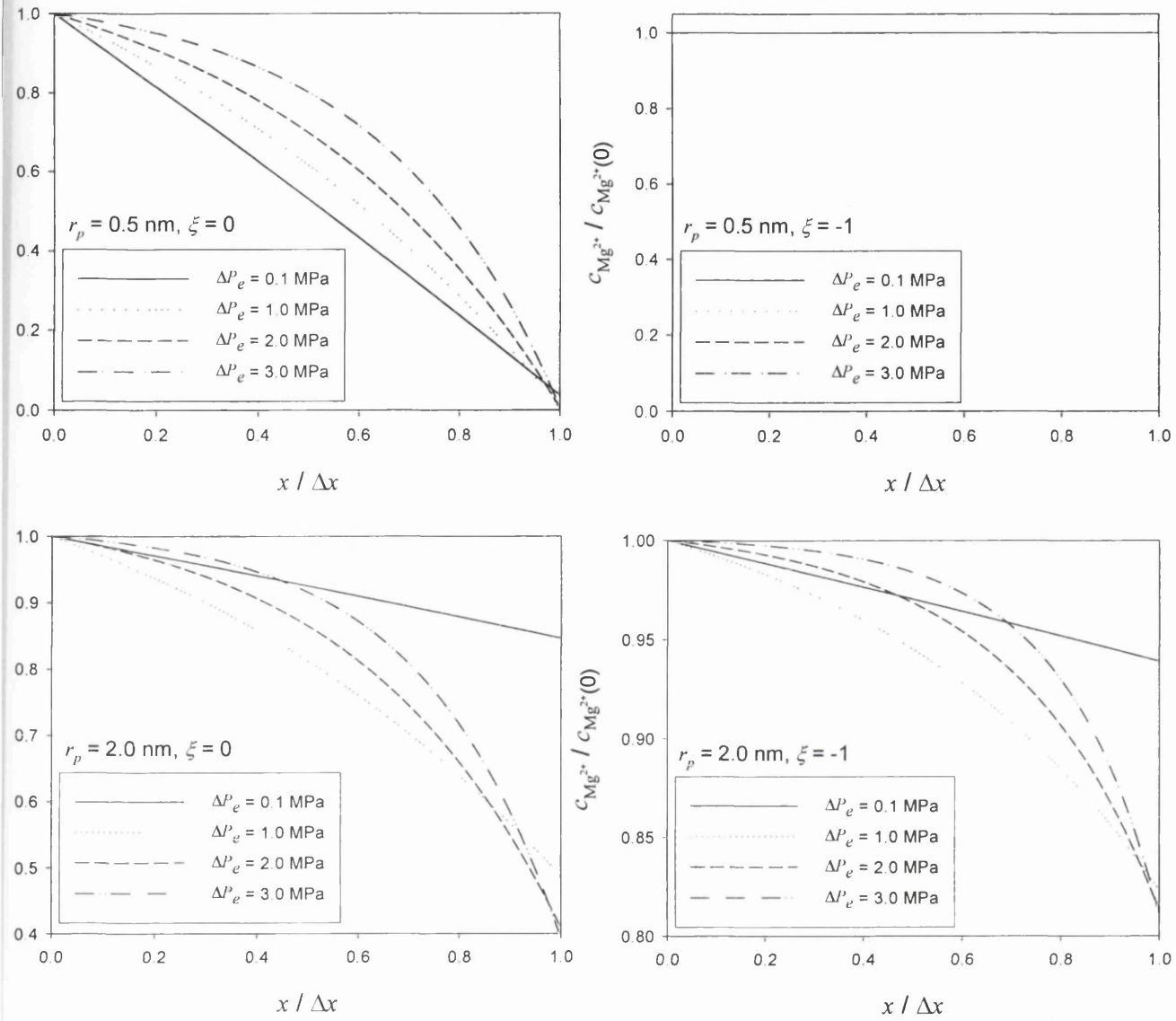

Figure 4.14: The dimensionless Mg^{2+} ion concentration through the hypothetical membrane for the calculations presented in Figure 4.13.

In summary, the linearised UDSPM model tends to over predict the calculated rejection with respect to the UDSPM model at pressures higher than 1 MPa and for large values of pore radius. This deviation tends to be more significant for large highly charged ions. The extent of the deviation for the four salts studied is of further interest. Table 4.1 summarises the deviation between the UDSPM and linearised UDSPM models for r_p = 2.0 nm and ΔP_e = 3 MPa.

Table 4.1: Linear UDSPM deviation at $r_p = 2.0$ nm and $\Delta P_e = 3$ MPa for binary salts.

Salt	Type	Deviation (%)		λ	Steric only (%)	ΔW (J)
		ξ = 0	ξ = -1			x10^{-30}
(Na)Cl	1:1	6	10	0.092	3.4	1.4
$Na_2(SO_4)$	1:2	8	12	0.115	5.0	4.5
$Mg(Cl_2)$	2:1	7	2	0.060	1.5	2.1
(Mg)SO4	2:2	10	12	0.175	9.5	2.9

(x) properties displayed for ion x.

The findings presented in Table 4.1 clearly indicate that the discrepancy between the UDSPM and linear UDSPM are not directly linked to steric phenomenon as there is no correlation between the expected steric deviation and that observed for the uncharged membrane. The largest deviation occurs for the salts Na_2SO_4 and $MgSO_4$ with a charged membrane. In the case of binary salts, the co-ion is more strongly rejected and thus, the overall rejection is dependent only on the co-ion. In this case there is a common co-ion (SO_4^{2-}) and the extent of deviation for both salts is the same, as would be expected. However, for the salts NaCl and $MgCl_2$, again there is a common co-ion but in this case the extent of deviation is not the same. Moreover, the deviation significantly decreases for the Mg^{2+} counter-ion, indicating that there are other interactions occurring. These additional interactions are not a result of steric properties or dielectric phenomenon as the expected deviation is approximately three fold and two fold respectively for the Mg^{2+} ion. Therefore, this reduced discrepancy between the two models must be attributed to either Donnan phenomena or a more complex combination of multiple phenomena.

4.2.3 Ternary salt solutions

Figure 4.15 illustrates the predicted rejection from a hypothetical membrane for a mixture of NaCl:Na_2SO_4 (an example of a 1:1:2 electrolyte) in 1:1 molar ratio. Other ratios of the salt mixture were studied but are not shown to avoid repetition as the trends were the same. Excellent agreement for the predicted rejection from both models was observed for each of the ions at small pore radius. Slight deviation

between the models was observed at the large pore radius for $\Delta P_e > 1.5$ MPa. These observations are analogous to those obtained for binary salt solutions. The discrepancy between the models was 8, 9 and 3 % for the uncharged membrane and 6, 3 and 16 % for the charged membrane for Na^+, SO_4^{2-} and Cl^- respectively, again with the linear model predicting higher values.

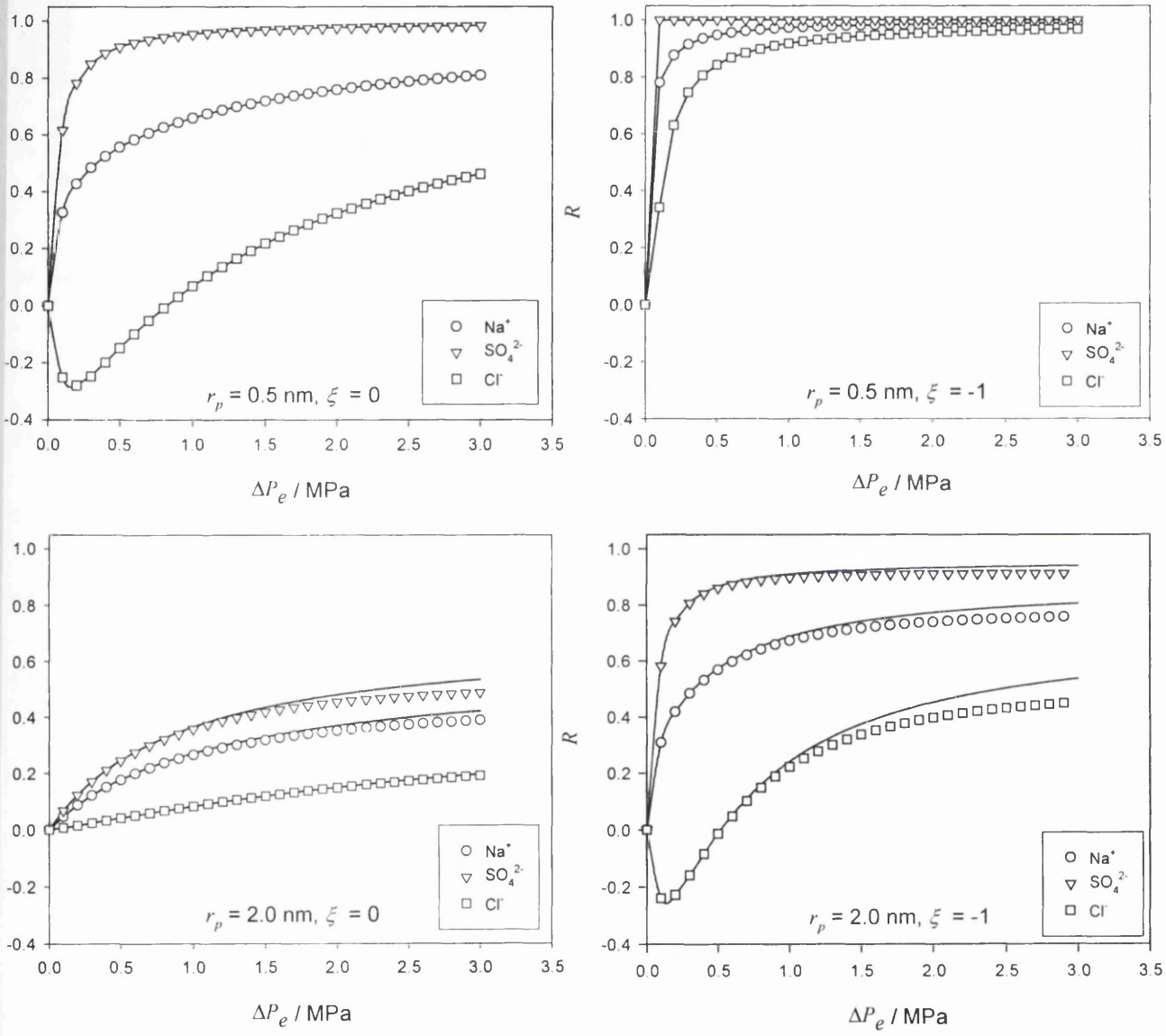

Figure 4.15: Predicted rejection from a hypothetical membrane for a solution of $NaCl:Na_2SO_4$ in a molar ratio 1:1. Symbols represent the full UDSPM model, lines represent the linearised UDSPM model ($\varepsilon^* = 35$).

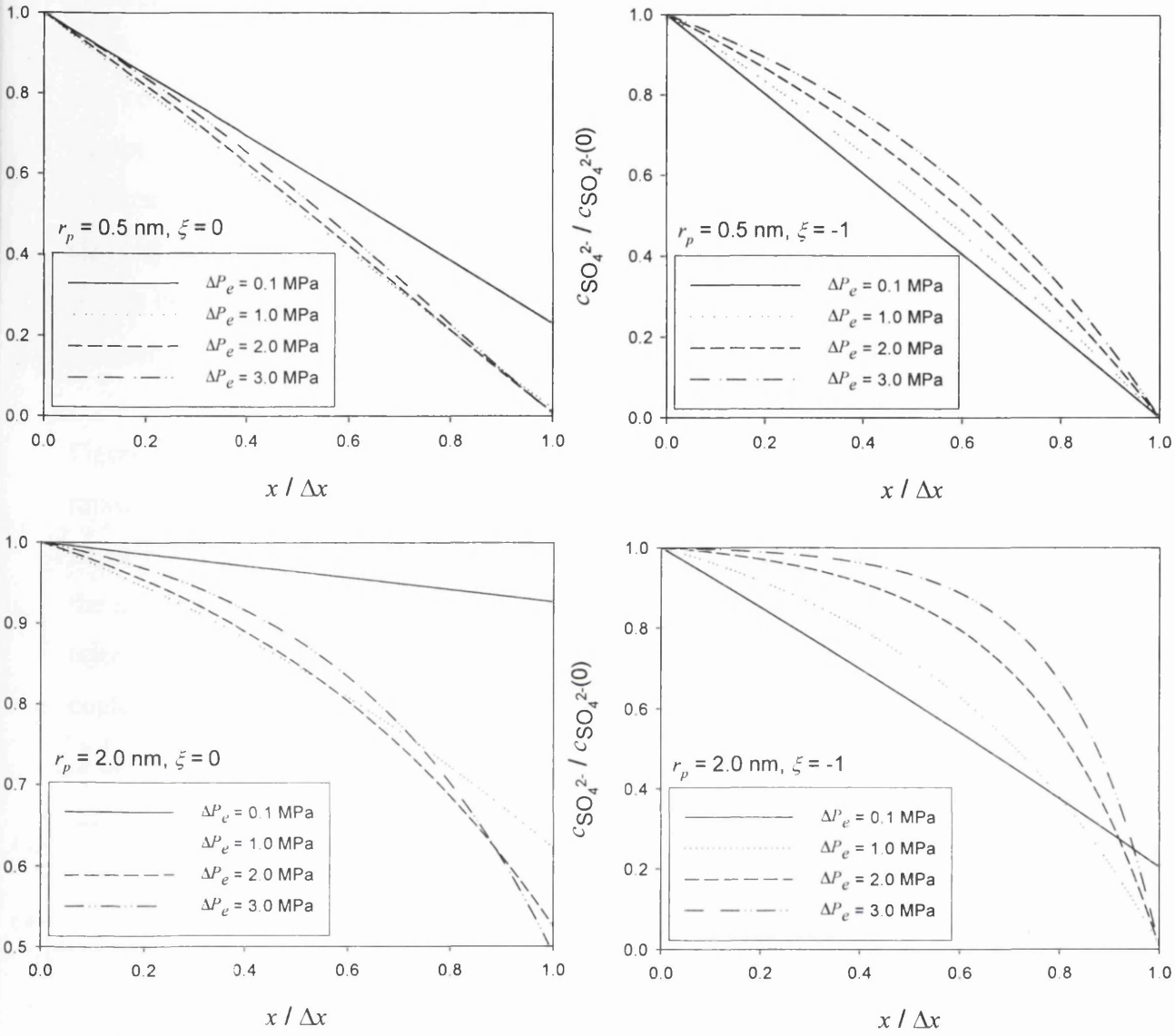

Figure 4.16: The dimensionless SO_4^{2-} ion concentration through the hypothetical membrane for the calculations presented in Figure 4.15.

Figure 4.16 represents the normalised concentration profile of SO_4^{2-} through the membrane for the calculations presented in Figure 4.15. The concentration of SO_4^{2-} has been illustrated as this molecule will dominate the rejection through the membrane. In strict terms each of the ions will have a different profile through the membrane. However, deviations from linearity were more predominant for divalent

ions in binary systems and have been selected here to amplify any possible discrepancy.

The concentration profile for the small pore radius shows slight curvature in all cases except for the lowest pressure (ΔP_e = 0.1 MPa), with the curvature being more apparent for the charged membrane. This trend is also observed for the larger pore size but with greater curvature in each case. The curvature is only really significant for the large pore highly charged membrane at higher pressures and explains the slight deviation between the UDSPM and linearised UDSPM models in this region.

Figure 4.17 illustrates the predicted rejection from a hypothetical membrane for a mixture of Na_2SO_4:$MgSO_4$ (an example of a 1:2:2 electrolyte) in 1:1 molar ratio. Other ratios of the salt mixture were studied but are not shown to avoid repetition as the trends were the same. The small pore radius was omitted in this case as complete rejection was calculated for all but low pressures and no meaningful interpretations could be made.

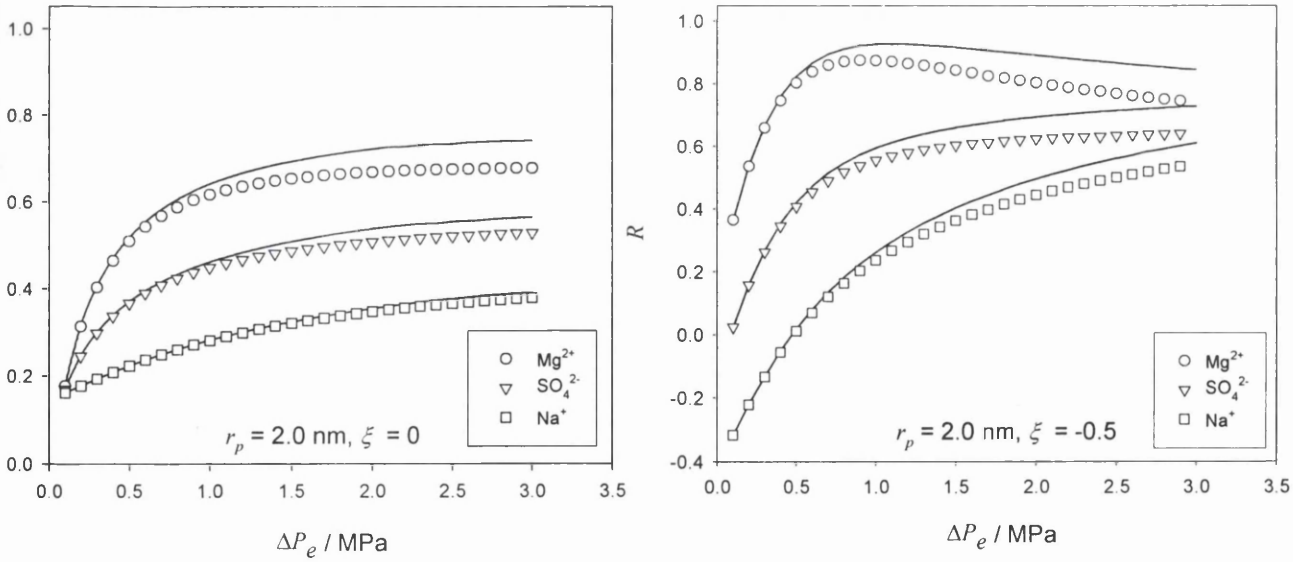

Figure 4.17: Predicted rejection from a hypothetical membrane for a solution of Na_2SO_4:$MgSO_4$ in a molar ratio 1:1. Symbols represent the full UDSPM model, lines represent the linearised UDSPM model (ε^* = 35).

The agreement between both models is good at low pressure (ΔP_e < 1 MPa), at higher pressures the models begin to deviate with the discrepancy being larger for the

charged membrane. The discrepancy between the models was 9, 6 and 3 % for the uncharged membrane and 12, 12 and 11 % for the charged membrane for Mg^{2+}, SO_4^{2-} and Na^+ respectively, again with the linear model predicting higher values.

Figure 4.18 represents the normalised concentration profile of SO_4^{2-} through the membrane for the calculations presented in Figure 4.17. The SO_4^{2-} profile has been illustrated for the same reasons given previously. The uncharged membrane exhibits only slight curvature at the higher pressures (ΔP_e > 2 MPa), with the charged membrane showing increased curvature for all but the lowest pressure.

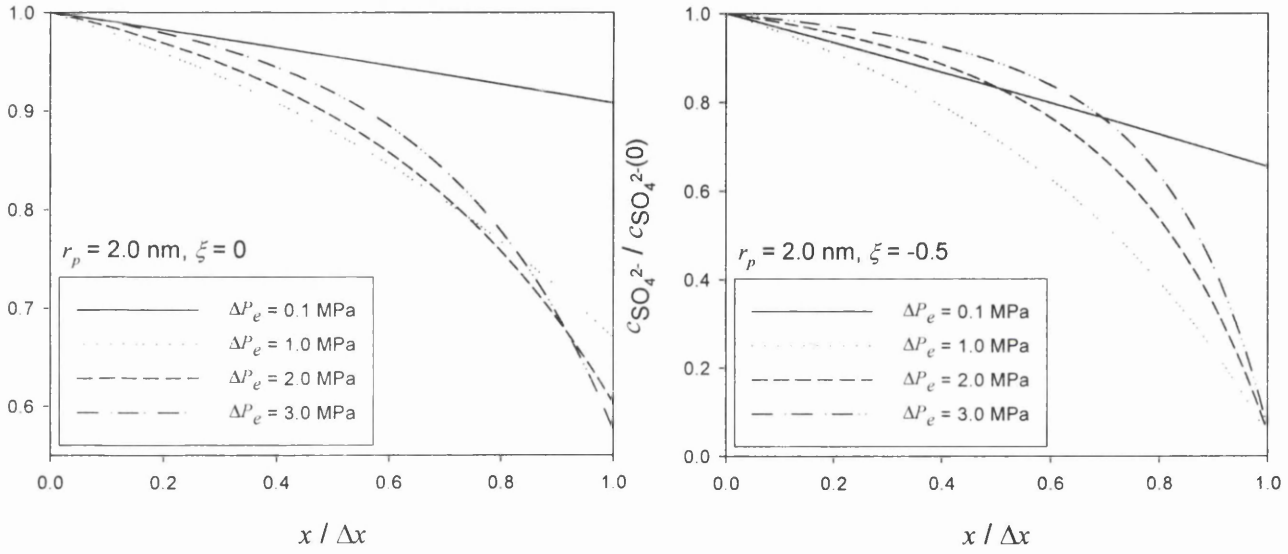

Figure 4.18: The dimensionless SO_4^{2-} ion concentration through the hypothetical membrane for the calculations presented in Figure 4.17.

In summary, the linearised UDSPM model tends to over predict the rejection with respect to the UDSPM model. The over prediction tends to be for the case of large pore radius, highly charged membranes and high pressures. Significantly, the over prediction is greater when two divalent ions are in the solution as opposed to only one, with the average deviation being of the order of 7.5 % and 9 % respectively. Thus, the trends observed for ternary salt solutions are analogous to those observed for binary systems.

4.2.4 Quaternary salt systems

Figure 4.19 illustrates the predicted rejection from a hypothetical membrane for a mixture of NaCl:$MgSO_4$ in a molar ratio 1:1 (example of a 1:1:2:2 electrolyte). Other ratios of the salt mixture were studied but are not shown to avoid repetition as the trends were the same. The small pore radius (r_p = 0.5 nm) was omitted in this case as complete rejection was calculated for all but low pressures and no meaningful interpretations could be made.

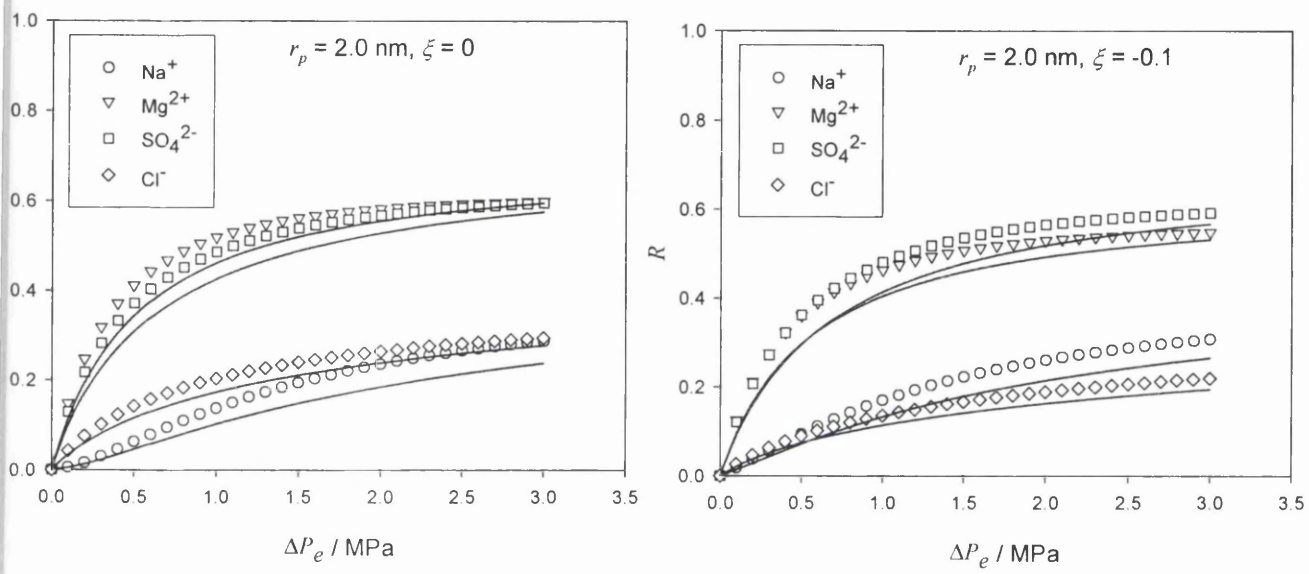

Figure 4.19: Predicted rejection from a hypothetical membrane for a solution of NaCl:$MgSO_4$ in a molar ratio 1:1. Symbols represent the full UDSPM model, lines represent the linearised UDSPM model (ε^* = 35).

The predicted rejection calculated using the linearised UDSPM deviates from the UDSPM prediction for both the charged and the uncharged membrane at all pressure values. Interestingly, the linearised model actually predicts a lower value for rejection in this case, opposite in nature to findings for both binary and ternary systems. The extent of the deviation is 17, 1, 3 and 6 % (average = 6.75 %) for the uncharged membrane and 14, 3, 4 and 12 % (average = 8.25 %) for the charged membrane.

Figure 4.20 represents the normalised concentration profile of SO_4^{2-} through the membrane for the calculations presented in Figure 4.19. The SO_4^{2-} profile has been illustrated for the same reasons given previously. The uncharged membrane exhibits curvature at all pressures except the lowest pressure value (ΔP_e = 0.1 MPa), with the charged membrane showing similar curvature to the uncharged membrane. This curvature explains the deviations observed between the two models and, as the extent of curvature is similar, confirms that the discrepancy between the two models should be of the same order of magnitude as observed.

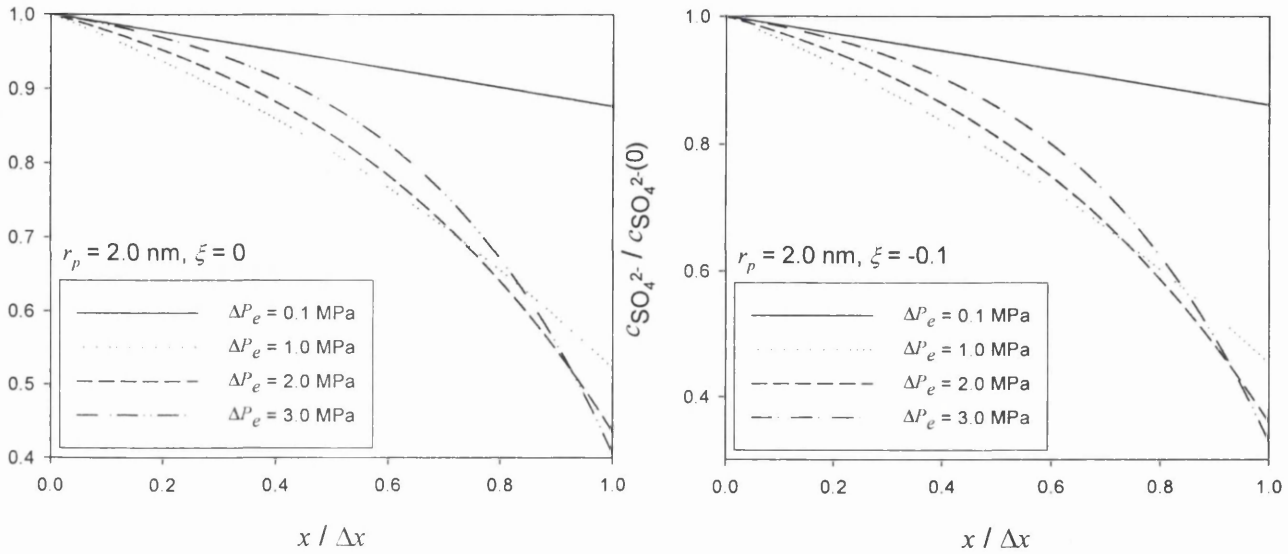

Figure 4.20: The dimensionless SO_4^{2-} ion concentration through the hypothetical membrane for the calculations presented in Figure 4.19.

4.3 Conclusions

An investigation into the numerical techniques required to solve the UDSPM model was made. The effect of step-size on the integration of the transport equations through the membrane was made and little dependence was found. 200 steps was suggested as adequate to produce reliable results. The effect of step-size on the integration over time for the diafiltration concentrations inside the diafiltration vessel was made. Reducing the step-size in this case was found to have a significant influence on the overall result and a time period of less than 5 minutes was suggested adequate to produce reliable results. The initial guesstimate for permeate

concentrations to solve the iteration procedure was found to be of extreme importance. If the initial guesstimate is placed within the invalid electroneutrality zone, no result can be obtained or a meaningless solution will be found. Therefore, the initial guesstimate of concentration must be in the valid concentration region. The solution of the iteration procedure is then obtained by minimisation of the error function. The accuracy of the result is extremely dependent on the tolerance used in this optimisation procedure and a tolerance of $1x10^{-12}$ was recommended to give reliable results.

A comparison was made between the predicted rejection calculated using the UDSPM model and the linearised UDSPM in order to evaluate if there is any discrepancy between the model predictions over a range of NF conditions. A mathematical analysis for uncharged solutes was made and the conclusion was made that the two models should indeed deviate from one another and that this deviation was expected to occur at high pressures. A qualitative comparison was made between the error functions of both models for an NaCl solution, which confirmed that the models should also deviate for charged solutes.

The extent of deviation between the two models was studied over a range of NF conditions for a number of different salt solutions. Generally, the linearised UDSPM was found to over estimate the predicted rejection with respect to the UDSPM. This was the case for both binary and ternary solutions. However, for quaternary systems the linearised UDSPM actually under predicted the rejection. A deviation trend was apparent in that the deviation was greater depending on the level of complexity in the system, i.e. the higher the ion valence or the number of ions in the solution the greater the deviation. Therefore, in real systems, the deviation between the two models could be estimated based upon the ionic solution in question. In all cases studied, the average deviation between the two models was no more than 10 %, which is suitable for engineering purposes. Therefore, the linearised UDSPM can be employed with confidence when predicting higher order systems such as ternary and quaternary ion solutions. This has the advantage over the UDSPM of greatly reducing the calculation complexity and, most importantly, reducing solution time.

5 Comparison of Dielectric Exclusion Mechanisms

In this chapter, the current mechanisms proposed for the description of dielectric exclusion at the surface of NF membranes are discussed. A comprehensive description of each method proposed is given and the individual merits and disadvantages are highlighted. A theoretical and experimental comparison of both models is performed and an overall assessment to evaluate which method is more practical for use in theoretical modelling is made.

5.1 Introduction to dielectric exclusion

The transport of ions through charged membranes has been extensively discussed in relation to reverse osmosis [Kedem and Katchalsky (1963), Spiegeler and Kedem (1966), Dressner (1972)] and more recently for NF [Tsuru *et al.* (1991), Bowen and Mohammad (1998), Garba et al. (1999), Hagmeyer and Gimbel (1998), Deen(1987)]. In this work, all electrostatic interactions occurring at the membrane interface were based solely on Donnan equilibrium theory [Donnan (1911)]. In order to obtain a more detailed understanding of the complex phenomena involved in ion partitioning at nanopores additional interactions between the ion and the local pore environment must be taken into account. Unfortunately, in pores of only a few molecular diameters, continuum theory begins to break down and the solvent physical properties such as dielectric constant, viscosity and diffusivity are not strictly homogeneous and can be very different from that of the bulk solution. When an ion passes from the bulk solution into the nanopore, the ion-solvent and ion-membrane interactions give rise to further rejection mechanisms known collectively as dielectric exclusion.

Dielectric exclusion in itself is an extremely complex mechanism and in order to fully understand and appreciate this phenomena a detailed knowledge of particle electrochemistry and molecular dynamics is required. Descriptions for dielectric exclusion arising from such theories are mathematically extensive and computationally demanding. Also, to add yet further complexity to this challenging area of interest, the relationship between Donnan equilibrium and dielectric exclusion

is non-trivial [Dukhin *et al.* (1988), Yaroshchuk (2000)]. For these reasons, the intention of this work is not to further develop dielectric exclusion theory. The aim is however, to provide the reader with an understanding of the complex issues involved and to compare and contrast two existing practical methods for the determination of dielectric effects for NF membranes.

5.1.1 Dielectric exclusion, first method

Dielectric exclusion may arise when an ion interacts with the bound electrical charges (induced by the ion) at interfaces between materials of different dielectric constant, in this case the membrane matrix and the solvent. The ion polarises the two different media according to their relative dielectric constant and a distribution of polarisation charge builds up at the discontinuity surface. For a single planar interface the interaction can be described formally as an interaction with a fictitious charge or *image*, the phenomena being described is then usually referred to as polarisation or image forces (see Figure 5.1). If we consider a membrane matrix of dielectric constant ε_m, and a solvent of dielectric constant ε_s, the nature of the image force will be repulsive if $\varepsilon_m < \varepsilon_s$ for both cations and anions [Israelachvili (1991)]. Also, the extent of the image force is dependent on the magnitude of the ion valence, the ratio $\varepsilon_m/\varepsilon_s$ and the pore geometry [Dukhin *et al.* (1988), Yaroshchuk (2000)]. Effectively, for the same pore size, the energy barrier is higher for spherical pores with respect to cylindrical pores and lower for plane geometry (slit-like pores).

The argument developed thus far has only considered the electrostatic interactions between a single ion and the polarisation layer of the NF membrane. However, at least two other electrostatic effects must be taken into account. Both ion-ion interactions and the effective membrane charge density have a natural tendency to screen the ion-polarisation charge interactions. The low electrolyte concentration expected within the nanopore has a Debye length typically much larger than the pore size, this leads to a weak screening effect of the image forces. Also, the polymeric matrix exhibits a small ion-exchange capacity and consequently provides a weak screening effect. Therefore, to evaluate the magnitude of the energy barrier arising from these dielectric partitioning effects an approximate relationship was proposed by

Bandini and Vezzani (2003) taken from recent reviews of dielectric exclusion theory by Yaroshchuk (2000).

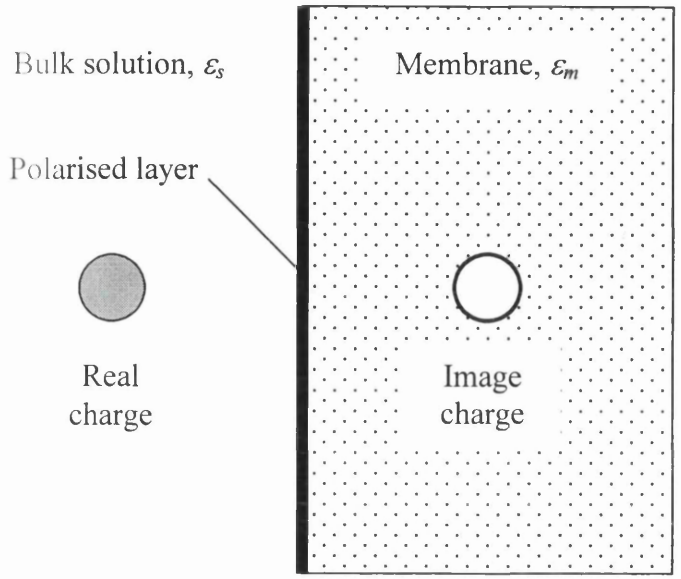

Figure 5.1: Ionic charge interaction at the membrane surface.

The energy barrier ΔW_{DE}, is calculated under the following assumptions:

- the ion is located on the axis line of symmetry,
- continuous membrane and solvent dielectric constant,
- ion-ion interactions in the bulk and pore solvent phase are described through the classical Debye-Huckel theory, and
- a slit-like pore geometry.

The dielectric theory described by Yaroshchuk (2000) was successfully adapted and introduced into the original DSPM model to form the DSPM&DE model [Vezzani and Bandini (2002)], in which the average pore diameter coincides with the slit height and the effect of water structure on dielectric constant inside the pore ε_p, is taken into account (i.e. when $\varepsilon_p < \varepsilon_s$), yielding the following expression for the dielectric exclusion partitioning effect at the feed side membrane interface

$$\Delta W_{DE} = W(0^+) - W(0^-) = r_B \left\{ \kappa(0^-) - \frac{\varepsilon_s}{\varepsilon_p} \left[\kappa(0^+) + \frac{1}{r_p} \ln\left(1 - \gamma e^{-2r_p \kappa(0^+)}\right) \right] \right\} \qquad (5.1)$$

Where r_B is the Bjerrum radius, κ is the inverse Debye length, (0^-) and (0^+) represent locations just outside the membrane and just inside the membrane respectively, with

$$r_B = \frac{F^2}{8\pi\varepsilon_s RTN_A} \tag{5.2}$$

$$\gamma = \frac{1-\varepsilon_m/\varepsilon_p}{1+\varepsilon_m/\varepsilon_p} \tag{5.3}$$

$$\kappa(0^-) = F\sqrt{\frac{2I(0^-)}{\varepsilon_s RT}} \tag{5.4}$$

$$\kappa(0^+) = F\sqrt{\frac{2I(0^+)}{\varepsilon_p RT}} \tag{5.5}$$

Where I is the ionic strength. For simplification purposes and practical use of the model, the dielectric constant of the pore solution was assumed equal to the bulk (i.e. $\varepsilon_p = \varepsilon_s$) and the membrane material dielectric constant equal to 3.

Eq. (5.1) represents two different mechanisms of interaction. The first two terms in brace parenthesis represent the difference between the reciprocal of the Debye lengths, calculated inside the membrane pore and in bulk solution. The parameter κ is derived from the Debye-Huckel theory and is related to the logarithm of the activity coefficient for a single charged ion and describes the changing ion-ion interactions between the bulk and pore solutions. The third term describes the ion-polarization energy of interaction [Dunkin *et al.* (1988)]. This energy is strongly dependent on pore radius, $\varepsilon_m/\varepsilon_p$ and the Debye length of the pore solution. Moreover, the exponential term describes the typical decay of any screened electric field; $2r_p\kappa(0^+)$ is the decay rate [Israelachvili (1991)] and is the ratio between pore size and Debye length inside the membrane pore. Finally, the screening is relevant when the dimensionless parameter $2r_p\kappa(0^+) \sim 1$, i.e. for large pores or concentrated solutions.

The dependence of the dimensionless energy term [Eq. (5.1)] on the dielectric constant ratio $\varepsilon_m/\varepsilon_s$, for different values of pore radius is illustrated in Figure 5.2.

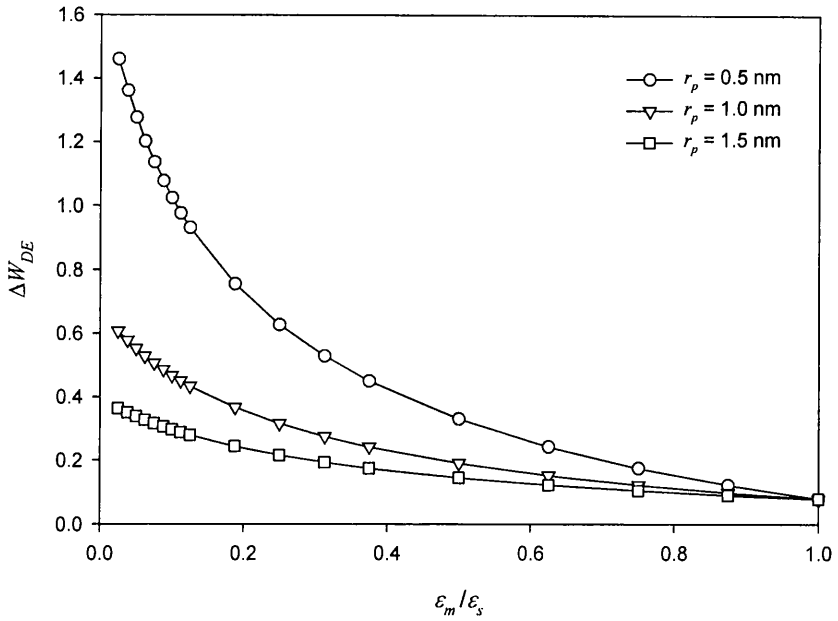

Figure 5.2: Dependence of the dimensionless dielectric energy term on the ratio of membrane to solvent dielectric constant.

As expected, the dielectric effect is more prevalent when the dielectric ratio between the materials is small. Moreover, the effect is significantly increased for the very narrow pores expected in the NF range. In the limiting region as $\varepsilon_m/\varepsilon_p \rightarrow 1$, all the curves for different values of pore radius converge to a common non-zero value. The dielectric ratio describes the interaction of the ion-polarisation charges and as $\varepsilon_m/\varepsilon_p \rightarrow 1$, $\gamma \rightarrow 0$. However, the reciprocal of the Debye lengths remains and is independent of pore radius.

Figure 5.3 illustrates the dependence of ΔW_{DE} on electrolyte concentration inside the membrane pore and the pore radius. As the pore size is increased, the ion-polarisation charge interactions decrease and the overall energy tends to the ion-ion interaction term, which is much smaller in magnitude as $\kappa(0^+) \rightarrow \kappa(0^-)$. For very narrow pores (typically less than 1 nm), the contribution of the ion-polarisation interactions are significantly higher than the ion-ion interactions, even when $\kappa(0^+)$ is increased (i.e. higher concentration inside the membrane) causing an enhanced screening effect.

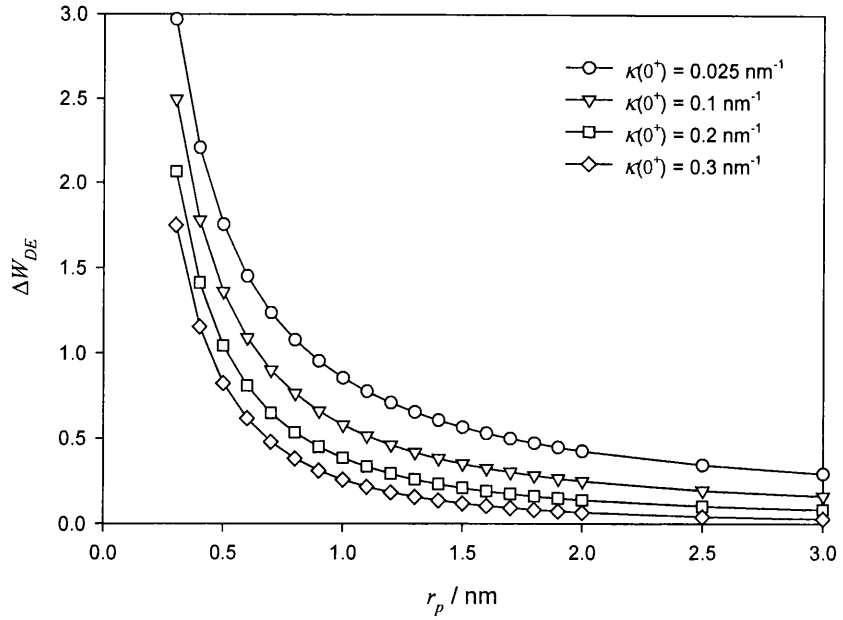

Figure 5.3: Dependence of the dimensionless energy term on pore radius.

5.1.2 Dielectric exclusion, second method

The second mechanism of dielectric exclusion is attributed to the variation in the solvent dielectric constant inside the membrane pore. Under normal circumstances the bulk solvent will be a continuous dielectric media. However, in the discrete molecular structure of a nano-pore, the liquid medium can no longer be considered as a simple structureless continuum. The confined geometry of the pore causes localised structuring of the liquid medium and the individual liquid molecules become ordered into discrete but diffuse layers. This re-orientation of the solvent within the constrained geometry causes a local reduction in the dielectric constant. The energy associated with the transfer of an ion from the bulk solvent into the reduced dielectric media of the nano-pore is always positive, i.e. there is an energy barrier to overcome and naturally there will be a tendency for the ion to remain in the bulk solvent. The localised solvent structure is particularly sensitive to three things [Israelachvili (1987)]: the surface roughness, the rigidity or fluidity of the solvent, and the presence of other components. These structural forces are commonly referred to as ion-solvation forces or, when the solvent is water, hydration forces.

The earliest model for the determination of the ion-solvation forces was proposed by Born (1920). His model considered the thermodynamic cycle associated with the transfer of an ion from vacuum to a polarisable solvent. The free energy was calculated as the sum of the work terms arising from discharging the ion in vacuum, transferring the neutral species to the solvent, recharging the species in the solvent, and restoring the aligned solvent dipoles to their precharging state after the ion is returned to the vacuum. Born considered only the electrostatic energy terms in this process. Also, his model was based upon the assumption of a structureless dielectric continuum with an infinitely dilute concentration of hard ion spheres. Defining the solvation energy as W and the dielectric constant of the bulk solvent as ε_s

$$\Delta W_i = \frac{z_i^2 e^2}{8\pi\varepsilon_o}\left[\frac{1}{a_v} - \frac{1}{a_s\varepsilon_s}\right] \tag{5.6}$$

Where ε_o is the permitivity of free space, z is the ion valence, e is electron charge, a_v and a_s represent the ion radii in vacuum and solvent respectively. Born calculated free energies by setting a_v and a_s equal to the Pauling crystallographic radius. Note that ΔW_i has dimensions of energy, J, and as a result, to compare this value with the dimensionless energy term obtained from Eq. 5.1 there must be a division by the product k_BT, i.e.

$$\frac{\Delta W_i}{k_BT} = \Delta W_{DE} \tag{5.7}$$

Where k_B is the Boltzmann constant. Unfortunately, the predicted values of ΔW obtained from the Born model are far greater in magnitude than those obtained experimentally, with errors greater than 50 % in some cases [Bontha and Pintauro (1992)]. For this reason, many attempts have been made to modify the original Born theory. The majority of these attempts have focussed either on the value selected for ion radii or the value used for the solvent dielectric constant. Latimer *et al.* (1939) suggested the addition of 0.85 Å for cations and 0.1 Å for anions to the crystallographic radius of the ions in vacuum and solution, this modification showed some success in the prediction of ΔW for alkali metals and univalent ions.

Noyes (1962) recognised that the strong electric field around an ion in solution will align the solvent dipoles and lower the dielectric constant of the solvent surrounding the ion, the value for ΔW was then calculated using an effective solvent dielectric constant. Although the modifications suggested above have made improvements to the original Born equation, they are essentially empirical corrections which lack a physiochemical basis. Other attempts to modify the original Born theory were made by Stokes (1964), Rashin and Honig (1985), Abraham and Liszi (1978).

The first case where Born theory has been applied to porous membranes was given by Parsegian (1969). If the Born model is rearranged to account for an ion of radius a_s passing from bulk solvent into a cylindrical membrane pore of dielectric constant ε_p

$$\Delta W_i = \frac{z_i^2 e^2}{8\pi\varepsilon_o a_s}\left[\frac{1}{\varepsilon_p} - \frac{1}{\varepsilon_s}\right] \qquad (5.8)$$

Thus, in order to calculate the magnitude of dielectric exclusion partitioning using the Born theory, an estimate of the pore dielectric constant is required. The dielectric constant of the solvent phase inside a nanopore is a matter of great debate. Booth (1951) derived an expression for the change in dielectric constant within a pore by taking into account the permanent dipoles and dipole-dipole interactions of the solvent species. However, this expression was also dependent on the radial potential gradient across the pore. In the case of small pores (as in NF) the radial potential distribution is small and can be neglected [Bowen *et al.* (1997), Wang *et al.* (1995)]. Therefore, this expression was not considered here. Bowen and Welfoot (2002) proposed an expression that assumed that the change in solvent dielectric properties within the pore could be attributed to a single layer of orientated solvent molecules. This assumption is similar to that taken by Abraham and Lizzi (1978) and was found to be a reasonable approximation for large univalent ions [Bontha and Pintauro (1992)]. If the dielectric constant of the orientated solvent layer is ε^*, the variation in average pore dielectric constant is calculated on a geometric basis

$$\varepsilon_p = \varepsilon_s - 2(\varepsilon_s - \varepsilon^*)\left(\frac{d}{r_p}\right) + (\varepsilon_s - \varepsilon^*)\left(\frac{d}{r_p}\right)^2 \qquad (5.9)$$

Where d is the thickness of the orientated solvent layer (d = 0.28 nm for water). The value of the parameter ε^* is obtainable from experimental salt rejection data at the membrane isoelectric point or from experimental salt rejection at high concentration if the membrane exhibits no isoelectric point [Welfoot (2001)].

The dependence of the solvation energy barrier on the pore dielectric constant is illustrated in Figure 5.4. Ionic hydrodynamic (Stokes) radii have been used in all calculations, which lessen the errors in the Born approach. As expected, the profile for the solvation energy is linear with respect to $1/\varepsilon_p$ and is inversely proportional to the ionic radius of the species in question. Also, ΔW_i is dependent on the square of the ion valence, thus, the larger the ion and the more strongly charged, the greater the magnitude of the dielectric partitioning. This effect is clearly demonstrated by Na^+ and SO_4^{2-}, with the solvation energy being more than double for the latter.

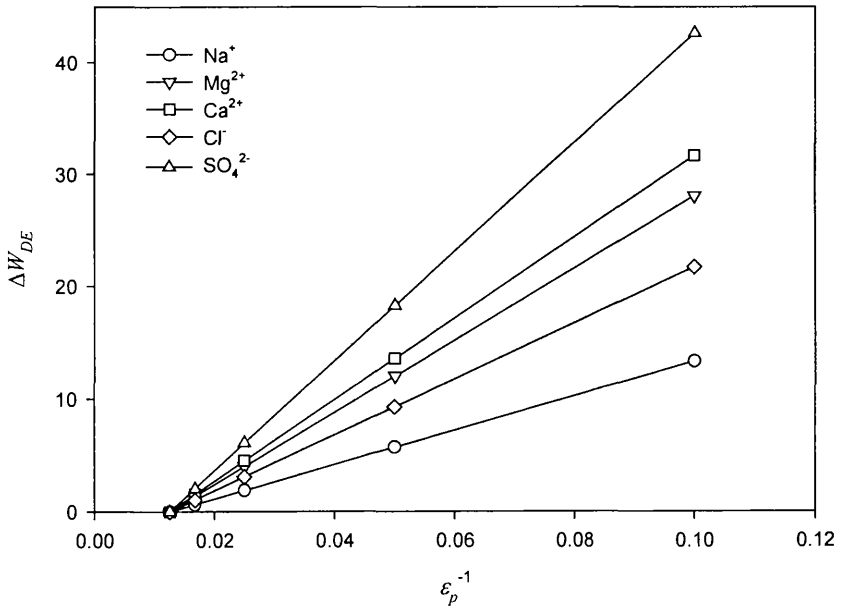

Figure 5.4: The dependence of the dielectric energy on the pore dielectric constant.

Figure 5.5 illustrates the dependence of the pore dielectric constant on the pore radius for various values of ε^*. One can clearly observe that as the confinement within the pore increases (i.e. $r_p \rightarrow 0$), the pore dielectric constant becomes decreased. This effect becomes especially significant below a pore radius of ~ 0.8 nm (in the NF range). Also, as the dielectric constant of the orientated solvent layer decreases, the

deviation of the pore dielectric constant from that of the bulk further increases. Both effects contribute to an increase in the magnitude of the ion solvation energy increasing the dielectric partitioning. The effects of ion solvation described here are not included in the DSPM&DE model as the assumption is made that the pore solvent dielectric constant is equal to that of the bulk.

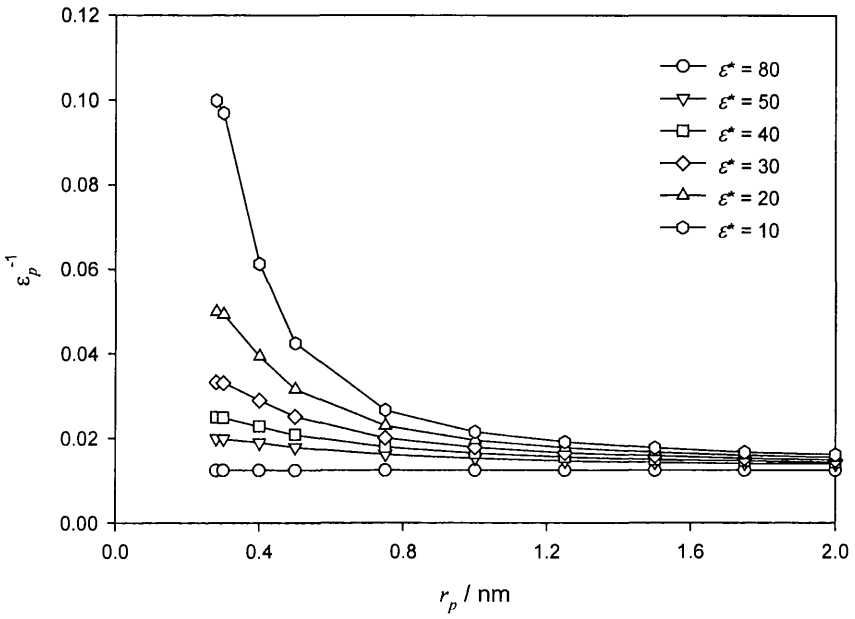

Figure 5.5: The dependence of the pore dielectric constant on the pore radius.

5.2 Results and discussion

For the comparison of the different mechanisms for dielectric exclusion a two-fold approach was taken. Firstly, partitioning coefficients and ion rejection were evaluated theoretically for constant model parameters. Secondly, the results from independent fitting of the same experimental data were analysed and the magnitude of the partitioning coefficients evaluated.

5.2.1 Theoretical comparison

In order to study the different partitioning mechanisms involved in NF, a common basis for analysis was established. In addition to dielectric partitioning, the

parameters affecting electrolyte rejection are: pore radius (r_p), electrolyte concentration (C_b), dimensionless effective membrane charge density (ξ) and Peclet number (Pe). The latter two are defined as

$$\xi = \frac{X_d}{C_f} \tag{5.10}$$

$$Pe = \frac{J_V \Delta x}{D_e} = \frac{r_p^2}{8\eta D_e} \Delta P_e \tag{5.11}$$

where D_e is the harmonic mean type hindered diffusivity of the ion as suggested by Cussler (1995).

$$D_e = \frac{|z_1| + |z_2|}{\frac{|z_1|}{D_{2p}} + \frac{|z_2|}{D_{1p}}} \tag{5.12}$$

The above-mentioned parameters completely define the transport and separation phenomena involved in the presented models for NF. Thus, once the salt and concentration are defined, pore radius specifies the steric partitioning effects, ξ expresses the magnitude of the effective membrane charge density and defines the Donnan partitioning term and finally, Peclet number provides an estimation of the transport phenomena (i.e. driving forces – pressure or volume flux) occurring inside the membrane pore.

By defining a value for the Peclet number [Eq. (5.11)], there is no longer a requirement to specify the value of the effective membrane thickness, Δx. Also, the effects of viscosity on the ion diffusivity and the volume flux across the membrane can be disregarded. If we now introduce Peclet number [Eq. (5.11)] and define $d\bar{x} = dx / \Delta x$ with $\bar{x} \in [0,1]$, then the extended Nernst-Planck equation [Eq. (3.18) or Eq. (3.43)] can be rearranged to give

$$\frac{dc_i}{d\bar{x}} = \left\{ \frac{1}{D_{i,p}} \left[K_{i,c} c_i - C_{i,p} \right] - z_i c_i \left[\frac{\sum_{i=1}^{n} \frac{z_i}{D_{i,p}} \left[K_{i,c} c_i - C_{i,p} \right]}{\sum_{i=1}^{n} z_i^2 c_i} \right] \right\} PeD_e \qquad (5.13)$$

Where $dc_i / d\bar{x}$ is the concentration gradient of the solute i across the membrane. This result is analogous to that obtained by either the DSPM&DE or the UDSPM models. The viscosity correction factor for hindered diffusion to account for the enhanced viscosity inside the membrane pore then becomes:

$$D_{ip}^{*} = \frac{\eta_o}{\eta} D_{ip} \rightarrow D_e^{*} = \frac{\eta_o}{\eta} D_e \qquad (5.14)$$

where η_o is the bulk solution viscosity and η is the enhanced viscosity due to pore confinement. Note that the effects of enhanced viscosity cancel when introduced into Eq. (5.13). The overall partitioning coefficients were defined as

$$\Gamma_i = \frac{c_i}{C_i} = \Phi_i Exp\left(-\frac{z_i F}{RT} \Delta\psi_D \right) Exp\left(-\Delta W_{DE} \right) = \Phi_i \Gamma_{Di} \Gamma_{DEi} \qquad (5.15)$$

Thus, starting from the same basis, the main difference between the two models (DSPM&DE and UDSPM) lies in the description of the dielectric phenomena considered for the equilibrium partitioning coefficient. Consequently, when maintaining the above mentioned parameters (r_p, C_b, ξ, Pe) constant, the dielectric effects over a wide range of conditions for NF can be investigated theoretically. In this work, values for the above mentioned parameters typical of those for NF membrane applications were considered:

- pore radius, r_p = 0.5 and 1.0 nm.
- feed concentration, C_b = 1 and 10 mol m^{-3}.
- dimensionless membrane charge, ξ = -0.1, -1 and –10 (membranes considered as negatively charged).
- Peclet number, Pe = 0.01 → 5.

In the following Figures and Tables calculated results are reported in order to compare the two model predictions for the contributions to dielectric exclusion. The rejection for single salt solutions for selected values of the four membrane parameters are plotted as a function of the Peclet number. Tabulated values for the partitioning coefficients, defined according to Eq. (5.15), are reported for the feed-membrane interface. In particular, attention is focussed on the Donnan and dielectric terms. The steric partitioning coefficients (Φ_i) are not reported as there is no difference between the values calculated from either model. For the DSPM&DE model, the results reported are calculated using the *integral* version of the transport equations, in which the potential gradient is considered constant over the membrane thickness [Bandini and Vezzani (2003)]. For the UDSPM model, the results reported are calculated using the linearised version of the transport equations, in which the concentration gradient is considered linear over the membrane thickness [Eq. (3.58)], note that the parameter Y was omitted from the calculations to maintain consistency.

The results obtained for NaCl (1:1 electrolyte) are reported in Table 5.1 and illustrated in Figure 5.6. A value of $\varepsilon^* = 30$, typical of an NF membrane [Welfoot (2001)], was used in the calculations. As expected, the rejection of NaCl increases with Pe number and reducing pore size. The selectivity is predicted higher for the UDSPM with respect to the DSPM&DE model over the entire range of Peclet number, with the UDSPM predicting a high limiting rejection (even in the case of r_p = 1 nm). In addition, the increased Donnan partitioning coefficient for the counter-ion (and relative decrease for the co-ion) for highly charged membranes is a well known behaviour directly related to the Donnan equilibrium and is not qualitatively affected by the introduction of dielectric phenomena. Moreover, the DSPM&DE curves illustrate dependence on electrolyte concentration, this dependence was negligible in the case of the UDSPM for the concentration and membrane charge range studied.

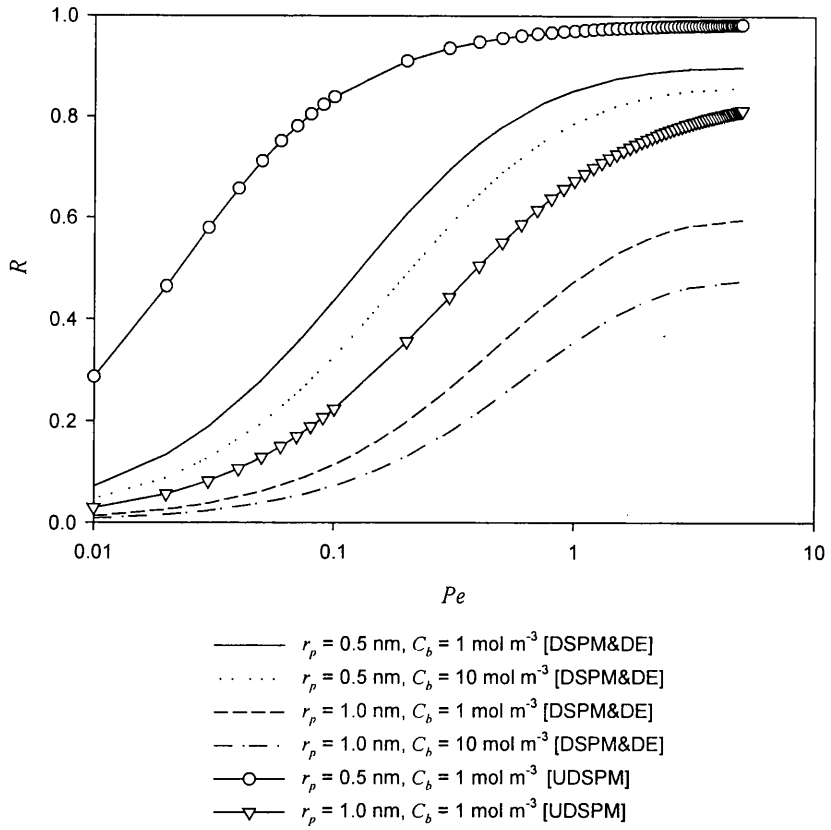

Figure 5.6: Predicted rejection for NaCl versus Peclet number.

The higher rejection predicted by the UDSPM was a result of the lower values calculated for the dielectric partitioning coefficients (especially for Cl^-) with respect to those from the DSPM&DE. The low value for the chloride partitioning coefficient corresponds to a small concentration of Cl^- inside the membrane and, with respect to pore electroneutrality, a lower concentration of Na^+. Thus, the predicted rejection will be higher for the UDSPM. The DSPM&DE has no dependence on ion size for any given ion. However, there is a dependence on ion valence, thus, the dielectric term is the same for the cation and anion in the case of symmetrical salts. All significant differences between the rejections predicted by the models are not a result of differences in the calculated Donnan terms as the results from both models are comparable for each concentration and dimensionless membrane charge (except in the case 10 mol m^{-3}, ξ = -1). Additionally, the dependence of ion concentration and membrane charge on screening the ion polarisation charges is evident from the values reported in Table 5.1. The larger the screening effect (resulting from an increase in concentration or membrane charge), the greater the dielectric partitioning coefficient,

i.e. the energy of interaction is lower. This behaviour is more evident for larger pore radii in which the distribution coefficients tend to unity.

Table 5.1: Model parameters for NaCl. No background – UDSPM model, shaded background – DSPM&DE model.

r_p	0.5 nm				1.0 nm			
C_b	1 mol m^{-3}		10 mol m^{-3}		1 mol m^{-3}		10 mol m^{-3}	
ξ	-0.1	-1	-0.1	-1	-0.1	-1	-0.1	-1
Γ_D [Na^+]	2.00	17.0	2.00	17.0	1.10	3.60	1.10	3.60
Γ_D [Cl^-]	0.50	0.058	0.50	0.058	0.95	0.28	0.95	0.28
Γ_D [Na^+]	2.01	10.3	1.75	6.71	1.23	2.99	1.20	2.47
Γ_D [Cl^-]	0.498	0.0974	0.572	0.149	0.811	0.334	0.835	0.405
Γ_{DE} [Na^+]	0.14		0.14		0.44		0.44	
Γ_{DE} [Cl^-]	0.052		0.052		0.29		0.29	
Γ_{DE}	0.199	0.247	0.281	0.386	0.547	0.579	0.714	0.756

Table 5.2: Model parameters for $CaCl_2$. No background – UDSPM model, shaded background – DSPM&DE model.

r_p	0.5 nm				1.0 nm			
C_b	1 mol m^{-3}		10 mol m^{-3}		1 mol m^{-3}		10 mol m^{-3}	
ξ	-0.1	-1	-0.1	-1	-0.1	-1	-0.1	-1
Γ_D [Ca^{2+}]	36.0	340	36.0	340	1.90	7.90	1.90	7.90
Γ_D [Cl^-]	0.17	0.054	0.17	0.054	0.72	0.35	0.72	0.35
Γ_D [Ca^{2+}]	225	517	84.1	86.8	4.81	8.57	2.60	3.67
Γ_D [Cl^-]	0.0667	0.0440	0.109	0.107	0.456	0.342	0.620	0.522
Γ_{DE} [Ca^{2+}]	0.010		0.010		0.14		0.14	
Γ_{DE} [Cl^-]	0.052		0.052		0.29		0.29	
Γ_{DE} [Ca^{2+}]	1.49E-03	5.67E-03	4.60E-03	0.0350	0.106	0.156	0.320	0.455
Γ_{DE} [Cl^-]	0.196	0.274	0.260	0.433	0.570	0.628	0.752	0.821

The results obtained for $CaCl_2$ (2:1 electrolyte) are reported in Table 5.2 and illustrated in Figure 5.7. The predicted rejection for the UDSPM is remarkably higher than that of the DSPM&DE for values of $Pe < 0.5$ and for $r_p = 1$ nm. The difference

between Γ_D and Γ_{DE} for the Ca^{2+} ion predicted by the two models is significant for the case of the small pore, low concentration and weakly charged membrane.

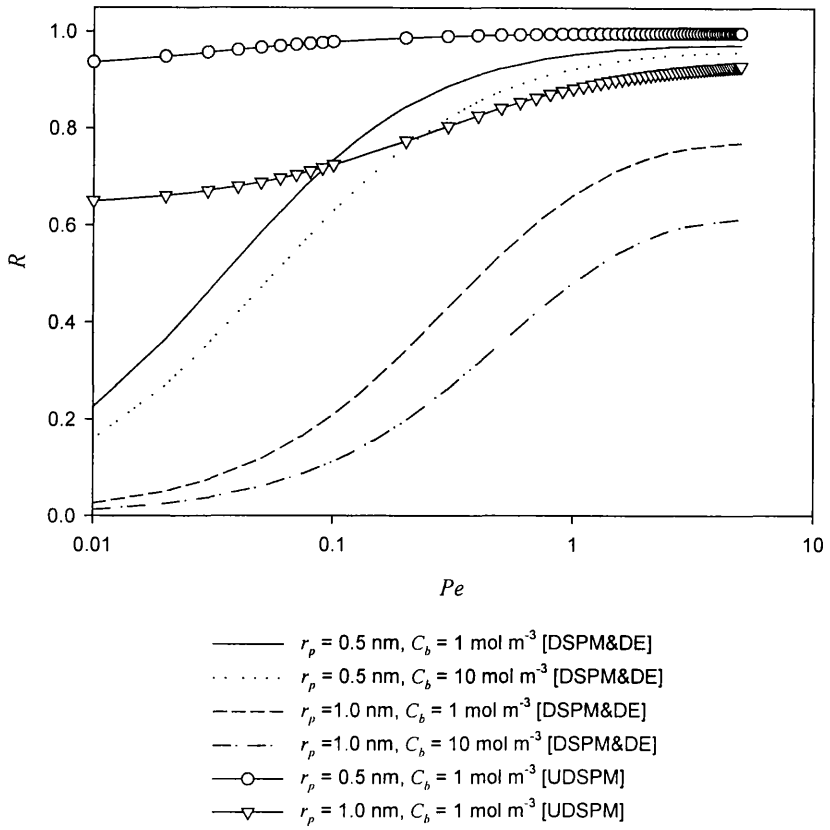

Figure 5.7: Predicted rejection for $CaCl_2$ versus Peclet number.

The Donnan potential calculated from the DSPM&DE with respect to the UDSPM is higher. This is caused by the larger values of the solvation energy predicted by the Born model, which significantly reduces the calcium concentration inside the membrane pore and increases the rejection. The values for Γ_D predicted by the DSPM&DE do not increase to the same extent as that for the UDSPM for an increase in membrane charge density. For a 2:1 electrolyte and a negatively charged membrane, the rejection normally increases with an increase in membrane charge density. Thus, for the DSPM&DE model, there is effectively a compensation between charge density and dielectric partitioning: if the membrane charge density increases, by increasing ξ, the Donnan potential is also expected to increase (reducing Γ_D) as in the case of the UDSPM. However, for the DSPM&DE model, the Donnan potential remains reasonably constant for an increase in charge density, while the energy of dielectric interaction (ΔW) is lowered due to the screening effect of membrane charge

on image forces. Finally, the ratio between the partitioning coefficients of Ca^{2+} and Cl^- predicted for the DSPM&DE with respect to the UDSPM are greater for r_p = 0.5 nm and 1 mol m^{-3}. However, this ratio reduces as the pore radius and electrolyte concentration are increased (i.e. Γ_{DE} increases). Similar behaviour would be expected for Na_2SO_4 filtration across a positively charged membrane.

The results obtained for Na_2SO_4 (1:2 electrolyte) are reported in Table 5.3 and illustrated in Figure 5.8. The calculated rejections for Na_2SO_4 are very similar for both models, especially for r_p = 0.5 nm, for which the UDSPM curve is roughly intermediate to the equivalent DSPM&DE curves.

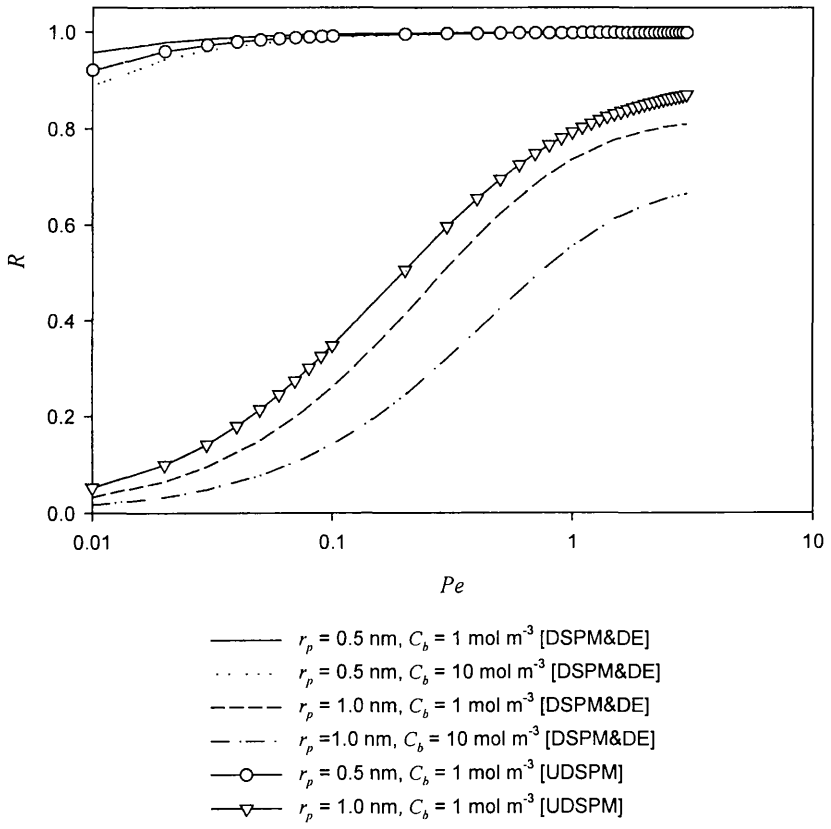

Figure 5.8: Predicted rejection for Na_2SO_4 versus Peclet number.

The Donnan term (Γ_D) for the sulphate ion at ξ = -0.1 is larger in magnitude than that for the sodium ion, while the opposite occurs for ξ = -1. This indicates that the Donnan potential is positive for the low charged membrane (typical of positively charged membranes) and negative for the high charged membrane (typical of

negatively charged membranes). For low charged membranes, steric partitioning tends to promote the concentration of small ions, while the dielectric effect arising from image forces enhances the concentration of monovalent ions and the dielectric effect arising from ion solvation enhances the concentration of large monovalent ions. Therefore, for the case of sodium and sulphate ions, the sulphate ion is drastically rejected. However, the pore solution (rich in Na^+ ions) has to maintain electroneutrality and develops a small positive Donnan potential at the pore interface to counter balance the excess sodium ions inside the membrane pore. A similar situation, opposite in nature, will occur qualitatively for $CaCl_2$ in slightly positively charged membranes.

Table 5.3: Model parameters for Na_2SO_4. No background – UDSPM model, shaded background – DSPM&DE model.

r_p	0.5 nm				1.0 nm			
C_b	1 mol m^{-3}		10 mol m^{-3}		1 mol m^{-3}		10 mol m^{-3}	
ξ	-0.1	-1	-0.1	-1	-0.1	-1	-0.1	-1
$\Gamma_D[Na^+]$	0.880	8.70	0.880	8.70	0.590	1.80	0.590	1.80
$\Gamma_D[SO_4^{2-}]$	1.30	0.0130	1.30	0.0130	2.90	0.330	2.90	0.330
$\Gamma_D[Na^+]$	0.703	5.22	0.607	3.59	0.579	1.43	0.733	1.26
$\Gamma_D[SO_4^{2-}]$	2.02	0.0367	2.71	0.0777	2.98	0.492	1.86	0.626
$\Gamma_{DE}[Na^+]$	0.14		0.14		0.44		0.44	
$_{DE}[SO_4^{2-}]$	2.10E-03		2.10E-03		0.073		0.073	
$\Gamma_{DE}[Na^+]$	0.180	0.240	0.213	0.349	0.551	0.556	0.725	0.699
$_{DE}[SO_4^{2-}]$	1.06E-03	3.31E-03	2.05E-03	0.0149	0.092	0.0958	0.276	0.238

Therefore, starting from different descriptions of dielectric phenomena and making reasonable assumptions to simplify the mathematical effort, the conclusion is made that the theoretical behaviour of both models is in qualitative agreement in the typical range of parameters influencing NF.

5.2.2 Experimental comparison

In order to gain a quantitative assessment between the two models and their performance against real NF processes a comparison was made through the fitting of

measured solute rejection across the Desal-5 DK membrane. For the DSPM&DE model the fitting procedure is analogous to that described by Bandini and Vezzani (2003) as Procedure C, except for non-symmetrical salts for which the simplified version of the model is not valid. In these cases, the *integral* version of the model was used. For both models, the effective membrane pore radius is assessed through the rejection data for uncharged solutes, described in Section (3.2.2.3).

Based on the experimental rejection data for glycerol (MW 92 Da) and glucose (MW 180 Da), the effective membrane pore radius was determined as r_p = 0.45 nm for the UDSPM model and r_p = 0.48 nm for the DSPM&DE model. The slight discrepancy in the two values is due to the hypothesis made for the solvent velocity profile inside the pore. For the UDSPM a parabolic profile is considered and for the DSPM&DE a constant velocity profile across the pore is considered. This has a small effect on the description of the hindered convection coefficient, $K_{i,c}$, and causes the slight deviation in the value for pore radius.

Having established the pore radius, the other structural parameters required for characterisation of the membrane active layer are obtained through the fitting of experimental data for salt solutions. For the DSPM&DE the effective membrane thickness, Δx, is required and for the UDSPM the dielectric constant in the confined oriented solvent layer, ε^*, is required. In the present work, only single salt solutions of NaCl, $MgCl_2$ and Na_2SO_4 are considered. With reference to aqueous NaCl solutions, the estimated values of the parameters required were Δx = 25.0 μm and $\varepsilon^* = 31$.

The results for the fitting the experimental data for the three salts are illustrated in Figures 5.9, 5.10 and 5.11 and the calculated values for the effective membrane charge density and partitioning coefficients are tabulated in Tables 5.4, 5.5 and 5.6. Again, the steric partitioning coefficient was omitted as the value is effectively the same for both models.

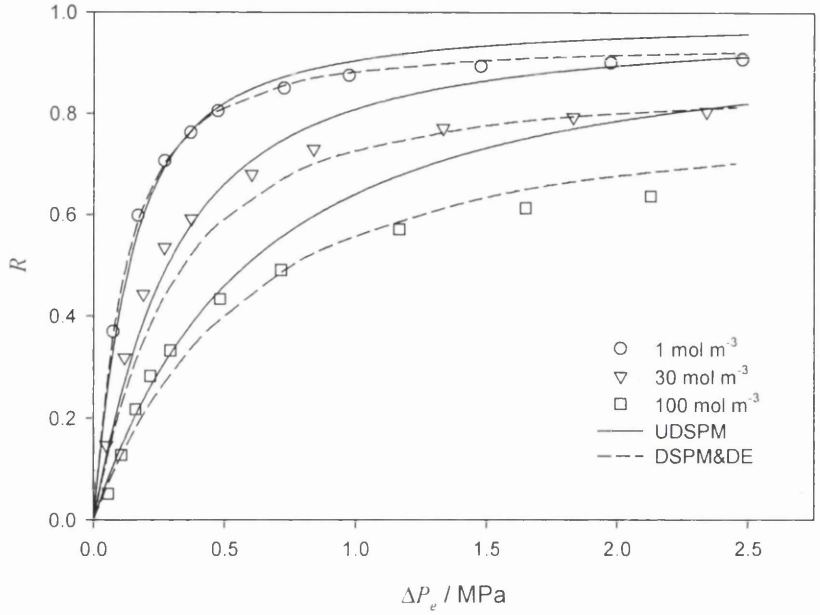

Figure 5.9: Comparison of model best fit parameters for NaCl.

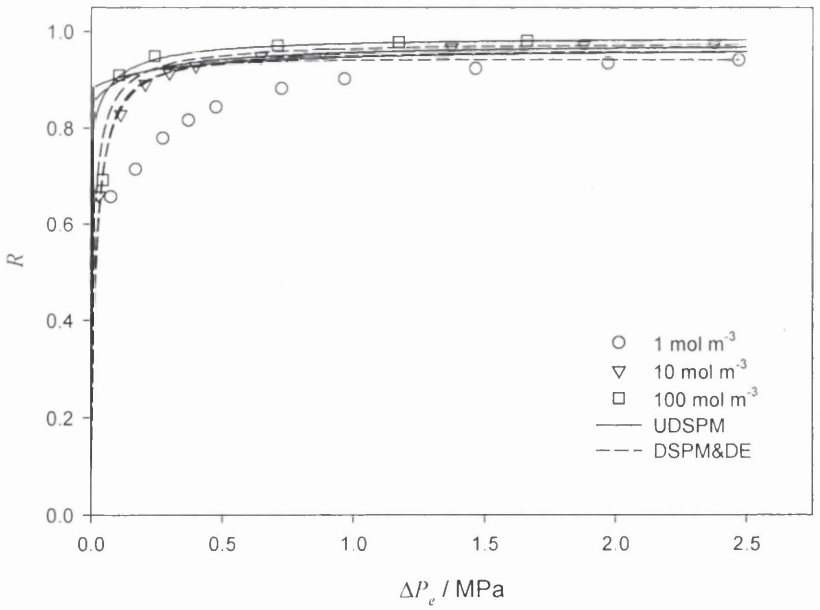

Figure 5.10: Comparison of model best fit parameters for $MgCl_2$.

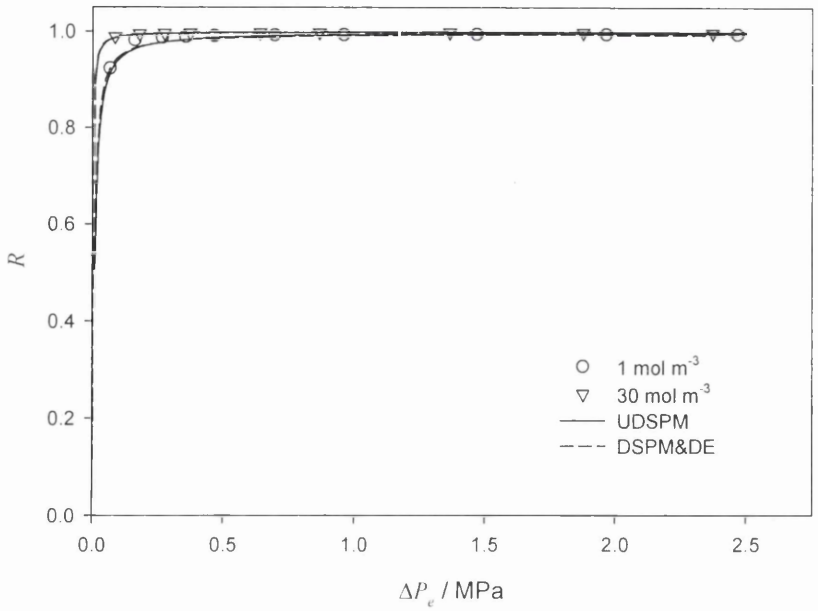

Figure 5.11: Comparison of model best fit parameters for Na_2SO_4.

Table 5.4: Model parameters for best fit of experimental NaCl rejection data. No background – UDSPM model, shaded background – DSPM&DE model.

C_b, mol m^{-3}	1.44	3.73	11.0	37.6
ξ_{UDSPM}	-0.35	-0.29	-0.19	-0.16
$\xi_{DSPM\&DE}$	-0.41	-0.46	-0.51	-0.77
$\Gamma_D[Na^+]$	8.20	7.00	4.60	3.90
$\Gamma_D[Cl^-]$	0.12	0.14	0.22	0.26
$\Gamma_D[Na^+]$	5.28	5.05	4.49	4.67
$\Gamma_D[Cl^-]$	0.19	0.20	0.22	0.21
$\Gamma_{DE}[Na^+]$	0.12			
$\Gamma_{DE}[Cl^-]$	0.04			
Γ_{DE}	0.215	0.254	0.321	0.462

Table 5.5: Model parameters for best fit of experimental $MgCl_2$ rejection data. No background – UDSPM model, shaded background – DSPM&DE model.

C_b, mol m^{-3}	1.25	11.8	100
ξ_{UDSPM}	-0.35	-0.29	-0.16
$\xi_{DSPM\&DE}$	-0.80	-0.12	-0.040
$\Gamma_D[Mg^{2+}]$	71.0	41.0	18.0
$\Gamma_D[Cl^-]$	0.12	0.16	0.23
$\Gamma_D[Mg^{2+}]$	891	168	82.0
$\Gamma_D[Cl^-]$	0.0335	0.0771	0.110
$\Gamma_{DE}[Mg^{2+}]$	0.012		
$\Gamma_{DE}[Cl^-]$	0.040		
$\Gamma_{DE}[Mg^{2+}]$	4.36E-03	4.05E-03	4.27E-03
$\Gamma_{DE}[Cl^-]$	0.256	0.252	0.255

The agreement between the models and the experimental rejection data for NaCl and Na_2SO_4 was good, however, for the $MgCl_2$ data the agreement is poor. The rejection behaviour of $MgCl_2$ is similar to that of $CaCl_2$ with the Desal-5 DK membrane ($CaCl_2$ rejection with the Desal-5 DK membrane was reported by Bandini [Bandini and Vezzani(2003)]) and increases with increasing concentration. To describe this behaviour, the dimensionless membrane charge, ξ, has to decrease (in absolute value) for more concentrated salt solutions. This is in agreement with the values reported in Table 5 for $MgCl_2$ obtained from both the DSPM&DE and UDSPM models. The dimensionless charge density varies between – 0.009 and – 0.80 for both models over the entire range of salts and salt concentrations, thus justifying the use of the values assumed in the theoretical comparison.

The fitted effective membrane charge density increases with feed concentration for NaCl, while the dimensionless membrane charge increases for the DSPM&DE model and decreases for the UDSPM model. The relationship between the effective membrane charge density and the salt concentration is commonly described using a Freundlich isotherm, detailed in Section (3.2.1.4). For the case of NaCl, the power of the concentration in the Freundlich expression is slightly higher than 1 for the DSPM&DE model and is lower than 1 (≈ 0.6) for the UDSPM model. The Donnan

partitioning terms are of the same order of magnitude for both models and both ions, while the dielectric partitioning terms are noticeably different. As indicated in the theoretical comparison, the dielectric coefficients are lower for the UDSPM than those calculated for the DSPM&DE. As a direct consequence, the required membrane charge to achieve the same rejection value is lower for the UDSPM model than the DSPM&DE model. The DSPM&DE model correctly describes the NaCl experimental data over the entire range of ΔP_e (Figure 5.9), while the fits for the UDSPM are satisfactory at low to moderate pressures and over estimate the asymptotic limiting rejection. This behaviour is a direct result of the linearisation of the UDSPM model, an identical argument is described in Section (4.2.2), and is not the result of differences in the contributions of dielectric exclusion. Bowen and Welfoot (2002) attributed this increased prediction in rejection to an overestimated salt diffusivity inside the membrane pore.

The problem of a correct assessment for Peclet number, defined according to structural parameters (Δx) and/or measured quantities (J_V or ΔP_e), seems to be more troublesome for $MgCl_2$ solutions (Figure 5.10). The agreement is satisfactory for the DSPM&DE model, except for 1 mol m^{-3}, for which the best fitting could be obtained for a different value of the effective thickness parameter, Δx, i.e. a different Peclet number (losing parameter generality) and a higher value for membrane charge density with respect to a Freundlich-type isotherm calculated for NaCl data. A similar observation was made for $CaCl_2$, at the same salt concentration, through NF experiments on Desal-5 DK flat sheet membrane [Bandini and Vezzani (2003)]. The arguments presented in the theoretical analysis section for $CaCl_2$ (Table 5.2) are completely analogous to the experimental fitting results for $MgCl_2$ (Table 5.5). The dielectric partitioning terms for the DSPM&DE model are practically independent of salt concentration, with the magnesium coefficients being considerably lower than the chloride coefficients. The difference in the dielectric coefficients for the UDSPM is not as remarkable.

The correct evaluation of Peclet number is not as relevant for Na_2SO_4 solutions (Figure 5.11), for which the results for both models are in excellent agreement with the experimental data and with each other. This is reflected by comparing the

partitioning coefficients in Table 5.6, where only small differences are shown for dimensionless membrane charge density values and no meaningful observation comes out from comparison of Donnan and dielectric terms for the two models. Moreover, the dielectric coefficients from both models are in good agreement with each other, especially for the low concentration data. The performance of both models is significantly better for Na_2SO_4 than the other salts as the both ions have similar hydrodynamic radii, 0.184 nm and 0.231 nm respectively. As a direct result of the similar ion radii and if the sources of screening are not significant (i.e. ionic shells and membrane charge), the dielectric terms calculated from each model are similar and the dimensionless dielectric energy (ΔW_{DE}) is only proportional to z_i^2 as an approximation. When the ion radii are significantly different, the dielectric coefficients calculated form the two models are remarkably different (e.g. NaCl in Table 5.1 and $CaCl_2$ in Table 5.2 at the lowest concentration and for the narrow pores).

5.3 Conclusions

The models used in this chapter to describe dielectric exclusion phenomena have included a number of fundamental assumptions. The dielectric properties in the DSPM&DE model are based upon slit-like pore geometry, no solvation and the Debye-Hückel theory. Slit-like pores for NF membranes (especially as $r_p \rightarrow 0$) is a reasonable assumption. The application of Debye-Huckel theory has been seriously questioned at the nanometer length scale [Glueckauf (1976), Dressner (1974)]. Solvation forces are well documented and should not be excluded. Image forces do not take into account finite ion size, an important parameter in the determination of electrostatic forces. In addition, the hindrance factors are developed for a flat velocity profile in the DSPM&DE model, this is clearly not the case in a pore of nanometer dimensions.

By the same token, the proposed Born theory assumes that the hydrodynamic Stokes radius is applicable inside the membrane pore. This is a questionable assumption when considering the state of ionic hydration in materials of different dielectric properties. The Born approach also assumes that the model for solvent dielectric

constant inside the pore is valid and makes no attempt to describe concentration dependent phenomena involved in the dielectric partitioning. Nevertheless, even with these assumptions, the models discussed are consistent in themselves and, more remarkably, calculate the total contribution of the dielectric partitioning coefficient to the same order of magnitude.

Overall, a decision has to be made over which model for dielectric partitioning is most appropriate for NF modelling. In this chapter, both models have clearly demonstrated their ability to describe this complex phenomena with reasonable accuracy. Therefore, the most practical model to proceed with at present is the Born model. This conclusion is based primarily on the fact that the model is very simple and lacks the complexity of calculation required for the description of dielectric phenomena used in the DSPM&DE model. Furthermore, as a result of the coupled nature of membrane charge and dielectric effects, a more detailed description of dielectric phenomena is simply not worth pursuing until a practical and reliable independent measurement of membrane charge is available.

Acknowledgements:

The experimental data used for the comparison of the dielectric mechanisms made in this chapter is taken from a previous study by Welfoot (2001).

The calculations using the DSPM&DE model were conducted by Mr. Daniele Vezzani, Dipartimento di Ingegneria Chimica, Mineraria e delle Tecnologie Ambientali, Alma Mater Studiorum, Universiti di Bologna, Viale Risorgimento 2, I-40136, Bologna, Italy.

6 Application of Membrane Theory to an Industrially Relevant Separation

For traditional separation processes there are widely available process design methodologies for scale up and optimisation. However, there is an increasing need for such a rational approach to membrane separation processes, identifying at an early stage operating limits and process options. Such predictive models will reduce development risk and time, thus promoting the wider use of membrane technology in process industries such as pharmaceutical manufacture. The NF models discussed in Chapter 3 have been verified experimentally at the laboratory scale for simple aqueous solutions and there is now a requirement to evaluate the applicability of these existing models to more complex separations of real industrial importance. This process requires a systematic approach, firstly, in order to obtain the relevant characterisation information required for modelling purposes, and secondly, to gain a better understanding of the separation in order to maximise modelling success.

In this chapter this philosophy is demonstrated by describing the rationale for modelling the performance of membrane NF used in the isolation of *N*-acetyl-D-neuraminic acid (Neu5Ac) an industrially important example of an equilibrium-controlled biotransformation reaction. The chemoenzymatic synthesis of Neu5Ac is already achieved at large scale and its derivatives are important as precursors for a range of antiviral drugs such as the commercially available anti influenza agent 4-guanidino-Neu5Ac-2-en (zanamivir, *Relenza*™). The separation involves the removal of pyruvate from the process stream, which is complicated by the fact that Neu5Ac and pyruvate have similar pK_a values.

6.1 Introduction to *N*-acetyl-D-neuraminic acid (Neu5Ac)

Influenza has probably affected mankind for several millennia and is feared because of dramatic impact during pandemics. The pandemic of 1918-1919 caused approximately 40 million deaths world wide [Taubenberger *et al.* (2000)]. Influenza is a self-limiting respiratory tract infection caused by the influenza virus. Each year,

infection occurs in 10 – 15 % the population (this value can be as high as 60 % in closed environments such as student halls or nursing homes). Influenza is characterised by a range of symptoms, notably cough, headache, myalgia and fever. When infected, patients typically can not continue in their normal activities for several days, giving rise to serious socio-economic impact. In addition to morbidity, there is also the risk of added complications and mortality in those patients deemed *high risk* (people with underlying illness such as diabetes, respiratory or cardio-pulmonary disease and the over 65's). The annual toll from influenza over the past few decades has averaged 114, 000 hospitalisations and 20, 000 deaths in the U.S.A alone [Ison and Hayden (2001)].

Vaccines protect against influenza by stimulating an immune response in recipients. To do so, the antigens contained in the vaccine must resemble those of the circulating virus. In contrast, the mechanism of action of influenza antivirals is independent of the antigenic make-up of the circulating viruses. Two classes of influenza antivirals are available for use and can be administered for both treatment and prophylaxis. Each class inhibits a different step in the viral replication cycle. Type A influenza viruses contain a protein commonly known as M2. This protein is responsible for uncoating the viral nucleoprotein during replication. Amantadine and rimantadine inhibit this activity and are termed M2 inhibitors [Sugrue and Hay (1991), Hay (1989)]. This class of antivirals have no effect on type B or C influenza viruses as these viruses do not posses the M2 protein.

Relenza™ (zanamivir) is the first in a new class of drugs for the treatment of influenza type A and B. All influenza A and B viruses express neuraminidase, a surface glycoprotein possessing enzymatic activity. Influenza type C does not express this enzyme. The neuraminidase cleaves the α-ketosidic bond linking a terminal neuraminic acid residue to the adjacent oligosaccharide moiety. Inhibition of this viral neuraminidase prevents the virus from being able to effectively pass through respiratory secretions and prevents virus spread as the virions remain attached to the inside of the infected cell membrane and to each other [Coleman (1994)]. Neuraminidase has a highly conserved active site and is critical to viral replication. Therefore, drugs that inhibit the enzyme function are actively sought [Ison and

Hayden (2001)]. Elucidation of the neuraminidase crystal structure led to the discovery of the two currently available inhibitors, Relenza™ (zanamivir) manufactured by GlaxoSmithKline and Tamiflu™ (oseltamivir) manufactured by Roche [Gubareva *et al.* (2000)].

Neu5Ac is the obvious choice of starting material for synthesis of zanamivir [Dawson *et al.* (1999)]. The chemical synthesis of Neu5Ac is lengthy and does not offer much potential for economic large scale production. Neu5Ac can be isolated from biological materials such as milk, eggs, edible birds nests or bacterial cell wall polymers. However, the quantities in each case are modest at best and purification is difficult. The most promising production route for Neu5Ac remains at present biosynthesis with appropriate enzymes [Blayer *et al.* (1999), Dawson *et al.* (1999), Mahmoudian *et al.* (1997), Kragl *et al.* (1991), Blayer *et al.* (1996), Von Itzstein *et al.* (1993)].

Neu5Ac is produced from *N*-acetyl-D-glucosamine (GlcNAc) and pyruvate in two steps (Figure 6.1). The first step is the base-catalysed epimerisation of GlcNAc to *N*-acetyl-D-mannosamine (ManNAc), and the second is the enzymatic catalysed condensation of pyruvate and ManNAc to synthesise Neu5Ac. The latter reaction is catalysed by Neu5Ac aldolase from *Escherichia coli*. The most important issue in this reaction scheme is that the equilibrium of the second reaction lies towards ManNAc and pyruvate. The solution to this problem is to increase the concentration of pyruvate and drive the second equilibrium towards Neu5Ac. The resulting product stream contains a mixture of ManNAc, pyruvate and Neu5Ac. The separation of these components is made more difficult by the fact that the p*Ka* values of Neu5Ac and pyruvate are very similar, in the region around 2.2 [Kragl *et al.* (1991)]. A separation is possible by ion exchange chromatography but large volumes of resin are needed to obtain the desired separation. In the literature, many process options have been considered to end up with a reaction composition, which does not contain a large excess of pyruvate over Neu5Ac [Kragl *et al.*(1991), Blayer *et al.*(1996), Blayer *et al.* (1999)]. Indeed, a low concentration of pyruvate in the reaction mixture is also beneficial to the reaction itself, as high concentrations of pyruvate inhibit the Neu5Ac aldolase enzyme [Dawson *et al.* (1999)]. However, the preferred reaction method is

with a large excess of pyruvate due to the high cost of ManNAc [Mahmoudian *et al.* (1997)].

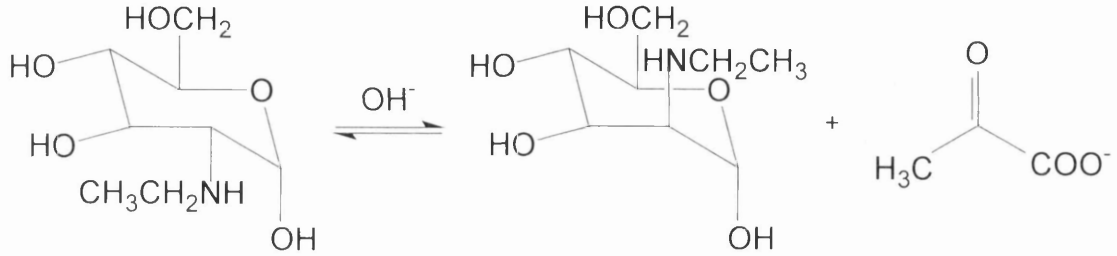

N-Acetyl-D-glucosamine (GlcNAc)

N-Acetyl-D-mannosamine (ManNAc)

pyruvate

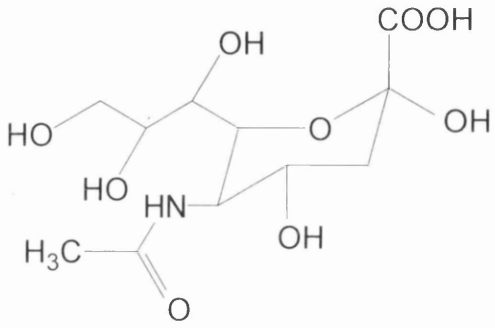

N-Acetyl-D-neuraminic acid (Neu5Ac)

Figure 6.1: Chemoenzymatic synthesis of *N*-acetyl-D-neuraminic acid catalysed by Neu5Ac aldolase from *E. coli*. [adapted from Mahmoudian *et al.* (1997)]

6.1.1 Materials and methods

Sample analysis involved several different techniques. Glucose concentrations were analysed using the GOD-Perid assay kit supplied by Roche Diagnostics GmbH (Manheim, Germany) and a spectrophotometer (Philips Scientific (Cambridge, UK) (Model No. PU 8625 UV/VIS)). Individual sodium pyruvate and Neu5Ac salt concentrations were calculated from conductivity measurements at 25 °C, using a conductivity meter supplied by Thermo Russell (Auchtermuchty, Fife, UK) (Model No. RL105) and probe.

HPLC Assay: ManNAc, and mixtures of ManNAc, pyruvate and Neu5Ac concentrations were determined using ion-moderated partition chromatography [Kragl *et al.* (1991)]. 1 μL sample of the reaction mixture was analysed through a Spherisorb® NH_2, 5 μm, column (150 x 4.6 mm, Alltech Associates Applied Science Ltd., Carnforth, Lancs., U.K.): assay conditions 35 °C, mobile phase, isocratic 0.01 M ammonium dihydrogen orthophosphate: acetonitrile 20:80 by volume, adjusted to pH 3.0 with phosphoric acid; flow rate 1.5 mL min^{-1}; UV detection at 210 nm.

The experimental set-up is described in Section 2.1. All experiments were conducted at 25 °C, and between 0.1-0.5 MPa applied pressure.

6.2 Results and discussion

6.2.1 Characterisation of the Nanomax™-50 membrane

Glucose was selected to evaluate r_p as the molecule has a reasonable range of rejection in the expected narrow pores of the Nanomax™-50 membrane. The manufacturer's rejection for sucrose using this membrane was very high (> 0.97) and so this molecule was not studied. The rejection of the ManNAc molecule was required as part of this study, so this molecule was included in the analysis. The experimental rejection for glucose and ManNAc are illustrated in Figure 6.2. The value obtained from the best-fit data from both components was r_p = 0.55 nm.

Pore dielectric effects and effective membrane charge density normally exhibit coupled behaviour, as described in Chapter 5. Thus, in order to evaluate a single effect their relationship must be decoupled. The membrane isoelectric point provides an opportunity to study only dielectric effects due to the membrane charge density being effectively neutralised. Figure 6.3 represents the rejection obtained over a range of pH. From the plot, one can see that the membrane exhibits no distinct pH giving a minimum rejection and therefore does not have a distinct isoelectric point.

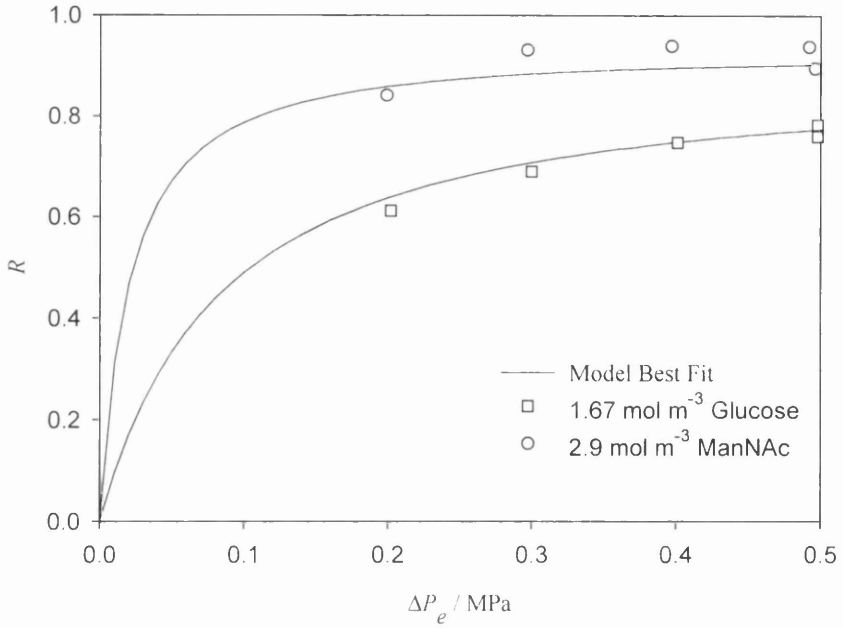

Figure 6.2: Experimental rejection and best fit data for glucose and ManNAc using the Nanomax™-50 membrane.

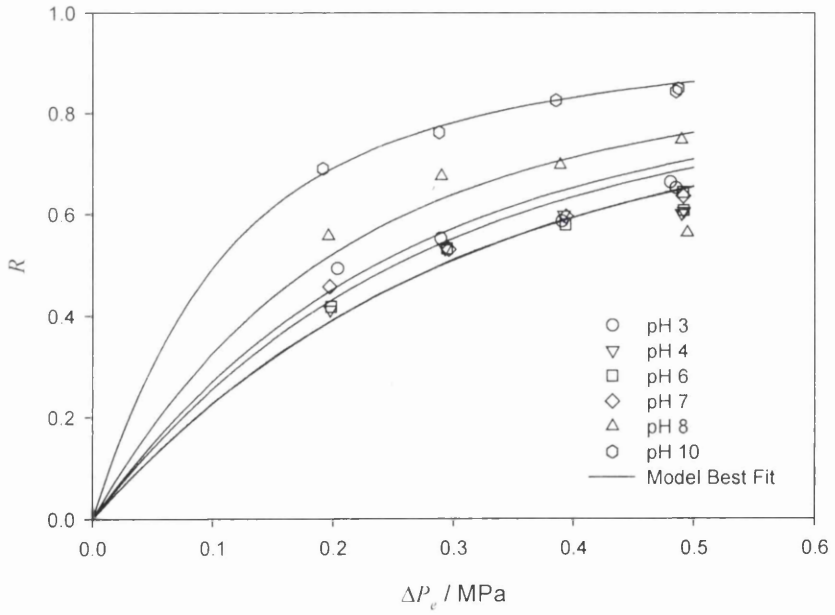

Figure 6.3: Rejection of 3 mol m^{-3} NaCl solutions for a range of pH values.

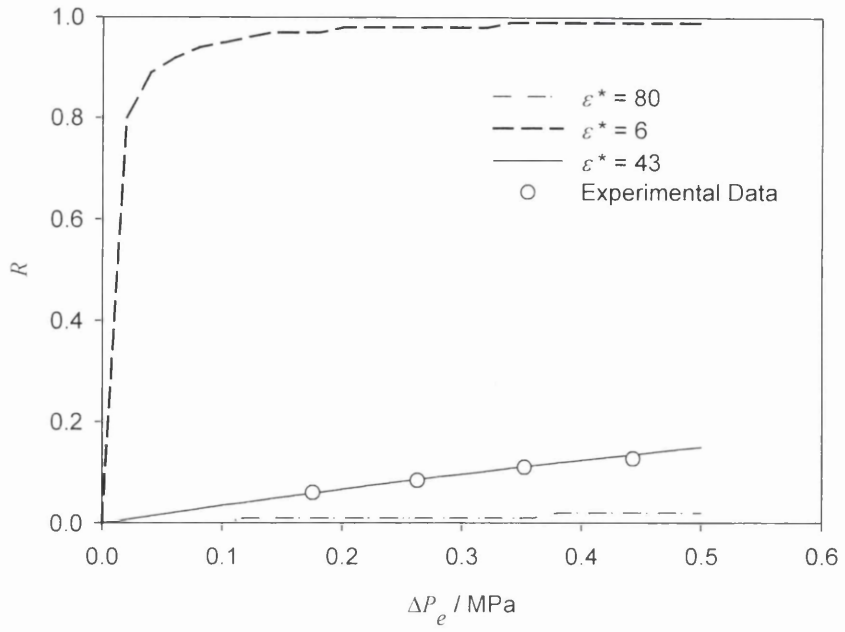

Figure 6.4: Evaluation of the dielectric constant for the orientated solvent layer within the pore (ε^*) from 100 mol m^{-3} NaCl rejection data.

An alternative method suggested for evaluation of ε^* is at high salt concentrations [Welfoot (2001)]. Concentrations of 100 mol m^{-3} NaCl are significant enough such that Donnan exclusion is likely to be small. The experimental rejection of 100 mol m^{-3} NaCl is given in Figure 6.4. The value calculated for ε^* by this method was 43. This value is similar in magnitude to that obtained for other polyamide membranes [Welfoot (2001)] and was therefore used as the value for the Nanomax™-50 membrane. The small variation in rejection over the pH range 3 – 7 in Figure 6.3 also indicates that X_d is independent of pH in this range. Thus, all further experiments were conducted in this pH range. The experimental rejection for different concentrations of NaCl was measured in order to develop an isotherm for predicting the value of X_d for various concentrations of ions in solution and is illustrated in Figure 6.5.

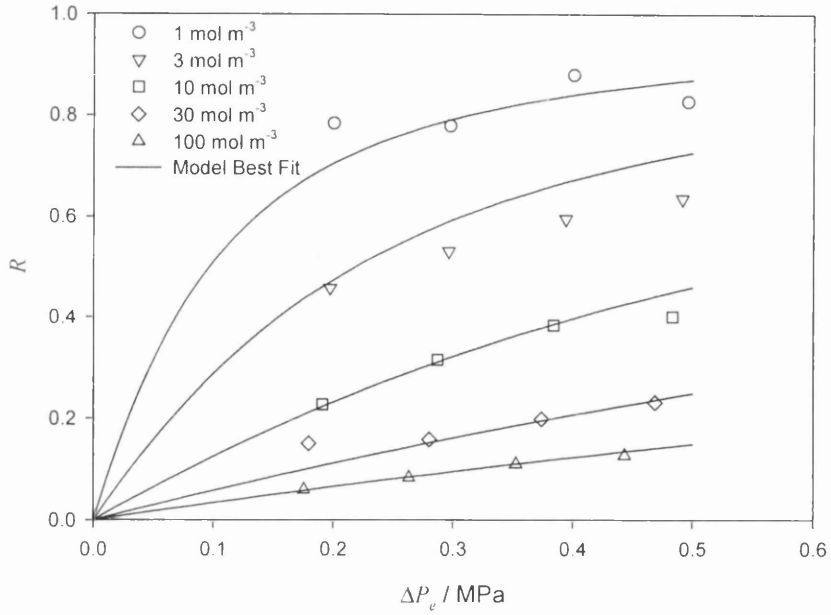

Figure 6.5: Rejection of various concentrations of NaCl.

6.22 Rejection of individual components

The rejections of different concentrations of both Neu5Ac and sodium pyruvate as individual components are illustrated in Figure 6.6. Plot a) indicates that the rejection of Neu5Ac is very high, greater than 95 % at modest effective pressures. The nature of the rejection for this molecule is predominantly steric ($\lambda = 0.9$) and thus, Neu5Ac is expected to show little dependence on membrane charge. Plot b) shows the experimental rejection of sodium pyruvate solutions. The fitted curves for this component using the isotherm developed for NaCl were poor and, as a result, the isotherm was recalculated to obtain the best-fit for sodium pyruvate (illustrated in plot d)). The rejection for sodium pyruvate depends on charge, dielectric effects and steric effects ($\lambda = 0.33$). Plot c) shows the flux measured for each of the experiments along with the pure water flux. The small deviation from the best-fit line further validates that concentration polarisation is small and also indicates that the osmotic pressure is low for the solutes studied.

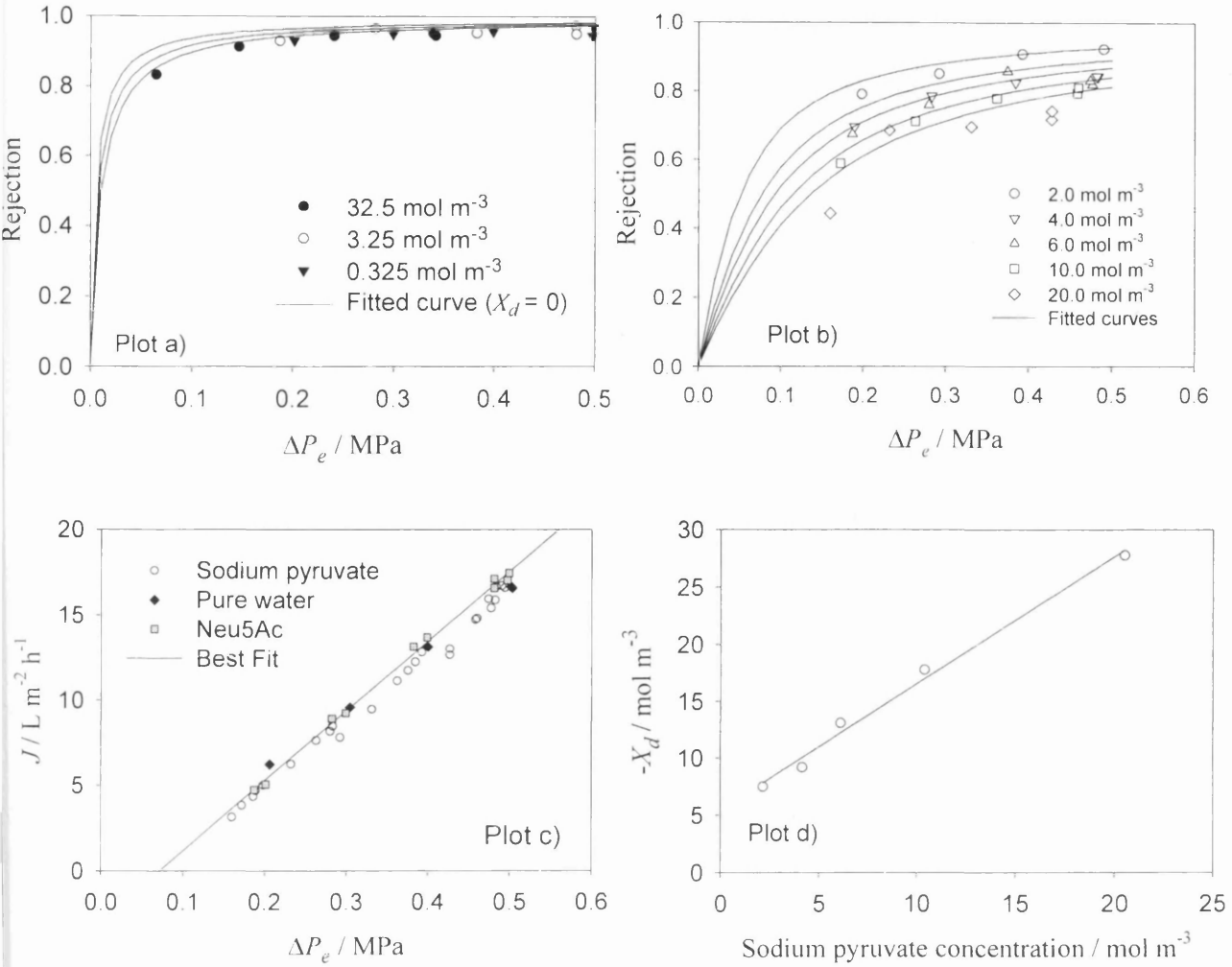

Figure 6.6: Experimental rejection and fluxes of individual components versus effective pressure. a) Neu5Ac rejection, b) sodium pyruvate rejection, c) experimental solvent flux and d) membrane charge isotherm for sodium pyruvate.

6.2.3 Rejection of component mixtures

To successfully model the diafiltration experiment, the rejections of each component in the mixture was studied using concentrations representative of different stages during the diafiltration experiment. The concentration of Neu5Ac throughout the diafiltration was expected to remain reasonably constant, due to the high rejection value for the individual component. For this reason, the concentration of this component in the mixtures studied was maintained at the diafiltration feed value of

32.5 mol m^{-3}. The concentrations of pyruvate used were 2.0, 6.9 and 20.2 mol m^{-3}. The experimental findings for these experiments are illustrated in Figure 6.7.

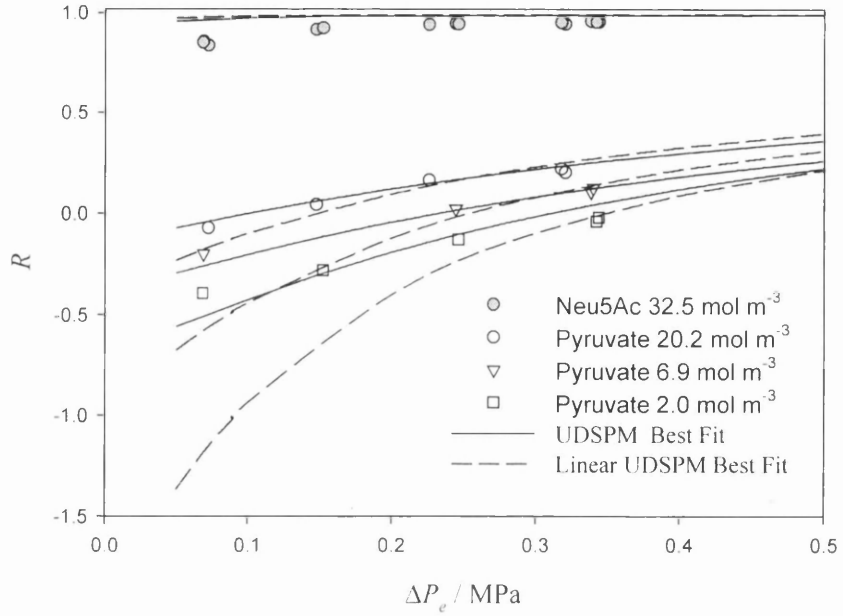

Figure 6.7: Rejection of Neu5Ac with various concentrations of pyruvate.

The rejection profile of Neu5Ac in Figure 6.7 is directly comparable to that in Figure 6.6. This confirms that Neu5Ac is not dependent on membrane charge and predominantly undergoes steric rejection even amongst a mixture of ions. The pyruvate ion rejection is again strongly influenced by membrane charge. However, in this case the membrane charge isotherms developed for both NaCl and sodium pyruvate as individual components are inadequate to describe the rejection behaviour. Thus, the charging mechanism of the membrane differs not only for different individual ions in solution but also for mixtures of different ions. A new membrane charge isotherm was developed for predicting the rejection behaviour of mixtures of the components and is illustrated in Figure 6.8.

The predictions (Figure 6.7) using this isotherm and the UDSPM model describe the rejection of both Neu5Ac and pyruvate very well. However, the linear UDSPM predictions are not as good as the UDSPM and deviate significantly at low concentration and low effective pressures. The model agreement becomes better as the effective pressure is raised and at effective pressures greater than 0.25 MPa the difference between the two models is small. This discrepancy between the two model

predictions is completely analogous to the behaviour observed for quaternary mixtures and charged membranes in Section (4.2.4). However, the magnitude of the deviation at low pressures is significantly larger than expected and indicates that the two models deviate even further for real systems as opposed to the ideal solutions considered in Chapter 4. At the low effective pressures where the two models deviate the membrane flux will be extremely low. Real NF processes demand high membrane flux for efficient operation and under the conditions of normal NF operation, the expected effective pressure driving force will be high and the linearised UDSPM will predict results similar to the UDSPM. Therefore, the significant deviations between the two models observed at low pressure will have no bearing on a real NF process and the linearised UDSPM can be used with confidence.

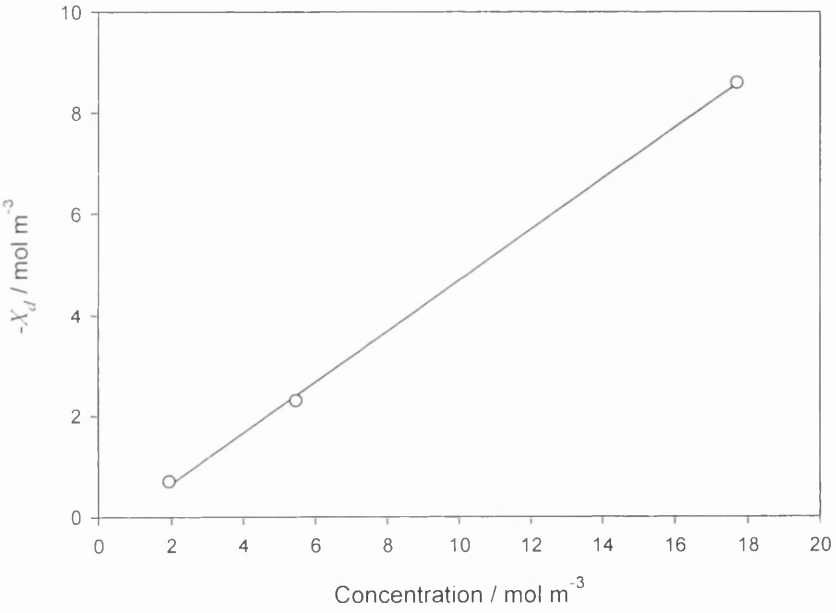

Figure 6.8: Membrane charge isotherm for Neu5Ac / pyruvate mixtures.

Figure 6.8 represents the membrane charge isotherm developed for the component mixtures. As the concentration of Neu5Ac is effectively the same for all cases considered the line is dependent only upon the pyruvate ion concentration in solution. The profile of this plot is linear, which is consistent with the behaviour observed for the individual pyruvate ion in Figure 6.7(d).

6.2.4 Diafiltration

The diafiltration experiment was carried out with initial feed concentrations of 32.8 mol m^{-3} Neu5Ac, 20.2 mol m^{-3} sodium pyruvate and 3.3 mol m^{-3} ManNAc. The experiment was continued until the concentration of the pyruvate ion was close to zero, based on a mass balance analysis for the system. During the diafiltration experiment, the flux of the system was maintained at a constant value by adjusting the applied pressure. The pH of the vessel contents throughout the diafiltration experiment was pH 2.4 and the relative dissociation of Neu5Ac was calculated from the pK_a value. Figure 6.9 shows the diafiltration vessel contents as a function of time for the diafiltration experiment (the Fortran™ code used to calculate the theoretical values is provided in the Appendix A2).

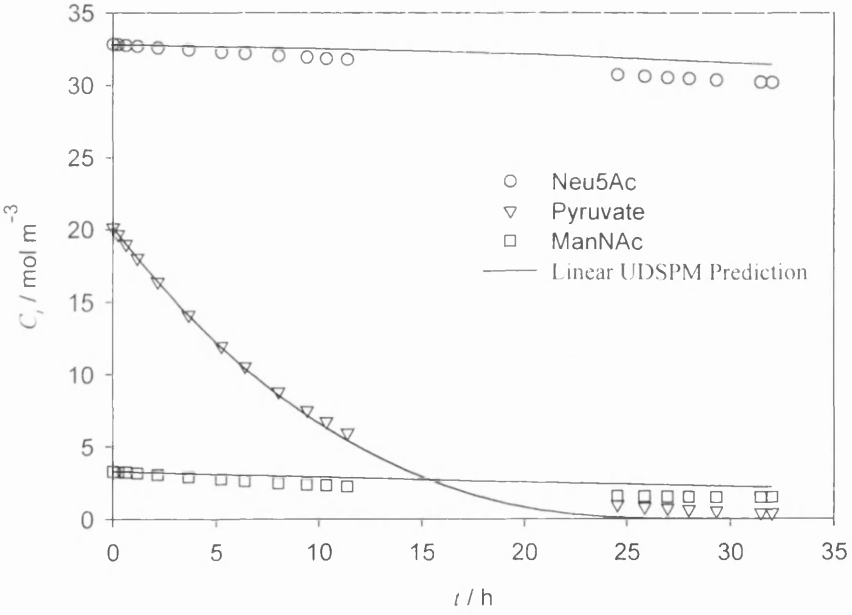

Figure 6.9: Diafiltration vessel contents as a function of time.

The experimental data was predicted using the linear UDSPM and the charge isotherm obtained from Figure 6.8. The predicted values show excellent agreement with the experimental data, Sy = 0.492. The diafiltration time to reduce the pyruvate ion concentration below 2 mol m^{-3} was 17.6 hours. This value represents a ten-fold reduction in the concentration of pyruvate from the reaction stream. At this stage in the diafiltration the ratio Neu5Ac/pyruvate is 15 and well above that required for high resolution purification [Dawson *et al.* (1999)]. The rejection of Neu5Ac remained

above 95 % at all times and the percentage loss of Neu5Ac over the experimental run was 8 %.

6.3 Conclusions

Uncharged solute rejection at the membrane surface was studied and the effective pore radius for the Nanomax™-50 membrane was evaluated as 0.55 nm. The electrical properties of the membrane were studied using NaCl. The dielectric constant for the orientated water layer within the pore confines of the membrane was evaluated as 43. The effective membrane charge density was found to be independent of pH in the range pH 3 to 7. A membrane charge isotherm for various concentrations of NaCl was established for this pH range. The effective membrane charge density was found to vary with different salt concentrations, for different salts and for mixtures of salts. Thus, the simple charge isotherm developed for NaCl would not be sufficient for use in predictive purposes with other salts and a new isotherm was developed for the actual diafiltration components.

A comparison was made between the UDSPM and linear UDSPM predictions for the rejection of mixtures of different concentrations of the diafiltration components and the difference between the two was small at effective pressures higher than 0.25 MPa. The small deviations observed between the two models predictions and the experimental findings represent a successful application of the both models to a real quaternary industrial process stream.

The linearised model was then used to simulate the membrane separation performance for diafiltration to remove pyruvate. Excellent agreement with the experimental findings was observed when the effective membrane charge density was varied with pyruvate ion concentration. To remove pyruvate to below detectable levels, the loss of Neu5Ac over the entire process was low (8 %).

Overall, the work detailed in this chapter represents the first successful application of the Linear UDSPM NF model to a real multi-component downstream industrial separation.

7 Recovery of a High Value Product From a Process Waste Stream

In the previous chapter, the linear UDSPM was successfully applied to an existing downstream industrial separation not previously achieved using membranes. The aim of this chapter is to further develop the theoretical approach to predictive modelling of membrane processes by considering a novel value added separation; recovering a valuable antibiotic from a process waste stream. Such a recovery process, if possible, has the potential of lowering the environmental burden of the original manufacturing process, improving the process yield and subsequently improving the process economics. The suggested recovery process differs greatly from the separation example used in Chapter 6 as there is no prior industrial experience and the concentration of the antibiotic considered is extremely low in comparison to the impurity. In addition, the rationale required for design and scale up of full industrial NF processes incorporating NF modelling as a design tool is considered.

NF operations are becoming increasingly favoured over traditional processes for the treatment of industrial process effluents. Frank *et al.* (2002) used a two step NF process to remove colour from an effluent stream and recycled the process water. Noronha *et al.* (2002) used a membrane bioreactor followed by NF integrated with UV treatment to reduce the chemical oxygen demand (COD) levels of effluent from the fruit juice industry and produce clean drinking water. Both of these NF operations were installed to produce effluent of suitable quality for disposal via municipal wastewater treatment plants and were deemed economically viable. Although NF is clearly capable of improving effluent quality, the interest here lies in the value added recovery from a process effluent. Recovery of high value products from industrial effluent not only reduces the environmental burden of the effluent, but also increases the overall yield of the manufacturing process, which is highly desirable in today's economic climate.

Vandanjon *et al.* (2002) used a combination of UF, NF and RO to reduce the COD levels of an effluent stream from seafood cooking waters and recover the valuable marine flavour compounds. Shaalan *et al.* (2001) and Cassano *et al.* (1997) used

membrane processes for the recovery of chromium in the tanning industries. Zhu *et al.* (2003) used NF to recover the antibiotic clindamycin from fermentation wastewater. Nguyen *et al.* (2003) used NF to recover whey products from effluent in the cottage cheese industry for incorporation into other dairy products such as ice cream and yoghurt. Scarpello *et al.* (2002) used solvent resistant NF as a non-destructive separation technique to recover high value organometallic homogeneous catalysts from reaction mixtures allowing the catalyst to be reused. All of these NF applications were deemed economically viable with most of them having short pay back periods as a direct result of the value added recovery. However, all of the examples given were purely experimental investigations and none of them used any form of predictive modelling to obtain a better understanding of the separation and aid in the construction of a full industrial NF process.

In this section, further demonstration of the practical use of NF modelling applied to the design, optimisation and scale-up of industrial pharmaceutical processes is provided by considering the isolation of sodium cefuroxime. The antibiotic sodium cefuroxime is the sodium salt of (6R,7R)-3-carbamoyloxymethyl-7-[(Z)-2-(fur-2-yl)-2-methoxyimino-acetamido] ceph-3-em-4-carboxylic acid and is one of around thirteen second generation cephalosporins having activity against most gram-positive cocci [Hotchkies *et al.* (1996)]. Traditionally, penicillin has long been used as a first line treatment for infectious disease. However, with the emergence of drug resistant strains of bacteria, intravenous cephalosporins have gained popularity. Cephalosporins are part of the β-lactam group of antibiotics that now constitute a large proportion of the multibillion dollar antibiotics market [Ghosh *et al.* (1997)] and are produced in an annual quantities of approximately 30,000 tonnes [Barboza *et al.* (2002)].

7.1 Introduction to cefuroxime sodium

Cephalosporin C was first discovered in 1955 and is the fundamental starting material in the manufacture of all semi synthetic cephalosporins. Almost all commercially manufactured cephalosporin C is produced by fermentation using high yield strains of the organism *Cephalosporium acremonium*. The first unit operation in the production

process of sodium cefuroxime is the recovery of cephalosporin C from the whole cell broth. The recovery of cephalosporin C is complicated by the hydrophilic nature of the α-aminoadipyl side chain (see Figure 7.1) rendering the molecule highly soluble in water and therefore precludes direct solvent extraction.

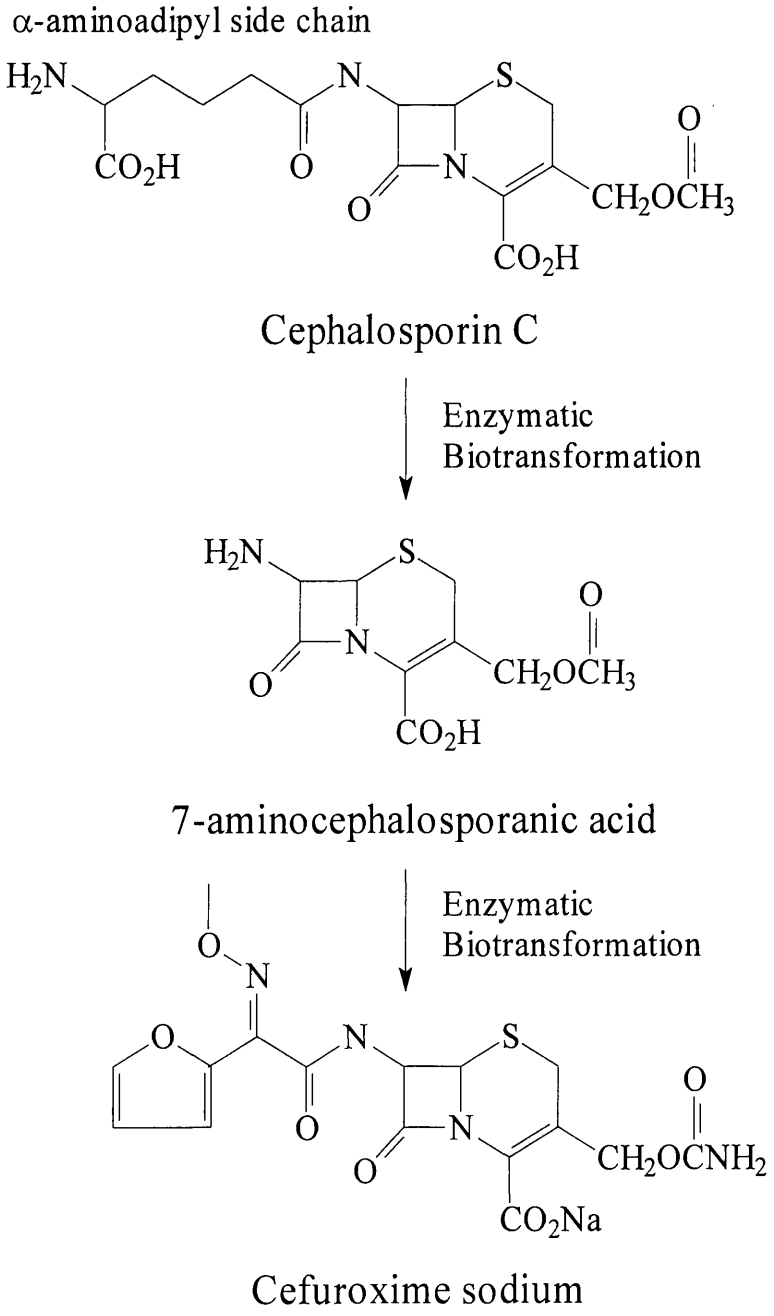

Figure 7.1: Basic outline of the biosynthetic production route for sodium cefuroxime manufacture from *Cephalosporium acremonium*. [adapted from Ghosh *et al.* (1997)]

A number of techniques, namely adsorption, reactive extraction, ion exchange and enzymic modification have been used either separately or sometimes in combination for the isolation of cephalosporin C [Smith (1985)]. After recovery, cephalosporin C is subjected to enzymatic biotransformation to produce the intermediate material 7-aminocephalosporanic acid (7-ACA). Any of the numerous commercially available cephalosporins can then be manufactured from 7-ACA by either direct synthesis or multi-step biotransformation with appropriate enzymes. A basic outline for the synthesis of sodium cefuroxime is provided in Figure 7.1. The final cephalosporin product is then obtained by isolation and purification from the reaction mixture. For the case of sodium cefuroxime, the final stage purification is achieved by crystallization using large quantities of sodium lactate.

The production of sodium cefuroxime represents a typical multi-stage industrial biochemical manufacturing production process. Optimisation of the overall yield of isolation is essential, as even a 1 % increase in the yield of a cephalosporin typically produced on a plant of 100 tonnes per annum at a product cost of around $100 per kilogram will result in an extra annual benefit of $100 000 which is economically attractive [Ghosh *et al.* (1997)]. The yield from the crystallization stages in many industrial production plants will not approach 100 %. The typical crystallisation yield for cephalosporins is not readily available in the literature, however, data is available for paracetamol and xylitol and typical yields for these materials are in the range 30-60 % [Al-Zoubi and Malamataris (2003), De Faveri *et al.* (2004)]. Thus, the effluent from sodium cefuroxime crystallization will contain small amounts of the high value product material along with other by-products and the large quantities of sodium lactate. This waste stream is normally sent for industrial disposal as the quantities of cefuroxime are too low for traditional separation processes to recover economically. This industrial disposal is made more expensive due to the fact that an antibiotic is present. Thus, if the antibiotic was removed from the process effluent, a cheaper disposal method may be possible.

The aim is to select a suitable NF membrane and demonstrate that NF is capable of recovering sodium cefuroxime from the waste stream. Secondly, by removal of a sufficient amount of lactate, show that the sodium cefuroxime can be recycled to the crystallization feed to improve the overall yield of the recovery process. In addition

to the benefits of product recovery, the waste stream, now free from antibiotic contamination, has possibilities of either becoming commercially viable or can be disposed of by more economical methods. Furthermore, in addition to the obvious benefits of a reliable model, the intention is to show that inclusion of NF processes to existing manufacturing plants has the potential to improve process performance with higher product yields, lower demand for raw materials and lower effluent emissions.

7.1.1 Materials and methods

Sample analysis involved several different techniques. Glucose concentrations were analysed using the GAGO-20 assay kit supplied by Sigma-Aldrich Ltd. (Poole Dorset, UK) and a spectrophotometer (Philips Scientific (Cambridge, UK) (Model No. PU 8625 UV/VIS)). Sodium lactate salt concentrations were calculated from conductivity measurements at 25 °C, using a conductivity meter supplied by Thermo Russell (Auchtermuchty, Fife, UK) (Model No. RL105) and probe. Lactate ion concentrations were analysed using the lactate reagent 735-10 assay kit supplied by Trinity Biotech U.K. Sales Ltd. (Abingdon, Oxford, U.K.). Particle size analysis was measured using the High Performance Particle Sizer (HPPS) with NIBS™ technology from Malvern Instruments (Malvern, Worces., U.K.)

HPLC Assay: Sodium cefuroxime was determined using high performance liquid chromatography. 1μL sample of the reaction mixture was analysed through a Spherisorb® hexyl, 5 μm, column (150 x 4.6mm, Alltech Associates Applied Science Ltd., Carnforth Lancs., U.K.): assay conditions 30 °C, mobile phase, sodium acetate 0.37 g, glacial acetic acid 5.16 g, water 901 g and acetonitrile 78 g ; flow rate 2.0 mL min^{-1}; UV detection at 273 nm.

The experimental set-up is described in Chapter 2. All experiments were conducted at 25 °C, between pH 6.0-7.0 and between 0.1-0.5 MPa applied pressure. The pH was maintained in this region to avoid chemical degradation of the cefuroxime molecule.

7.1.2 Characterisation of the membranes and process stream

Glucose was used as an uncharged solute to evaluate the effective membrane pore radius (r_p). The dielectric constant of the orientated water layer within the pore (ε^*) for the Nanomax™-50 membrane was determined in Chapter 6 and the value for the Desal-5-DK membrane was determined in previous study by Welfoot (2001). This measurement was not made for the SelRO® MPF-44 membrane. The effective membrane charge density (X_d) was then determined as necessary for the given solutions.

The physical properties required for modelling the process stream are the material diffusion coefficient at infinite dilution and the hydrodynamic Stokes radius, evaluation of these parameters has been discussed in Chapter 2. The pK_a for sodium cefuroxime is 2.04 [Lin *et al.* (2000)], thus the molecule is fully dissociated for the pH of the solutions studied and similarly for sodium lactate.

7.2 Results and discussion

7.2.1 Characterisation of the membranes

Glucose was selected to evaluate r_p as the molecule has a reasonable range of rejection in the expected narrow pores of the three membranes studied. The manufacturer's rejection for sucrose using these membranes was very high (> 0.97) and so this molecule was not studied. The experimental glucose rejection for each membrane is illustrated in Figure 7.2.

The Nanomax™-50 membrane was characterised in Chapter 6, however, this membrane is considered in this chapter also and will therefore be included in the discussion. The values obtained for the best-fit data were r_p = 0.55 nm for the Nanomax™-50 membrane, r_p = 0.52 nm for the Desal-5-DK membrane and r_p = 0.49 nm for the SelRO® MPF-44 membrane.

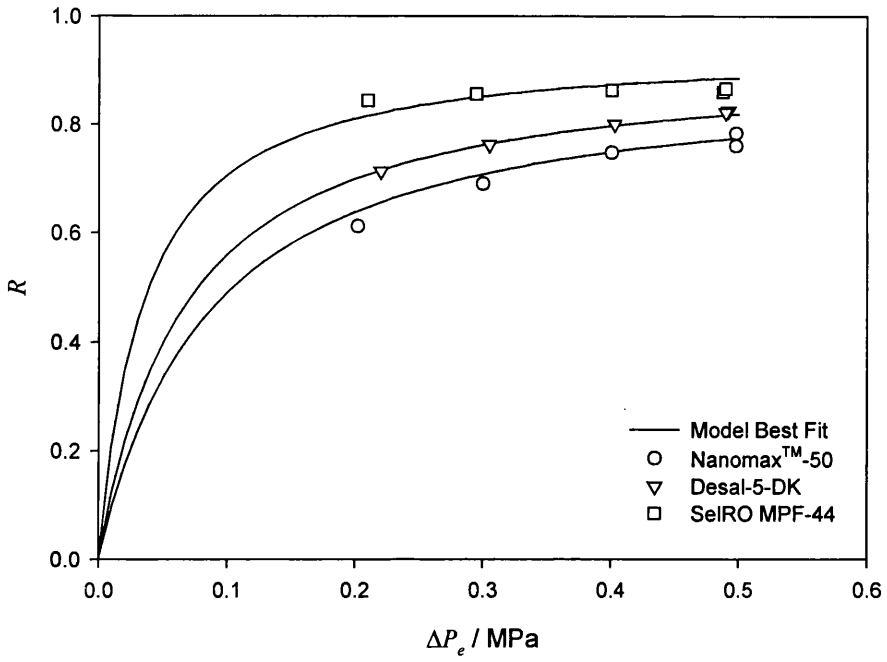

Figure 7.2: Glucose rejection versus effective pressure for the three commercially available membranes studied.

7.2.2 Rejection of individual components

7.2.2.1 Nanomax™-50 membrane

The rejection of sodium cefuroxime and sodium lactate from the Nanomax™-50 membrane are illustrated in Figure 7.3. The nature of the rejection for cefuroxime (plot a) is predominantly steric (λ = 0.82) with the limiting rejection being 93 % and 89 % at modest effective pressures for a 1 and 10 mol m^{-3} solution respectively. The nature of the rejection for sodium lactate (plot b) is both steric and charge based (λ = 0.42) with the rejection being strongly influenced by concentration. The rejection behaviour is typical of that expected for a small single salt with this membrane as similar concentration dependence is observed for NaCl, see Figure 6.5.

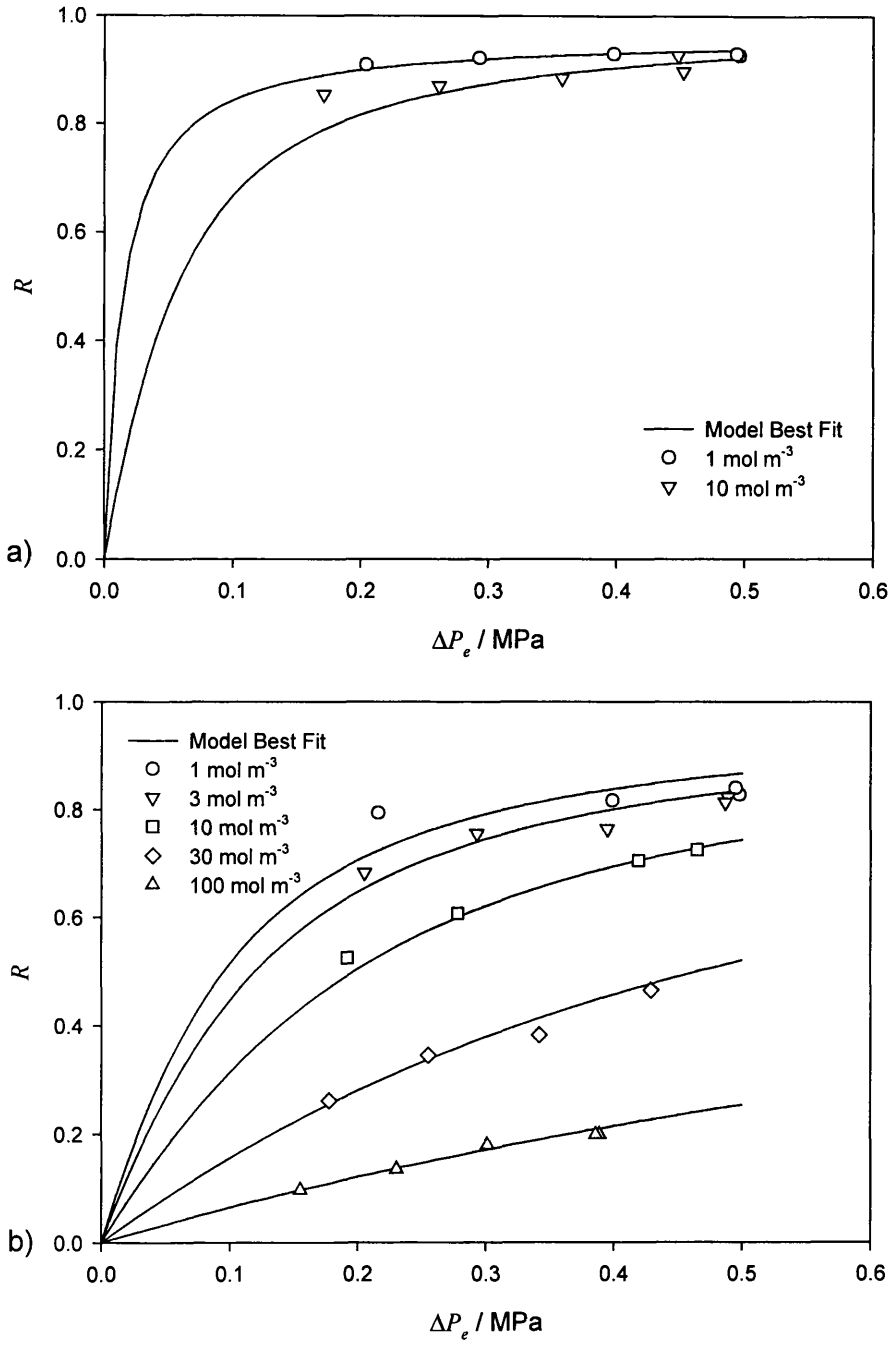

Figure 7.3: Rejection from the Nanomax™-50 membrane versus effective pressure for a) sodium cefuroxime and b) sodium lactate.

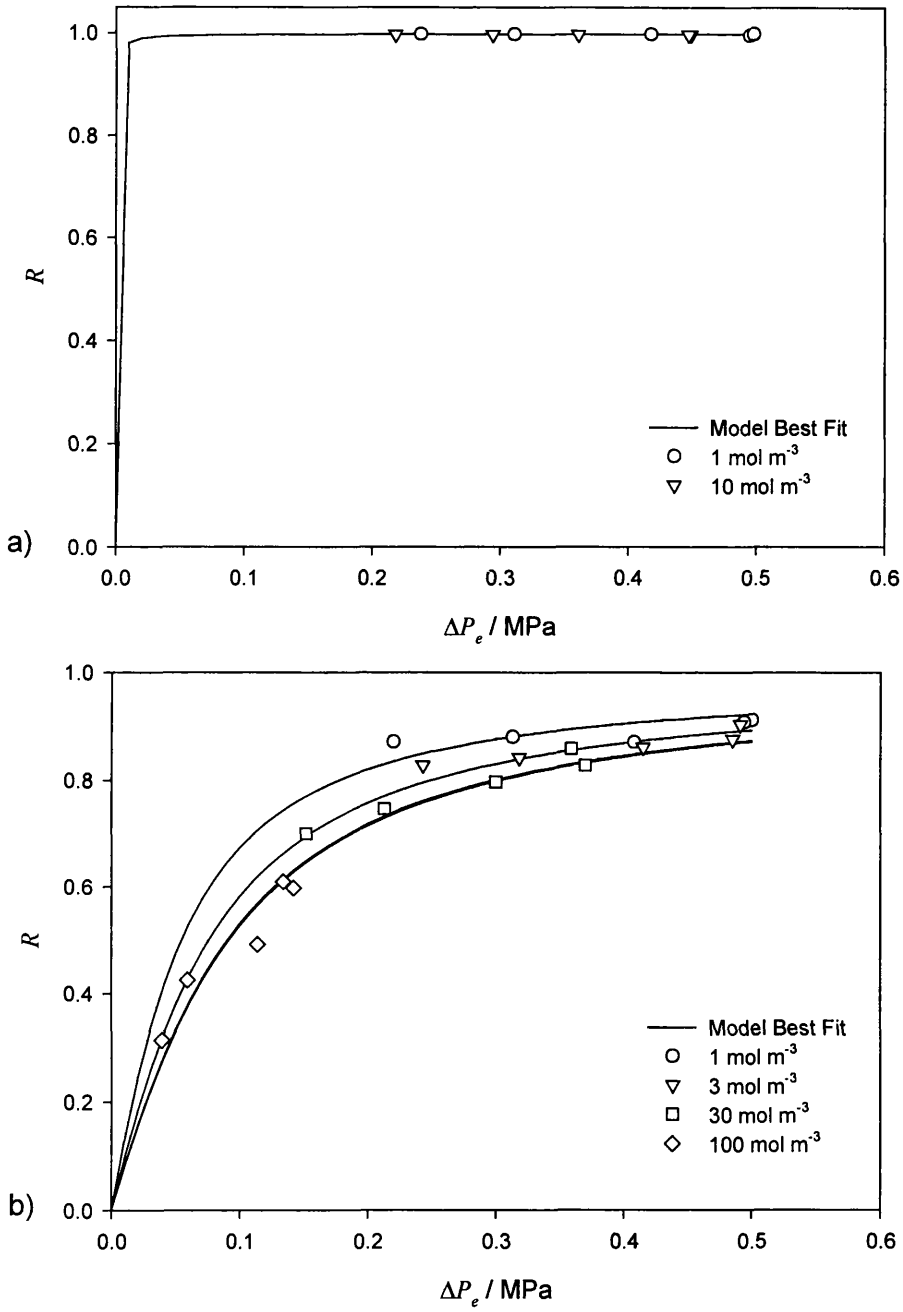

Figure 7.4: Rejection from the Desal-5-DK membrane versus effective pressure for a) sodium cefuroxime and b) sodium lactate.

7.2.2.2 Desal-5-DK membrane

The rejection of sodium cefuroxime and sodium lactate from the Desal-5-DK membrane are illustrated in Figure 7.4. The nature of the rejection for cefuroxime (plot a) is predominantly steric ($\lambda = 0.87$) with the limiting rejection being 99.7 % for all effective pressures studied and concentrations of 1 and 10 mol m^{-3}. The rejection for sodium lactate (plot b) is both steric and charged based ($\lambda = 0.44$). However, the variation in rejection observed with increased concentration is smaller than that for the Nanomax™-50 membrane, indicating that the Donnan contribution to overall rejection is lower for this membrane and, as a direct result, the influence of effective membrane charge is lower.

7.2.2.3 SelRO® MPF-44 membrane

The rejection of sodium lactate from the SelRO® MPF-44 membrane is illustrated in Figure 7.5.

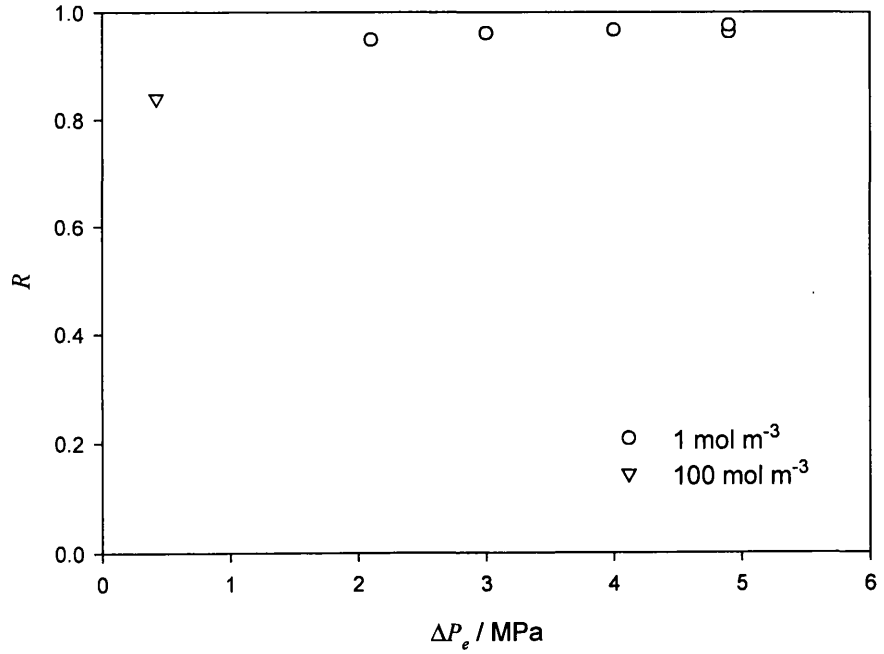

Figure 7.5: Rejection from the SelRO® MPF-44 membrane versus effective pressure for sodium lactate.

The nature of the rejection for this species was predominantly steric and dielectric with a limiting rejection of 97 % for a concentration of 1 mol m^{-3}. The rejection showed very little concentration dependence. As the rejection of sodium lactate was extremely high, the expected rejection of sodium cefuroxime was 100 %. However, although separation of these two molecules with this membrane is theoretically possible, in practice this is not a viable economic separation as the sodium lactate rejection is too high. Therefore, the SelRO® MPF-44 membrane was not considered suitable for this separation and was not studied further.

7.2.2.4 Conclusive remarks

The three membranes were characterised in order to assess which, if any, of them would be most suitable for the desired separation. As a direct result of the extremely high rejection of sodium lactate at all effective pressures and concentrations from the SelRO® MPF-44 membrane, this membrane was deemed most unsuitable for this separation and was not studied further. The Nanomax™-50 membrane showed favourable cefuroxime rejection, in the range 89-93 %, and had low sodium lactate rejection. The Desal-5-DK membrane exhibited the highest rejection of sodium cefuroxime measured (99.7 %) and allowed reasonable permeation of the sodium lactate. Thus, a conflict of interests has developed in relation to which membrane to proceed with for the desired separation.

The Nanomax™-50 membrane, exhibits very favourable sodium lactate permeation, however, this membrane also allows the permeation of a significant quantity of sodium cefuroxime. If any suggested separation is to be economically viable the process must recover as much of the most valuable product as possible. Therefore, the economics of this process depend on the efficient recovery of sodium cefuroxime from the feed solution. For this reason, the Desal-5-DK membrane was selected as the most suitable membrane for this separation and all subsequent experiments were performed using only this membrane.

7.2.3 Rejection of component mixtures

To successfully model the diafiltration experiment, the rejections of each component in the mixture were studied using concentrations representative of different stages during the diafiltration experiment. The concentration of sodium cefuroxime throughout the diafiltration was expected to remain constant, due to the high rejection value for the individual component. For this reason, the concentration of this component in the mixtures studied was maintained at the diafiltration feed concentration. A value of 5 mol m^{-3} was selected as representative of a low concentration pharmaceutical effluent. The concentrations of sodium lactate used were 100, 30 and 10 mol m^{-3}. The experimental findings for these experiments are illustrated in Figure 7.6.

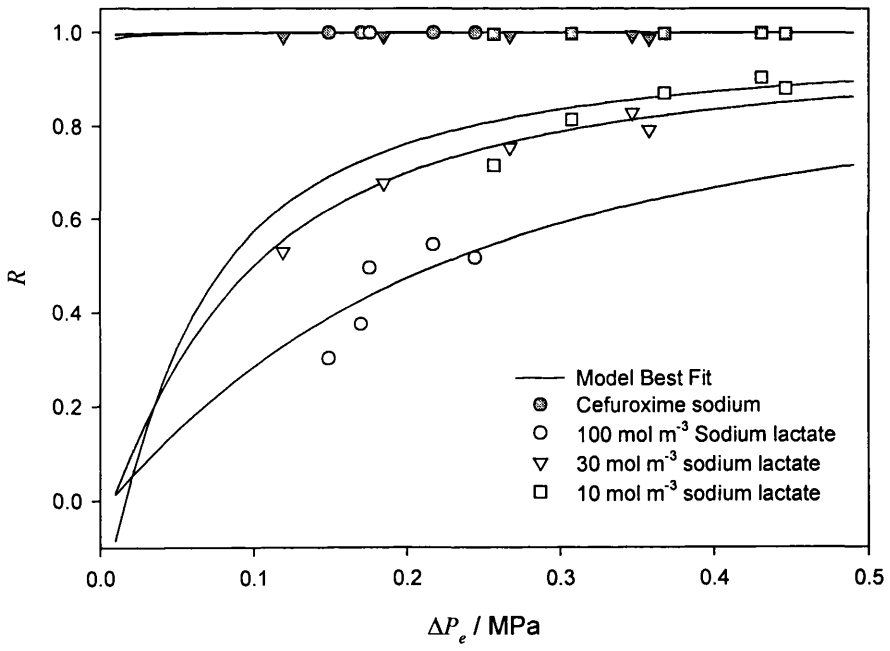

Figure 7.6: Rejection of 5 mol m^{-3} sodium cefuroxime with varying concentrations of sodium lactate.

The rejection profile of sodium cefuroxime in Figure 7.6 is directly comparable to that in Figure 7.4. This confirms that sodium cefuroxime is not dependent on membrane charge and predominantly undergoes steric rejection even amongst a mixture of ions. The rejection of sodium cefuroxime is above 99.5 % at all times and is favourable for

our minimum loss criteria. The sodium lactate rejection is also very similar to that observed for the individual component rejection, and again, the concentration dependence upon rejection is small. The rejection for sodium lactate is in the range 70-90 % for an effective pressure of 0.5 MPa. This is rather high for a material that one would wish to remove and will cause an increase in the expected processing time.

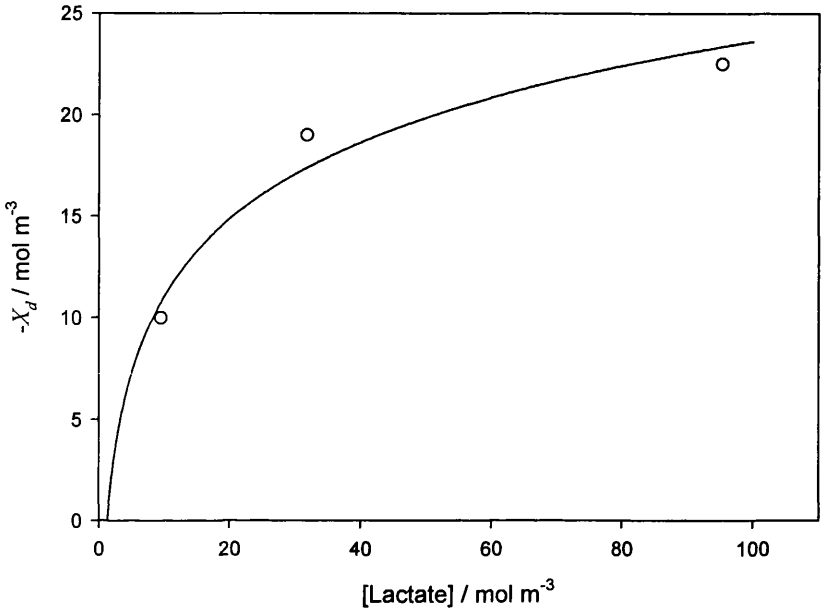

Figure 7.7: Membrane charge isotherm developed for sodium cefuroxime and sodium lactate for the Desal-5-DK membrane.

However, as a direct result of our minimum loss criteria for sodium cefuroxime, we have to accept this as a consequence. A membrane charge isotherm was developed from the experimental rejection data and is shown in Figure 7.7. As the concentration of cefuroxime is effectively the same for all cases considered, the charge isotherm is dependent upon the sodium lactate concentration in solution.

7.2.4 Diafiltration

The diafiltration experiment was carried out with initial feed concentrations of 5 mol m^{-3} sodium cefuroxime and 100 mol m^{-3} sodium lactate. The experiment was carried out over a 200 hour period. During the diafiltration experiment, the flux of the system was maintained at a constant value by adjusting the applied pressure. The diafiltration vessel contents as a function of time are illustrated in Figure 7.8.

The diafiltration was predicted using the charge isotherm developed from Figure 7.7 and shows excellent agreement with the experimental results, Sy = 0.555. Over the diafiltration period, the sodium lactate concentration was reduced by a factor of 2.5, confirming that NF was indeed a viable method for this separation. The rejection of sodium cefuroxime remained above 99.7 % at all times during the diafiltration and the overall recovery was 99.6 %. Thus, the extremely high recovery of sodium cefuroxime satisfies our minimum loss criteria with a loss of only 0.4 % of the initial feed.

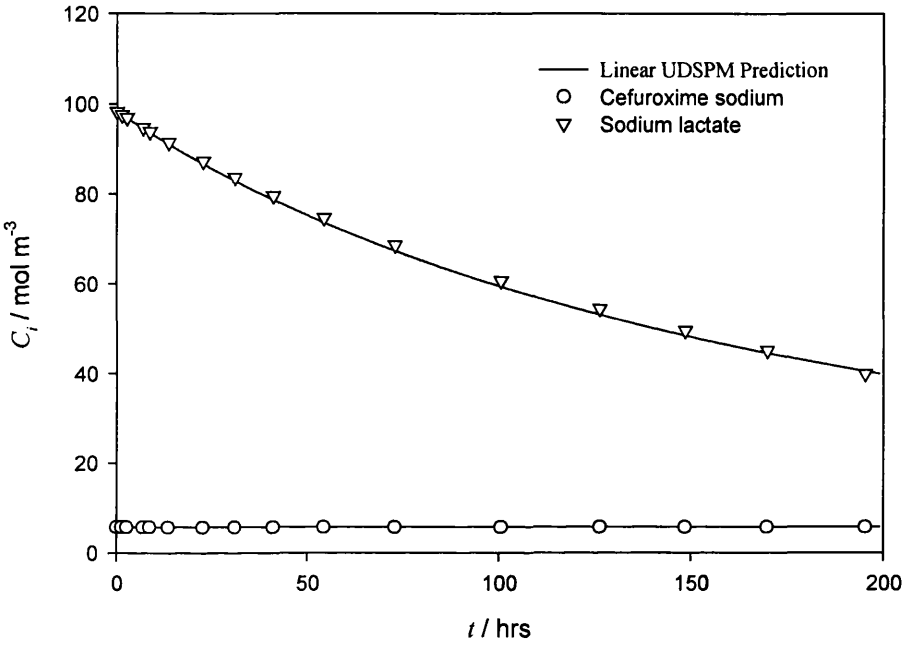

Figure 7.8: Vessel contents over time for the diafiltration experiment.

7.2.5 Industrial recovery process

Having demonstrated the effectiveness of the modelling system by considering the diafiltration in section 7.2.4. The aim now was to progress further and theoretically apply the linear UDSPM for the case of the real industrial waste recovery process. If the production of 100 tonnes per annum (see section 7.1) is considered as the typical production basis for a cefuroxime plant, this will be the equivalent of 614 moles per day on a 365 day production basis. By considering that the final crystallization stage is 70 % efficient (above that expected, section 7.1), then the total daily production rate will be 877.1 moles. The actual industrial crystallization concentration specifications

for sodium cefuroxime are available in a U.S. patent [Stables (1980)] and use concentrations of 140 mol m^{-3} sodium cefuroxime and 2,230 mol m^{-3} sodium lactate. If these concentrations are scaled for the production rate a crystallization solution volume of 6.3 m^3 is obtained. Therefore, the feed solution to the NF unit will be 6.3 m^3 of 2,230 mol m^{-3} sodium lactate and 41.8 mol m^{-3} sodium cefuroxime. The proposed NF recovery process is outlined in Figure 7.9.

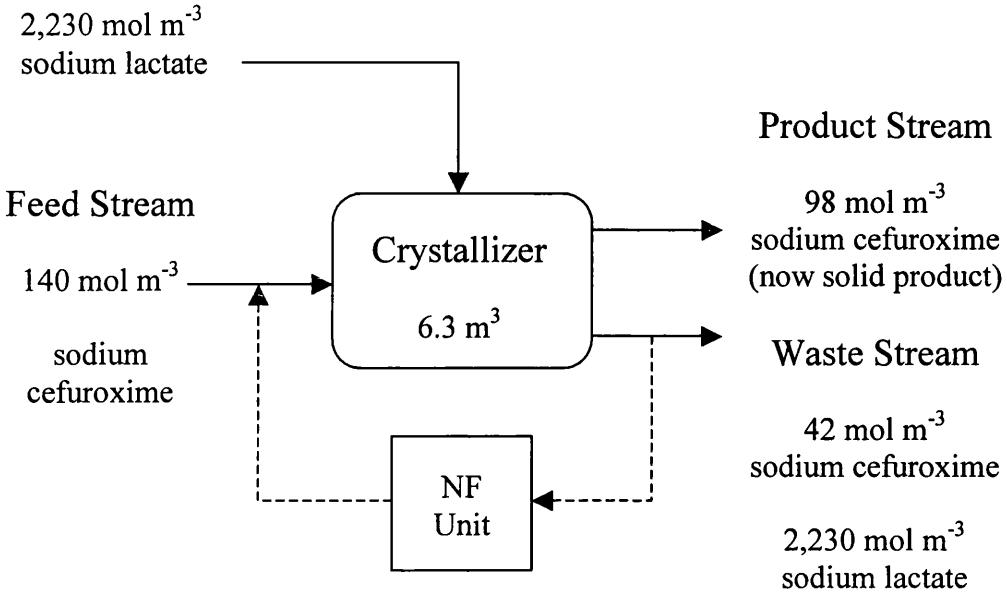

Figure 7.9: The proposed NF recovery process to recycle sodium cefuroxime from the industrial process effluent.

The expected osmotic pressure of the feed stream will be beyond the operational pressure for the Desal-5-DK membrane (3 MPa). Therefore, dilution of the feed stream is required. If we take a dilution ratio of 1 in 5, then the expected osmotic pressure for the feed stream will be of the order of 1.4 MPa, providing a driving force of 1.6 MPa for the diafiltration stage. The flux for the industrial spiral wound Desal-5-DK membrane is available from a previous study [Welfoot (2001)] and is equivalent to 1.278 x10^{-11} m^3 m^{-2} s^{-1} Pa^{-1}. The assumption will be made that there are no mass transfer effects limiting the full scale industrial recovery process, i.e. the cross-flow is sufficient to neglect concentration polarisation. The results from

modelling the full scale recovery process using the linear UDSPM are provided in Table 7.1 and Figure 7.10.

The recovery process was modelled to obtain the same ratio of sodium lactate to sodium cefuroxime as in the feed stream to the crystallization unit (16:1). Then, by concentration of the recovered waste stream, the product stream from the NF unit is recycled to the crystallization units where an appropriate amount of raw feed is added to form the exact same feed solution as in the original process. This is a very important consideration as industrial crystallization units are very sensitive to changes in the feed composition and throughput, i.e. no extra burden is now placed on the crystallization unit as the new feed solution is identical to the original feed solution. As an example of the linear UDSPM prediction, if the proposed NF unit contains 200 m^2 of Desal-5-DK membrane then the total process time for the combined diafiltration and concentration stages will be 10.7 hours. Therefore, if the NF process is operated on the same 24 hour time scale as the original process, then assuming the time required to remove the 1.85 m^3 excess water to obtain the crystallization concentrations can be calculated and the manufacturers recommendations for cleaning in place are known, the area for the NF unit may then specified to achieve a processing time less than the required 24 hours.

Table 7.1: Predicted values of process parameters for the full scale industrial recovery of sodium cefuroxime.

Membrane Area	Time [h]			Final concentration [mol m^{-3}]		Ratio	Recovery	Final Volume
m^2	Diafiltration Phase	Concentration Phase	Total	Cefuroxime	Lactate	-	%	m^3
1000	1.1	0.9	1.9	54.9	893.5	16.3	98.59	4.73
900	1.3	0.9	2.2	53.8	870.7	16.2	98.57	4.83
800	1.5	1.0	2.5	53.6	855.5	16.0	98.54	4.85
700	1.7	1.2	2.9	53.2	852.1	16.0	98.55	4.88
600	2.1	1.4	3.4	52.9	839.0	15.9	98.53	4.91
500	2.5	1.6	4.1	51.4	828.6	16.1	98.54	5.05
400	3.3	2.0	5.2	51.9	820.1	15.8	98.51	5.00
300	4.4	2.6	7.0	49.9	796.6	16.0	98.51	5.21
200	6.9	3.8	10.7	48.9	779.8	16.0	98.50	5.31
150	9.3	5.0	14.4	48.2	768.4	15.9	98.50	5.38
100	14.0	7.5	21.5	46.8	756.2	16.1	98.51	5.54

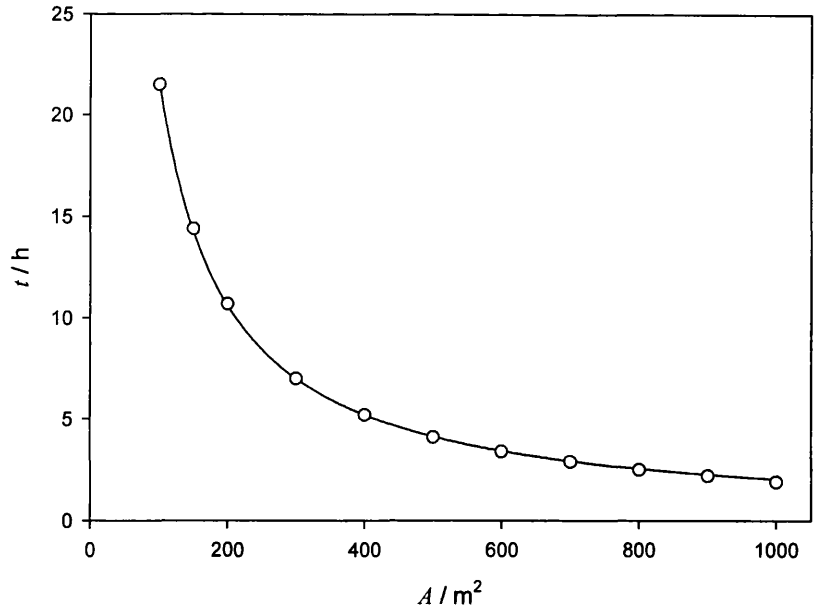

Figure 7.10: Predicted values of membrane area required for the full scale industrial recovery of sodium cefuroxime versus total processing time.

The percentage recovery of sodium cefuroxime from the NF unit in all cases was 98.5 % [justifying the use of constant mass in Eq. (3.81)]. If the process is operated to recover the same quantity of sodium cefuroxime per day, then the production rate is effectively lowered as a direct result of the increase in recovery efficiency caused by the inclusion of NF technology. In addition, the crystallization unit will have an identical load to that previous and will perform with the same efficiency.

The original feed to the crystallization unit was 882 moles day^{-1}, recycling the treated waste stream would reduce this value to 622 moles day^{-1}. This is a reduction in the manufacturing of sodium cefuroxime by 260 moles day^{-1} or 116 kg day^{-1}. The recovery efficiency will increase from 70 % to 99.5 %. This increase in recovery efficiency and in-situ decrease in product manufacturing clearly illustrates that the inclusion of NF technology to the recovery of high value products is indeed an attractive economic proposal.

7.3 Conclusions

Three commercially available NF membranes, namely Nanomax™-50, Desal-5-DK and SelRO® MPF-44, were characterised and assessed for suitability for the sodium cefuroxime recovery process. The Desal-5-DK membrane was selected as most suitable with a sodium cefuroxime rejection of greater than 99.7 % and reasonable sodium lactate transmission. A membrane charge isotherm was developed from the experimental rejection data of different concentration mixtures of sodium cefuroxime and sodium lactate and was employed to predict the diafiltration experiment. Excellent agreement between the experimental findings and the model prediction was observed when the effective membrane charge density was varied with lactate ion concentration.

The model was then used to assess the performance of a possible full scale industrial recovery process. The model results indicate that inclusion of NF technology will indeed facilitate the recovery of the high value antibiotic and produce an effluent of significantly improved quality. The improvement in recovery efficiency values will allow a reduction of the fermentation production rate for the antibiotic which has obvious economic benefit as the new process uses less raw materials and has reduced power and labour demands. In addition, the removal of the antibiotic from the process waste stream produces an effluent of higher quality, which not only has a reduced environmental cost burden but may indeed offer a significantly cheaper disposal method.

8 Overall Conclusions and Recommendations

The objective of the work presented in this thesis was to perform an industrial assessment of the UDSPM and linear UDSPM models for membrane nanofiltration and address several unanswered questions pertaining to the limitations of such theoretical descriptions when applied to separations of real industrial interest.

8.1 Conclusions

Nanofiltration membranes are being increasingly employed as a viable alternative to more established separation processes in a diverse range of industries due to their ability to separate and concentrate small solutes effectively. Reliable predictive NF models are required that can identify at an early stage possible process options and operating limits. Such predictive models will reduce development risk and time, thus promoting the wider use of membrane technology in process industries such as pharmaceutical and fine chemical manufacture.

The main advantage of using the laboratory scale dead-end experimental apparatus in this study was that experiments could be conducted with real industrial materials. Unfortunately, pharmaceuticals of industrial importance are extremely expensive to obtain and the costs of operating a pilot-scale nanofiltration plant are significant when considering the quantities of material needed. Sufficient experimental evidence has been reported in the literature to suggest that the results obtained from laboratory scale apparatus are representative of full scale industrial equipment. An experimental analysis of the mass transfer characteristics of the laboratory scale dead-end filtration cell used in all experiments showed that the concentration polarisation effects could be neglected.

Previous theoretical descriptions of NF processes have been successful in describing the separations of simple ideal systems such as uncharged solutes and monovalent salts. However, the success of the DSPM model was largely due to the arbitrary optimisation of the parameter $\Delta x/A_k$ at constant r_p, which is physically inconsistent as

these two parameters are linked through the membrane permeability and rejection is independent of membrane thickness. For this reason, the descriptions of NF used in this study focus on the updated DSPM model (UDSPM) and the more recent linearised UDSPM model. The linearised UDSPM has distinct advantages over the UDSPM model in terms of computational time and complexity.

A comprehensive theoretical comparison was made between the predicted rejection obtained from both the UDSPM model and the linearised UDSPM model in order to ascertain the range of validity of the linearised model. Predicted rejection for uncharged solutes, binary, ternary and quaternary salt solutions was evaluated over a range of expected NF conditions for both models and the results compared. In general, the linearised UDSPM was found to over predict solute rejection when compared to the UDSPM. This result was confirmed mathematically for the simple case of uncharged solutes and qualitatively for binary salt solutions. The extent of deviation between the two models followed a simple trend in that the discrepancy becomes more significant depending on the level of complexity in the system, i.e. the deviation will be less for a mono-valent binary salt system than for a multi-valent quaternary system. In all cases studied, the average discrepancy between the two models was no more than 10 %, which is suitable for engineering purposes.

The transport of ions through charged membranes has been extensively discussed throughout the literature and separation is considered to occur due to a combination of size (steric) effects, electrical (Donnan) effects and non-steric (dielectric) effects. The mechanism of dielectric exclusion is currently a matter of great debate. At present, the available descriptions of dielectric exclusion are based upon continuum theories (which in themselves are questionable at the near atomic dimensions considered for nanofiltration) and is complicated by the fact that the relationship between Donnan and dielectric effects is non-trivial. For these reasons, current descriptions of dielectric exclusion have been reviewed and two practical models containing dielectric effects have been compared theoretically and experimentally. The results of the comparison indicate that both models, although derived from entirely different mechanisms of dielectric exclusion, calculate the magnitude of the dielectric partitioning coefficient to the same order of magnitude and are equally capable of describing this complex phenomenon with reasonable accuracy. The Born model was

suggested as the most practical method to proceed with at present due to the models practicality and simplicity in comparison with the alternative. Furthermore, as a direct consequence of the coupled nature between membrane charge and dielectric effects, a more detailed description of this phenomena is simply not worth pursuing until a practical and reliable independent measurement of membrane charge is available.

Both the UDSPM and the linearised UDSPM models were then used to predict the performance of membrane nanofiltration in the isolation of *N*-acetyl-D-neuraminic acid (Neu5Ac) an important precursor in the production of the anti-influenza agent Relenza™. The separation involves the removal of pyruvate from the process stream, which is complicated by the fact that Neu5Ac and pyruvate have similar pK_a values. Excellent agreement was observed between the two models for the prediction of component mixtures representative of different stages in the diafiltration process. The linearised UDSPM was then used to simulate the membrane separation performance for the removal of pyruvate by diafiltration. Excellent agreement with the experimental findings was observed when the effective membrane charge density was varied with pyruvate ion concentration. However, the effective membrane charge density proved difficult to predict. Isotherms developed from independent salts and the individual components of the stream in question were inadequate to effectively simulate membrane charge and only the isotherm developed from varying concentrations of the diafiltration components was successful. This indicated that the charging mechanism of the membrane was complex and differs greatly depending on the ionic environment of the feed solution.

The successful application of the UDSPM models in the isolation of Neu5Ac has established two fundamental points: Firstly, the existing nanofiltration models are indeed capable of describing and predicting real multi-component industrial separations. Secondly, the predicted rejection calculated using the linearised UDSPM is representative of the predictions obtained using the UDSPM. This confirms that the linearised UDSPM is sufficient for use as a predictive tool for real process streams which greatly reduces computational time and complexity.

A further investigation of real industrial process separations was made by considering the value added recovery of a high value antibiotic from a process waste stream. The separation involved the recovery of a low concentration cephalosporin antibiotic from the waste stream which contained a high concentration of sodium lactate. Three commercially available membranes were characterised and the Desal-5-DK membrane was found to be most suitable for the required separation. Excellent agreement was observed for the laboratory scale diafiltration when the effective membrane charge density was varied with lactate ion concentration. Again, as was the case for the isolation of Neu5Ac, the effective membrane charge density proved difficult to predict and only an isotherm developed from the diafiltration components was sufficient for modelling purposes. The model was then used to assess the feasibility of a possible full scale industrial recovery process and preliminary outline of design options, product recovery, product purity and operating limits were suggested.

Overall, as a result of the rational approach taken in this study, the use of existing predictive NF models developed for separations at the laboratory scale for application to more complex industrially relevant separations has been established. The isolation and recovery processes used as industrial examples are sufficient to illustrate the power of the modelling tool to facilitate the initial assessment of operating limits and process options including the use of higher concentrations and in-situ product recovery. In this way, such predictive models can guide the process engineer along with economic constraints in defining possible process operating regions and process options for subsequent scale-up, reducing overall development risk and time.

8.2 Recommendations for future work

The work presented in this thesis will be further developed by the following suggestions:

1. The effective membrane charge density is the most troublesome parameter required for NF process prediction to simulate theoretically. Presently there exist a number of experimental methods by which to independently verify

membrane charge densities. However, these methods are severely limited due to the fact that the membrane charge is either measured at the membrane surface or through the membrane pore, none of which accurately describes the volumetric effective membrane charge density. Development of a new measuring technique that will allow unambiguous quantification of the membrane charge density would be invaluable in the characterisation of the active layer of NF membranes and provide increased reality in membrane process prediction. Furthermore, if such a measurement technique was available, a more detailed investigation into dielectric exclusion effects at the membrane-solvent interface could be made using more detailed continuum theories and sophisticated molecular dynamic simulations. At present, these approaches are limited by the sheer lack of quantifiable experimental evidence available.

2. Application of the model to predict further industrial separations of varying complexity in order to gain an understanding of the limits of the predicting capacity. In addition, having established that the linearised UDSPM is capable of predicting process performance for real separations, further reality may be brought into the calculations by considering:

    - A separation where the effects of mass transfer are apparent and must be characterised in order to successfully model the separation.
    - The separation of two species of similar properties where the membrane pore size distribution has a significant effect and must be considered (this has already been achieved theoretically).
    - Modelling a separation that contains fouling materials. This could be achieved by characterisation of the extent of fouling over time and modelling the subsequent change in pore size distribution.

3. Application of the model to predict separations in non-aqueous solvents. Many industrial separations take place in solvents other than water and a systematic study of such separations will further develop understanding in the field of nanofiltration.

4. Develop a computer simulation package to allow non-specialised engineers to use the available NF predictive models for the optimisation of existing NF plants and also perform feasibility studies for new processes. This will guide the process engineer along with economic constraints in defining possible process operating regions and process options for subsequent scale-up, reducing overall development risk and time.

Finally, the work presented in this thesis has improved the understanding of the relative importance of the various separation mechanisms of NF membranes. The use of available NF models for application in the prediction of real industrial process separations has been established and represents a significant contribution to the field of NF modelling.

Appendices

Appendix A1: Theoretical information

In the section that follows, mathematical expressions related to the UDSPM model will be presented which are developed from the equations derived in Chapter 3. Note that the parameter Y has been omitted as this parameter was not used throughout the numerical simulations as the specific volume of the solutes used was not available.

Derivation of the linearised uncharged solute equation

The uncharged solute form of Eq. (3.58) gives

$$\frac{\Delta c_i}{\Delta x} = \frac{V}{D_{i,p}}\left[K_{i,c}c_{i,av} - C_{i,p}\right] \tag{A1}$$

Rearrangement of Eq. (A1) gives

$$\Delta c_i = \frac{K_{i,c}V\Delta x}{D_{i,p}}\left[c_{i,av} - \frac{C_{i,p}}{K_{i,c}}\right] \tag{A2}$$

Substitution of the Peclet number gives

$$\Delta c_i = Pe\left[c_{i,av} - \frac{C_{i,p}}{K_{i,c}}\right] \tag{A3}$$

The boundary conditions for an uncharged membrane are derived from equilibrium partitioning and are given as

$$c_{i,(0)} = \Phi_i C_{i,w} \tag{A4}$$

$$c_{i,(\Delta x)} = \Phi_i C_{i,p} \tag{A5}$$

By definition

$$\Delta c_i = c_{i,(\Delta x)} - c_{i,(0)} \tag{A6}$$

Substitution of Eqs. (A4) and (A5) into Eq. (A6) yields

$$\Delta c_i = \Phi_i \left(C_{i,p} - C_{i,w} \right) \tag{A7}$$

By definition

$$c_{i,av} = \frac{1}{2} \left(c_{i,(0)} + c_{i,(\Delta x)} \right) \tag{A8}$$

Substitution of Eqs. (A4) and (A5) into Eq. (A8) yields

$$c_{i,av} = \frac{1}{2} \Phi_i \left(C_{i,p} + C_{i,w} \right) \tag{A9}$$

Substitution of Eqs. (A7) and (A9) into Eq. (A3) yields

$$\Phi_i \left(C_{i,p} - C_{i,w} \right) = Pe \left[\frac{1}{2} \Phi_i \left(C_{i,p} + C_{i,w} \right) - \frac{C_{i,p}}{K_{i,c}} \right] \tag{A10}$$

Rearrangement of Eq. (A10) gives

$$\frac{C_{i,p}}{C_{i,w}} = \frac{\frac{1}{2} \Phi_i K_{i,c} + \frac{\Phi_i K_{i,c}}{Pe}}{\frac{\Phi_i K_{i,c}}{Pe} + 1 - \frac{1}{2} \Phi_i K_{i,c}} \tag{A11}$$

By definition

$$\frac{C_{i,p}}{C_{i,w}} = 1 - R \tag{A12}$$

Substitution of Eq. (A12) into Eq. (A11) gives

$$1-R=\frac{\frac{1}{2}\Phi_i K_{i,c}+\frac{\Phi_i K_{i,c}}{Pe}}{\frac{\Phi_i K_{i,c}}{Pe}+1-\frac{1}{2}\Phi_i K_{i,c}} \tag{A13}$$

Rearrangement of Eq. (A13) yields the result

$$R=\frac{1-\Phi_i K_{i,c}}{1-\frac{1}{2}\Phi_i K_{i,c}+\frac{\Phi_i K_{i,c}}{Pe}} \tag{A14}$$

Transport equations for binary, ternary and quaternary systems

The full derivation of the extended Nernst-Planck equation has been provided in Chapter 3 and will not be detailed here to avoid repetition. Eq. (3.43) gives

$$\frac{dc_i}{dx}=\frac{V}{D_{i,p}}\left[\left\{K_{i,c}-Y\right\}c_i-C_{i,p}\right]-z_i c_i\left[\frac{\sum_{i=1}^{n}\frac{z_i V}{D_{i,p}}\left[\left\{K_{i,c}-Y\right\}c_i-C_{i,p}\right]}{\sum_{i=1}^{n}z_i^2 c_i}\right] \tag{A15}$$

As Eq. (A15) contains a summation, each multi-component system will require a different form of the transport equation. Consider that Eq. (A15) is of the general form

$$\frac{dc_i}{dx}=\frac{V}{D_{i,p}}\left[K_{i,c}c_i-C_{i,p}\right]-c_i z_i\frac{F}{RT}\frac{d\psi}{dx} \tag{A16}$$

The unique expression for a binary solution is then obtained by substitution of the following expression into Eq. (A16)

$$\frac{d\psi}{dx} = \frac{a_1 c_1 + a_2 C_{1,p} - a_3 X_d}{a_4 c_1 - a_5 X_d} \tag{A17}$$

Where the constants in Eq. (A17) are given by

$$a_1 = z_1 V\left(\frac{K_{1,c}}{D_{1,p}} - \frac{K_{2,c}}{D_{2,p}}\right) \tag{A18a}$$

$$a_2 = z_1 V\left(\frac{1}{D_{2,p}} - \frac{1}{D_{1,p}}\right) \tag{A18b}$$

$$a_3 = \frac{V K_{2,c}}{D_{2,p}} \tag{A18c}$$

$$a_4 = \frac{F}{RT}\left(z_1^2 - z_1 z_2\right) \tag{A18d}$$

$$a_5 = \frac{F}{RT} z_2 \tag{A18e}$$

The unique expression for a ternary solution is then obtained by substitution of the following expression into Eq. (A16)

$$\frac{d\psi}{dx} = \frac{a_1 c_1 + a_2 c_2 + a_3 C_{1,p} + a_4 C_{2,p} - a_5 X_d}{a_6 c_1 + a_7 c_2 - a_8 X_d} \tag{A19}$$

Where the constants in Eq. (A19) are given by

$$a_1 = z_1 V\left(\frac{K_{1,c}}{D_{1,p}} - \frac{K_{3,c}}{D_{3,p}}\right) \tag{A20a}$$

$$a_2 = z_2 V\left(\frac{K_{2,c}}{D_{2,p}} - \frac{K_{3,c}}{D_{3,p}}\right) \tag{A20b}$$

$$a_3 = z_1 V\left(\frac{1}{D_{3,p}} - \frac{1}{D_{1,p}}\right) \tag{A20c}$$

$$a_4 = z_2 V\left(\frac{1}{D_{3,p}} - \frac{1}{D_{2,p}}\right) \tag{A20d}$$

$$a_5 = \frac{VK_{3,c}}{D_{3,p}} \tag{A20e}$$

$$a_6 = \frac{F}{RT}\left(z_1^2 - z_1 z_3\right) \tag{A20f}$$

$$a_7 = \frac{F}{RT}\left(z_2^2 - z_2 z_3\right) \tag{A20g}$$

$$a_8 = \frac{F}{RT} z_3 \tag{A20h}$$

The unique expression for a quaternary solution is then obtained by substitution of the following expression into Eq. (A16)

$$\frac{d\psi}{dx} = \frac{a_1 c_1 + a_2 c_2 + a_3 c_3 + a_4 C_{1,p} + a_5 C_{2,p} + a_6 C_{3,p} - a_7 X_d}{a_8 c_1 + a_9 c_2 + a_{10} c_3 - a_{11} X_d} \tag{A21}$$

Where the constants in Eq. (A21) are given by

$$a_1 = z_1 V\left(\frac{K_{1,c}}{D_{1,p}} - \frac{K_{4,c}}{D_{4,p}}\right) \tag{A22a}$$

$$a_2 = z_2 V\left(\frac{K_{2,c}}{D_{2,p}} - \frac{K_{4,c}}{D_{4,p}}\right) \tag{A22b}$$

$$a_3 = z_3 V\left(\frac{K_{3,c}}{D_{3,p}} - \frac{K_{4,c}}{D_{4,p}}\right) \tag{A22c}$$

$$a_4 = z_1 V\left(\frac{1}{D_{4,p}} - \frac{1}{D_{1,p}}\right) \tag{A22d}$$

$$a_5 = z_2 V\left(\frac{1}{D_{4,p}} - \frac{1}{D_{2,p}}\right) \tag{A22e}$$

$$a_6 = z_3 V\left(\frac{1}{D_{4,p}} - \frac{1}{D_{3,p}}\right) \tag{A22f}$$

$$a_7 = V\frac{K_{4,c}}{D_{4,p}} \tag{A22g}$$

$$a_8 = \frac{F}{RT}\left(z_1^2 - z_1 z_4\right) \tag{A22h}$$

$$a_9 = \frac{F}{RT}\left(z_2^2 - z_2 z_4\right) \tag{A22i}$$

$$a_{10} = \frac{F}{RT}\left(z_3^2 - z_3 z_4\right) \tag{A22j}$$

$$a_{11} = \frac{F}{RT} z_4 \tag{A22k}$$

Note that there is a successive pattern between the evolution of the transport equations for the three systems considered. Therefore, the transport equations for a system of any order may be rapidly obtained without the need for tedious derivation.

The linearised forms of the transport equations are then obtained by simple substitution of the following expressions into the relevant transport equation.

$$\frac{dc}{dx} = \frac{\Delta c}{\Delta x} \text{ and } c_i = c_{i,av} \tag{A23}$$

Where the average solute concentration and the linearised solute concentration gradient are defined as

$$\frac{dc_i}{dx} \approx \frac{\Delta c_i}{\Delta x} = \frac{c_i(\Delta x) - c_i(0)}{\Delta x} \tag{A24}$$

$$c_{i,av} = \frac{c_i(0) + c_i(\Delta x)}{2} \tag{A25}$$

Equilibrium partitioning expressions for binary, ternary and quaternary systems

The generalised equilibrium equation was provided in the full text as Eq. (3.50) and is represented as

$$\frac{\gamma_i c_i}{\gamma_i^o C_i} = \Phi_i \exp\left(-\frac{z_i F}{RT}\Delta\psi_D\right)\exp\left(-\frac{\Delta W_i}{k_B T}\right) \quad \text{(A26)}$$

Neglecting activity coefficients and rearranging Eq. (A26) gives

$$\frac{c_i}{C_i} = \Phi_i' \exp\left(-\frac{z_i F}{RT}\Delta\psi_D\right) \quad \text{(A27)}$$

Considering the feed side of the membrane and rearranging Eq. (A27) gives

$$\Delta\psi_D = -\frac{RT}{z_i F}\ln\left|\frac{c_{i(0)}}{C_{i,p}\Phi_i'}\right| \quad \text{(A28)}$$

The Donnan term for a given bulk solution-membrane interface will be equal for all ions (the magnitude of this value will differ at a different interface, i.e. the magnitude of the Donnan term will be different for the feed-membrane interface and the permeate-membrane interface). Therefore expressions can be developed for all ions in relation to ion 1, i.e.

$$c_{2(0)} = C_{2,w}\Phi_2'\left(\frac{c_{1(0)}}{C_{1,w}\Phi_1'}\right)^{\frac{z_2}{z_1}} \quad \text{(A29a)}$$

$$c_{3(0)} = C_{3,w}\Phi_3'\left(\frac{c_{1(0)}}{C_{1,w}\Phi_1'}\right)^{\frac{z_3}{z_1}} \quad \text{(A29b)}$$

$$c_{4(0)} = C_{4,w}\Phi_4'\left(\frac{c_{1(0)}}{C_{1,w}\Phi_1'}\right)^{\frac{z_4}{z_1}} \quad \text{(A29c)}$$

Electroneutrality inside the pore gives

$$\sum_{i=1}^{i=n} z_i c_i + X_d = 0 \qquad \text{(A30)}$$

Substitution of Eqs. (29a,b and c) into Eq. (A30) will yield (for a quaternary system)

$$z_1 c_{1(0)} + z_2 C_{2,w} \Phi'_2 \left(\frac{c_{1(0)}}{C_{1,w} \Phi'_1} \right)^{\frac{z_2}{z_1}} + z_3 C_{3,w} \Phi'_3 \left(\frac{c_{1(0)}}{C_{1,w} \Phi'_1} \right)^{\frac{z_3}{z_1}} + z_4 C_{4,w} \Phi'_4 \left(\frac{c_{1(0)}}{C_{1,w} \Phi'_1} \right)^{\frac{z_4}{z_1}} + X_d = 0 \qquad \text{(A31)}$$

Eq. (A31) is a polynomial expression in terms of $c_{1(0)}$ with, for the case of the feed side, all values of $C_{i,w}$ are known. Therefore, $c_{1(0)}$ is evaluated from standard polynomial solution techniques and the other feed side membrane concentrations are then evaluated from Eqs. (29a,b and c). For the lower order systems, i.e. binary and ternary, Eq. (A31) is simply reduced by eliminating the higher order terms.

For the case of the permeate side of the membrane, completely analogous expressions exist and Eq. (A31) becomes

$$z_1 c_{1(\Delta x)} + z_2 C_{2,p} \Phi'_2 \left(\frac{c_{1(\Delta x)}}{C_{1,p} \Phi'_1} \right)^{\frac{z_2}{z_1}} + z_3 C_{3,p} \Phi'_3 \left(\frac{c_{1(\Delta x)}}{C_{1,p} \Phi'_1} \right)^{\frac{z_3}{z_1}} + z_4 C_{4,p} \Phi'_4 \left(\frac{c_{1(\Delta x)}}{C_{1,p} \Phi'_1} \right)^{\frac{z_4}{z_1}} + X_d = 0 \qquad \text{(A32)}$$

Again, Eq. (A32) is a polynomial expression in terms of $c_{1(\Delta x)}$. However, in this case the bulk permeate values are the guess values for the iteration step. Solution is obtained in exactly the same way as for Eq. (A31) and the remaining membrane concentrations are obtained from

$$c_{2(\Delta x)} = C_{2,p} \Phi'_2 \left(\frac{c_{1(\Delta x)}}{C_{1,p} \Phi'_1} \right)^{\frac{z_2}{z_1}} \qquad \text{(A33a)}$$

$$c_{3(\Delta x)} = C_{3,p}\Phi'_3\left(\frac{c_{1(\Delta x)}}{C_{1,p}\Phi'_1}\right)^{\frac{z_3}{z_1}} \qquad \text{(A33b)}$$

$$c_{4(\Delta x)} = C_{4,p}\Phi'_4\left(\frac{c_{1(\Delta x)}}{C_{1,p}\Phi'_1}\right)^{\frac{z_4}{z_1}} \qquad \text{(A33c)}$$

Similarly, for the lower order solutions, the higher order terms are eliminated from Eq. (A32).

Appendix A2: Examples of the Fortran™ code

In order to solve the equations for ion transport developed throughout this thesis, computer codes using the programming language Fortran™ were developed. Only examples of the more sophisticated codes are provided here. Codes for simple salt systems were provided by Welfoot (2001).

Full UDSPM model, quaternary prediction of rejection versus ΔP_e

This code was written in order to predict the rejection of the individual ions in a quaternary system. The code has been developed to accept ions of any given valence.

```
C============================4IONS.FOR=============================C
C--- Calculation of the ion rejection versus pressure for a system -C
C--- of 4 ions. Final version for 4 ions written by D. Oatley on   -C
C--- 30/10/2001.                                                   -C
C--- SYSTEM: Na +(1); Mg 2+(2); SO4 2-(3); Cl -(4);                -C
C============================MAIN PROGRAM============================C
      PROGRAM MAIN
      IMPLICIT DOUBLE PRECISION (A-Z)
      INTEGER*4 I,J,K,N,NMAX,SWITCH
      PARAMETER (NMAX=5)
      DIMENSION C0(1:NMAX),CW(1:NMAX),D0(1:NMAX),DELTAW(1:NMAX),
     +          DP(1:NMAX),KD(1:NMAX),KC(1:NMAX),
     +          LAMBDA(1:NMAX),PHI(1:NMAX),RSOL(1:NMAX),SVOL(1:NMAX),
     +          TESTFUNC(1:7),Y(1:NMAX),Z(1:NMAX)
      COMMON /SUB_RK/ C0,DELTAW,DP,DX,KC,PHI,VEL,Y,Z
      COMMON /ALL/    BOLTZC,F,N,R,TEMP,XD
C
C=====FIXED INPUT DATA=====
      PI=DACOS(-1D0)
```

```
C---Effective pore radius [m]
C      RP=2D-9
C---Pore length [m]
       DX=1D-6
C---Effective charge density [mol m-3]
C      XD=-0.01D0
C---Faraday constant [C mol-1]
       F=96487D0
C---Gas constant [J mol-1 K-1]
       R=8.314D0
C---Boltzmann constant [J K-1]
       BOLTZC=1.38066D-23
C---Temperature [K]
       TEMP=298D0
C---Electric field constant [C V-1 m-1]
       ELEFIELDC=8.85419D-12
C---Elemental electron charge [J V-1]
       CHARGE=1.602177D-19
C---Bulk solvent viscosity at given temp [kg m-1 s-1]
       VISCOS=0.893D-3
C---Bulk dielectric constant
       DIELECB=80D0
C---Dielectric constant in oriented solvent layer
       DIELECL=35D0
C
C=====ION DATA=====
C---Number of ion species
       N=4
C---Valence of ions
       Z(1)=1D0
       Z(2)=2D0
       Z(3)=-2D0
       Z(4)=-1D0
C---Bulk ion diffusion coefficients [m2 s-1]
       D0(1)=1.333D-9
       D0(2)=0.705D-9
       D0(3)=1.602D-9
       D0(4)=2.301D-9
C---Ion radius in solvent [m]
       RSOL(1)=1.840D-10
       RSOL(2)=3.479D-10
       RSOL(3)=2.309D-10
       RSOL(4)=1.207D-10
C---Bulk ion concentration on wall side [mol m-3]
       CW(1)=2.43D0
       CW(2)=20.2D0
       CW(3)=CW(2)
       CW(4)=CW(1)
C---Partial molar volume [m3 mol-1]
       SVOL(1)=-1.20D-6
       SVOL(2)=-21.57D-6
       SVOL(3)=14.18D-6
       SVOL(4)=17.82D-6
C
       RP=2D-9
       DCHARGE=-0.1D0
       XD=DCHARGE*(CW(1)+CW(2)+CW(3)+CW(4))
C=====CALCULATION OF PORE SIZE DEPENDENT TRANSPORT PROPERTIES=====
C---Calculation of pore viscosity
       IF (RP.LE.0.28D-9) THEN
          VISCP=10D0*VISCOS
```

```
      ELSE
         RATIO=0.28D-9/RP
         VISCP=VISCOS*(1D0+(18D0*RATIO)-(9D0*(RATIO**2)))
      ENDIF
C---Calculation of hindrance factors
      DO I=1,N
         LAMBDA(I)=RSOL(I)/RP
         PHI(I)=(1D0-LAMBDA(I))**2
         KD(I)=1D0-(2.3D0*LAMBDA(I))+(1.154D0*(LAMBDA(I))**2)
     +                  +(0.224D0*(LAMBDA(I))**3)
         KC(I)=(1D0+(0.054D0*LAMBDA(I))-(0.988D0*(LAMBDA(I))**2)
     +                  +(0.441D0*(LAMBDA(I))**3))*(2D0-PHI(I))
         DP(I)=(KD(I)*D0(I)*VISCOS)/VISCP
         Y(I)=(8D0*DP(I)*SVOL(I)*VISCP)/(R*TEMP*(RP**2))
      ENDDO
C---Calculation of the pore dielectric constant
      IF (RP.LE.0.28D-9) THEN
         DIELECP=DIELECL
      ELSE
         MU=0.28D-9/RP
         FUNC=DIELECB-DIELECL
         DIELECP=DIELECB-(2D0*MU*FUNC)+(FUNC*(MU**2))
      ENDIF
C---Calculation of the Born energy barrier
      FUNC2=(1D0/DIELECP)-(1D0/DIELECB)
      DO I=1,N
          DELTAW(I)=(((Z(I)**2)*(CHARGE**2))/
     +           (8D0*PI*ELEFIELDC*RSOL(I)))*FUNC2
      ENDDO
C
C=====CALL PORE INLET CONCENTRATIONS FROM SUBROUTINE PARTITN=====
      CALL PARTITN(CW,DELTAW,PHI,Z,C0)
C
C=====CALCULATION OF THE REJECTION=====
C---Initial pressure and step size
      PRESS=0.0D6
      DPRESS=0.1D6
C---Initial CP1 maximum and minimum values
      CP1MIN=1D-4*CW(1)
      CP1MAX=CW(1)
C---Initial CP2 maximum and minimum values
      CP2MIN=1D-4*CW(2)
      CP2MAX=CW(2)
C---Initial CP3 maximum and minimum values
      CP3MIN=1D-4*CW(3)
      CP3MAX=CW(3)
C---Starting CP(i) values
      CP1START=(CP1MIN+CP1MAX)/2D0
      CP2START=(CP2MIN+CP2MAX)/2D0
      CP3START=(CP3MIN+CP3MAX)/2D0
C---Open output file
      OPEN(5,FILE='4IONS.RES')
      WRITE(5,3600)0D0,0D0,0D0,0D0,0D0
C---Calculation
      DO J=1,30
         PRESS=PRESS+DPRESS
         VEL=(PRESS*(RP**2))/(8D0*DX*VISCP)
         CP1STEP=(CP1MAX-CP1MIN)/5D0
         CP2STEP=(CP2MAX-CP2MIN)/5D0
         CP3STEP=(CP3MAX-CP3MIN)/5D0
C---Initial Cp1 values
```

```
          CP1C=CP1START
          CP1N=CP1C
          CP1E=CP1C+CP1STEP
          CP1SE=CP1C
          CP1S=CP1C
          CP1W=CP1C-CP1STEP
          CP1NW=CP1C
C---Initial Cp2 values
          CP2C=CP2START
          CP2N=CP2C+CP2STEP
          CP2E=CP2C
          CP2SE=CP2C
          CP2S=CP2C-CP2STEP
          CP2W=CP2C
          CP2NW=CP2C
C---Initial Cp3 values
          CP3C=CP3START
          CP3N=CP3C
          CP3E=CP3C
          CP3SE=CP3C+CP3STEP
          CP3S=CP3C
          CP3W=CP3C
          CP3NW=CP3C-CP3STEP
C---Initial test function
          TEST=10D0
          DOWHILE (TEST.GT.1D-12)
C---Calculation of concentration at each point
             CALL ROOT(CP1C,CP2C,CP3C,CP4C,CDX1C,CDX2C,CDX3C,CDX4C)
             CALL ROOT(CP1N,CP2N,CP3N,CP4N,CDX1N,CDX2N,CDX3N,CDX4N)
             CALL ROOT(CP1E,CP2E,CP3E,CP4E,CDX1E,CDX2E,CDX3E,CDX4E)
             CALL ROOT(CP1SE,CP2SE,CP3SE,CP4SE,CDX1SE,CDX2SE,CDX3SE,
     +                 CDX4SE)
             CALL ROOT(CP1S,CP2S,CP3S,CP4S,CDX1S,CDX2S,CDX3S,CDX4S)
             CALL ROOT(CP1NW,CP2NW,CP3NW,CP4NW,CDX1NW,CDX2NW,CDX3NW,
     +                 CDX4NW)
             CALL ROOT(CP1W,CP2W,CP3W,CP4W,CDX1W,CDX2W,CDX3W,CDX4W)
C---Determination of test functions
             CALL CONC(CP1N,CP2N,CP3N,CP4N,CDX1N,CDX2N,CDX3N,CDX4N,
     +                 SWITCH)
             IF (SWITCH.EQ.0) THEN
                CALL RK(CP1N,CP2N,CP3N,CP4N,CDX1N,CDX2N,CDX3N,CDX4N,
     +                  TESTN)
             ELSE
                TESTN=100D0
                SWITCH=0
             ENDIF
             CALL CONC(CP1E,CP2E,CP3E,CP4E,CDX1E,CDX2E,CDX3E,CDX4E,
     +                 SWITCH)
             IF (SWITCH.EQ.0) THEN
                CALL RK(CP1E,CP2E,CP3E,CP4E,CDX1E,CDX2E,CDX3E,CDX4E,
     +                  TESTE)
             ELSE
                TESTE=100D0
                SWITCH=0
             ENDIF
             CALL CONC(CP1SE,CP2SE,CP3SE,CP4SE,CDX1SE,CDX2SE,CDX3SE,
     +                 CDX4SE,SWITCH)
             IF (SWITCH.EQ.0) THEN
                CALL RK(CP1SE,CP2SE,CP3SE,CP4SE,CDX1SE,CDX2SE,CDX3SE,
     +                  CDX4SE,TESTSE)
             ELSE
```

```
               TESTSE=100D0
               SWITCH=0
            ENDIF
            CALL CONC(CP1S,CP2S,CP3S,CP4S,CDX1S,CDX2S,CDX3S,CDX4S,
     +                  SWITCH)
            IF (SWITCH.EQ.0) THEN
               CALL RK(CP1S,CP2S,CP3S,CP4S,CDX1S,CDX2S,CDX3S,CDX4S,
     +                  TESTS)
            ELSE
               TESTS=100D0
               SWITCH=0
            ENDIF
            CALL CONC(CP1W,CP2W,CP3W,CP4W,CDX1W,CDX2W,CDX3W,CDX4W,
     +                  SWITCH)
            IF (SWITCH.EQ.0) THEN
               CALL RK(CP1W,CP2W,CP3W,CP4W,CDX1W,CDX2W,CDX3W,CDX4W,
     +                  TESTW)
            ELSE
               TESTW=100D0
               SWITCH=0
            ENDIF
            CALL CONC(CP1NW,CP2NW,CP3NW,CP4NW,CDX1NW,CDX2NW,CDX3NW,
     +                  CDX4NW,SWITCH)
            IF (SWITCH.EQ.0) THEN
               CALL RK(CP1NW,CP2NW,CP3NW,CP4NW,CDX1NW,CDX2NW,CDX3NW,
     +                  CDX4NW,TESTNW)
            ELSE
               TESTNW=100D0
               SWITCH=0
            ENDIF
            CALL CONC(CP1C,CP2C,CP3C,CP4C,CDX1C,CDX2C,CDX3C,CDX4C,
     +                  SWITCH)
            IF (SWITCH.EQ.0) THEN
               CALL RK(CP1C,CP2C,CP3C,CP4C,CDX1C,CDX2C,CDX3C,CDX4C,
     +                  TESTC)
            ELSE
               TESTC=100D0
               SWITCH=0
            ENDIF
C---Evaluation of minimum
            TESTFUNC(1)=TESTC
            TESTFUNC(2)=TESTN
            TESTFUNC(3)=TESTE
            TESTFUNC(4)=TESTSE
            TESTFUNC(5)=TESTS
            TESTFUNC(6)=TESTW
            TESTFUNC(7)=TESTNW
            TESTMIN=20000D0
            DO I=1,7
               IF (TESTFUNC(I).LT.TESTMIN) THEN
                  TESTMIN=TESTFUNC(I)
                  K=I
               ENDIF
            ENDDO
            IF (K.EQ.1) THEN
               TEST=TESTC
               CP1STEP=CP1STEP/1.1D0
               CP2STEP=CP2STEP/1.1D0
               CP3STEP=CP3STEP/1.1D0
               CP1C=CP1C
               CP1N=CP1C
```

```
      CP1E=CP1C+CP1STEP
      CP1SE=CP1C
      CP1S=CP1C
      CP1W=CP1C-CP1STEP
      CP1NW=CP1C
      CP2C=CP2C
      CP2N=CP2C+CP2STEP
      CP2E=CP2C
      CP2SE=CP2C
      CP2S=CP2C-CP2STEP
      CP2W=CP2C
      CP2NW=CP2C
      CP3C=CP3C
      CP3N=CP3C
      CP3E=CP3C
      CP3SE=CP3C+CP3STEP
      CP3S=CP3C
      CP3W=CP3C
      CP3NW=CP3C-CP3STEP
   ENDIF
   IF (K.EQ.2) THEN
      TEST=TESTN
      CP1C=CP1N
      CP1N=CP1C
      CP1E=CP1C+CP1STEP
      CP1SE=CP1C
      CP1S=CP1C
      CP1W=CP1C-CP1STEP
      CP1NW=CP1C
      CP2C=CP2N
      CP2N=CP2C+CP2STEP
      CP2E=CP2C
      CP2SE=CP2C
      CP2S=CP2C-CP2STEP
      CP2W=CP2C
      CP2NW=CP2C
      CP3C=CP3N
      CP3N=CP3C
      CP3E=CP3C
      CP3SE=CP3C+CP3STEP
      CP3S=CP3C
      CP3W=CP3C
      CP3NW=CP3C-CP3STEP
   ENDIF
   IF (K.EQ.3) THEN
      TEST=TESTE
      CP1C=CP1E
      CP1N=CP1C
      CP1E=CP1C+CP1STEP
      CP1SE=CP1C
      CP1S=CP1C
      CP1W=CP1C-CP1STEP
      CP1NW=CP1C
      CP2C=CP2E
      CP2N=CP2C+CP2STEP
      CP2E=CP2C
      CP2SE=CP2C
      CP2S=CP2C-CP2STEP
      CP2W=CP2C
      CP2NW=CP2C
      CP3C=CP3E
```

```
      CP3N=CP3C
      CP3E=CP3C
      CP3SE=CP3C+CP3STEP
      CP3S=CP3C
      CP3W=CP3C
      CP3NW=CP3C-CP3STEP
   ENDIF
   IF (K.EQ.4) THEN
      TEST=TESTSE
      CP1C=CP1SE
      CP1N=CP1C
      CP1E=CP1C+CP1STEP
      CP1SE=CP1C
      CP1S=CP1C
      CP1W=CP1C-CP1STEP
      CP1NW=CP1C
      CP2C=CP2SE
      CP2N=CP2C+CP2STEP
      CP2E=CP2C
      CP2SE=CP2C
      CP2S=CP2C-CP2STEP
      CP2W=CP2C
      CP2NW=CP2C
      CP3C=CP3SE
      CP3N=CP3C
      CP3E=CP3C
      CP3SE=CP3C+CP3STEP
      CP3S=CP3C
      CP3W=CP3C
      CP3NW=CP3C-CP3STEP
   ENDIF
   IF (K.EQ.5) THEN
      TEST=TESTS
      CP1C=CP1S
      CP1N=CP1C
      CP1E=CP1C+CP1STEP
      CP1SE=CP1C
      CP1S=CP1C
      CP1W=CP1C-CP1STEP
      CP1NW=CP1C
      CP2C=CP2S
      CP2N=CP2C+CP2STEP
      CP2E=CP2C
      CP2SE=CP2C
      CP2S=CP2C-CP2STEP
      CP2W=CP2C
      CP2NW=CP2C
      CP3C=CP3S
      CP3N=CP3C
      CP3E=CP3C
      CP3SE=CP3C+CP3STEP
      CP3S=CP3C
      CP3W=CP3C
      CP3NW=CP3C-CP3STEP
   ENDIF
   IF (K.EQ.6) THEN
      TEST=TESTW
      CP1C=CP1W
      CP1N=CP1C
      CP1E=CP1C+CP1STEP
      CP1SE=CP1C
```

```
            CP1S=CP1C
            CP1W=CP1C-CP1STEP
            CP1NW=CP1C
            CP2C=CP2W
            CP2N=CP2C+CP2STEP
            CP2E=CP2C
            CP2SE=CP2C
            CP2S=CP2C-CP2STEP
            CP2W=CP2C
            CP2NW=CP2C
            CP3C=CP3W
            CP3N=CP3C
            CP3E=CP3C
            CP3SE=CP3C+CP3STEP
            CP3S=CP3C
            CP3W=CP3C
            CP3NW=CP3C-CP3STEP
         ENDIF
         IF (K.EQ.7) THEN
            TEST=TESTNW
            CP1C=CP1NW
            CP1N=CP1C
            CP1E=CP1C+CP1STEP
            CP1SE=CP1C
            CP1S=CP1C
            CP1W=CP1C-CP1STEP
            CP1NW=CP1C
            CP2C=CP2NW
            CP2N=CP2C+CP2STEP
            CP2E=CP2C
            CP2SE=CP2C
            CP2S=CP2C-CP2STEP
            CP2W=CP2C
            CP2NW=CP2C
            CP3C=CP3NW
            CP3N=CP3C
            CP3E=CP3C
            CP3SE=CP3C+CP3STEP
            CP3S=CP3C
            CP3W=CP3C
            CP3NW=CP3C-CP3STEP
         ENDIF
         WRITE(*,3601) TEST,J
      ENDDO
      CP4C=-( (Z(1)*CP1C)+(Z(2)*CP2C)+(Z(3)*CP3C) )/
     +                    ( Z(4) )
      REJ1=(1D0-(CP1C/CW(1)))*100D0
      REJ2=(1D0-(CP2C/CW(2)))*100D0
      REJ3=(1D0-(CP3C/CW(3)))*100D0
      REJ4=(1D0-(CP4C/CW(4)))*100D0
      WRITE(5,3600) (PRESS/1D6),(REJ1/100),(REJ2/100),
     +                      (REJ3/100),(REJ4/100)
3600  FORMAT(1X,T4,F12.6,T18,F12.6,T32,F12.6,T46,F12.6,T60,F12.6
     +                                    ,T74,F12.6)
3601  FORMAT(1X,T4,F15.12,T21,I4)
      CP1START=CP1C
      CP2START=CP2C
      CP3START=CP3C
    ENDDO
    CLOSE(5)
    STOP
```

```
      END
C=======================END OF MAIN PROGRAM=========================C
C
C=====================PARTITIONING SUBROUTINE=======================C
      SUBROUTINE PARTITN(CW,DELTAW,PHI,Z,C0)
      IMPLICIT DOUBLE PRECISION (A-Z)
      INTEGER*4 COUNT,I,N,NMAX
      PARAMETER (NMAX=5)
      DIMENSION C0(1:NMAX),CONC(1:NMAX),CW(1:NMAX),DELTAW(1:NMAX),
     +          PHI(1:NMAX),Z(1:NMAX)
      COMMON /ALL/    BOLTZC,F,N,R,TEMP,XD
C
C=====CALCULATION=====
C---Initial values
      PSI=0D0
      TEST=20D0
      COUNT=0
C---Iteration
      DOWHILE (TEST.GT.1D-6)
         PSINEW=PSI
         SUM=0D0
         DO I=1,N
            CONC(I)=CW(I)*PHI(I)*DEXP((-Z(I)*F*PSINEW)/(R*TEMP))*
     +                  DEXP(-DELTAW(I)/(BOLTZC*TEMP))
            SUM=SUM+(Z(I)*CONC(I))
         ENDDO
         TESTNEW=SUM+XD
         IF (COUNT.EQ.0) THEN
            IF (TESTNEW.GT.0) THEN
               PSI=PSINEW+0.1D0
               PSIABOVE=PSINEW
               TEST=DABS(TESTNEW)
               COUNT=1
            ENDIF
            IF (TESTNEW.LT.0) THEN
               PSI=PSINEW-0.1D0
               PSIBELOW=PSINEW
               TEST=DABS(TESTNEW)
               COUNT=2
            ENDIF
         ENDIF
         IF (COUNT.EQ.1) THEN
            IF (TESTNEW.GT.0) THEN
               PSI=PSINEW+0.1D0
               PSIABOVE=PSINEW
               TEST=DABS(TESTNEW)
            ENDIF
            IF (TESTNEW.LT.0) THEN
               PSI=PSINEW-0.1D0
               PSIBELOW=PSINEW
               TEST=DABS(TESTNEW)
               COUNT=3
            ENDIF
         ENDIF
         IF (COUNT.EQ.2) THEN
            IF (TESTNEW.GT.0) THEN
               PSI=PSINEW+0.1D0
               PSIABOVE=PSINEW
               TEST=DABS(TESTNEW)
               COUNT=3
            ENDIF
```

```
            IF (TESTNEW.LT.0) THEN
               PSI=PSINEW-0.1D0
               PSIBELOW=PSINEW
               TEST=DABS(TESTNEW)
            ENDIF
         ENDIF
         IF (COUNT.EQ.3) THEN
            IF (TESTNEW.GT.0) THEN
               PSIABOVE=PSINEW
               TEST=DABS(TESTNEW)
            ENDIF
            IF (TESTNEW.LT.0) THEN
               PSIBELOW=PSINEW
               TEST=DABS(TESTNEW)
            ENDIF
            PSI=(PSIABOVE+PSIBELOW)/2D0
         ENDIF
      ENDDO
C
C=====CONCENTRATION AT PORE ENTRANCE=====
      DO I=1,N
         C0(I)=CONC(I)
      ENDDO
C
C---Return to main program
      RETURN
      END
C====================END OF PARTITIONING SUBROUTINE==================C
C
C=======================RUNGE-KUTTA SUBROUTINE====================C
      SUBROUTINE RK(CP1,CP2,CP3,CP4,CDX1,CDX2,CDX3,CDX4,TEST)
      IMPLICIT DOUBLE PRECISION (A-Z)
      INTEGER*4 I,J,N,NMAX,NSTEP
      PARAMETER (NMAX=5)
      DIMENSION C0(1:NMAX),C1(1:NMAX),C2(1:NMAX),C3(1:NMAX),
     +          C4(1:NMAX),CION1(1:500),CION2(1:500),CION3(1:500),
     +          CION4(1:500),CP(1:NMAX),DELTAW(1:NMAX),DP(1:NMAX),
     +          K1(1:NMAX),K2(1:NMAX),K3(1:NMAX),K4(1:NMAX),
     +          KC(1:NMAX),PHI(1:NMAX),Y(1:NMAX),Z(1:NMAX)
      COMMON /SUB_RK/ C0,DELTAW,DP,DX,KC,PHI,VEL,Y,Z
      COMMON /ALL/    BOLTZC,F,N,R,TEMP,XD
C
C=====CALCULATION=====
C---Step size
      NSTEP=200
      H=-DX/NSTEP
C      DIST=DX
C---Initial concentrations
      CION1(1)=CDX1
      CION2(1)=CDX2
      CION3(1)=CDX3
      CION4(1)=CDX4
C---PREPARING OUTPUT FILE
C      OPEN(6,FILE='CONCPRO.RES')
C      WRITE(6,13) DIST/DX,CDX3/C0(3)
C---Initial permeate concentrations
      CP(1)=CP1
      CP(2)=CP2
      CP(3)=CP3
      CP(4)=CP4
C---Setting up loop
```

```
      DO J=1,NSTEP
C---Runge-Kutta method
         C1(1)=CION1(J)
         C1(2)=CION2(J)
         C1(3)=CION3(J)
         C1(4)=CION4(J)
C---1st order Runge-Kutta algorithm
         TOP=0D0
         BOT=0D0
         DO I=1,N
            TOP=TOP+((Z(I)*VEL/DP(I))*(((KC(I)-Y(I))*C1(I))-CP(I)))
            BOT=BOT+((Z(I)**2)*C1(I))
         ENDDO
         DPSIDX=TOP/((F*BOT)/(R*TEMP))
         DO I=1,N
            K1(I)=((VEL/DP(I))*(((KC(I)-Y(I))*C1(I))-CP(I))) -
     +              ((Z(I)*C1(I)*F*DPSIDX)/(R*TEMP))
         ENDDO
C---2nd order Runge-Kutta algorithm
         C2(1)=C1(1)+(0.5D0*H*K1(1))
         C2(2)=C1(2)+(0.5D0*H*K1(2))
         C2(3)=C1(3)+(0.5D0*H*K1(3))
         C2(4)=C1(4)+(0.5D0*H*K1(4))
         TOP=0D0
         BOT=0D0
         DO I=1,N
            TOP=TOP+((Z(I)*VEL/DP(I))*(((KC(I)-Y(I))*C2(I))-CP(I)))
            BOT=BOT+((Z(I)**2)*C2(I))
         ENDDO
         DPSIDX=TOP/((F*BOT)/(R*TEMP))
         DO I=1,N
            K2(I)=((VEL/DP(I))*(((KC(I)-Y(I))*C2(I))-CP(I))) -
     +              ((Z(I)*C2(I)*F*DPSIDX)/(R*TEMP))
         ENDDO
C---3rd order Runge-Kutta algorithm
         C3(1)=C2(1)+(0.5D0*H*K2(1))
         C3(2)=C2(2)+(0.5D0*H*K2(2))
         C3(3)=C2(3)+(0.5D0*H*K2(3))
         C3(4)=C2(4)+(0.5D0*H*K2(4))
         TOP=0D0
         BOT=0D0
         DO I=1,N
            TOP=TOP+((Z(I)*VEL/DP(I))*(((KC(I)-Y(I))*C3(I))-CP(I)))
            BOT=BOT+((Z(I)**2)*C3(I))
         ENDDO
         DPSIDX=TOP/((F*BOT)/(R*TEMP))
         DO I=1,N
            K3(I)=((VEL/DP(I))*(((KC(I)-Y(I))*C3(I))-CP(I))) -
     +              ((Z(I)*C3(I)*F*DPSIDX)/(R*TEMP))
         ENDDO
C---4th order Runge-Kutta algorithm
         C4(1)=C3(1)+(H*K3(1))
         C4(2)=C3(2)+(H*K3(2))
         C4(3)=C3(3)+(H*K3(3))
         C4(4)=C3(4)+(H*K3(4))
         TOP=0D0
         BOT=0D0
         DO I=1,N
            TOP=TOP+((Z(I)*VEL/DP(I))*(((KC(I)-Y(I))*C4(I))-CP(I)))
            BOT=BOT+((Z(I)**2)*C4(I))
         ENDDO
```

```
          DPSIDX=TOP/((F*BOT)/(R*TEMP))
          DO I=1,N
             K4(I)=((VEL/DP(I))*(((KC(I)-Y(I))*C4(I))-CP(I))) -
     +               ((Z(I)*C4(I)*F*DPSIDX)/(R*TEMP))
          ENDDO
C---Final concentrations
          CION1(J+1)=CION1(J) +
     +               ( (H/6D0)*(K1(1)+(2D0*K2(1))+(2D0*K3(1))+K4(1)) )
          CION2(J+1)=CION2(J) +
     +               ( (H/6D0)*(K1(2)+(2D0*K2(2))+(2D0*K3(2))+K4(2)) )
          CION3(J+1)=CION3(J) +
     +               ( (H/6D0)*(K1(3)+(2D0*K2(3))+(2D0*K3(3))+K4(3)) )
          CION4(J+1)=CION4(J) +
     +               ( (H/6D0)*(K1(4)+(2D0*K2(4))+(2D0*K3(4))+K4(4)) )
C
C---OUTPUTTING PROFILE
C
C          DIST=DIST+H
C          WRITE(6,13) DIST/DX,CION3(J+1)/C0(3)
C
       ENDDO
C
       IF (CION1(J).LT.0D0.OR.CION2(J).LT.0D0.OR.CION3(J).LT.0D0.
     +    OR.CION4(J).LT.0D0) THEN
          TEST=100D0
       ELSE
          TEST1=(CION1(J)-C0(1))
          TEST2=(CION2(J)-C0(2))
          TEST3=(CION3(J)-C0(3))
          TEST=(TEST1**2)+(TEST2**2)+(TEST3**2)
       ENDIF
C---CLOSING OUTPUT FILE
C  13  FORMAT(1X,T4,F8.4,T15,F12.6)
C       CLOSE(6)
C
C---Return to main program
       RETURN
       END
C====================END OF RUNGE-KUTTA SUBROUTINE==================C
C
C============================ROOT SUBROUTINE=======================C
       SUBROUTINE ROOT(CP1,CP2,CP3,CP4,CDX1,CDX2,CDX3,CDX4)
       IMPLICIT DOUBLE PRECISION (A-Z)
       INTEGER*4 I,N,NMAX,SWITCH,COUNT
       PARAMETER (NMAX=5)
       DIMENSION A(1:NMAX),C0(1:NMAX),DELTAW(1:NMAX),DP(1:NMAX),
     +          KC(1:NMAX),PHI(1:NMAX),Y(1:NMAX),Z(1:NMAX)
       COMMON /SUB_RK/ C0,DELTAW,DP,DX,KC,PHI,VEL,Y,Z
       COMMON /ALL/    BOLTZC,F,N,R,TEMP,XD
C
C=====CALCULATION=====
C---Cp3 value from electroneutrality
       CP4=-( (Z(1)*CP1)+(Z(2)*CP2)+(Z(3)*CP3) )/
     +                  ( Z(4) )
C---Functions
       DO I=1,N
          A(I)=PHI(I)*DEXP(-DELTAW(I)/(BOLTZC*TEMP))
       ENDDO
C
C=====CHECK CONCENTRATIONS=====
       SWITCH=0
```

```
      IF (CP1.LT.0) THEN
         SWITCH=1
      ENDIF
      IF (CP2.LT.0) THEN
         SWITCH=1
      ENDIF
      IF (CP3.LT.0) THEN
         SWITCH=1
      ENDIF
      IF (CP4.LT.0) THEN
         SWITCH=1
      ENDIF
C
C=====SWITCH=====
      IF (SWITCH.EQ.0) THEN
C=====NEWTON-RAPHSON=====
C---Initial guess for concentration
         COLD=C0(1)
         CCOMP=1D0
         COUNT=0
         S1=Z(2)*CP2*A(2)/((CP1*A(1))**2)
         S2=Z(1)
         S3=XD
         S4=Z(4)*CP1*A(1)*CP4*A(4)
         S5=Z(3)*CP3*A(3)*((CP1*A(1))**2)
         DOWHILE (CCOMP.GT.1D-6)
            FUNC=(S1*(COLD**4))+(S2*(COLD**3))+
     +           (S3*(COLD**2))+(S4*COLD)+S5
            DERIVF=(4D0*S1*(COLD**3))+(3D0*S2*(COLD**2))+
     +             (2D0*S3*COLD)+S4
            CNEW=COLD-(FUNC/DERIVF)
            CCOMP=100D0*DABS((CNEW-COLD)/CNEW)
            CRES=COLD
            COLD=CNEW
            COUNT=COUNT+1
            IF (COUNT.GT.1000) THEN
               CRES=-1D0
               CCOMP=1D-9
               PRINT*,'no ROOT!!!'
            ENDIF
         ENDDO
      ELSE
         CRES=-1D0
      ENDIF
C---Ci(dx) values
      CDX1=CRES
      CDX2=(CP2*A(2)*(CDX1**2))/((CP1*A(1))**2)
      CDX3=CP3*A(3)*((CP1*A(1))**2)/(CDX1**2)
      CDX4=CP1*A(1)*CP4*A(4)/CDX1
C
C---Return to main program
      RETURN
      END
C=======================END OF ROOT
SUBROUTINE=========================C
C
C==========================CONC
SUBROUTINE=========================C
      SUBROUTINE CONC(CP1,CP2,CP3,CP4,CDX1,CDX2,CDX3,CDX4,SWITCH)
      IMPLICIT DOUBLE PRECISION (A-Z)
      INTEGER*4 SWITCH
```

```
C
C=====SEARCH FOR NEGATIVE CONCENTRATION VALUES=====
      SWITCH=0
      IF (CP1.LT.0D0) THEN
         SWITCH=1
      ENDIF
      IF (CP2.LT.0D0) THEN
         SWITCH=1
      ENDIF
      IF (CP3.LT.0D0) THEN
         SWITCH=1
      ENDIF
      IF (CP4.LT.0D0) THEN
         SWITCH=1
      ENDIF
      IF (CDX1.LT.0D0) THEN
         SWITCH=1
      ENDIF
      IF (CDX2.LT.0D0) THEN
         SWITCH=1
      ENDIF
      IF (CDX3.LT.0D0) THEN
         SWITCH=1
      ENDIF
      IF (CDX4.LT.0D0) THEN
         SWITCH=1
      ENDIF
C---Return to main program
      RETURN
      END
C=======================END OF CONC SUBROUTINE=====================C
```

Linearised model, ternary prediction of rejection, diafiltration and concentration

This was the code used to calculate the component concentrations over time for the diafiltration and concentration of the sodium cefuroxime separation.

```
*=====================================================================
=
*      Original 22/07/03
*
*   Program: Diafilt_Conc.for
*
*   BACKGROUND OF THE PROGRAM...
*
*   A program to predict the diafiltration and concentration of a
*   3 ion system. Theoretical rejection is predicted as a function of
*   effective pressure using the linearised version of the extended
*   Nernst-Planck equation.  The code is written in algebraic terms
*   such that the equilibrium partitioning and transport equations
*   are universal and will accept ions of any given valence.
*
*   ---------------------------------------------------------------
*   ===============================================================
```

```
*    ---------------------------------------------------------------
*
       PROGRAM MAIN
       IMPLICIT DOUBLE PRECISION (A-Z)
       INTEGER          I,K,SWITCH,NMAX,Z,J
       PARAMETER       (NMAX=3)
       DIMENSION        D0(NMAX),RSOL(NMAX),Z(NMAX),CW(NMAX),PHI(NMAX),
      +                 LAMBDA(NMAX),KD(NMAX),KC(NMAX),DELTAW(NMAX),
      +                 DP(NMAX),C0(NMAX),TESTFUNC(5),OSMOTIC(NMAX)
       COMMON /ALL/     BOLTZC,F,R,TEMP,XD
       COMMON /OTHERS/ C0,DELTAW,PHI,Z,VEL,KC,DP,DX
*
*---INPUTTING SOLUTE DATA
*---Na+,Cefuroxime-,lactate-
       D0(1)=1.333D-9
       D0(2)=0.540D-9
       D0(3)=1.060D-9
       RSOL(1)=0.184D-9
       RSOL(2)=0.453D-9
       RSOL(3)=0.231D-9
       Z(1)=1
       Z(2)=-1
       Z(3)=-1
       C2START=8.364D0
       C3START=446.0D0
       C1START=C2START+C3START
       CW(1)=C1START
       CW(2)=C2START
       CW(3)=C3START
*---DIAFILTRATION ENDS WHEN
       C3END=225D0
*---CONCENTRATION ENDS WHEN
       C2END=140D0
*---INPUTTING MEMBRANE PORE SIZE [M]
       RP=0.519D-9
*---INPUTTING FLUX [M3 M-2 S-1]
       FLUX=2.143D-5
*---EFFECTIVE PRESSURE [BAR]
       PRESS=16.3D0
       PRESS=PRESS*1D5
*---DIAFILTRATION VESSEL VOLUME [M3]
       VOL=31.5D0
*---MEMBRANE AREA [M2]
       AREA=100D0
*---INPUTTING TIME DIFFERENCE [S]
       DELTIME=100D0
       TIME=0D0
*---INPUT DIAFILTRATION TIME [HRS]
       TDIA=100D0
       TDIA=TDIA*3600D0
*
*---INPUTTING CONSTANTS
       PI=DACOS(-1D0)
*---FARADAY  [C mol-1]
       F=96487D0
*---GAS [J mol-1 K-1]
       R=8.314D0
*---BOLTZMANN [J K-1]
       BOLTZC=1.38066D-23
*---TEMPERATURE [K]
       TEMP=298D0
```

```
*---ELECTRIC FIELD [C V-1 m-1]
      ELEFIELDC=8.85419D-12
*---ElEMENTAL ELECTRON CHARGE [J V-1]
      CHARGE=1.602177D-19
*---BULK SOLVENT VISCOSITY (@ 298 K) [kg m-1 s-1]
      VISCOS=0.893D-3
*---BULK SOLVENT DIELECTRIC
      DIELECB=80D0
*---ORIENTED SOLVENT LAYER DIELECTRIC
      DIELECL=31D0
*---MEMBRANE THICKNESS [m]
      DX=1D-6
*
*---CALCULATION OF THE PORE SIZE DEPENDANT PROPERTIES
*
*---POREWISE VISCOSITY
      IF (RP.LE.0.28D-9) THEN
         VISCP=10D0*VISCOS
      ELSE
         RATIO=0.28D-9/RP
         VISCP=VISCOS*(1D0+(18D0*RATIO)-(9D0*(RATIO**2)))
      ENDIF
*---HINDERANCE FACTORS (7TH ORDER VERSION)
      DO I=1,NMAX
         LAMBDA(I)=RSOL(I)/RP
         PHI(I)=(1D0-LAMBDA(I))**2
*
*---CONSTANTS FOR KD
         KD1=1.0000D0
         KD2=-2.1812D0
         KD3=0.7328D0
         KD4=-0.9065D0
         KD5=6.7272D0
         KD6=-10.2324D0
         KD7=6.3293D0
         KD8=-1.4692D0
*
         IF(LAMBDA(I).GT.0.98D0)THEN
            KD(I)=3D-5
         ELSE

KD(I)=KD1+KD2*LAMBDA(I)+KD3*LAMBDA(I)**2+KD4*LAMBDA(I)**3+
     +            KD5*LAMBDA(I)**4+KD6*LAMBDA(I)**5+KD7*LAMBDA(I)**6+
     +            KD8*LAMBDA(I)**7
         END IF
*
*---CONSTANTS FOR KC
         KC1=1.0000D0
         KC2=0.0650D0
         KC3=-1.9370D0
         KC4=8.5211D0
         KC5=-27.3398D0
         KC6=44.4150D0
         KC7=-34.5582D0
         KC8=10.3358D0
*
         KC(I)=(KC1+KC2*LAMBDA(I)+KC3*LAMBDA(I)**2+KC4*LAMBDA(I)**3+
     +          KC5*LAMBDA(I)**4+KC6*LAMBDA(I)**5+KC7*LAMBDA(I)**6+
     +          KC8*LAMBDA(I)**7)*(2D0-PHI(I))
*
*
```

```
*
         DP(I)=KD(I)*D0(I)*VISCOS/VISCP
       ENDDO
*---PORE DIELECTRIC CONSTANT
       IF (RP.LE.0.28D-9) THEN
          DIELECP=DIELECL
       ELSE
          MU=0.28D-9/RP
          FUNC=DIELECB-DIELECL
          DIELECP=DIELECB-(2D0*MU*FUNC)+(FUNC*(MU**2))
       ENDIF
*---BORN ENERGY BARRIER
       FUNC2=(1D0/DIELECP)-(1D0/DIELECB)
       DO I=1,NMAX
          DELTAW(I)=(((Z(I)**2)*(CHARGE**2))/
     +            (8D0*PI*ELEFIELDC*RSOL(I)))*FUNC2
       ENDDO
*
*---SETTING MAX AND MIN VALUES FOR OUTPUT CONCENTRATIONS
*
       CP1MIN=1D-6*CW(1)
       CP1MAX=CW(1)
       CP2MIN=1D-6*CW(2)
       CP2MAX=1D-2*CW(2)
*
       CP1START=(CP1MAX+CP1MIN)/2D0
       CP2START=(CP2MAX+CP2MIN)/2D0
*
*---OPENING OUTPUT FILE
*
       OPEN (5,FILE='3ionDiafil.res')
       WRITE(5,3702) 'Time','Conc 1','Conc 2','Conc 3'
       WRITE(5,10)   TIME,C1START,C2START,C3START
*
*---SETTING UP DIAFILTRATION LOOP
*
       DOWHILE(CW(3).GT.C3END)
*
*---SETTING MEMBRANE CHARGE
*
          IF(CW(3).LT.1.313D0)THEN
             XD=0D0
             ELSE
             XD=-(5.4508D0*LOG(CW(3))-1.4868)
          END IF
*
*---CALLING FOR INLET CONCENTRATIONS C0(I) FROM PARTITN
*
          CALL PARTITN(CW,LAMBDA,DELTAW,PHI,Z,C0)
*
          TIME=TIME+DELTIME
          VEL=(PRESS*RP**2)/(8D0*DX*VISCP)
          CP1STEP=CP1MAX/5D0
          CP2STEP=CP2MAX/5D0
*
*---INITIAL CONCENTRATION GUESSES
*
          CP1C=CP1START
          CP1N=CP1C
          CP1S=CP1C
          CP1E=CP1C+CP1STEP
```

```
          CP1W=CP1C-CP1STEP
*
          CP2C=CP2START
          CP2N=CP2C+CP2STEP
          CP2S=CP2C-CP2STEP
          CP2E=CP2C
          CP2W=CP2C
*
*---INITIAL VALUES FOR TEST FUNCTIONS
*
          TEST=10D0
          TESTMIN=2D5
          K=0
          DOWHILE(TEST.GT.1D-12)
*
*---CALCULATION OF EXIT CONCENTRATIONS CDXi FOR EACH POINT
*
             CALL ROOT(CP1C,CP2C,CDX1C,CDX2C)
             CALL ROOT(CP1N,CP2N,CDX1N,CDX2N)
             CALL ROOT(CP1S,CP2S,CDX1S,CDX2S)
             CALL ROOT(CP1E,CP2E,CDX1E,CDX2E)
             CALL ROOT(CP1W,CP2W,CDX1W,CDX2W)
*
*---CHECKING FOR NEGATIVE CONCENTRATIONS AND CALCULATING PROFILES
*
             CALL CONC(CP1C,CP2C,CDX1C,CDX2C,SWITCH)
             IF(SWITCH.EQ.0)THEN
                CALL LINEAR(CP1C,CP2C,CDX1C,CDX2C,TESTC)
                ELSE
                   TESTC=1000D0
                   SWITCH=0
             END IF
             CALL CONC(CP1N,CP2N,CDX1N,CDX2N,SWITCH)
             IF(SWITCH.EQ.0)THEN
                CALL LINEAR(CP1N,CP2N,CDX1N,CDX2N,TESTN)
                ELSE
                   TESTN=1000D0
                   SWITCH=0
             END IF
             CALL CONC(CP1S,CP2S,CDX1S,CDX2S,SWITCH)
             IF(SWITCH.EQ.0)THEN
                CALL LINEAR(CP1S,CP2S,CDX1S,CDX2S,TESTS)
                ELSE
                   TESTS=1000D0
                   SWITCH=0
             END IF
             CALL CONC(CP1E,CP2E,CDX1E,CDX2E,SWITCH)
             IF(SWITCH.EQ.0)THEN
                CALL LINEAR(CP1E,CP2E,CDX1E,CDX2E,TESTE)
                ELSE
                   TESTE=1000D0
                   SWITCH=0
             END IF
             CALL CONC(CP1W,CP2W,CDX1W,CDX2W,SWITCH)
             IF(SWITCH.EQ.0)THEN
                CALL LINEAR(CP1W,CP2W,CDX1W,CDX2W,TESTW)
                ELSE
                   TESTW=1000D0
                   SWITCH=0
             END IF
*
```

```
*---EVALUATION OF THE MINIMUM TEST FUNCTION
*
            TESTFUNC(1)=TESTC
            TESTFUNC(2)=TESTN
            TESTFUNC(3)=TESTS
            TESTFUNC(4)=TESTE
            TESTFUNC(5)=TESTW
*
            K=1
            DO J=1,5
               IF(TESTFUNC(J).LT.TESTMIN)THEN
                  TESTMIN=TESTFUNC(J)
                  K=J
               END IF
            END DO
*
            IF(K.EQ.1)THEN
               CP1STEP=CP1STEP/1.1D0
               CP2STEP=CP2STEP/1.1D0
               CP1C=CP1C
               CP1N=CP1C
               CP1S=CP1C
               CP1E=CP1C+CP1STEP
               CP1W=CP1C-CP1STEP
*
               CP2C=CP2C
               CP2N=CP2C+CP2STEP
               CP2S=CP2C-CP2STEP
               CP2E=CP2C
               CP2W=CP2C
               TEST=TESTC
            END IF
            IF(K.EQ.2)THEN
               CP1C=CP1N
               CP1N=CP1C
               CP1S=CP1C
               CP1E=CP1C+CP1STEP
               CP1W=CP1C-CP1STEP
*
               CP2C=CP2N
               CP2N=CP2C+CP2STEP
               CP2S=CP2C-CP2STEP
               CP2E=CP2C
               CP2W=CP2C
               TEST=TESTN
            END IF
            IF(K.EQ.3)THEN
               CP1C=CP1S
               CP1N=CP1C
               CP1S=CP1C
               CP1E=CP1C+CP1STEP
               CP1W=CP1C-CP1STEP
*
               CP2C=CP2S
               CP2N=CP2C+CP2STEP
               CP2S=CP2C-CP2STEP
               CP2E=CP2C
               CP2W=CP2C
               TEST=TESTS
            END IF
            IF(K.EQ.4)THEN
```

```
                CP1C=CP1E
                CP1N=CP1C
                CP1S=CP1C
                CP1E=CP1C+CP1STEP
                CP1W=CP1C-CP1STEP
*
                CP2C=CP2E
                CP2N=CP2C+CP2STEP
                CP2S=CP2C-CP2STEP
                CP2E=CP2C
                CP2W=CP2C
                TEST=TESTE
             END IF
             IF(K.EQ.5)THEN
                CP1C=CP1W
                CP1N=CP1C
                CP1S=CP1C
                CP1E=CP1C+CP1STEP
                CP1W=CP1C-CP1STEP
*
                CP2C=CP2W
                CP2N=CP2C+CP2STEP
                CP2S=CP2C-CP2STEP
                CP2E=CP2C
                CP2W=CP2C
                TEST=TESTW
             END IF
*             PRINT 11 ,TEST,(TIME/3.6D3),CW(3)
*  11         FORMAT(1X,F14.12,4X,F8.3,4X,F12.6)
          END DO
          CP3C=-(Z(1)*CP1C+Z(2)*CP2C)/Z(3)
          REJ1=1D0-CP1C/CW(1)
          REJ2=1D0-CP2C/CW(2)
          REJ3=1D0-CP3C/CW(3)
          CP1START=CP1C
          CP2START=CP2C
*
*---CONVERTING CONCENTRATIONS FOR CALCULATION
*
          C1OLD=CW(1)
          C2OLD=CW(2)
          C3OLD=CW(3)
*
*---SETTING UP THE RUNGA CUTTA CONSTANTS
*
          FUNCR=-FLUX*AREA/VOL
*---FOR COMPONENT 1
          K11=FUNCR*(1-REJ1)*C1OLD
          K21=FUNCR*(1-REJ1)*(C1OLD+0.5D0*DELTIME*K11)
          K31=FUNCR*(1-REJ1)*(C1OLD+0.5D0*DELTIME*K21)
          K41=FUNCR*(1-REJ1)*(C1OLD+DELTIME*K31)
*---FOR COMPONENT 2
          K12=FUNCR*(1-REJ2)*C2OLD
          K22=FUNCR*(1-REJ2)*(C2OLD+0.5D0*DELTIME*K12)
          K32=FUNCR*(1-REJ2)*(C2OLD+0.5D0*DELTIME*K22)
          K42=FUNCR*(1-REJ2)*(C2OLD+DELTIME*K32)
*---FOR COMPONENT 3
          K13=FUNCR*(1-REJ3)*C3OLD
          K23=FUNCR*(1-REJ3)*(C3OLD+0.5D0*DELTIME*K13)
          K33=FUNCR*(1-REJ3)*(C3OLD+0.5D0*DELTIME*K23)
          K43=FUNCR*(1-REJ3)*(C3OLD+DELTIME*K33)
```

```
*
*---CALCULATING NEW CONCENTRATIONS
*
          C1NEW=C1OLD+DELTIME*((1D0/6D0)*(K11+2D0*K21+2D0*K31+K41))
          C2NEW=C2OLD+DELTIME*((1D0/6D0)*(K12+2D0*K22+2D0*K32+K42))
          C3NEW=C3OLD+DELTIME*((1D0/6D0)*(K13+2D0*K23+2D0*K33+K43))
*
*---CONVERTING CONCENTRATIONS BACK TO AN ARRAY
*
          CW(1)=C1NEW
          CW(2)=C2NEW
          CW(3)=C3NEW
*
          WRITE(5,10)  (TIME/3.6D3),CW(1),CW(2),CW(3)
          WRITE(*,10)  (TIME/3.6D3),CW(2),CW(3)
 10       FORMAT(1X,T4,F12.3,T18,F12.4,T32,F12.4,T46,F12.4,T60,F12.4)
*
       END DO
*
*    ---------------------------------------------------------------
*    ===================== END OF DIAFILTRATION ====================
*    ---------------------------------------------------------------
*
*
*    ---------------------------------------------------------------
*    -------------------- START OF CONCENTRATION -------------------
*    ---------------------------------------------------------------
*
*
*---SET APPLIED PRESSURE FOR CONCENTRATION PHASE [BAR]
       APRESS=30D0
       APRESS=APRESS*1D5
*
*---CALCULATING THE MASS OF CEF
       MASS=CW(2)*VOL
*
*---SETTING THE TIME INTERVAL FOR CONCENTRATION [s]
*
       DELTIME=4D0
*---SETTING UP THE PRIMARY CONCENTRATION LOOP
       DOWHILE(CW(2).LT.C2END)
*
*---SETTING XD
          IF(CW(3).LT.1.313D0)THEN
             XD=0D0
             ELSE IF(CW(3).GT.95.3D0)THEN
             XD=-22.5D0
             ELSE
             XD=-(5.4508D0*LOG(CW(3))-1.4868)
          END IF
*
*---CALCULATING OSMOTIC PRESSURE
          TOTAL=0D0
          DO I=1,NMAX
             OSMOTIC(I)=CW(I)*R*TEMP
             TOTAL=TOTAL+OSMOTIC(I)
          END DO
          PERM=(CP1C+CP2C+CP3C)*R*TEMP
          OPRESS=TOTAL-PERM
*
```

```
*---SETTING EFFECTIVE PRESSURE
         PRESS=APRESS-OPRESS
         IF(PRESS.LE.0D0)THEN
            GOTO 17
         END IF
*
*---CALCULATING THE MEMBRANE FLUX
*   (BASED UPON DESAL DATA FROM WELFOOT CES)
         FLUX=1.278D-11*PRESS+6D-7
*
*---CALCULATING REJECTION
*
*---SETTING MAX AND MIN VALUES FOR OUTPUT CONCENTRATIONS
*
         CP1MIN=1D-6*CW(1)
         CP1MAX=CW(1)
         CP2MIN=1D-6*CW(2)
         CP2MAX=1D-2*CW(2)
*
         CP1START=(CP1MAX+CP1MIN)/2D0
         CP2START=(CP2MAX+CP2MIN)/2D0
*
*---CALLING FOR INLET CONCENTRATIONS C0(I) FROM PARTITN
*
         CALL PARTITN(CW,LAMBDA,DELTAW,PHI,Z,C0)
*
         TIME=TIME+DELTIME
         VEL=(PRESS*RP**2)/(8D0*DX*VISCP)
         CP1STEP=CP1MAX/5D0
         CP2STEP=CP2MAX/5D0
*
*---INITIAL CONCENTRATION GUESSES
*
         CP1C=CP1START
         CP1N=CP1C
         CP1S=CP1C
         CP1E=CP1C+CP1STEP
         CP1W=CP1C-CP1STEP
*
         CP2C=CP2START
         CP2N=CP2C+CP2STEP
         CP2S=CP2C-CP2STEP
         CP2E=CP2C
         CP2W=CP2C
*
*---INITIAL VALUES FOR TEST FUNCTIONS
*
         TEST=10D0
         TESTMIN=2D5
         K=0
         DOWHILE(TEST.GT.1D-12)
*
*---CALCULATION OF EXIT CONCENTRATIONS CDXi FOR EACH POINT
*
            CALL ROOT(CP1C,CP2C,CDX1C,CDX2C)
            CALL ROOT(CP1N,CP2N,CDX1N,CDX2N)
            CALL ROOT(CP1S,CP2S,CDX1S,CDX2S)
            CALL ROOT(CP1E,CP2E,CDX1E,CDX2E)
            CALL ROOT(CP1W,CP2W,CDX1W,CDX2W)
*
*---CHECKING FOR NEGATIVE CONCENTRATIONS AND CALCULATING PROFILES
```

```
*
            CALL CONC(CP1C,CP2C,CDX1C,CDX2C,SWITCH)
            IF(SWITCH.EQ.0)THEN
               CALL LINEAR(CP1C,CP2C,CDX1C,CDX2C,TESTC)
               ELSE
                  TESTC=1000D0
                  SWITCH=0
            END IF
            CALL CONC(CP1N,CP2N,CDX1N,CDX2N,SWITCH)
            IF(SWITCH.EQ.0)THEN
               CALL LINEAR(CP1N,CP2N,CDX1N,CDX2N,TESTN)
               ELSE
                  TESTN=1000D0
                  SWITCH=0
            END IF
            CALL CONC(CP1S,CP2S,CDX1S,CDX2S,SWITCH)
            IF(SWITCH.EQ.0)THEN
               CALL LINEAR(CP1S,CP2S,CDX1S,CDX2S,TESTS)
               ELSE
                  TESTS=1000D0
                  SWITCH=0
            END IF
            CALL CONC(CP1E,CP2E,CDX1E,CDX2E,SWITCH)
            IF(SWITCH.EQ.0)THEN
               CALL LINEAR(CP1E,CP2E,CDX1E,CDX2E,TESTE)
               ELSE
                  TESTE=1000D0
                  SWITCH=0
            END IF
            CALL CONC(CP1W,CP2W,CDX1W,CDX2W,SWITCH)
            IF(SWITCH.EQ.0)THEN
               CALL LINEAR(CP1W,CP2W,CDX1W,CDX2W,TESTW)
               ELSE
                  TESTW=1000D0
                  SWITCH=0
            END IF
*
*---EVALUATION OF THE MINIMUM TEST FUNCTION
*
            TESTFUNC(1)=TESTC
            TESTFUNC(2)=TESTN
            TESTFUNC(3)=TESTS
            TESTFUNC(4)=TESTE
            TESTFUNC(5)=TESTW
*
            K=1
            DO J=1,5
               IF(TESTFUNC(J).LT.TESTMIN)THEN
                  TESTMIN=TESTFUNC(J)
                  K=J
               END IF
            END DO
*
            IF(K.EQ.1)THEN
               CP1STEP=CP1STEP/1.1D0
               CP2STEP=CP2STEP/1.1D0
               CP1C=CP1C
               CP1N=CP1C
               CP1S=CP1C
               CP1E=CP1C+CP1STEP
               CP1W=CP1C-CP1STEP
```

```
*
                CP2C=CP2C
                CP2N=CP2C+CP2STEP
                CP2S=CP2C-CP2STEP
                CP2E=CP2C
                CP2W=CP2C
                TEST=TESTC
              END IF
              IF(K.EQ.2)THEN
                CP1C=CP1N
                CP1N=CP1C
                CP1S=CP1C
                CP1E=CP1C+CP1STEP
                CP1W=CP1C-CP1STEP
*
                CP2C=CP2N
                CP2N=CP2C+CP2STEP
                CP2S=CP2C-CP2STEP
                CP2E=CP2C
                CP2W=CP2C
                TEST=TESTN
              END IF
              IF(K.EQ.3)THEN
                CP1C=CP1S
                CP1N=CP1C
                CP1S=CP1C
                CP1E=CP1C+CP1STEP
                CP1W=CP1C-CP1STEP
*
                CP2C=CP2S
                CP2N=CP2C+CP2STEP
                CP2S=CP2C-CP2STEP
                CP2E=CP2C
                CP2W=CP2C
                TEST=TESTS
              END IF
              IF(K.EQ.4)THEN
                CP1C=CP1E
                CP1N=CP1C
                CP1S=CP1C
                CP1E=CP1C+CP1STEP
                CP1W=CP1C-CP1STEP
*
                CP2C=CP2E
                CP2N=CP2C+CP2STEP
                CP2S=CP2C-CP2STEP
                CP2E=CP2C
                CP2W=CP2C
                TEST=TESTE
              END IF
              IF(K.EQ.5)THEN
                CP1C=CP1W
                CP1N=CP1C
                CP1S=CP1C
                CP1E=CP1C+CP1STEP
                CP1W=CP1C-CP1STEP
*
                CP2C=CP2W
                CP2N=CP2C+CP2STEP
                CP2S=CP2C-CP2STEP
                CP2E=CP2C
```

```
                CP2W=CP2C
                TEST=TESTW
              END IF
*              PRINT 12 ,TEST,(TIME/3.6D3),CW(3)
*  12          FORMAT(1X,F14.12,4X,F8.3,4X,F12.6)
          END DO
          CP3C=-(Z(1)*CP1C+Z(2)*CP2C)/Z(3)
          REJ1=1D0-CP1C/CW(1)
          REJ2=1D0-CP2C/CW(2)
          REJ3=1D0-CP3C/CW(3)
          CP1START=CP1C
          CP2START=CP2C
*
*-----------------------------------------------------------------
*---------------- ALL VARIABLES NOW AQUIRED ----------------------
*-----------------------------------------------------------------
*
*---STARTING THE RUNGA-KUTTA INTEGRAL FOR CONCENTRATION
*
*---CONVERTING CONCENTRATIONS FOR CALCULATION
*
          C1OLD=CW(1)
          C2OLD=CW(2)
          C3OLD=CW(3)
*
*---SETTING UP THE RUNGA CUTTA CONSTANTS
*
          FUNCR=FLUX*AREA/MASS
*
*---FOR CEFUROXIME
*
          K11=FUNCR*REJ2*C2OLD**2
          K21=FUNCR*REJ2*(C2OLD+0.5D0*DELTIME*K11)**2
          K31=FUNCR*REJ2*(C2OLD+0.5D0*DELTIME*K21)**2
          K41=FUNCR*REJ2*(C2OLD+DELTIME*K31)**2
*
*---CALCULATING NEW CONCENTRATION
*
          C2NEW=C2OLD+DELTIME*((1D0/6D0)*(K11+2D0*K21+2D0*K31+K41))
*
*---FOR LACTATE ION
*
          K13=FUNCR*REJ3*C2OLD*C3OLD
          K23=FUNCR*REJ3*C2OLD*(C3OLD+0.5D0*DELTIME*K13)
          K33=FUNCR*REJ3*C2OLD*(C3OLD+0.5D0*DELTIME*K23)
          K43=FUNCR*REJ3*C2OLD*(C3OLD+DELTIME*K33)
*
*---CALCULATING NEW CONCENTRATIONS
*
          C3NEW=C3OLD+DELTIME*((1D0/6D0)*(K13+2D0*K23+2D0*K33+K43))
*
*---CALCULATING SODIUM CONCENTRATION
*
          C1NEW=-(Z(2)*C2NEW+Z(3)*C3NEW)/Z(1)
*
*---CONVERTING CONCENTRATIONS BACK TO AN ARRAY
*
          CW(1)=C1NEW
          CW(2)=C2NEW
          CW(3)=C3NEW
*
```

```
*---ADJUSTING TIME INCREMENT
*
         TIME=TIME+DELTIME
*
*---RECALULATING FOR SMALL LOSS IN MASS
*
         LIQUID=FLUX*AREA*DELTIME
         PCONC=CP2C
         PMASS=PCONC*LIQUID
         MASS=MASS-PMASS
*
         WRITE(5,10) (TIME/3.6D3),CW(1),CW(2),CW(3)
         WRITE(*,10) (TIME/3.6D3),CW(2),CW(3)
*
      END DO
   17 IF(PRESS.LE.0D0)THEN
         WRITE(5,*)''
         WRITE(5,*)'ZERO PRESSURE'
         WRITE(*,*)'ZERO PRESSURE'
      END IF
*
*-----------------------------------------------------------------
*------------------- CALCULATING FINAL VALUES --------------------
*-----------------------------------------------------------------
*
*---CALCULATING FINAL VOLUME
*
      FVOL=MASS/CW(2)
*
*---PERCENTAGE RECOVERY
*
      RECOV=MASS/(C2START*VOL)*100D0
*
*---RATIO OF CEF TO LACTATE
*
      RATIO=CW(3)/CW(2)
*
*
      WRITE(5,*) ''
      WRITE(5,15) '[L/C]','REC[%]','VOL[L]'
      WRITE(5,16) RATIO,RECOV,FVOL
      WRITE(*,*) ''
      WRITE(*,15) 'VOL[L]','REC[%]','[L/C]'
      WRITE(*,16) FVOL*1D3,RECOV,RATIO
*
   15 FORMAT(1X,T4,A12,T18,A12,T32,A12)
   16 FORMAT(1X,T4,F12.3,T18,F12.2,T32,F12.4)
*
3702  FORMAT(1X,T4,A12,T18,A12,T32,A12,T46,A12,T60,A12)
*
      CLOSE(5)
      STOP
      END
*
*   ----------------------------------------------------------------
*   ====================== END OF MAIN PROGRAM =====================
*   ----------------------------------------------------------------
*
*---PARTITIONING SUBROUTINE TO FIND C0(I)
*
      SUBROUTINE PARTITN(CW,LAMBDA,DELTAW,PHI,Z,C0)
```

```
      IMPLICIT DOUBLE PRECISION (A-Z)
      INTEGER*4     COUNT,I,NMAX,Z
      PARAMETER    (NMAX=3)
      DIMENSION     C0(1:NMAX),CONC(1:NMAX),CW(1:NMAX),DELTAW(1:NMAX),
     +              PHI(1:NMAX),Z(1:NMAX),LAMBDA(1:NMAX)
      COMMON /ALL/ BOLTZC,F,R,TEMP,XD
*
*===== CALCULATION =====
*---Initial values
      PSI=0D0
      TEST=20D0
      COUNT=0
*---Iteration
      DOWHILE (TEST.GT.1D-6)
         PSINEW=PSI
         SUM=0D0
         DO I=1,NMAX
            IF(LAMBDA(I).GE.1D0)THEN
               CONC(I)=0D0
            ELSE
               CONC(I)=CW(I)*PHI(I)*DEXP((-Z(I)*F*PSINEW)/(R*TEMP))*
     +                 DEXP(-DELTAW(I)/(BOLTZC*TEMP))
            END IF
            SUM=SUM+(Z(I)*CONC(I))
         ENDDO
         TESTNEW=SUM+XD
         IF (COUNT.EQ.0) THEN
            IF (TESTNEW.GT.0) THEN
               PSI=PSINEW+0.1D0
               PSIABOVE=PSINEW
               TEST=DABS(TESTNEW)
               COUNT=1
            ENDIF
            IF (TESTNEW.LT.0) THEN
               PSI=PSINEW-0.1D0
               PSIBELOW=PSINEW
               TEST=DABS(TESTNEW)
               COUNT=2
            ENDIF
         ENDIF
         IF (COUNT.EQ.1) THEN
            IF (TESTNEW.GT.0) THEN
               PSI=PSINEW+0.1D0
               PSIABOVE=PSINEW
               TEST=DABS(TESTNEW)
            ENDIF
            IF (TESTNEW.LT.0) THEN
               PSI=PSINEW-0.1D0
               PSIBELOW=PSINEW
               TEST=DABS(TESTNEW)
               COUNT=3
            ENDIF
         ENDIF
         IF (COUNT.EQ.2) THEN
            IF (TESTNEW.GT.0) THEN
               PSI=PSINEW+0.1D0
               PSIABOVE=PSINEW
               TEST=DABS(TESTNEW)
               COUNT=3
            ENDIF
            IF (TESTNEW.LT.0) THEN
```

```
               PSI=PSINEW-0.1D0
               PSIBELOW=PSINEW
               TEST=DABS(TESTNEW)
            ENDIF
         ENDIF
         IF (COUNT.EQ.3) THEN
            IF (TESTNEW.GT.0) THEN
               PSIABOVE=PSINEW
               TEST=DABS(TESTNEW)
            ENDIF
            IF (TESTNEW.LT.0) THEN
               PSIBELOW=PSINEW
               TEST=DABS(TESTNEW)
            ENDIF
            PSI=(PSIABOVE+PSIBELOW)/2D0
         ENDIF
      ENDDO
*
*---CONCENTRATION AT PORE ENTRANCE
      DO I=1,NMAX
         C0(I)=CONC(I)
      ENDDO
*
*---RETURN TO MAIN PROGRAM
      RETURN
      END
*
*
*---SUBROUTINE ROOT FOR CDXi VALUES
*
      SUBROUTINE ROOT(CP1,CP2,CDX1,CDX2)
      IMPLICIT DOUBLE PRECISION (A-Z)
      INTEGER*4        I,NMAX,SWITCH,COUNT,Z
      PARAMETER       (NMAX=3)
      DIMENSION        A(NMAX),C0(NMAX),DELTAW(NMAX),Z(NMAX),DP(NMAX),
     +                 PHI(NMAX),KC(NMAX)
      COMMON /ALL/     BOLTZC,F,R,TEMP,XD
      COMMON /OTHERS/ C0,DELTAW,PHI,Z,VEL,KC,DP,DX
*
*---CP3 VALUE FROM ELECTRONEUTRALITY
      CP3=-(Z(1)*CP1+Z(2)*CP2)/Z(3)
*---FUNCTIONS
      DO I=1,NMAX
         A(I)=PHI(I)*DEXP(-DELTAW(I)/(BOLTZC*TEMP))
      ENDDO
*
*---CHECK CONCENTRATIONS
      SWITCH=0
      IF (CP1.LT.0) THEN
         SWITCH=1
      ENDIF
      IF (CP2.LT.0) THEN
         SWITCH=1
      ENDIF
      IF (CP3.LT.0) THEN
         SWITCH=1
      ENDIF
*
*---SWITCH
      IF (SWITCH.EQ.0) THEN
*---NEWTON METHOD
```

```
*---INITIAL GUESS FOR CDX1
          COLD=C0(1)
          CCOMP=1D0
          COUNT=0
          DOWHILE (CCOMP.GT.1D-6)
*---FUNC FUNCTIONS
          P1=Z(1)*COLD
          P2=Z(2)*A(2)*CP2*((COLD/(CP1*A(1)))**(Z(2)/Z(1)))
          P3=Z(3)*A(3)*CP3*((COLD/(CP1*A(1)))**(Z(3)/Z(1)))
          P4=XD
*---DERIVF FUNCTIONS
          S1=Z(1)
          S2=((A(2)*CP2*Z(2)**2)/(Z(1)*CP1*A(1)))*((COLD/(CP1*A(1)))**
     +       ((Z(2)/Z(1))-1))
          S3=((A(3)*CP3*Z(3)**2)/(Z(1)*CP1*A(1)))*((COLD/(CP1*A(1)))**
     +       ((Z(3)/Z(1))-1))
*
             FUNC=P1+P2+P3+P4
             DERIVF=S1+S2+S3
             CNEW=COLD-(FUNC/DERIVF)
             CCOMP=100D0*DABS((CNEW-COLD)/CNEW)
             CRES=COLD
             COLD=CNEW
             COUNT=COUNT+1
             IF (COUNT.GT.1000) THEN
                CRES=-1D0
                CCOMP=1D-9
                PRINT*,'no ROOT!!!'
             ENDIF
          ENDDO
*---CDXi VALUES
       CDX1=CRES
       CDX2=A(2)*CP2*((CDX1/(A(1)*CP1))**(Z(2)/Z(1)))
*
       ELSE
          CRES=-1D0
          CDX1=CRES
          CDX2=CRES
       ENDIF
*---RETURN TO MAIN PROGRAM
       RETURN
       END
*
*---SUBROUTINE CONC TO SEARCH FOR NEGATIVE VALUES
*
       SUBROUTINE CONC(CP1,CP2,CDX1,CDX2,SWITCH)
       IMPLICIT DOUBLE PRECISION (A-Z)
       INTEGER*4 SWITCH
*
*===== SEARCH FOR NEGATIVE CONCENTRATION VALUES =====
       SWITCH=0
       IF (CP1.LT.0D0) THEN
          SWITCH=1
       ENDIF
       IF (CP2.LT.0D0) THEN
          SWITCH=1
       ENDIF
       IF (CDX1.LT.0D0) THEN
          SWITCH=1
       ENDIF
       IF (CDX2.LT.0D0) THEN
```

```
         SWITCH=1
       ENDIF
*---RETURN TO MAIN PROGRAM
       RETURN
       END
*
*---SUBROUTINE LINEAR TO CALCULATE CONCENTRATION PROFILES
*
       SUBROUTINE LINEAR(CP1,CP2,CDX1,CDX2,TEST)
       IMPLICIT DOUBLE PRECISION (A-Z)
       INTEGER*4        NMAX,Z
       PARAMETER       (NMAX=3)
       DIMENSION        C0(NMAX),Z(NMAX),KC(NMAX),DP(NMAX),
      +                 DELTAW(NMAX),PHI(NMAX)
       COMMON /ALL/     BOLTZC,F,R,TEMP,XD
       COMMON /OTHERS/ C0,DELTAW,PHI,Z,VEL,KC,DP,DX
*
*===== CALCULATION =====
*
       T=TEMP
*---CALCULATION OF CAVi
       CAV1=(C0(1)+CDX1)/2
       CAV2=(C0(2)+CDX2)/2
*
*---CALCULATION OF CHARGE FUNCTION (DSI/DX)
*
*---FUNCTIONS
       A=Z(1)*VEL*(KC(1)/DP(1)-KC(3)/DP(3))
       B=Z(2)*VEL*(KC(2)/DP(2)-KC(3)/DP(3))
       G=Z(1)*VEL*(1/DP(3)-1/DP(1))
       H=Z(2)*VEL*(1/DP(3)-1/DP(2))
       L=VEL*KC(3)/DP(3)
       M=(F/(R*T))*((Z(1)**2)-Z(1)*Z(3))
       N1=(F/(R*T))*((Z(2)**2)-Z(2)*Z(3))
       Q=(F/(R*T))*Z(3)
*
       DSIDX=(A*CAV1+B*CAV2+G*CP1+H*CP2-L*XD)/
      +       (M*CAV1+N1*CAV2-Q*XD)
*
*---CALCULATION OF CONCENTRATION GRADIENTS
*
       DC1DX=(VEL/DP(1))*(KC(1)*CAV1-CP1)-((CAV1*Z(1)*F)/(R*T))*DSIDX
       DC2DX=(VEL/DP(2))*(KC(2)*CAV2-CP2)-((CAV2*Z(2)*F)/(R*T))*DSIDX
*
*---CALCULATING CDXi(CALC) FROM GRADIENTS
       CDX1C=DC1DX*DX+C0(1)
       CDX2C=DC2DX*DX+C0(2)
*
*---EVALUATING TEST FUNCTION
*
       T1=(CDX1C-CDX1)**2
       T2=(CDX2C-CDX2)**2
       TEST=SQRT(T1+T2)
*
*---RETURN TO MAIN PROGRAM
       RETURN
       END
*    ------------------------------------------------------------------
*    ====================== END OF SUBROUTINES ======================
*    ------------------------------------------------------------------
```

Linearised model, quaternary prediction of rejection and diafiltration

This was the code used to calculate the component concentrations over time for the diafiltration used in the Neu5Ac separation.

```
*  4ionlinearDiafilt_Nana.for
*=================================================================
*-                                                               -
*- Calculation of rejection vs. time for the complex Nana system  -
*- using the linearised form of the extended Nernst-Planck equation.-
*- Both Nana and pyruvate are dissociating in solution.          -
*-                                                               -
*- Original code written by D. Oatley on 12/08/2002.             -
*-                                                               -
*=================================================================
      PROGRAM MAIN
      IMPLICIT DOUBLE PRECISION (A-Z)
      INTEGER   I,K,N,NMAX,SWITCH,Z
      PARAMETER (NMAX=4)
      DIMENSION C0(1:NMAX),CW(1:NMAX),D0(1:NMAX),DELTAW(1:NMAX),
     +          DP(1:NMAX),KD(1:NMAX),KC(1:NMAX),LAMBDA(1:NMAX),
     +          PHI(1:NMAX),RSOL(1:NMAX),Z(1:NMAX),TESTFUNC(1:7)
      COMMON /ALL/    BOLTZC,F,N,R,TEMP,XD
      COMMON /OTHERS/ C0,DELTAW,PHI,Z,VEL,KC,DP,DX
*
*===== FIXED INPUT DATA =====
*
*---EFFECTIVE PORE RADIUS [m]
      RP=0.55D-9
*---EFFECTIVE MEMBRANE PRESSURE [BAR]
      PRESS=3.5D0
      PRESS=PRESS*1D5
*---MEMBRANE FLUX [M3 M-2 S-1]
      FLUX=3.3667D-6
*---MEMBRANE AREA [M2]
      AREA=4.18D-3
*---DIAFILTRATION VESSEL VOLUME [M3]
      VOL=0.4D-3
*---DIAFILTRATION TIME INTERVAL [S]
      DELTIME=1200D0
      TIME=0D0
*---SOLUTION PH
      PH=2.4D0
*
*===== CONSTANTS =====
      PI=DACOS(-1D0)
*---PKa FOR NANA
      PKAN=2.2D0
*---pKa FOR PYRUVATE
      PKAP=1.9D0
*---FARADAY  [C mol-1]
      F=96487D0
*---GAS [J mol-1 K-1]
      R=8.314D0
*---BOLTZMANN [J K-1]
      BOLTZC=1.38066D-23
```

```
*---TEMPERATURE [K]
      TEMP=298D0
*---ELECTRIC FIELD [C V-1 m-1]
      ELEFIELDC=8.85419D-12
*---ElEMENTAL ELECTRON CHARGE [J V-1]
      CHARGE=1.602177D-19
*---BULK SOLVENT VISCOSITY (@ 298 K) [kg m-1 s-1]
      VISCOS=0.893D-3
*---BULK SOLVENT DIELECTRIC
      DIELECB=80D0
*---ORIENTED SOLVENT LAYER DIELECTRIC
      DIELECL=43D0
*---MEMBRANE THICKNESS [m]
      DX=1D-6
*
*===== ION DATA =====
*
*---NUMBER OF SPECIES
      N=4
*Ion(1)=Sodium
*Ion(2)=Hydrogen
*Ion(3)=Nana-
*Ion(4)=Pyruvate
*SOLUTE(5)=Nana(Neutral)
*---ION VALENCES
      Z(1)=1
      Z(2)=1
      Z(3)=-1
      Z(4)=-1
*---BULK ION DIFFUSION COEFFICIENTS [m2 s-1]
      D0(1)=1.333D-9
      D0(2)=9.31D-9
      D0(3)=0.499D-9
      D0(4)=1.05D-9
*---STOKES RADIUS IN SOLVENT [m]
      RSOL(1)=0.184D-9
      RSOL(2)=0.026D-9
      RSOL(3)=0.490D-9
      RSOL(4)=0.233D-9
*---RAW FEED CONCENTRATIONS [mol m-3]
      NANAC=32.81D0
      NAPYRC=20.15D0
      PYRCONC=NAPYRC
*---CALCULATING THE DISSOCIATION FACTOR
      DISFUNC1=1D0/10D0**(PKAN)
      DISFUNC2=1D0/10D0**(PH)
      DISFUNC3=DISFUNC1/DISFUNC2
      DISFUNC4=1D0/10D0**(PKAP)
      DISFUNC5=DISFUNC4/DISFUNC2
      FRAC1=DISFUNC3/(1D0+DISFUNC3)
      FRAC2=DISFUNC5/(1D0+DISFUNC5)
*---BULK FEED CONCENTRATION [mol m-3]
      CW(1)=FRAC2*NAPYRC
      CW(2)=FRAC1*NANAC
      CW(3)=FRAC1*NANAC
      CW(4)=FRAC2*NAPYRC
      CONCN1=(1D0-FRAC1)*NANAC
      CONCN2=(1D0-FRAC2)*NAPYRC
*
*---DIAFILTRATION END CONCENTRATION [MOL M-3]
      CEND=0.01D0
```

```
*
*---Na+,Mg2+,SO4 2-,Cl-
*---ION VALENCES
*       Z(1)=1
*       Z(2)=2
*       Z(3)=-2
*       Z(4)=-1
*---BULK ION DIFFUSION COEFFICIENTS [m2 s-1]
*       D0(1)=1.333D-9
*       D0(2)=0.705D-9
*       D0(3)=1.602D-9
*       D0(4)=2.301D-9
*---STOKES RADIUS IN SOLVENT [m]
*       RSOL(1)=0.1840D-9
*       RSOL(2)=0.3479D-9
*       RSOL(3)=0.2309D-9
*       RSOL(4)=0.1207D-9
*---BULK FEED CONCENTRATION [mol m-3]
*       CW(1)=0.461D0
*       CW(2)=7.107D0
*       CW(3)=CW(2)
*       CW(4)=CW(1)
*
*===== PORE SIZE DEPENDENT TRANSPORT PROPERTIES =====
*
*---POREWISE VISCOSITY
       IF (RP.LE.0.28D-9) THEN
          VISCP=10D0*VISCOS
       ELSE
          RATIO=0.28D-9/RP
          VISCP=VISCOS*(1D0+(18D0*RATIO)-(9D0*(RATIO**2)))
       ENDIF
*---HINDERANCE FACTORS (7TH ORDER VERSION)
       DO I=1,N
          LAMBDA(I)=RSOL(I)/RP
          PHI(I)=(1D0-LAMBDA(I))**2
*
*---CONSTANTS FOR KD
          KD1=1.0000D0
          KD2=-2.1812D0
          KD3=0.7328D0
          KD4=-0.9065D0
          KD5=6.7272D0
          KD6=-10.2324D0
          KD7=6.3293D0
          KD8=-1.4692D0
*
          IF(LAMBDA(I).GT.0.98D0)THEN
             KD(I)=0D0
          ELSE

KD(I)=KD1+KD2*LAMBDA(I)+KD3*LAMBDA(I)**2+KD4*LAMBDA(I)**3+
     +            KD5*LAMBDA(I)**4+KD6*LAMBDA(I)**5+KD7*LAMBDA(I)**6+
     +            KD8*LAMBDA(I)**7
          END IF
*
*---CONSTANTS FOR KC
          KC1=1.0000D0
          KC2=0.0650D0
          KC3=-1.9370D0
          KC4=8.5211D0
```

```
         KC5=-27.3398D0
         KC6=44.4150D0
         KC7=-34.5582D0
         KC8=10.3358D0
*
         KC(I)=(KC1+KC2*LAMBDA(I)+KC3*LAMBDA(I)**2+KC4*LAMBDA(I)**3+
     +          KC5*LAMBDA(I)**4+KC6*LAMBDA(I)**5+KC7*LAMBDA(I)**6+
     +          KC8*LAMBDA(I)**7)*(2D0-PHI(I))
*
*
*
         DP(I)=KD(I)*D0(I)*VISCOS/VISCP
      ENDDO
*---PECLET NUMBER FOR NEUTRAL NANA
      PE1=(KC(3)*PRESS*RP**2)/(8D0*VISCP*DP(3))
*---PECLET NUMBER FOR NEUTRAL PYRUVATE
      PE2=(KC(4)*PRESS*RP**2)/(8D0*VISCP*DP(4))
*---PORE DIELECTRIC CONSTANT
      IF (RP.LE.0.28D-9) THEN
         DIELECP=DIELECL
      ELSE
         MU=0.28D-9/RP
         FUNC=DIELECB-DIELECL
         DIELECP=DIELECB-(2D0*MU*FUNC)+(FUNC*(MU**2))
      ENDIF
*---BORN ENERGY BARRIER
      FUNC2=(1D0/DIELECP)-(1D0/DIELECB)
      DO I=1,N
         DELTAW(I)=(((Z(I)**2)*(CHARGE**2))/
     +           (8D0*PI*ELEFIELDC*RSOL(I)))*FUNC2
      ENDDO
*
*===== MAX AND MIN VALUES FOR OUTPUT CONCENTRATIONS =====
*
*---Initial CP1 maximum and minimum values
      CP1MIN=1D-6*CW(1)
      CP1MAX=CW(1)
*---Initial CP2 maximum and minimum values
      CP2MIN=1D-6*CW(2)
      CP2MAX=CW(2)
*---Initial CP3 maximum and minimum values
      CP3MIN=1D-6*CW(3)
      CP3MAX=CW(3)
*
*---STARTING CP VALUES
      CP1START=(CP1MIN+CP1MAX)/2D0
      CP2START=(CP2MIN+CP2MAX)/2D0
      CP3START=(CP3MIN+CP3MAX)/2D0
*
*===== OPENING OUTPUT FILE =====
      OPEN(5,FILE='4ionlDiafilt.res')
      WRITE(5,3601)'Time','Na','H','Pyr -','Nana -','Nana T','PYR T'
      WRITE(5,3600) TIME,CW(1),CW(2),CW(4),CW(3),NANAC,NAPYRC
*
*===== SETTING UP DIAFILTRATION LOOP =====
*
*      DOWHILE(PYRCONC.GE.CEND)
      DOWHILE(TIME.LE.1.188D5)
*
*---CALCULATION OF REJECTION
*
```

```
*---SETTING MEMBRANE CHARGE
*
          IF(CW(4).GT.17.7D0)THEN
             XD=-8.6D0
             ELSE
             XD=-(0.5051D0*CW(4)-0.3616)
          END IF
          IF(XD.GT.0D0)THEN
             XD=0D0
          END IF
*
*===== CALLING C0(I) FROM SUBROUTINE PARTITN =====
       CALL PARTITN(CW,LAMBDA,DELTAW,PHI,Z,C0)
*
          TIME=TIME+DELTIME
          VEL=(PRESS*(RP**2))/(8D0*DX*VISCP)
          CP1STEP=(CP1MAX-CP1MIN)/5D0
          CP2STEP=(CP2MAX-CP2MIN)/5D0
          CP3STEP=(CP3MAX-CP3MIN)/5D0
*---Initial Cp1 values
          CP1C=CP1START
          CP1N=CP1C
          CP1E=CP1C+CP1STEP
          CP1SE=CP1C
          CP1S=CP1C
          CP1W=CP1C-CP1STEP
          CP1NW=CP1C
*---Initial Cp2 values
          CP2C=CP2START
          CP2N=CP2C+CP2STEP
          CP2E=CP2C
          CP2SE=CP2C
          CP2S=CP2C-CP2STEP
          CP2W=CP2C
          CP2NW=CP2C
*---Initial Cp3 values
          CP3C=CP3START
          CP3N=CP3C
          CP3E=CP3C
          CP3SE=CP3C+CP3STEP
          CP3S=CP3C
          CP3W=CP3C
          CP3NW=CP3C-CP3STEP
*---INITIAL TEST FUNCTION
          TEST=10D0
          TESTMIN=1D6
          DOWHILE (TEST.GT.1D-10)
*---CALCULATION OF CONCENTRATION AT EACH POINT
             CALL ROOT(CP1C,CP2C,CP3C,CP4C,CDX1C,CDX2C,CDX3C,CDX4C)
             CALL ROOT(CP1N,CP2N,CP3N,CP4N,CDX1N,CDX2N,CDX3N,CDX4N)
             CALL ROOT(CP1E,CP2E,CP3E,CP4E,CDX1E,CDX2E,CDX3E,CDX4E)
             CALL ROOT(CP1SE,CP2SE,CP3SE,CP4SE,CDX1SE,CDX2SE,CDX3SE,
     +                 CDX4SE)
             CALL ROOT(CP1S,CP2S,CP3S,CP4S,CDX1S,CDX2S,CDX3S,CDX4S)
             CALL ROOT(CP1NW,CP2NW,CP3NW,CP4NW,CDX1NW,CDX2NW,CDX3NW,
     +                 CDX4NW)
             CALL ROOT(CP1W,CP2W,CP3W,CP4W,CDX1W,CDX2W,CDX3W,CDX4W)
*
*---CHECKING FOR NEGATIVE CONCENTRATIONS
             CALL CONC(CP1C,CP2C,CP3C,CP4C,CDX1C,CDX2C,CDX3C,CDX4C,
     +                 SWITCH)
```

```
*---CALLING FOR CONCENTRATION PROFILE ACROSS MEMBRANE
            IF (SWITCH.EQ.0) THEN
               CALL LINEAR(CP1C,CP2C,CP3C,CDX1C,CDX2C,CDX3C,TESTC,
     +                           G1,G2,G3          )
            ELSE
               TESTC=1D7
               SWITCH=0
            ENDIF
*
*---REPEATING FOR OTHER GUESSES i.e. N,E,SE...
            CALL CONC(CP1N,CP2N,CP3N,CP4N,CDX1N,CDX2N,CDX3N,CDX4N,
     +                 SWITCH)
            IF (SWITCH.EQ.0) THEN
               CALL LINEAR(CP1N,CP2N,CP3N,CDX1N,CDX2N,CDX3N,TESTN,
     +                           G11,G12,G13          )
            ELSE
               TESTN=1D7
               SWITCH=0
            ENDIF
*
            CALL CONC(CP1E,CP2E,CP3E,CP4E,CDX1E,CDX2E,CDX3E,CDX4E,
     +                 SWITCH)
            IF (SWITCH.EQ.0) THEN
               CALL LINEAR(CP1E,CP2E,CP3E,CDX1E,CDX2E,CDX3E,TESTE,
     +                            G11,G12,G13          )
            ELSE
               TESTE=1D7
               SWITCH=0
            ENDIF
*
            CALL CONC(CP1SE,CP2SE,CP3SE,CP4SE,CDX1SE,CDX2SE,CDX3SE,
     +                 CDX4SE,SWITCH)
            IF (SWITCH.EQ.0) THEN
               CALL LINEAR(CP1SE,CP2SE,CP3SE,CDX1SE,CDX2SE,CDX3SE,
     +                      TESTSE,G11,G12,G13)
            ELSE
               TESTSE=1D7
               SWITCH=0
            ENDIF
*
            CALL CONC(CP1S,CP2S,CP3S,CP4S,CDX1S,CDX2S,CDX3S,CDX4S,
     +                 SWITCH)
            IF (SWITCH.EQ.0) THEN
               CALL LINEAR(CP1S,CP2S,CP3S,CDX1S,CDX2S,CDX3S,TESTS,
     +                              G11,G12,G13          )
            ELSE
               TESTS=1D7
               SWITCH=0
            ENDIF
*
            CALL CONC(CP1NW,CP2NW,CP3NW,CP4NW,CDX1NW,CDX2NW,CDX3NW,
     +                 CDX4NW,SWITCH)
            IF (SWITCH.EQ.0) THEN
               CALL LINEAR(CP1NW,CP2NW,CP3NW,CDX1NW,CDX2NW,CDX3NW,
     +                         TESTNW,G11,G12,G13)
            ELSE
               TESTNW=1D7
               SWITCH=0
            ENDIF
*
            CALL CONC(CP1W,CP2W,CP3W,CP4W,CDX1W,CDX2W,CDX3W,CDX4W,
```

```
     +                SWITCH)
              IF (SWITCH.EQ.0) THEN
                 CALL LINEAR(CP1W,CP2W,CP3W,CDX1W,CDX2W,CDX3W,TESTW,
     +                        G11,G12,G13          )
              ELSE
                 TESTW=1D7
                 SWITCH=0
              ENDIF
*---EVALUATION OF MINIMUM
              TESTFUNC(1)=TESTC
              TESTFUNC(2)=TESTN
              TESTFUNC(3)=TESTE
              TESTFUNC(4)=TESTSE
              TESTFUNC(5)=TESTS
              TESTFUNC(6)=TESTNW
              TESTFUNC(7)=TESTW
c              TESTMIN=20000D0
              K=1
              DO I=1,7
                 IF (TESTFUNC(I).LT.TESTMIN) THEN
                    TESTMIN=TESTFUNC(I)
                    K=I
                 ENDIF
              ENDDO
              IF (K.EQ.1) THEN
                 TEST=TESTC
                 CP1STEP=CP1STEP/5D0
                 CP2STEP=CP2STEP/5D0
                 CP3STEP=CP3STEP/5D0
                 CP1C=CP1C
                 CP1N=CP1C
                 CP1E=CP1C+CP1STEP
                 CP1SE=CP1C
                 CP1S=CP1C
                 CP1W=CP1C-CP1STEP
                 CP1NW=CP1C
                 CP2C=CP2C
                 CP2N=CP2C+CP2STEP
                 CP2E=CP2C
                 CP2SE=CP2C
                 CP2S=CP2C-CP2STEP
                 CP2W=CP2C
                 CP2NW=CP2C
                 CP3C=CP3C
                 CP3N=CP3C
                 CP3E=CP3C
                 CP3SE=CP3C+CP3STEP
                 CP3S=CP3C
                 CP3W=CP3C
                 CP3NW=CP3C-CP3STEP
              ENDIF
              IF (K.EQ.2) THEN
                 TEST=TESTN
                 CP1C=CP1N
                 CP1N=CP1C
                 CP1E=CP1C+CP1STEP
                 CP1SE=CP1C
                 CP1S=CP1C
                 CP1W=CP1C-CP1STEP
                 CP1NW=CP1C
                 CP2C=CP2N
```

```
      CP2N=CP2C+CP2STEP
      CP2E=CP2C
      CP2SE=CP2C
      CP2S=CP2C-CP2STEP
      CP2W=CP2C
      CP2NW=CP2C
      CP3C=CP3N
      CP3N=CP3C
      CP3E=CP3C
      CP3SE=CP3C+CP3STEP
      CP3S=CP3C
      CP3W=CP3C
      CP3NW=CP3C-CP3STEP
   ENDIF
   IF (K.EQ.3) THEN
      TEST=TESTE
      CP1C=CP1E
      CP1N=CP1C
      CP1E=CP1C+CP1STEP
      CP1SE=CP1C
      CP1S=CP1C
      CP1W=CP1C-CP1STEP
      CP1NW=CP1C
      CP2C=CP2E
      CP2N=CP2C+CP2STEP
      CP2E=CP2C
      CP2SE=CP2C
      CP2S=CP2C-CP2STEP
      CP2W=CP2C
      CP2NW=CP2C
      CP3C=CP3E
      CP3N=CP3C
      CP3E=CP3C
      CP3SE=CP3C+CP3STEP
      CP3S=CP3C
      CP3W=CP3C
      CP3NW=CP3C-CP3STEP
   ENDIF
   IF (K.EQ.4) THEN
      TEST=TESTSE
      CP1C=CP1SE
      CP1N=CP1C
      CP1E=CP1C+CP1STEP
      CP1SE=CP1C
      CP1S=CP1C
      CP1W=CP1C-CP1STEP
      CP1NW=CP1C
      CP2C=CP2SE
      CP2N=CP2C+CP2STEP
      CP2E=CP2C
      CP2SE=CP2C
      CP2S=CP2C-CP2STEP
      CP2W=CP2C
      CP2NW=CP2C
      CP3C=CP3SE
      CP3N=CP3C
      CP3E=CP3C
      CP3SE=CP3C+CP3STEP
      CP3S=CP3C
      CP3W=CP3C
      CP3NW=CP3C-CP3STEP
```

```
ENDIF
IF (K.EQ.5) THEN
   TEST=TESTS
   CP1C=CP1S
   CP1N=CP1C
   CP1E=CP1C+CP1STEP
   CP1SE=CP1C
   CP1S=CP1C
   CP1W=CP1C-CP1STEP
   CP1NW=CP1C
   CP2C=CP2S
   CP2N=CP2C+CP2STEP
   CP2E=CP2C
   CP2SE=CP2C
   CP2S=CP2C-CP2STEP
   CP2W=CP2C
   CP2NW=CP2C
   CP3C=CP3S
   CP3N=CP3C
   CP3E=CP3C
   CP3SE=CP3C+CP3STEP
   CP3S=CP3C
   CP3W=CP3C
   CP3NW=CP3C-CP3STEP
ENDIF
IF (K.EQ.6) THEN
   TEST=TESTNW
   CP1C=CP1NW
   CP1N=CP1C
   CP1E=CP1C+CP1STEP
   CP1SE=CP1C
   CP1S=CP1C
   CP1W=CP1C-CP1STEP
   CP1NW=CP1C
   CP2C=CP2NW
   CP2N=CP2C+CP2STEP
   CP2E=CP2C
   CP2SE=CP2C
   CP2S=CP2C-CP2STEP
   CP2W=CP2C
   CP2NW=CP2C
   CP3C=CP3NW
   CP3N=CP3C
   CP3E=CP3C
   CP3SE=CP3C+CP3STEP
   CP3S=CP3C
   CP3W=CP3C
   CP3NW=CP3C-CP3STEP
ENDIF
IF (K.EQ.7) THEN
   TEST=TESTW
   CP1C=CP1W
   CP1N=CP1C
   CP1E=CP1C+CP1STEP
   CP1SE=CP1C
   CP1S=CP1C
   CP1W=CP1C-CP1STEP
   CP1NW=CP1C
   CP2C=CP2W
   CP2N=CP2C+CP2STEP
   CP2E=CP2C
```

```
                CP2SE=CP2C
                CP2S=CP2C-CP2STEP
                CP2W=CP2C
                CP2NW=CP2C
                CP3C=CP3W
                CP3N=CP3C
                CP3E=CP3C
                CP3SE=CP3C+CP3STEP
                CP3S=CP3C
                CP3W=CP3C
                CP3NW=CP3C-CP3STEP
              ENDIF
              PRINT 11,TEST,(TIME/3.6D3),PYRCONC
   11         FORMAT(1X,F16.12,4X,F12.2,4X,F12.4)
           ENDDO
           CP4C=-( (Z(1)*CP1C)+(Z(2)*CP2C)+(Z(3)*CP3C) )/
     +                        ( Z(4) )
*
*---CALCULATING REJECTION OF IONS
           REJ1=(1D0-(CP1C/CW(1)))
           REJ2=(1D0-(CP2C/CW(2)))
           REJ3=(1D0-(CP3C/CW(3)))
           REJ4=(1D0-(CP4C/CW(4)))
*---CALCULATING REJECTION OF NEUTRAL NANA
           REJ5=1D0-(KC(3)*PHI(3))/(1D0-(1D0-(KC(3)*PHI(3)))*EXP(-PE1))
*---CALCULATING REJECTION OF NEUTRAL PYRUVATE
           REJ6=1D0-(KC(4)*PHI(4))/(1D0-(1D0-(KC(4)*PHI(4)))*EXP(-PE2))
*
*---CONVERTING CONCENTRATIONS FOR CALCULATION
*
           C1OLD=CW(1)
           C2OLD=CW(2)
           C3OLD=CW(3)
           C4OLD=CW(4)
           C5OLD=CONCN1
           C6OLD=CONCN2
*
*---SETTING UP THE INTEGRAL CONSTANTS
*
           FUNCR=-FLUX*AREA/VOL
*---FOR COMPONENT 1
           K11=FUNCR*(1-REJ1)*C1OLD
           K21=FUNCR*(1-REJ1)*(C1OLD+0.5D0*DELTIME*K11)
           K31=FUNCR*(1-REJ1)*(C1OLD+0.5D0*DELTIME*K21)
           K41=FUNCR*(1-REJ1)*(C1OLD+DELTIME*K31)
*---FOR COMPONENT 2
           K12=FUNCR*(1-REJ2)*C2OLD
           K22=FUNCR*(1-REJ2)*(C2OLD+0.5D0*DELTIME*K12)
           K32=FUNCR*(1-REJ2)*(C2OLD+0.5D0*DELTIME*K22)
           K42=FUNCR*(1-REJ2)*(C2OLD+DELTIME*K32)
*---FOR COMPONENT 3
           K13=FUNCR*(1-REJ3)*C3OLD
           K23=FUNCR*(1-REJ3)*(C3OLD+0.5D0*DELTIME*K13)
           K33=FUNCR*(1-REJ3)*(C3OLD+0.5D0*DELTIME*K23)
           K43=FUNCR*(1-REJ3)*(C3OLD+DELTIME*K33)
*---FOR COMPONENT 4
           K14=FUNCR*(1-REJ4)*C4OLD
           K24=FUNCR*(1-REJ4)*(C4OLD+0.5D0*DELTIME*K14)
           K34=FUNCR*(1-REJ4)*(C4OLD+0.5D0*DELTIME*K24)
           K44=FUNCR*(1-REJ4)*(C4OLD+DELTIME*K34)
*---FOR COMPONENT 5
```

```
          K15=FUNCR*(1-REJ5)*C5OLD
          K25=FUNCR*(1-REJ5)*(C5OLD+0.5D0*DELTIME*K15)
          K35=FUNCR*(1-REJ5)*(C5OLD+0.5D0*DELTIME*K25)
          K45=FUNCR*(1-REJ5)*(C5OLD+DELTIME*K35)
*---FOR COMPONENT 6
          K16=FUNCR*(1-REJ6)*C6OLD
          K26=FUNCR*(1-REJ6)*(C6OLD+0.5D0*DELTIME*K16)
          K36=FUNCR*(1-REJ6)*(C6OLD+0.5D0*DELTIME*K26)
          K46=FUNCR*(1-REJ6)*(C6OLD+DELTIME*K36)
*
*---CALCULATING NEW CONCENTRATIONS
*

          C1NEW=C1OLD+DELTIME*((1D0/6D0)*(K11+2D0*K21+2D0*K31+K41))
          C2NEW=C2OLD+DELTIME*((1D0/6D0)*(K12+2D0*K22+2D0*K32+K42))
          C3NEW=C3OLD+DELTIME*((1D0/6D0)*(K13+2D0*K23+2D0*K33+K43))
          C4NEW=C4OLD+DELTIME*((1D0/6D0)*(K14+2D0*K24+2D0*K34+K44))
          C5NEW=C5OLD+DELTIME*((1D0/6D0)*(K15+2D0*K25+2D0*K35+K45))
          C6NEW=C6OLD+DELTIME*((1D0/6D0)*(K16+2D0*K26+2D0*K36+K46))
*
*---CALCULATING THE CONCENTRATIONS FOR NANA
*
          NANCONC=C3NEW+C5NEW
          PYRCONC=C4NEW+C6NEW
*---CONVERTING CONCENTRATIONS BACK TO AN ARRAY
*
          CW(1)=C1NEW
          CW(2)=C2NEW
          CW(3)=NANCONC*FRAC1
          CW(4)=PYRCONC*FRAC2
          CONCN1=NANCONC*(1D0-FRAC1)
          CONCN2=PYRCONC*(1D0-FRAC2)
*
*
          WRITE(5,3600)  (TIME/3.6D3),CW(1),CW(2),CW(4),CW(3),NANCONC,
     +                                                        PYRCONC
 3600     FORMAT(1X,T4,F12.2,T18,F12.6,T32,F12.6,T46,F12.6,T60,F12.6,
     +           T74,F12.6,T92,F12.6)
 3601     FORMAT(1X,T4,A12,T18,A12,T32,A12,T46,A12,T60,A12,T74,A12,
     +           T92,A12)
          CP1START=CP1C
          CP2START=CP2C
          CP3START=CP3C
       ENDDO
       CLOSE(5)
       STOP
       END
*
*=====================================================================
*-                                                                   -
*-                       END OF MAIN PROGRAM                         -
*-                                                                   -
*=====================================================================
*=====================================================================
*-                                                                   -
*-                            SUBROUTINES                            -
*---------------------------------------------------------------------
*
*===== PARTITIONING SUBROUTINE TO FIND C0(I) =====
*
       SUBROUTINE PARTITN(CW,LAMBDA,DELTAW,PHI,Z,C0)
```

```
      IMPLICIT DOUBLE PRECISION (A-Z)
      INTEGER*4 COUNT,I,N,NMAX,Z
      PARAMETER (NMAX=4)
      DIMENSION C0(1:NMAX),CONC(1:NMAX),CW(1:NMAX),DELTAW(1:NMAX),
     +          PHI(1:NMAX),Z(1:NMAX),LAMBDA(1:NMAX)
      COMMON /ALL/    BOLTZC,F,N,R,TEMP,XD
*
*===== CALCULATION =====
*---Initial values
      PSI=0D0
      TEST=20D0
      COUNT=0
*---Iteration
      DOWHILE (TEST.GT.1D-6)
         PSINEW=PSI
         SUM=0D0
         DO I=1,N
            IF(LAMBDA(I).GE.1D0)THEN
               CONC(I)=0D0
               ELSE
               CONC(I)=CW(I)*PHI(I)*DEXP((-Z(I)*F*PSINEW)/(R*TEMP))*
     +                 DEXP(-DELTAW(I)/(BOLTZC*TEMP))
            END IF
            SUM=SUM+(Z(I)*CONC(I))
         ENDDO
         TESTNEW=SUM+XD
         IF (COUNT.EQ.0) THEN
            IF (TESTNEW.GT.0) THEN
               PSI=PSINEW+0.1D0
               PSIABOVE=PSINEW
               TEST=DABS(TESTNEW)
               COUNT=1
            ENDIF
            IF (TESTNEW.LT.0) THEN
               PSI=PSINEW-0.1D0
               PSIBELOW=PSINEW
               TEST=DABS(TESTNEW)
               COUNT=2
            ENDIF
         ENDIF
         IF (COUNT.EQ.1) THEN
            IF (TESTNEW.GT.0) THEN
               PSI=PSINEW+0.1D0
               PSIABOVE=PSINEW
               TEST=DABS(TESTNEW)
            ENDIF
            IF (TESTNEW.LT.0) THEN
               PSI=PSINEW-0.1D0
               PSIBELOW=PSINEW
               TEST=DABS(TESTNEW)
               COUNT=3
            ENDIF
         ENDIF
         IF (COUNT.EQ.2) THEN
            IF (TESTNEW.GT.0) THEN
               PSI=PSINEW+0.1D0
               PSIABOVE=PSINEW
               TEST=DABS(TESTNEW)
               COUNT=3
            ENDIF
            IF (TESTNEW.LT.0) THEN
```

```
               PSI=PSINEW-0.1D0
               PSIBELOW=PSINEW
               TEST=DABS(TESTNEW)
            ENDIF
         ENDIF
         IF (COUNT.EQ.3) THEN
            IF (TESTNEW.GT.0) THEN
               PSIABOVE=PSINEW
               TEST=DABS(TESTNEW)
            ENDIF
            IF (TESTNEW.LT.0) THEN
               PSIBELOW=PSINEW
               TEST=DABS(TESTNEW)
            ENDIF
            PSI=(PSIABOVE+PSIBELOW)/2D0
         ENDIF
      ENDDO
*
*===== CONCENTRATION AT PORE ENTRANCE =====
      DO I=1,N
         C0(I)=CONC(I)
      ENDDO
*
*---RETURN TO MAIN PROGRAM
      RETURN
      END
*
*===== END OF SUBROUTINE PARTITN =====
*
*===== ROOT SUBROUTINE TO FIND CDXi VALUES FOR CPi GUESSES =====
*
      SUBROUTINE ROOT(CP1,CP2,CP3,CP4,CDX1,CDX2,CDX3,CDX4)
      IMPLICIT DOUBLE PRECISION (A-Z)
      INTEGER*4 I,N,NMAX,SWITCH,COUNT,Z
      PARAMETER (NMAX=4)
      DIMENSION A(1:NMAX),C0(1:NMAX),DELTAW(1:NMAX),Z(1:NMAX),
     +          PHI(1:NMAX),KC(1:NMAX),DP(1:NMAX)
      COMMON /ALL/    BOLTZC,F,N,R,TEMP,XD
      COMMON /OTHERS/ C0,DELTAW,PHI,Z,VEL,KC,DP,DX
*
*===== CALCULATION =====
*
*---CP4 VALUE FROM ELECTRONEUTRALITY
      CP4=-( (Z(1)*CP1)+(Z(2)*CP2)+(Z(3)*CP3) )/
     +                   ( Z(4) )
*---FUNCTIONS
      DO I=1,N
         A(I)=PHI(I)*DEXP(-DELTAW(I)/(BOLTZC*TEMP))
      ENDDO
*
*===== CHECK CONCENTRATIONS =====
      SWITCH=0
      IF (CP1.LT.0) THEN
         SWITCH=1
      ENDIF
      IF (CP2.LT.0) THEN
         SWITCH=1
      ENDIF
      IF (CP3.LT.0) THEN
         SWITCH=1
      ENDIF
```

```
      IF (CP4.LT.0) THEN
         SWITCH=1
      ENDIF
*
*===== SWITCH =====
      IF (SWITCH.EQ.0) THEN
*===== NEWTON METHOD =====
*---INITIAL GUESS FOR CDX1
         COLD=C0(1)
         CCOMP=1D0
         COUNT=0
         DOWHILE (CCOMP.GT.1D-6)
*---FUNC FUNCTIONS
         P1=Z(1)*COLD
         P2=Z(2)*A(2)*CP2*((COLD/(CP1*A(1)))**(Z(2)/Z(1)))
         P3=Z(3)*A(3)*CP3*((COLD/(CP1*A(1)))**(Z(3)/Z(1)))
         P4=Z(4)*A(4)*CP4*((COLD/(CP1*A(1)))**(Z(4)/Z(1)))
         P5=XD
*---DERIVF FUNCTIONS
         S1=Z(1)
         S2=((A(2)*CP2*Z(2)**2)/(Z(1)*CP1*A(1)))*((COLD/(CP1*A(1)))**
     +       ((Z(2)/Z(1))-1))
         S3=((A(3)*CP3*Z(3)**2)/(Z(1)*CP1*A(1)))*((COLD/(CP1*A(1)))**
     +       ((Z(3)/Z(1))-1))
         S4=((A(4)*CP4*Z(4)**2)/(Z(1)*CP1*A(1)))*((COLD/(CP1*A(1)))**
     +       ((Z(4)/Z(1))-1))
*
            FUNC=P1+P2+P3+P4+P5
            DERIVF=S1+S2+S3+S4
            CNEW=COLD-(FUNC/DERIVF)
            CCOMP=100D0*DABS((CNEW-COLD)/CNEW)
            CRES=COLD
            COLD=CNEW
            COUNT=COUNT+1
            IF (COUNT.GT.1000) THEN
               CRES=-1D0
               CCOMP=1D-9
               PRINT*,'no ROOT!!!'
            ENDIF
         ENDDO
*---CDXi VALUES
      CDX1=CRES
      CDX2=A(2)*CP2*((CDX1/(A(1)*CP1))**(Z(2)/Z(1)))
      CDX3=A(3)*CP3*((CDX1/(A(1)*CP1))**(Z(3)/Z(1)))
      CDX4=A(4)*CP4*((CDX1/(A(1)*CP1))**(Z(4)/Z(1)))
*
      ELSE
         CRES=-1D0
         CDX1=CRES
         CDX2=CRES
         CDX3=CRES
         CDX4=CRES
      ENDIF
*---RETURN TO MAIN PROGRAM
      RETURN
      END
*
*===== END OF SUBROUTINE ROOT =====
*
*===== CONC SUBROUTINE TO FIND NEGATIVE CONCENTRATIONS =====
*
```

```
      SUBROUTINE CONC(CP1,CP2,CP3,CP4,CDX1,CDX2,CDX3,CDX4,SWITCH)
      IMPLICIT DOUBLE PRECISION (A-Z)
      INTEGER*4 SWITCH
*
*===== SEARCH FOR NEGATIVE CONCENTRATION VALUES =====
      SWITCH=0
      IF (CP1.LT.0D0) THEN
         SWITCH=1
      ENDIF
      IF (CP2.LT.0D0) THEN
         SWITCH=1
      ENDIF
      IF (CP3.LT.0D0) THEN
         SWITCH=1
      ENDIF
      IF (CP4.LT.0D0) THEN
         SWITCH=1
      ENDIF
      IF (CDX1.LT.0D0) THEN
         SWITCH=1
      ENDIF
      IF (CDX2.LT.0D0) THEN
         SWITCH=1
      ENDIF
      IF (CDX3.LT.0D0) THEN
         SWITCH=1
      ENDIF
      IF (CDX4.LT.0D0) THEN
         SWITCH=1
      ENDIF
*---RETURN TO MAIN PROGRAM
      RETURN
      END
*
*===== END OF SUBROUTINE CONC =====
*
*===== LINEAR SUBROUTINE TO CALCULATE CONCENTRATION PROFILE =====
*
      SUBROUTINE LINEAR(CP1,CP2,CP3,CDX1,CDX2,CDX3,TEST,
     +                        DSIDX,DC1DX,CDX1C)
      IMPLICIT DOUBLE PRECISION (A-Z)
      INTEGER*4 NMAX,N,Z
      PARAMETER (NMAX=4)
      DIMENSION C0(1:NMAX),Z(1:NMAX),KC(1:NMAX),DP(1:NMAX),
     +          DELTAW(1:NMAX),PHI(1:NMAX)
      COMMON /ALL/    BOLTZC,F,N,R,TEMP,XD
      COMMON /OTHERS/ C0,DELTAW,PHI,Z,VEL,KC,DP,DX
*
*===== CALCULATION =====
*
      T=TEMP
*---CALCULATION OF CAVi
      CAV1=(C0(1)+CDX1)/2
      CAV2=(C0(2)+CDX2)/2
      CAV3=(C0(3)+CDX3)/2
*
*---CALCULATION OF CHARGE FUNCTION (DSI/DX)
*
*---FUNCTIONS
      A=Z(1)*VEL*(KC(1)/DP(1)-KC(4)/DP(4))
      B=Z(2)*VEL*(KC(2)/DP(2)-KC(4)/DP(4))
```

```
      E=Z(3)*VEL*(KC(3)/DP(3)-KC(4)/DP(4))
      G=Z(1)*VEL*(1/DP(4)-1/DP(1))
      H=Z(2)*VEL*(1/DP(4)-1/DP(2))
      J=Z(3)*VEL*(1/DP(4)-1/DP(3))
      L=VEL*KC(4)/DP(4)
      M=(F/(R*T))*((Z(1)**2)-Z(1)*Z(4))
      N1=(F/(R*T))*((Z(2)**2)-Z(2)*Z(4))
      P=(F/(R*T))*((Z(3)**2)-Z(3)*Z(4))
      Q=(F/(R*T))*Z(4)
*
      DSIDX=(A*CAV1+B*CAV2+E*CAV3+G*CP1+H*CP2+J*CP3-L*XD)/
     +      (M*CAV1+N1*CAV2+P*CAV3-Q*XD)
*
*---CALCULATION OF CONCENTRATION GRADIENTS
*
      DC1DX=(VEL/DP(1))*(KC(1)*CAV1-CP1)-((CAV1*Z(1)*F)/(R*T))*DSIDX
      DC2DX=(VEL/DP(2))*(KC(2)*CAV2-CP2)-((CAV2*Z(2)*F)/(R*T))*DSIDX
      DC3DX=(VEL/DP(3))*(KC(3)*CAV3-CP3)-((CAV3*Z(3)*F)/(R*T))*DSIDX
*
*---CALCULATING CDXi(CALC) FROM GRADIENTS
      CDX1C=DC1DX*DX+C0(1)
      CDX2C=DC2DX*DX+C0(2)
      CDX3C=DC3DX*DX+C0(3)
*
*---EVALUATING TEST FUNCTION
*
      T1=(CDX1C-CDX1)**2
      T2=(CDX2C-CDX2)**2
      T3=(CDX3C-CDX3)**2
      TEST=SQRT(T1+T2+T3)
*
*---RETURN TO MAIN PROGRAM
      RETURN
      END
*
*===== END OF SUBROUTINE LINEAR =====
```

Appendix A3: Sample analysis

The general description of the methods used for sample analysis are provided in Chapter 2. The individual assay details along with relevant calibration plots will be provided here.

Glucose analysis, GOD Perid assay

Glucose concentration in the feed and permeate samples was analysed using a GOD-Perid assay kit supplied by Roche Diagnostics GmbH (Manheim, Germany).

The details of the assay are outlined in the document MPR 2 124028 and are briefly outlined here. The test relies on the following principle reactions

$$glucose + O_2 + H_2O \xrightarrow{GOD} gluconate + H_2O_2 \quad \text{(A34)}$$

$$H_2O_2 + ABTS \xrightarrow{POD} chromogen + H_2O \quad \text{(A35)}$$

The reaction causes a colour change in the sample which is observed using a spectrophotometer. The concentration of glucose is then obtained by comparison of the optical density to that of a standard solution or a calibration curve. The optical density was recorded at 740 nm, the maximum absorbance of the GOD-Perid solution (see Figure A1), using the Phillips PU 8625 UV/Vis spectrophotometer. The concentration was then evaluated from the calibration curve provided as Figure A2.

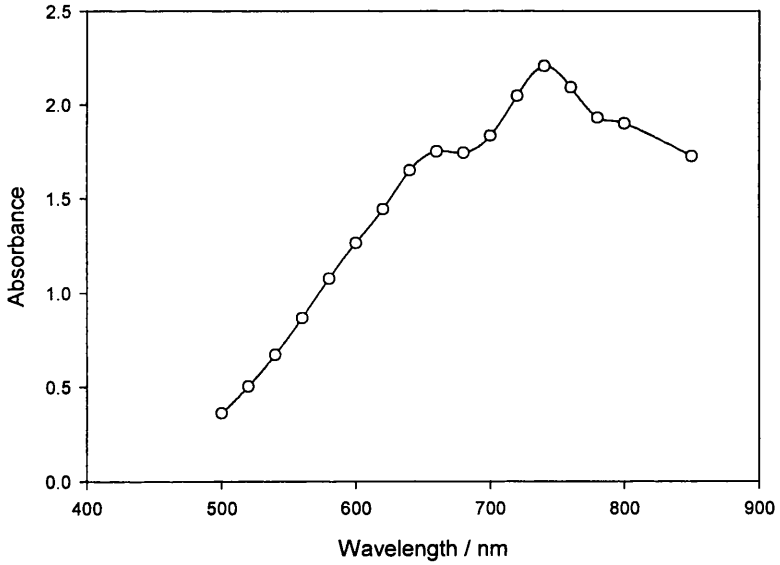

Figure A1: Absorbance of GOD-Perid assay solution versus light wavelength (maximum occurring at 740 nm).

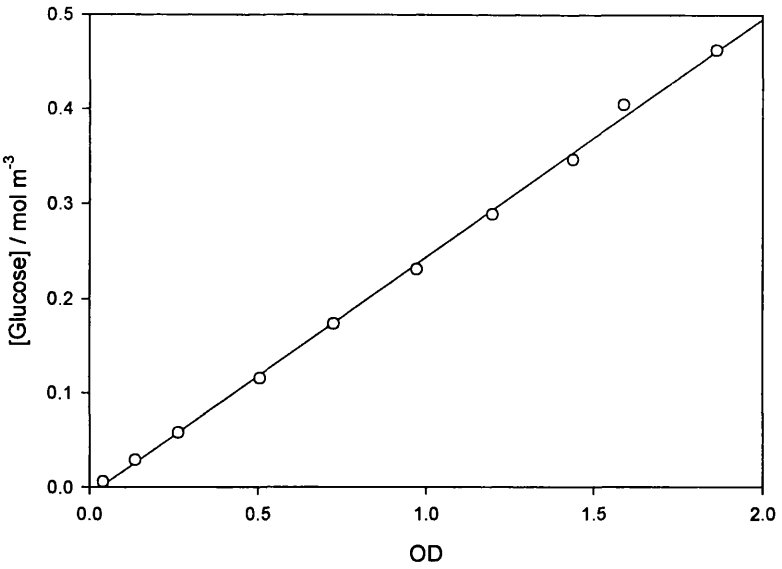

Figure A2: Glucose calibration curve using the GOD-Perid assay kit (detection at 740 nm).

Glucose analysis, GAGO-20 assay kit

Glucose concentration in the feed and permeate samples was also analysed using a GAGO-20 assay kit supplied by Sigma-Aldrich Ltd. (Poole, Dorset, U.K.). The details of the assay are outlined in the document Product Information GAGO-20 and are briefly outlined here. The test relies on the following principle reactions

$$Glucose + H_2O + O_2 \xrightarrow{Glucose\ Oxidase} Gluconic\ acid + H_2O_2 \quad \text{(A36)}$$

$$H_2O_2 + \text{Red. } Dianisidine \text{ (colourless)} \xrightarrow{Peroxidase} \text{Ox. } Dianisidine \text{ (brown)} \quad \text{(A37)}$$

$$\text{Ox. } Dianisidine \text{ (brown)} \xrightarrow{H_2SO_4} \text{Ox. } Dianisidine \text{ (pink)} \quad \text{(A38)}$$

The test then involves measuring the optical density of the samples and comparison against a known standard (*KS*) using the equation

$$\text{mg Glucose} = \frac{A_{540}Test}{A_{540}KS} \times \text{mg Glucose in } KS \quad \text{(A39)}$$

Sodium lactate analysis, Lactate reagent 735-10 assay kit

Lactate ion concentration in the feed and permeate samples was analysed using the Lactate reagent 735-10 assay kit supplied by Trinity Biotech U.K. Sales Ltd. (Abingdon, Oxford, U.K.). The details of the assay are outlined in the document Procedure No. 735 and are briefly outlined here. The test relies on the following principle reactions

$$Lactate \xrightarrow[Oxidase]{Lactate} Pyruvate + H_2O_2 \qquad \text{(A40)}$$

$$H_2O_2 + Pre\text{-}Chromogen \xrightarrow{Peroxidase} Chromogen \qquad \text{(A41)}$$

The reactions cause a colour change in the solution which is measured at 540 nm. The concentration of lactate ions in solution was then evaluated from a calibration curve provided as Figure A3.

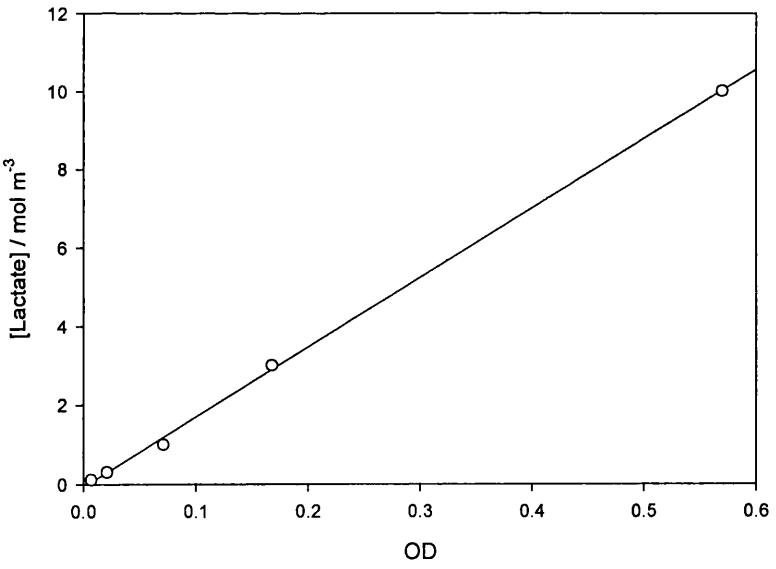

Figure A3: Lactate calibration curve using the 735-10 assay kit (detection at 540 nm).

Cefuroxime analysis, HPLC method 1

The concentration of cefuroxime ions in solution were analysed by HPLC. The details of the HPLC method are provided in Section 2.3 (method 1) and will not be repeated here. The concentration of cefuroxime was determined from a calibration curve produced from samples of known concentration and is provided as Figure A4.

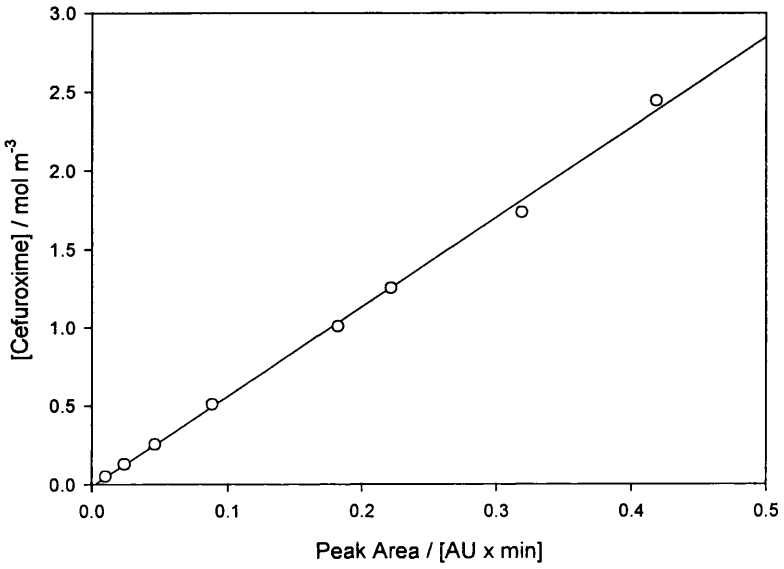

Figure A4: Cefuroxime calibration curve using HPLC method 1.

Neu5Ac analysis, HPLC method 2

The concentration of ManNAc and mixtures of Neu5Ac, ManNAc and pyruvate in solution were analysed by HPLC. The details of the HPLC method are provided in Section 2.3 (method 2) and will not be repeated here. The concentration of these components was determined from a calibration curve produced from samples of known concentration and is provided as Figure A5.

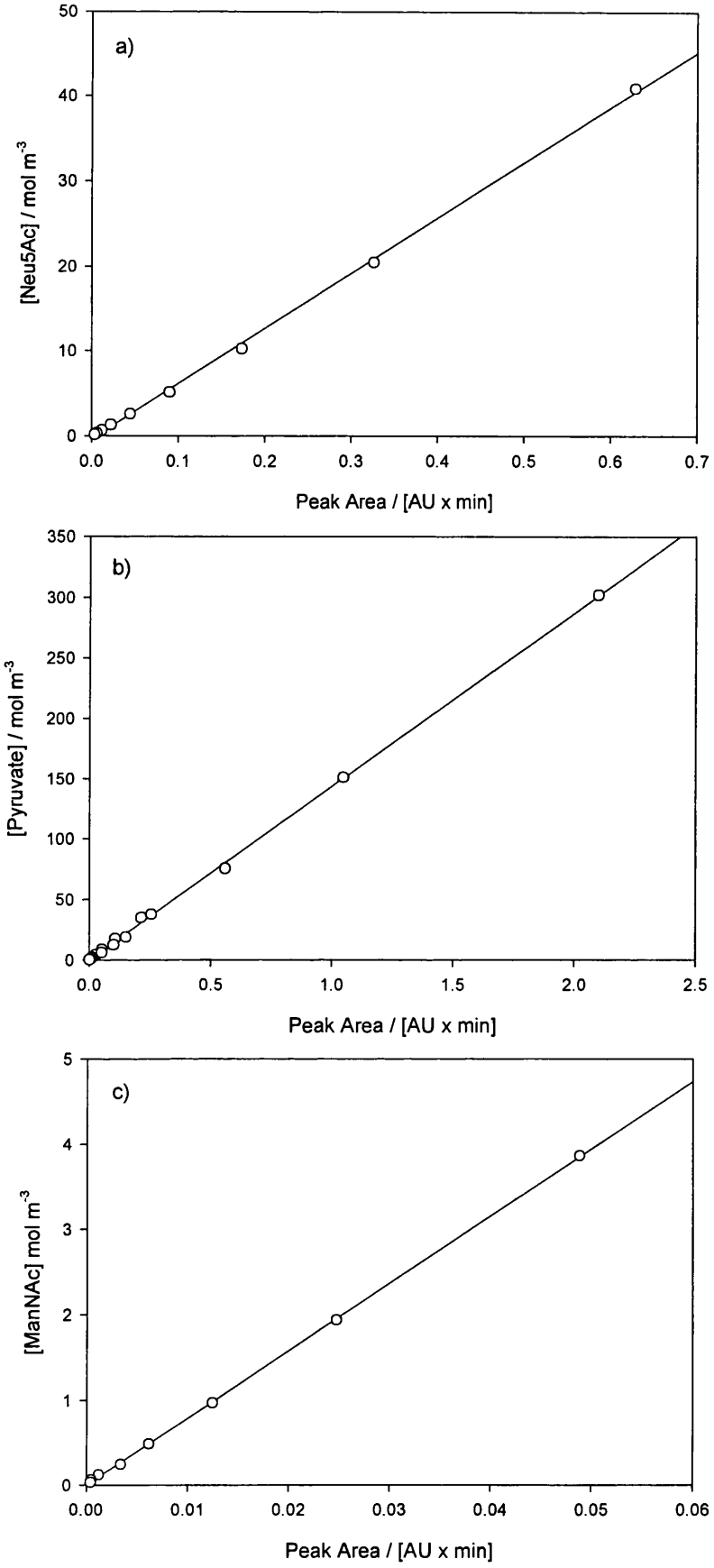

Figure A5: HPLC calibration curves for a) Neu5Ac, b) Pyruvate and c) ManNAc.

Appendix A4: High Performance Particle Sizing (HPPS)

The particle radius (a_i) has been used throughout this thesis and indeed is extremely important in many other areas of research. However, this simple property remains difficult to obtain with reliable accuracy from either predictive models or experimental measurements, even more so for very small solutes. Recently, Malvern Instruments (Malvern, Worces., U.K.) has developed the Malvern HPPS 3.1 which claims to have the ability to measure the solute radius of particles as small as 0.3 nm[1]. This is a significant improvement in relation to other equipment in the range and is useful as an independent measurement of particle size in the NF range.

Details of the HPPS principles of operation and functions are found in the operators guide referenced below.

A comparison between the measured particle radius using the HPPS, predicted particle radius using current models and literature values for various small solutes was made in order to gain an understanding of the accuracy of the equipment and current predictive models for particle size.

The predictive models used in this study were those of:
Hayduk and Laudie (1974), a general model for the diffusion of any species in any solvent, details provided in Section 2.4.3.

$$a_i = 0.045 MW^{0.44} \qquad \text{(A42)}$$

Combe *et al.* (1999), derived to predict the diffusion coefficients of various forms of PEG.

$$\log_{10} a_i = -1.3363 + 0.395 \log_{10} MW \qquad \text{(A43)}$$

Bowen and Mohammad (1998b), developed to predict small molecule diffusivity, and

$$a_i = 16.73 \times 10^{-3} MW^{0.557} \qquad \text{(A44)}$$

Singh *et al.* (1998), developed from intrinsic viscosity data.

[1] HPPS Operators Guide, MAN0314, Issue 1.0, Dec. 2001

Sample preparation

The physical process of making measurements is very simple – basically you insert the sample into the instrument and tell the software to measure ! For a particle size of less than 10 nm, a concentration greater than 0.5 g L^{-1} is recommended with no upper limit provided the material has no aggregation or gelation. In this study, a concentration of approximately 80 g L^{-1} was used in all cases. Samples were prepared using deionised water and were filtered with a 0.22 μm Millex syringe driven filter unit [obtained from Millipore (U.K.) Ltd. (Watford, Herts., U.K.)] into a 4.5 mL capacity UV range cuvette obtained from Merck Ltd. (Leics., U.K.).

Results and discussion

The results obtained for measuring the particle size of several solutes using the Malvern HPPS are provided in Table A1.

Table A1: Particle size measurement using the Malvern HPPS

Particle	MW	Particle size	Standard deviation	a_i	Standard deviation	Literature value	% Difference
	Da	nm	nm	nm	nm	nm	
Arginine	174	0.82	0.05	0.41	0.025	-	-
Glucose	180	0.81	0.03	0.41	0.015	0.36*	11.1
ManNAc	209	0.86	0.04	0.43	0.020	-	-
Neu5Ac	309	1.44	0.16	0.72	0.080	-	-
Sucrose	342	0.99	0.03	0.50	0.015	0.47*	5.1
Cefuroxime	423	0.87	0.03	0.44	0.015	-	-
Raffinose	504	1.28	0.18	0.64	0.090	0.58*	9.4
PEG 1,500	1514	2.22	0.19	1.11	0.095	1.13**	-1.7
PEG 3,400	3406	3.49	0.43	1.75	0.215	1.61**	7.6
PEG 4,600	4594	3.69	0.39	1.85	0.195	1.84**	0.3
PEG 10,000	10006	4.98	0.55	2.49	0.275	2.57**	-3.2

* Bowen and Mohammad (1998), ** Combe *et al.* (1999).

The results provided in Table A1 represent the particle size and standard deviation over a set of 40 individual experiments. The maximum deviation between the literature value (where available) and the experimental findings occurs for glucose. This represents the smallest molecule with an available literature size value and indicates the machine may be at the limit of operation for this molecule. However,

the deviation is approximately 10 % and becomes less as the particle size is increased. Therefore, the equipment is capable of providing a reasonable estimate of particle radius for these very small solutes. As the particle size is increased above MW 1000, the agreement becomes significantly improved.

The experimental findings were then compared to the values obtained from the predictive models and are illustrated in Figure A6.

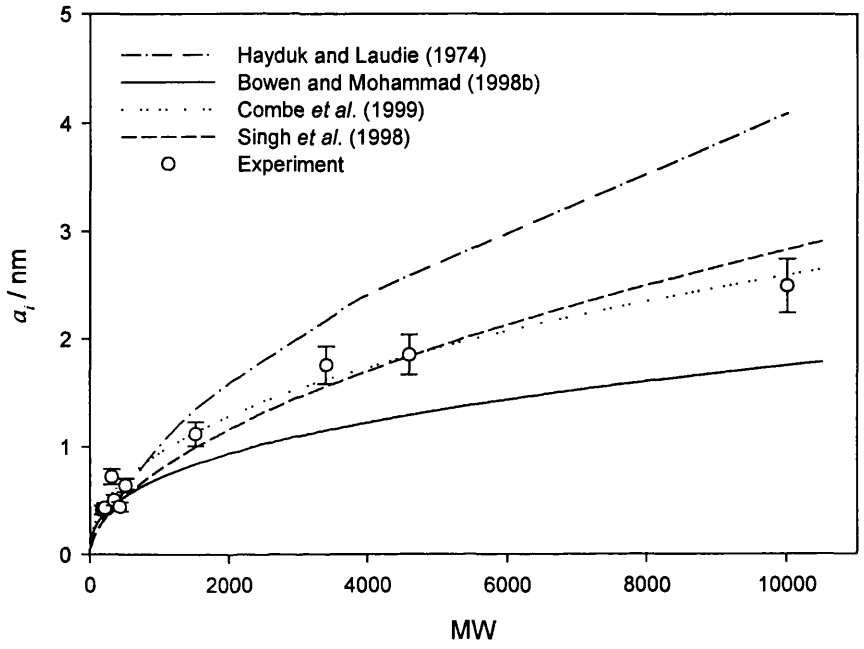

Figure A6: Comparison of experimental findings with correlations for solute radius.

The error bars in Figure A6 represent a standard error of 10 % in the experimentally obtained value of particle radius, the approximate maximum error expected. Both the models of Combe *et al.* (1999) and Singh *et al.* (1998) provide a reasonable estimate of solute radius over the entire range of materials studied. The model of Hayduk and Laudie (1974) significantly over estimates the solute radius as expected and justifies the scaling of the model result in Section 2.4.3. The model of Bowen and Mohammad (1998b) significantly under estimates the solute radius. However, this model was developed for solutes of MW < 1000, which may justify the significant deviation above this point.

Appendix A5: Hindrance factors

A description of the development of hindrance factors is given in Section 3.3.1 and will not be repeated here. The raw data used in developing the new descriptions is provided in Table A2 and the results of the curve fitting procedure are detailed.

Table A2: Raw data and calculated values for the hindrance factors

λ	K^1	G	Φ	$K_{i,c}$	$K_{i,d}$
0.0	1.000	1.000	1.0000	1.00000	1.00000
0.05		0.9985	0.9025	1.09585	
0.1	0.7886	0.9935	0.8100	1.18227	0.78860
0.2	0.5945	0.9740	0.6400	1.32464	0.59450
0.3	0.4198	0.9350	0.4900	1.41185	0.41980
0.4	0.2786	0.8945	0.3600	1.46698	0.27860
0.5	0.1673	0.8343	0.2500	1.46009	0.16734
0.6	0.0892	0.7660	0.1600	1.40946	0.08918
0.7	0.0407	0.7081	0.0900	1.35256	0.04067
0.8	0.0134	0.6379	0.0400	1.25032	0.01345
0.9	0.0021	0.5676	0.0100	1.12951	0.00213
0.92	0.0012	0.5540	0.0064	1.10447	0.00119
0.95	0.0004	0.5335	0.0025	1.06561	0.00035
0.98	0.0000	0.5128	0.0004	1.02531	0.00003

The values in Table A2 for $\lambda \leq 0.4$ are the original data from Anderson and Quinn (1974), the values for $l \geq 0.5$ were obtained from personal correspondence with Dr. Adel Sharif (Surrey University).

The lag coefficient, *G*

The results from the curve fitting exercise for *G* give:

f = y0+a*x+b*x^2+c*x^3+d*x^4+e*x^5+h*x^6+g*x^7
fit f to y

R = 0.99994488 Rsqr = 0.99988976 Adj Rsqr = 0.99976115

Standard Error of Estimate = 0.0029

	Coefficient	Std. Error	t	P
y0	1.0000	0.0029	344.1243	<0.0001
a	0.0650	0.1358	0.4782	0.6494

b	-1.9370	1.9372	-0.9999	0.3560
c	8.5211	11.2092	0.7602	0.4759
d	-27.3398	31.6748	-0.8631	0.4212
e	44.4150	46.5103	0.9549	0.3765
h	-34.5582	34.1007	-1.0134	0.3500
g	10.3358	9.8648	1.0477	0.3351

Analysis of Variance:

	DF	SS	MS	F	P
Regression	7	0.4733	0.0676	7774.4013	<0.0001
Residual	6	0.0001	0.0000		
Total	13	0.4733	0.0364		

PRESS = 0.0003

Durbin-Watson Statistic = 3.2359

Normality Test: Passed (P = 0.3282)

Constant Variance Test: Passed (P = 0.9035)

Power of performed test with alpha = 0.0500: 1.0000

The enhanced drag, K^{-1}

The results of the curve fitting exercise for K^{-1} give:

f = y0+a*x+b*x^2+c*x^3+d*x^4+e*x^5+h*x^6+g*x^7
fit f to y

R = 0.99999884 Rsqr = 0.99999769 Adj Rsqr = 0.99999499

Standard Error of Estimate = 0.0007

	Coefficient	Std. Error	t	P
y0	1.0000	0.0007	1341.5412	<0.0001
a	-2.1812	0.0428	-50.9867	<0.0001
b	0.7328	0.6078	1.2057	0.2733
c	-0.9065	3.3535	-0.2703	0.7960
d	6.7272	9.0477	0.7435	0.4852
e	-10.2324	12.7540	-0.8023	0.4530
h	6.3293	9.0191	0.7018	0.5091
g	-1.4692	2.5252	-0.5818	0.5819

Analysis of Variance:

	DF	SS	MS	F	P
Regression	7	1.4433	0.2062	370587.3978	<0.0001
Residual	6	0.0000	0.0000		
Total	13	1.4433	0.1110		

PRESS = 0.0000

Durbin-Watson Statistic = 3.4865

Normality Test: Passed (P = 0.0078)

Constant Variance Test: Passed (P = 0.0907)

Power of performed test with alpha = 0.0500: 1.0000

Both curve fitting procedures were performed using SigmaPlot 2001, version 7.0, SPSS Inc..

References

Abraham, M.H., and J. Liszi (1978)
Calculations on ionic solvation,
J. Chem. Soc. Farad. Trans. **74** 2858.

Afonso, M.D. and M.N. de Pinho (2000)
Transport of $MgSO_4$, $MgCl_2$ and Na_2SO_4 across an amphoteric nanofiltration membrane,
J. Membrane Sci., **179**, 137.

Afonso, M.D., G Hagmeyer and R. Gimbel (2001)
Streaming potential measurements to assess the variation of nanofiltration surface charge with the concentration of salt solutions,
Sep. Purification Tech., **22-23**, 529.

Ahn, K-H., K-G. Song, H-Y. Cha and I-T. Yeom (1999)
Removal of ions in nickel electroplating rinse water using low-pressure nanofiltration,
Desalination, **122**, 77.

Aitkuliev, K., V.D. Sobolev and N.V. Churaev (1984)
Influence of the flow rate and concentration of the electrolyte on the selectivity of reverse osmosis membranes.
Colloid J. USSR, **46**, 179.

Al-Zoubi, N. and S. Malamataris (2003)
Effects of initial concentration and seeding procedure on crystallisation of orthorhombic paracetamol from ethanolic solution,
Int. J. Pharmaceutics **260** 123.

Anderson, J.L. and J.A. Quinn (1974)
Restricted transport in small pores,
Biophys. J., **14**, 130.

Bandini, S. and D. Vezzani (2003)
Nanofiltration modelling: the role of dielectric exclusion in membrane characterisation,
Chem. Eng. Sci., In Press

Barboza, M., C.O. Hokka and F. Maugeri (2002)
Continuous cephalosporin C purification: dynamic modelling and parameter validation,
Bioprocess Biosyst. Eng. **25** 193.

Basu, S. and M.M. Sharma (1997)
An improved Space-Charge model for flow through charged microporous membranes,
J. Membrane Sci., **124**, 77.

Belfort, G., J. Scherig and D.O. Seevers (1974)
Nuclear magnetic resonance relaxation studies of adsorbed water on porous glass of varying sizes,
J. Colloid Interface Sci., **47**, 106.

Bessarabov, D. and Z. Twardowski (2002)
Industrial application of nanofiltration – new perspectives,
Membr. Tech., **9** 6.

Bhattacharyya, D., R. Adams and M. Williams (1989)
Separation of selected organic acid and inorganic solute by low pressure reverse osmosis membranes,
Biol. Synth. Membranes, **292**, 153.

Binnig, G., C.F. Quate and C. Gerber (1986)
Atomic Force Microscope,
Phys. Rev. Lett., **56**, 930.

Bird, R.B., W.E. Stewart and E.N. Lightfoot (1960)
Transport Phenomena
Wiley, New York.

Blayer, S., J.M. Woodley, M.D. Lilly and M.J. Dawson (1996)
Characterisation of the chemoenzymatic synthesis of *N*-acetyl-D-neuraminic acid (Neu5Ac),
Biotechnol. Prog., **12** 758.

Blayer, S., J.M. Woodley, M.D. Lilly and M.J. Dawson (1999)
Alkaline biocatalysis for the direct synthesis of *N*-acetyl-D-Neuraminic acid (Neu5Ac) from *N*-acetyl-D-Glucosamine (GlcNAc),
Biotech. Bioeng., **66** 131.

Bontha, J.R. and P.N. Pintauro (1992)
Prediction of ion solvation free energies in a polarizable dielectric continuum,
J. Phys. Chem. **96** 7778.

Booth, F. (1951)
The dielectric constant of water and the saturation effect,
J. Chem. Phys., **19**, 391.

Born, M. (1920)
Volumen and hydratationswärme der ionen,
Z. Physik. Chem., **1**, 45.

Boussahel, R., S. Bouland, K. M. Moussaoui and A. Montiel (2000)
Removal of pesticide residues in water using the nanofiltration process,
Desalination, **132**, 205.

Bowen, W.R. (1994)
Membrane Separation Processes, in J.M. Coulson and J.F. Richardson, Eds., *Chemical Engineering*, 4th Edition, Pergamon.

Bowen, W.R. and J.S. Welfoot (2002)
Modelling the performance of membrane nanofiltration-critical assessment and model development,
Chem. Eng. Sci., **57** 1121.

Bowen, W.R. and J.S. Welfoot (2002b)
Predictive modelling of nanofiltration: membrane specification and process optimisation,
Desalination, **147** 197.

Bowen, W.R. and A.O. Sharif (1994)
Transport through microfiltration membranes: particle hydrodynamics and flux reductions,
J. Colloid Interface Sci., **168**, 414.

Bowen, W.R. and A.W. Mohammad (1998)
Diafiltration by Nanofiltration: Prediction and Optimisation,
AIChE J., **44**, 1799.

Bowen, W.R. and A.W. Mohammad (1998b)
Characterisation and prediction of nanofiltration membrane performance – a general assessment,
Trans. IChemE., **76** 885.

Bowen, W.R. and H. Mukhtar (1996)
Characterisation and prediction of separation performance of nanofiltration membranes,
J. Membrane Sci., **112**, 263.

Bowen, W.R. and T.A. Doneva (2000)
Atomic force microscopy of nanofiltration membranes: surface morphology, pore size distribution and adhesion,
Desalination, **129**, 163.

Bowen, W.R. and T.A. Doneva (2000b)
Atomic force microscopy characterization of ultrafiltration membranes: correspondence between surface pore dimensions and molecular weight cut-off,
Surface Interface Sci., **29**, 544.

Bowen, W.R., A.W. Mohammad and N. Hilal (1997)
Characterisation of nanofiltration membranes for predictive purposes – use of salts, uncharged solutes and atomic force microscopy,
J. Membrane Sci., **126**, 91.

Bowen, W.R., J.S. Welfoot, and P.M. Williams (2002)
A linearised transport model for nanofiltration: development and assessment,
AIChE J., **48** 760.

Bruggen, B.V.D. and C. Vandecasteele (2002)
Distillation vs. membrane filtration: overview of process evolutions in seawater desalination,
Desalination **143** 207.

Bungay, P.M. and H. Brenner (1973)
The motion of a closely fitting sphere in a fluid-filled tube,
Int. J. Multiph. Flow **1** 25.

Burghoff, H.G., K.L. Lee and W. Pusch (1980)
Characterisation of transport across cellulose-acetate membranes in the presence of strong solute-membrane interactions,
J. App. Ploy. Sci. **25** 323.

Cadotte, J., R. Forester, M. Kim, R. Petersen and T. Stocker (1988)
Nanofiltration membranes broaden the use of membrane separation technology,
Desalination, **70**, 77.

Cassano, A., E. Drioli, R. Molinari (1997)
Recovery and reuse of chemicals in unhairing, degreasing and chromium tanning processes by membranes,
Desalination, **113** 251.

Chai, X., Y. Mi, P-L. Yue and G. Chen (1999)
Bean curd wastewater treatment by membrane separation,
Sep. Purification Tech., **15**, 175.

Chapra, J.C. & M. Canale (1989)
Numerical methods for engineers,
McGraw-Hill Inc., 603.

Childress, A.E. and M. Elimelech (1996)
Effect of solution chemistry on the surface-charge of polymeric reverse-osmosis and nanofiltration membranes,
J. Membrane Sci., **119**, 253.

Chmiel, H., M. Kascheck, C. Blocher, M. Noronha and V. Mavrov (2002)
Concepts for the treatment of spent process water in the food and beverage industries,
Desalination **152** 307.

Christy, C. and S. Vermant (2002)
The state-of-the-art of filtration in recovery processes for biopharmaceutical production,
Desalination **147** 1.

Colman, P.M. (1994)
Influenza virus neuraminidase: structure, antibodies and inhibitors,
Protein Sci. **3** 1687.

Combe, C., C. Guizard, P. Aimar and V. Sanchez (1997)
Synthesis and characterization of microporous zirconia powders: Application in nanofilters and nanofiltration characteristics,
J. Membrane Sci., **132** 109.

Combe, C., E. Molis, P. Lucas, R. Riley and M.M. Clark (1999)
The effect of CA membrane properties on adsorptive fouling by humic acid,
J. Membrane Sci., **154** 73.

Coulson, J.M. and J. F. Richardson (1996)
Chemical Engineering
Vol. 1-6, Pergamon.

Crow, D.R. (1994)
Principles and applications of electrochemistry, 4th Ed.
Blackie Academic & Professional, Glasgow.

Cussler, E.L. (1995)
Diffusion: Mass transfer in fluid systems
Cambridge University Press, U.K.

Dawson, M.J., Mahmoudian, M., Blayer, S. and Woodley, J.M. (1999)
Process options for *N*-acetyl-D-neuraminic acid production using the aldolase enzyme, Presentation in Bio Europe 99, Biocatalysis for fine chemicals and pharmaceuticals, March 4-5, Amsterdam, The Netherlands.

De Faveri, D., P. Torre, P. Perego and A. Converti (2004)
Optimisation of xylitol recovery by crystallization from synthetic solutions using response surface methodology,
J. Food Eng., **61** 407

Deen, W.M., (1987)
Hindered transport of large molecules in liquid-filled pores,
AIChE J., **33**, 1409.

Deen, W.M., B. Satvat and M. Jaimeson (1980)
Theoretical model for glomerular filtration of charged solutes,
Am. J. of Physiology **38** 126.

Dey, T.K., V. Ramachandhran and B.M. Misra (2000)
Selectivity of anionic species in binary mixed electrolyte systems for nanofiltration membranes,
Desalination, **127**, 165.

Dickson, J.M. (1988)
Fundamental aspects of reverse osmosis, In *Reverse Osmosis Technology*, Ed. B. S. Parekh, Marcel Dekker Inc., New York.

Donnan F.G. (1911)
Theory of membrane equilibria and membrane potentials in the presence of non-dialysing electrolytes. A contribution physical-chemical physiology,
Z. Elektrochem. Angew. Phys. Chem., **17** 572.

Dresch, M., G. Daufin and B. Chaufer (2001)
Integrated membrane regeneration process for dairy cleaning-in-place
Sep. Purification Tech., **22-23**, 181.

Dresner, L. (1974)
Ion exclusion from neutral and slightly charged pores,
Desalination, **15**, 39.

Dresner, L. and J.S. Johnson (1980)
Hyperfiltration (Reverse Osmosis)
in *Principles of Desalination*, 2nd edition, Academic Press.

Dresner, L., (1972)
Some remarks on the integration of extended Nernst-Planck equation in the hyperfiltration of multicomponent solutions,
Desalination, **10**, 27.

Dukhin, S.S., N.V. Churaev, V.N. Shilov and V.M. Starov (1988)
Modelling reverse osmosis,
Russian Chemical Reviews (English Translation), **57**, 572.

Ebert, K. and F.P. Cuperus (1999)
Solvent resistant nano-filtration membranes in edible oil processing,
Membrane Technology, **107**, 5.

Eman, M.I. and N.V. Churaev (1990)
Changes in the structure and selective properties of composite membranes under the influence of electrolyte concentration,
Colloid J. (English Translation), **52**, 813.

Eriksson, P. (1988)
Nanofiltration extended the range of membrane filtration,
Env. Prog., **7**, 58.

Ernst, M., A. Bismarck, J. Springer and M. Jekel (2000)
Zeta-potential and rejection rates of a polyethersulfone nanofiltration membrane in single salt solutions,
J. Membrane Sci., **165**, 251.

Frank, M.J.W., J.B. Westerink, A. Schokker (2002)
Recycling of industrial waste water by using a two-step nanofiltration process for the removal of colour,
Desalination, **145** 69.

Garba, Y., S. Taha, J. Cabon and G. Dorange (2003)
Modelling of cadmium salts rejection through a nanofiltration membrane: relationships between solute concentration and transport parameters,
J. Membr. Sci. **211** 51.

Garba, Y., S. Taha, N. Gondrexon and G. Dorange (1999)
Ion transport modelling through nanofiltration membranes,
J. Membrane Sci., **160**, 187.

Garem, A., G. Daufin, J.L. Maubois and J. Leonil (1997)
Selective separations of amino acids with a charged inorganic nanofiltration membrane: Effect of physicochemical parameters on selectivity,
Biotech. Bioeng., **54**, 291.

Ghosh, A.C., R.K. Mathur and N.N. Dutta (1997)
Extraction and purification of cephalosporin antibiotics, Th. Scheper (Ed.),
Adv. Biochem. Eng. Biotech. **56**, Springer, Berlin.

Giddings, J.C., E. Kucera, C.P. Russell and M.N. Myers (1968)
Statistical theory for the equilibrium distribution of rigid molecules in inert porous networks. Exclusion chromatography,
J. Phys. Chem., **72**, 4397.

Gilron, J., N. Gara and O. Kedem (2001)
Experimental analysis of negative salt rejection,
J. Membrane Sci., **185**, 223.

Glueckauf, E. (1976)
The distribution of electrolytes between cellulose acetate membranes and aqueous solutions,
Desalination, **18**, 155.

Goulas, A.K., P.G. Kapasakalidis, H.R. Sinclair, R.A. Rastall, A.S. Grandison (2002)
Purification of oligosaccharides by nanofiltration,
J. Membr. Sci. **209** 321.

Grib, H., M. Persin, C. Gavach, D. L. Piron, J. Sandeaux and N. Mameri (2000)
Amino acid retention with alumina nanofiltration membrane,
J. Membrane Sci., **172** 9.

Gross, R.J., and J.F. Osterle (1968)
Membrane transport characteristics in ultrafine capillaries,
J. Chem. Phys., **49**, 228.

Gubareva, L.V., L. Kaiser and F.G. Hayden (2000)
Influenza virus neuraminidase inhibitors,
Lancet **355** 827.

Hafiane, A., D. Lemordant and M. Dhahbi (2000)
Removal of hexavalent chromium by nanofiltration,
Desalination, **130**, 305.

Hagmeyer, G. and R. Gimbel (1998)
Modelling the salt rejection of nanofiltration for ternary ion mixtures and for single salts at different pH values,
Desalination, **117**, 247.

Hagmeyer, G. and R. Gimbel (1999)
Modelling the rejection of nanofiltration membranes using zeta potential measurements,
Sep. Purification Tech., **15**, 19.

Hall, M.S., D.R. Lloyd and V.M. Starov (1997b)
Reverse osmosis of multicomponent electrolyte solutions. Part II. Experimental verification,
J. Membrane Sci., **128**, 39.

Hall, M.S., V.M. Starov and D.R. Lloyd (1997) Reverse osmosis of multicomponent electrolyte solutions. Part I. theoretical development, *J. Membrane Sci.*, **128**, 23.

Hay, A.J. (1989)
The mechanism of action of amantadine and rimantadine against influenza viruses. In: Notkins, A.L. and Oldstone M.B.A, Concepts in viral pathogenesis III., Berlin: Springer 561.

Hayberman, W.L. and R.M. Sayre (1958)
Motion of rigid and fluid spheres in stationary and moving liquids inside cylindrical tubes, David Taylor Model Basin Report No. **1143**, Dept. of the Navy, U.S.A.

Hayduk, W and H. Laudie (1974)
Prediction of diffusion coefficients for nonelectrolytes in dilute aqueous solutions,
AIChE J., **20** 611.

Hotchkies, L., D.T. Grima and S. Hedayati (1996)
The total process cost of parental antibiotic therapy: beyond drug acquisition cost,
Clinical Therapeutics, **18** NO. 4.

International Critical Tables (1929)
Coefficients of diffusion in liquids
Volume V, 63, McGraw-Hill, New York.

Ison, M.G. and F.G. Hayden (2001)
Therapeutic options for the management of influenza,
Current Opinion in Pharmacology **1** 482.

Israelachvili, J. N. (1991)
Intermolecular and Surface Forces 2nd Edition
Academic Press, London.

Israelachvili, J.N. (1987)
Solvation forces and liquid structure, as probed by direct force measurements,
Acc. Chem. Res. **20** 415.

IUPAC (1996)
J. Membrane Sci., **120**, 149.

J.P.G. Villaluenga and A.T. Mohammadi (2000)
A review on the separation of benzene/cyclohexane mixtures by pervaporation processes,
J. Membr. Sci. **169** 159.

Jacazio, G., R.F. Probstein, A.A. Sonin and D. Yung (1972)
Electrokinetic salt rejection in hyperfiltration through porous materials. Theory and experiment,
J. Phys. Chem., **76**, 4015.

Kedem, O. and A. Katchalsky (1963)
Permeability of composite membranes: Part 1. Electric current, volume flow and flow of solute through membranes,
Trans. Faraday Soc., **59**, 163.

Kragl, U., Gygax, D., Ghisalba, O., and Wandrey, C (1991)
Enzymatic two-step synthesis of *N*-acetyl-D-neuraminic acid in the enzyme membrane reactor,
Angew Chem. Int. Ed. Engl. **30** 827.

Krishna, R. and J.A. Wesselingh (1997)
The Maxwell-Stefan approach to mass transfer,
Chem. Eng. Sci., **52**, 861.

Latimer, W.M., K.S. Pitzer and C.M. Slansky (1939)
The free energy of hydration of gaseous ions and the absolute potential of normal calomel electrode,
J. Phys. Chem. **7** 108.

Lebas (1915) The molecular volumes of liquid chemical compounds, in Perry, J.H., Chemical Engineers Handbook, 4th ed., McGraw-Hill, NY 1963 14.

Levenstein, R., D. Hasson and R. Semiat (1996)
Utilisation of the Donnan effect for improving electrolyte separation with nanofiltration membranes,
J. Membrane Sci., **116**, 77.

Levesque, M.A. (1928)
Les lois de la transmission de chaleur par convection,
Annales Mines, **13**, 201.

Li, S.L., C. Li, Y.S. Liu, X.L. Wang and Z.A. Cao (2003)
Separation of L-glutamine from fermentation broth by nanofiltration,
J. Membr. Sci. **222** 191.

Lin, C.E., H.W. Chen, E.C. Lin, K.S. Lin and H.C. Huang (2000)
Optimisation of separation and migration behaviour of cephalosporins in capillary zone electrophoresis,
J. Chromatogr. A, **879** 197.

Loeb, S. and S. Sourirajan (1960)
Seawater demineralization by means of a semi-permeable membrane,
University of California at Los Angeles Engineering Report No. 60-60.

Mahmoudian, M, D. Noble, C.S. Drake, R.F. Middleton, D.S. Montgomery, J.E. Piercey, D. Ramlakhan, M. Todd, and M.J. Dawson (1997)
An efficient process for production of N-acetylneuraminic acid using N-acetylneuraminic acid aldolase,
J. Enz. Micr. Tech., **20** 393.

Malone, D.M. and J.L. Anderson (1977)
Diffusional boundary-layer resistance for membranes with low porosity,
AIChE J. **23** 177.

Merry, A. (2001)
The right membrane for the job,
Filtration & Separation, **38**, 16.

Meyer, K.H. and J-F. Sievers (1936)
La perméabilité des membranes I. Théorie de la perméabilé ionique,
Helv. Chim. Acta, **19**, 649.

Mohammad, A.W. (1998)
Predictive Models for Nanofiltration Membrane Processes,
PhD Thesis, University of Wales Swansea.

Mohammad, A.W. and M.S. Takriff (2003)
Predicting flux and rejection of multicomponent salts mixture in nanofiltration membranes,
Desalination **157** 105.

Mukhtar, H. (1995)
Flux and Rejection at Charged Porous Membranes,
PhD Thesis, University of Wales Swansea.

Mulder, M. (1996)
Basic Principles of Membrane Technology 2nd Edition
Kluwer, Dordrecht.

Nakao, S. and Kimura, S. (1981)
Analysis of solutes rejection in ultrafiltration,
J. Chem. Eng. Japan, **14**, 32.

Nguyen, M., N. Reynolds, S. Vigneswaran (2003)
By-product recovery from cottage cheese production by nanofiltration,
J. Cleaner. Prod., **11** 803.

Noronha, M., T. Britz, V. Mavrov, H.D. Janke, H. Chmiel (2002)
Treatment of spent process water from a fruit juice company for purposes of reuse: hybrid process concept and on-site test operation of a pilot plant,
Desalination, **143** 183.

Noyes, R.M. (1962)
Thermodynamics of ion hydration as a measure of effective dielectric properties of water,
J. Am. Chem. Soc. **84** 513.

Nystrom, M., K. Ruohomaki and L. Kaipia (1996)
Humic acids as a fouling agent in filtration,
Desalination, **106**, 79.

Nystrom, M., L. Kaipia and S. Luque (1995)
Fouling and retention of nanofiltration membranes,
J. Membrane Sci., **98**, 249.

Opong, W.S. and A.L. Zydney (1991)
Diffusive and convective protein transport through asymmetric membranes,
AIChE J., **37** 1497.

Parsegian, A. (1969)
Energy of an ion crossing a low dielectric membrane: Solutions to four relevant electrostatic problems,
Nature, **221**, 844.

Peeters, J.M.M., J.P. Boom, M.H.V. Mulder and H. Strathmann (1998)
Retention measurements of nanofiltration membranes with electrolyte solutions,
J. Membrane Sci., **145**, 199.

Peeters, J.M.M., M.H.V. Mulder and H. Strathmann (1999)
Streaming potential measurements as a characterization method for nanofiltration membranes,
Colloids and Surfaces A: Physicochemical and Eng. Aspects **150** 247.

Pervov, A.G., E.V. Dudkin, O.A. Sidorenko, V.V. Antipov, S.A. Khakhanov and R.I. Makarov (2000)
RO and NF membrane systems for drinking water production and their maintenance techniques,
Desalination, **132**, 315.

Petersen, R.J. (1993)
Composite reverse osmosis and nanofiltration membranes,
Desalination, **83**, 81.

Pouliot, Y., M. C. Wijers, S. F. Gauthier and L. Nadeau (1999)
Fractionation of whey protein hydrolysates using charged UF/NF membranes,
J. Membrane Sci., 158, 105.

Radier, C. W. van Oers, A. Steenbergen and M. Wessling (2001)
Desalting a process cooling water using nanofiltration,
Sep. Purification Tech., **22-23**,159.

Raff, O. and R-D. Wilken (1999)
Removal of dissolved uranium by nanofiltration,
Desalination, **122**, 147.

Raman, L.P., M. Cheryan and N. Rajagopalan (1994)
Consider nanofiltration for membrane separations,
Chem. Eng. Prog., **90**, 68.

Rashin, A.A., and B. Honig (1985)
Re-evaluation of the Born model of ion hydration,
J. Phys. Chem. **89** 5588.

Rautenbach, R. and Gröschl, A. (1990)
Separation potential of nanofiltration membranes,
Desalination, **77**, 73.

Rautenbach, R. and R Albrecht (1994)
Membrane Processes
John Wiley, Chichester.

Rios, G.M., R. Joulie, S.J. Sarrade and M. Carles (1996)
Investigation of ion separation by microporous nanofiltration membranes,
AIChE J., **42**, 2521.

Scarpello, J.T., D. Nair, L.M. Freitas dos Santos, L.S. White, A.G. Livingston (2002)
The separation of homogeneous organometallic catalysts using solvent resistant nanofiltration,
J. Membr. Sci., **203** 71.

Schaep, J., C. Vandecasteele, A.W. Mohammad and W.R. Bowen (1999)
Analysis of the salt retention of nanofiltration membranes using the Donnan-steric partitioning pore model,
Sep. Sci. Tech., **34** 3009-3030.

Schaep, J., C. Vandecasteele, A.W. Mohammad and W.R. Bowen (2001)
Modelling the retention of ionic components for different nanofiltration membranes,
Sep. Purification Tech., **22-23**, 169.

Schlögl, R. (1966)
Membrane permeation in system far from equilibrium,
Berichte der Bunsengesellschaft Physik. Chem, **70**, 400.

Shaalan, H.F., M.H. Sorour, S.R. Tewfik (2001)
Simulation and optimisation of a membrane system for chromium recovery from tanning wastes,
Desalination, **141** 315.

Singh, S., K.C. Khulbe, T. Matsuura and P. Ramamurphy (1998)
Membrane characterisation by solute transport and atomic force microscopy,
J. Membr. Sci., **142** 111.

Smith, A. (1985)
Cephalosporins, in Comprehensive Biotechnology: the principles, applications and regulations of biotechnology in industry, agriculture and medicine, **3** 163, Pergamon Press, Oxford, U.K.

Smith, K.A., C.K. Colton, E.W. Merill and L.B. Evans (1968)
Convective transport in a batch dialyzer: determination of true membrane permeability from a single measurement,
Chem. Eng. Prog. Symp. Ser. **84** 45.

Spiegler, K.S. and O. Kedem (1966)
Thermodynamics of hyperfiltration (RO): criteria for efficient membranes,
Desalination, **1**, 311.

Stables, H.C. (1980)
Crystallization process
U.S. Patent 4 298 732.

Stokes, R.H. (1964)
The Van Der Waals radii of gaseous ions of the noble gas structure in relation to hydration energies,
J. Am. Chem. Soc. **86** 979.

Sugrue R.J. and A.J. Hay (1991)
Structural characteristics of the M2 protein of influenza A viruses: evidence that it forms a tetrameric channel,
Virology **180** 617.

Taubenberger, J.K., A.H. Reid and T.G. Fanning (2000)
The 1918 influenza virus: a killer comes into view,
Virology **274** 241.

Teorell, T. (1951)
Zur quantitativen behandlung der membranpermeabilität,
Z. Elektrochem., **55**, 460.

Tsuru, T., M. Miyawaki, H. Kondo, T. Yoshioka and M.Asaeda (2003)
Inorganic porous membranes for nanofiltration of nonaqueous solutions,
Sep. Purif. Tech. **32** 105.

Tsuru, T., M. Urairi, S. Nakao and S. Kimura (1991b)
Reverse osmosis of single and mixed electrolytes with charged membranes: experiment and analysis,
J. Chem. Eng. Japan, **24**, 518.

Tsuru, T., S. Nakao and S. Kimura (1991)
Calculation of ion rejection by extended Nernst-Planck equation with charged reverse osmosis membranes for single and mixed electrolyte solutions,
J. Chem. Eng. Japan, **24**, 511.

Tsuru, T., T. Shutou, S. Nakao and S. Kimura (1994)
Peptide and amino acid separation with nanofiltration membranes,
Sep. Sci. and Tech., **29**, 971.

Vandanjon, L., S. Cros, P. Jaouen, F. Quemeneur, P. Bourseau (2002)
Recovery by nanofiltration and reverse osmosis of marine flavours from seafood cooking waters,
Desalination, **144** 379.

Vezzani, D. and S. Bandini (2002)
Donnan equilibrium and dielectric exclusion for characterisation of nanofiltration membranes,
Desalination **149** 477.

Villaluenga, J.P. Garcia and A. Tabe-Mohammadi (2000)
A review on the separation of benzene/cyclohexane mixtures by pervaporation processes,
J. of Membrane Sci., **169**, 159.

Von Itzstein, M., W.Y. Wu, G.B. Kok, M.S. Pegg, J.C. Dyason, B. Jin, T. Van Phan, M.L. Smythe, H.F. White, S.W. Oliver, P.M. Coleman, J.N. Varghese, D.M. Ryan, J.M. Woods, R.C. Bethell, J.V. Hothman, J.M. Cameron and C.R Penn (1993)
Rational design of potent sialidase-based inhibitors of influenza virus replication,
Nature **363** 418.

Vrijenhoek, E.M. and J.J. Waypa (2000)
Arsenic removal from drinking water by a "loose" nanofiltration membrane,
Desalination, **130**, 265.

Wang, X-L., T. Tsuru, S. Nakao, and S. Kimura (1995)
Electrolyte transport through nanofiltration membranes by the space-charge model and the comparison with Teorell-Meyer-Sievers model,
J. of Membrane Sci., **103**, 117.

Weber, R., H. Chmiel and V. Mavrov (2003)
Characteristics and application of new ceramic nanofiltration membranes,
Desalination **157** 113.

Welfoot, J.S. (2001)
Predictive modelling of membrane nanofiltration
PhD Thesis, University of Wales Swansea.
Wilke, P.R. & P. Chang (1955)
Correlation of diffusion coefficients in dilute solutions,
AIChE J. **1** 264.

Xu, J-H., X-H. Xing, S. Yamamoto, Y. Tanji and H. Unno (1997)
Effect of ion adsorption on its permeation through a nanofiltration membrane,
J. Chem. Eng. Japan, 30, 806.

Yaroshchuk, A.E. (1998)
Rejection mechanisms of NF membranes,
Membrane Technology, **100**, 9.

Yaroshchuk, A.E. (2000)
Dielectric exclusion of ions from membranes,
Adv. Col. Int. Sci., **85** 193.

Zhu, A., W. Zhu, Z. Wu, Y. Jing (2003)
Recovery of clindamycin from fermentation wastewater with nanofiltration membranes,
Water Res., **37** 3718.

Nomenclature

a_i, a	hydrodynamic (Stokes) radius of ion *i* or uncharged solute, m
a_i	activity of ion *i*, mol m^{-3}
a_s	ion radius in solvent, m
a_v	ion radius in vacuum, m
A	membrane area, m^2
A_k	porosity, dimensionless
c_i, c	concentration of ion *i* or uncharged solute within pore, mol m^{-3}
$c_i(0), c(0)$	concentration of ion *i* or uncharged solute at the pore entrance, mol m^{-3}
$c_i(\Delta x), c(\Delta x)$	concentration of ion *i* or uncharged solute at the pore outlet, mol m^{-3}
$c_{i,av}, c_{av}$	average concentration of ion *i* or uncharged solute within pore, mol m^{-3}
c_T	total concentration, mol m^{-3}
C_i	ionic solute bulk solution concentration, mol m^{-3}
$C_{i,f}, C_f$	bulk feed concentration, mol m^{-3}
$\dot{C}_{i,f}$	bulk concentration of fully retained solute, mol m^{-3}
$C_{i,p}, C_p$	permeate concentration of ion *i* or uncharged solute, mol m^{-3}
$C_{i,w}, C_w$	wall concentration of ion *i* or uncharged solute, mol m^{-3}
d	thickness of the oriented solvent layer, m
D_p^*	corrected uncharged solute pore diffusion coefficient, $m^2\ s^{-1}$
D_e	harmonic mean diffusion coefficient, $m^2\ s^{-1}$
D_{eff}	effective bulk salt diffusion coefficient, $m^2\ s^{-1}$
$D_{i,p}, D_p$	pore diffusion coefficient of ion *i* or uncharged solute, $m^2\ s^{-1}$
$D_{i,\infty}, D_\infty$	bulk diffusion coefficient of ion *i* or uncharged solute, $m^2\ s^{-1}$
E	energy potential describing electrostatic forces, V
e	electronic charge, 1.602177×10^{-19} C
f_i	iterative method test function for ion *i*, mol m^{-3}
$f_{Overall}$	overall iterative method test function, mol m^{-3}
F	Faraday constant, 96487 C mol^{-1}

G	the lag coefficient, dimensionless
i	electrical current, A
I	ionic strength, mol m^{-3}
j_i	ionic flux of ion i (pore area basis), mol m^{-2} s^{-1}
J_v	volumetric flux, m^3 m^{-2} s^{-1}
J_w	pure water flux, m^3 m^{-2} s^{-1}
k	feed-side mass transfer coefficient, m s^{-1}
k'	mass transfer parameter in Eq. (2.8), variable dimensions
k_B	Boltzmann constant, 1.38066 x 10^{-23} J K^{-1}
K^{-1}	the enhanced drag coefficient, dimensionless
K_{cell}	cell constant of conductivity meter, dimensionless
$K_{i,c}, K_c$	hindrance factor for convection of ion i or uncharged solute, dimensionless
$K_{i,d}, K_d$	hindrance factor for diffusion of ion i or uncharged solute, dimensionless
M	mass of solute in bulk feed, kg
$\dot{M}$	mass of solute fully retained, kg
MW	molecular weight, Da
n	number of ions in an electrolyte mixtures, dimensionless
N_A	Avagadro's number, 6.023 x10^{23} g mol
N_{Re}	Reynolds number, dimensionless
N_{Sh}	Sherwood number, dimensionless
p	partial vapour pressure, N m^{-2}
P	pressure, N m^{-2}
Pe_i, Pe	Peclet number for ion i or uncharged solute, dimensionless
Pe'	modified Peclet number of uncharged solute, dimensionless
r	radius of the stirred cell, m
r	radial position within the pore, m
r_B	Bjerrum radius, m
r_p	effective pore radius, m
R, R_i	real rejection of salt or ion i, dimensionless
R	Universal Gas Constant, 8.314 J mol^{-1} K^{-1}
R	electrical resistance, Ω
R_{calc}	calculated rejection, dimensionless

R_{exp}	experimental rejection, dimensionless
R_{lim}	limiting rejection, dimensionless
R_{obs}	observed rejection, dimensionless
S_y	sum of squares objective function in fitting, dimensionless
t	elapsed time, s
T	absolute temperature, K
u_i	ionic mobility, $m^2\ s^{-1}\ V^{-1}$
u_s	solvent velocity inside pore, $m\ s^{-1}$
u_x	maximum solvent velocity inside pore, $m\ s^{-1}$
$\overline{V}$	solute molar volume, m^3
V	solvent velocity, $m\ s^{-1}$
V	sample volume, m^3
V_{si}	solute partial molar volume, $m^3\ mol^{-1}$
x	solvent association parameter, dimensionless
x	axial position within the pore, m
X_d	effective charge density, $mol\ m^{-3}$
Y	dimensionless group of ion *i*, dimensionless
z_i	valence of ion i, dimensionless

Greek Symbols

$\Delta c_i, \Delta c$	pore concentration difference for ion *i* or uncharged solute, $mol\ m^{-3}$
ΔP	applied pressure, $N\ m^{-2}$
ΔP_e	effective pressure driving force, $N\ m^{-2}$
$\Delta\pi$	osmotic pressure, $N\ m^{-2}$
ΔW_{DE}	dielectric exclusion energy, dimensionless
ΔW_i	Born solvation energy barrier, J
Δx	membrane thickness, m
$\Delta\psi_D$	Donnan potential at the pore inlet, V
β	radial position inside pore, dimensionless
δ	thickness of the feed-side boundary film, m

ε_b	bulk dielectric constant, dimensionless
ε_m	dielectric constant of membrane material, dimensionless
ε_p	pore dielectric constant, dimensionless
ε_s	dielectric constant of bulk solvent, dimensionless
ε_o	permittivity of free space, 8.85419×10^{-12} J^{-1} C^2 m^{-1}
ε^*	dielectric constant of the oriented water layer, dimensionless
κ	Debye screening length, m
γ	parameter defined by Eq. (5.3), dimensionless
Γ_i	overall partitioning coefficient, dimensionless
Γ_{Di}	Donnan partitioning coefficient, dimensionless
Γ_{DEi}	dielectric partitioning coefficient, dimensionless
Λ	equivalent electrical conductance, S m^2 mol^{-1}
Λ_o	limiting equivalent electrical conductance, S m^2 mol^{-1}
η	solvent viscosity within pores, N s m^{-2}
η_{layer}	viscosity of oriented solvent layer, N s m^{-2}
η_o, μ	bulk solvent viscosity, N s m^{-2}
ω	angular velocity, rad s^{-1}
γ_i	activity coefficient of ion *i* within pore, dimensionless
γ_i^o	bulk activity coefficient of ion *i*, dimensionless
ν	kinematic viscosity, m^2 s^{-1}
v_i	ionic velocity, m^2 s^{-1}
λ	ratio of ionic or uncharged solute radius to pore radius, dimensionless
ξ	ratio of effective membrane charge density to bulk feed concentration, dimensionless
Φ_i'	partial partition coefficient, dimensionless
Φ_i, Φ	steric partition coefficient of ion *i* or uncharged solute, dimensionless
μ	uncharged solute chemical potential, J mol^{-1}
μ_i	electrochemical potential of ion *i*, J mol^{-1}
ψ	electrical potential within the pore, V
Ψ	space charge potential within the pore as defined by Eq. (3.15), V

$\overline{\Psi}$	total pore electrical potential as defined by Eq. (3.15), V

Subscripts

+	anion
-	cation
±	both anion and cation
1	ion 1
2	ion 2
3	ion 3
4	ion 4
(0^+)	denotes feed-membrane interface (membrane side)
(0^-)	denotes feed-membrane interface (feed side)

Abbreviations

7-ACA	7-aminocephalosporanic acid
AFM	atomic force microscopy
DSPM	Donnan steric partitioning model
GlcNAc	*N*-acetyl-D-glucosamine
ManNAc	*N*-acetyl-D-mannosamine
MWCO	molecular weight cut off
Neu5Ac	*N*-acetyl-D-neuraminic acid
NF	nanofiltration
TFC	thin film composite
UDSPM	updated Donnan steric partitioning model